uOttawa

L'Université canadienne
Canada's university

FACULTÉ DES ÉTUDES SUPÉRIEURES
ET POSTOCTORALES

uOttawa

L'Université canadienne
Canada's university

FACULTY OF GRADUATE AND
POSDOCTORAL STUDIES

Kristina Haase

AUTEUR DE LA THÈSE / AUTHOR OF THESIS

M.Sc. (Mechanical Engineering)

GRADE / DEGREE

School of Information Technology and Engineering

FACULTÉ, ÉCOLE, DÉPARTEMENT / FACULTY, SCHOOL, DEPARTMENT

Finite Element Analysis of Orthopaedic Plates and Screws to Reduce the Effect of Stress Shielding

TITRE DE LA THÈSE / TITLE OF THESIS

G. Rouhi

DIRECTEUR (DIRECTRICE) DE LA THÈSE / THESIS SUPERVISOR

CO-DIRECTEUR (CO-DIRECTRICE) DE LA THÈSE / THESIS CO-SUPERVISOR

H. Frei

M. Labrosse

Gary W. Slater

Le Doyen de la Faculté des études supérieures et postdoctorales / Dean of the Faculty of Graduate and Postdoctoral Studies

Finite Element Analysis of Orthopaedic Plates and Screws to Reduce the Effects of Stress Shielding

by

Kristina Haase

A thesis submitted to the Faculty of Graduate and Postdoctoral Studies in partial fulfillment of the requirements for the degree of

Master of Applied Science

In Mechanical Engineering

Ottawa-Carleton Institute for Mechanical and Aerospace Engineering

University of Ottawa

Ottawa, Canada

Your file Votre référence
ISBN: 978-0-494-65495-8
Our file Notre référence
ISBN: 978-0-494-65495-8

Acknowledgements

I would like to express gratitude to my thesis supervisor, Dr. Gholamreza Rouhi, for his patient guidance and encouragement throughout my research.

A deep appreciation is extended to my family and friends, whom have all encouraged and supported me throughout this experience.

I would also like to recognize my academic peers and the staff of the Department of Mechanical Engineering.

Abstract

The biological adaptation of bone to changes in its environment is a continual process known as bone remodeling. Although it has been well observed that mechanical stimuli are required to initiate the bone remodeling response, the exact stimuli and mechanisms of this process remain unknown. When bone's normal level of mechanical stimuli is disrupted localized areas of bone experience changes in their rate of remodeling, (i.e. a rate of change in net bone mass and porosity). In the case of fracture healing with the use of fixation devices, a reduction in mechanical stimuli can lead to bone resorption. This phenomenon, known as stress shielding, is a common cause of failure in fracture fixation of long-bones.

Using finite element models, this thesis studies the effects of implant geometry and material properties in relation to stress shielding, by examining bone-implant interactions of stress and also strain energy density distributions as possible mechanical stimuli.

Contents

Acknowledgements ii

Abstract iii

List of Tables vii

List of Figures viii

Chapter 1: Introduction 1

1.1 Purpose of this research 1

1.2 Material properties of bone 2

1.3 Bone adaptation 3

1.4 Fracture healing 5

1.5 Stress shielding 7

1.6 Computational models and the use of FEA 8

1.7 Thesis objective 9

Chapter 2: Internal fixation plates 10

2.1 The progression of plating techniques 10

2.2 Predicting bone stresses using composite beam theory 14

Chapter 3: Three-dimensional FE plated-bone models 15

3.1 Simple bone-plate model 15

3.1.1 Model geometry and methods 15

3.1.2 Simulation results 18

3.1.3 Conclusions 28

3.2 Parametric model 29

3.2.1 Model geometry and methods 29

3.2.2 Simulation results 33

3.2.3 Conclusions 41

3.4 Discussion 42

Chapter 4: Orthopaedic screws 44

4.1 Employment of screws in bone fixation 45

4.2 Common Orthopaedic Screw Types 49

4.2.1 Cortical Screws 50

4.2.2 Cancellous Screws 50

4.2.3 Lag Screws 51
4.3 Stress shielding in the vicinity of screws 51
4.3.1 Stress concentrations caused by screw removal 51
4.3.2 Bone atrophy or hypertrophy? 52
4.3.3 Resorption may be critical in osteoporotic bone 57
4.4 Screw Pullout Strength 57
4.4.1 Pullout strength test methods 59
4.4.2 Host material density 59
4.4.3 Screw design factors 60
4.4.4 Pilot-hole size 62
4.4.5 Screw insertion angle 62
4.5 Theoretical analysis of shear failure force 63
Chapter 5: Two-dimensional FE screw-bone model 67
5.0 Model overview 67
5.1 Bone screw parameters 68
5.2 Finite element analyses methods 69
5.3 Simulation and evaluation of biocompatibility 70
5.3.1 Stress transfer parameters (STPs) 72
5.3.2 Strain energy density transfer parameters (SEDTPs) 73
5.4 Verification of the model 74
5.4.1 Testing the validity of quantifying parameters 74
5.4.2 Testing the effect of load magnitude 82
5.4.3 Testing the model under a compressive axial load 84
5.5 Simulation results 86
5.5.1 The difference between α & β values 87
5.5.2 The effect of varying thread profile shape 92
5.5.3 The effect of varying the number of screw threads 94
5.5.4 The effect of varying the shaft length 95
5.5.5 The effect of varying the screw thread diameter 97
5.5.6 The effect of varying the screw's modulus of elasticity 98
5.5.6 The effect of varying the screw shaft diameter 99
5.6 Conclusions 101

5.7 Discussion 102
Chapter 6: Concluding summary & suggestions for future work 108
6.1 Three-dimensional FE plated-bone model 108
6.2 Two-dimensional FE screw-bone model 111
6.3 A brief discussion on the use of FEA 116
References 119
Publications Arising from This Research 137
Appendix i: STP results 138
Appendix ii: SEDTP results 139
Appendix iii: Theoretical analysis 140
Composite beam theory 140
Beam on elastic foundation theory 147

List of Tables

Table 1: Resulting stresses and strains resulting from loads applied to the control and fixed-bone models 22

Table 2: Predicted shear strength(s) of bovine bone, pedilen, and experimental bovine bone results 65

Table 3: Shear force calculations for screw configurations tested in 2D bone-screw model 66

Table 4: STP and SEDTP values for the 1 GPa screw configurations 78

Table 5: STP parametric results 138

Table 6: Total STP values 138

Table 7: SEDTP parametric results 139

Table 8: Total SEDTP values 139

List of Figures

Figure 1: The phases of bone remodeling ... 4

Figure 2: Primary and secondary fracture healing ... 6

Figure 3: Stress shielding resulting from a reduction in mechanical stimulus ... 7

Figure 4: Simplified schematic diagram of FE models incorporating bone remodeling ... 8

Figure 5: Conventional compression plates and locking dynamic compression plates ... 11

Figure 6: Mesh of ¼ model of plated bone ... 17

Figure 7: Compressive axial load ... 17

Figure 8: Pure bending moment ... 18

Figure 9: Eccentric axial load ... 18

Figure 10: Theoretical prediction of stress in bone below the plate ... 19

Figure 11: Axial loading of a simple direct contact bone-plate model ... 20

Figure 12: Comparison of theoretical to FE model longitudinal stress values ... 21

Figure 13: Comparison of bone stresses for the control and the fixed bone model ... 21

Figure 14: Equivalent stress resulting from an axial compressive load: control bone model ... 23

Figure 15: Equivalent stress resulting from an axial compressive load: fixed-bone model ... 23

Figure 16: Equivalent stress resulting from a pure bending moment: control bone model ... 24

Figure 17: Equivalent stress resulting from a pure bending moment: fixed-bone model ... 24

Figure 18: Equivalent stress resulting from an eccentric axial load: control bone model ... 25

Figure 19: Equivalent stress resulting from an eccentric axial load: fixed-bone model ... 26

Figure 20: 3D parametric bone-plate model ... 31

Figure 21: Original mesh of the parametric model ... 32

Figure 22: Mesh refinement at the fixed end (representative of the fracture site) ... 32

Figure 23: Equivalent stress resulting from an applied bending moment on the 3D model ... 33

Figure 24: Equivalent strain resulting from an applied bending moment to the 3D model ... 34

Figure 25: Theoretical predictions of stress in bone underlying a plate of changing thickness ... 35

Figure 26: The effect of plate thickness on effective stress at the fracture site ... 36

Figure 27: Predicted change in bone stress below the plate with a change in plate angle ... 37

Figure 28: The effect of increasing the plate-bone contact area ... 38

Figure 29: Effect of changing the distal screw position (increased distance from the fracture site) ... 39

Figure 30: Comparison of stress distribution with stainless steel and titanium screws ... 40

Figure 31: Basic profile for Unified and ISO thread geometry ... 46

Figure 32: Alternate commercial screw thread profile shapes ... 47
Figure 33: Examples of commercially available cortical and cancellous bone screws (New Life Surgical Works) ... 50
Figure 34: 2D screw-bone model ... 68
Figure 35: Screw geometry ... 69
Figure 36: Mesh of 2D screw-bone model with mesh refinement along screw threads ... 71
Figure 37: Stress and strain path defined in ANSYS ... 72
Figure 38: (a-d) Examples of 1 GPa screw configurations under tensile loading ... 77
Figure 39: Comparison of STP and SEDTP total values for a screw with modulus of elasticity of 1 GPa ... 79
Figure 40: Difference between STP α values for screws with different moduli of elasticity ... 79
Figure 41: Difference between STP β values for screws with different moduli of elasticity ... 80
Figure 42: Example of stress distribution for the long shaft, 4 mm diameter, 9 thread configurations ... 81
Figure 43: Change in load distribution as the screw's elastic modulus increases ... 82
Figure 44: Stress and strain plot for 80 N tensile load ... 82
Figure 45: Stresses in bone and threads along the defined path ... 83
Figure 46: Stress in bone and screw versus an increase in load ... 84
Figure 47: The total deformation of the 2D bone-screw model under a compressive load of 80 N ... 85
Figure 48: Comparison of nodal solutions of equivalent stress for (a) compressive and (b) tensile loading. ... 85
Figure 49: Comparison of STP α and β values for 4 mm diameter thread ... 87
Figure 50: Comparison of STP α and β values for 6 mm diameter thread ... 88
Figure 51: Comparison of SEDTP α and β values for 4 mm thread diameter ... 90
Figure 52: Comparison of SEDTP α and β values for 6 mm diameter thread ... 91
Figure 53: Detail of nodal average solution of equivalent stress along thread contour ... 93
Figure 54: Total STP and SEDTP values for a change in shaft radius ... 100
Figure 55: STP trends for an increase in shaft diameter ... 100
Figure 57: The inclusion of an adaptive bone remodeling theory ... 111
Figure 57: STP/SEDTP average trend comparison ... 113
Figure 58: A 2D bi-cortical screw-bone model ... 115
Figure 60: Axial loading of a single-material beam ... 141
Figure 61: Single material beam under bending load ... 143

Chapter 1: Introduction

1.1 Purpose of this research

Prior to the 20^{th} century, scientists and researchers, already cognizant of the important role that stress and strain history plays in the development and transformation of skeletal biology, hypothesize an array of mechanistic theories based on the architecture of the skeleton and structure of bone. It is now a well known and accepted theory that bone adapts to changes in mechanical stimuli; an important process of whose knowledge has been greatly attributed to a German anatomist by the name of Julius Wolff (Wolff, 1892). Although the generalized theory, known as Wolff's law, has been proven to have some limitations, the concept of bone adaptation has been proven on countless occasions, through physiological experiments and the histological tracking of bone density in relation to mechanical activity and contrarily to disuse (Frost, 2001) (Carter, 1987) (Huiskes, Ruimerman, Van Lenthe, & Janssen, 2000) (Whalen & Carter, 1988). This adaptive behaviour that bone exhibits consists of 5 phases, namely activation, resorption, reversal, apposition, and quiescence (Bartel, Davy, & Keaveny, 2006, p. 109). Even though researchers accept the notion of bone adaptation, the current understanding of the bone remodeling process and the mechanisms involved is still one of ongoing debate.

Alongside the progression of remodeling theories, which has shed light into the mechanics of fracture healing, the development of internal fixation techniques has also been transformed. The transformation occurred as the primary concern of fixation which initially focused on the mechanical properties shifted to one increasingly concerned with biological properties. This transformation has occurred in response to a need to limit the negative effects resultant of internal fixation which have led to unsuccessful fracture healing or re-fracture following the removal of fixation (Uhthoff & Finnegan, 1983). One of the most influential effects relating to failure of fixation is stress shielding (Uhthoff & Jaworski, 1978). This thesis will discuss some of the controversies that arise in accordance with fixation techniques and the methods employed to promote a reduction in stress shielding.

So far, many researchers have contributed valuable insight into the nature of bone remodeling and fracture healing through experimental and pre-determinate analyses with the aid of finite element analysis (FEA) tools (Cheal, Hayes, & White III, 1985; Cheung, Zalzal, Bhandari, Spelt, & Papini, 2004; Kotha, Hsieh, Strigel, Muller, & Silva, 2004). As advancements in computational methods evolve, our ability to accurately predict both preventative measures and failure modes *in situ* also continue to flourish. A brief review of the historical changes in remodeling theories and the concurrent changes in internal fixation techniques reveals important considerations that must be noted by future researchers who try to span the gap between theory and application with the aid of computational technologies.

This introductory chapter provides basic background information on the material properties of bone, with a particular focus on its adaptive nature, and the biological methods involved in fracture healing. A discussion involves fracture treatment methods, associated negative effects of stress shielding, as well as the capability to measure these effects via computational methods. The objective of this thesis is outlined at the end of this chapter.

1.2 Material properties of bone

Research into the biological and mechanical properties of bone at the organ and tissue level is an ongoing challenge (Bartel, Davy, & Keaveny, 2006, p. 80) (Cowin, 2001). Responsible for mechanical, synthetic, and metabolic activities, bone as an organ is both responsive and adaptive to changes in its environment and is also inter- and intra-individually heterogeneous. Two distinct architectures exist, namely, cortical (compact, dense, or Haversian) bone, and trabecular (cancellous or spongy) bone. Cortical bone is composed of a dense arrangement of highly organized lamellar bone, whereas trabecular bone consists of a much more porous, scaffold-like arrangement of trabeculae. Both architectures exhibit an elastic anisotropic behavior. Stiffness and strength are dependent on the direction of loading as well as the local volume fraction and density of bone. The apparent density of hydrated human cortical bone varies little over a given specimen and is about 1.85 g/cm^3 (Bartel, Davy, & Keaveny, 2006, p. 79; Burstein & Wright, 1994). On the other hand, the apparent density of trabecular bone can range between 0.10 g/cm^3 and 0.50 g/cm^3 for different anatomic sites (Bartel, Davy, & Keaveny, 2006, p. 79). Subtle changes in bone density, caused by aging, disease, or disuse, largely affects both the strength and elastic modulus of bone. In vitro experimentation proves that a power law relationship best describes the Young's modulus of bone, which can be approximated by the cubic relationship between calcium content and volume fraction (Currey, 1988).

Bone is a composite material consisting of an organic phase of mostly type I collagen fibers, and an inorganic phase mainly composed of hydroxyapatite and water (Bartel, Davy, & Keaveny, 2006, p.

74). Bone's toughness is associated with its organic phase whereas the rigidity is provided by its mineral phase. The latter of which has a substantial affect on the mechanical properties of bone. After skeletal maturity is reached, the percent of mineralization no longer changes (Burstein & Wright, 1994). Fatigue, creep and viscoelastic behaviours of bone are also noted experimentally. Anisotropic behaviour is also demonstrated by bone's greater resistance to failure in compression than in tension (e.g. in the longitudinal direction the ultimate stress is 193 MPa in compression and 133 MPa in tension), and in the direction of the grain of the bone than in the transverse direction (Reilly & Burstein, 1975). Microtensile and ultrasonic testing proves these behaviours exist for both trabecular and cortical bone, although they act as separate materials, mechanically (Rho, Ashman, & Turner, 1993). So, one should expect anisotropic behaviour from both cortical and spongy bone, as this is the case in a fiber reinforced composite with a preferred fibers' direction.

Heterogeneity is a fundamental characteristic of biological tissues, although for the purposes of this work, bone is considered to be homogeneous, and have isotropic, material properties (so, just two independent constants will appear in the elasticity tensor, i.e. the modulus of elasticity and Poisson's ratio). In reality, considering this material as a continuum is a simplifying assumption and is highly dependent on the geometric scale of the model in question. Cortical bone is commonly modeled under these assumptions; however, trabecular bone should be on the order of 5-10 mm to be considered as a continuum (Dendorfer & Maier H.J.Hammer, 2009) (Gibson, 1985), as it is in our 2D bone-screw study.

1.3 Bone adaptation

An important capability of bone is its ability to adapt micro-structurally in response to changes in mechanical loading. This phenomenon is known as the process of bone remodeling. Through feedback control, bone reorganizes itself to optimize mechanical properties where necessary. This concept originated as early as 1892 when Julius Wolff, a German anatomist, postulated that bone adapts to changes in its environment (Wolff, 1892) (Vahdati & Rouhi, 2007).

Growth, repair, and maintenance of bone are executed by four types of cells, namely osteoclasts, osteoblasts, osteocytes, and bone lining cells. These cells are involved in the remodeling process, which follows a pattern of activation, resorption, reversal, formation, and quiescence (see Figure 1) (Bartel, Davy, & Keaveny, 2006, p. 109) (Cowin, 2001, p. 26). It has been proposed by many researchers that, during the activation phase, osteocytes act as sensors to mechanical stimuli such as strain or strain energy density (Cowin & Hegedus, 1976). The mechanical signal is converted to a chemical one that initiates the response of osteoclasts and osteoblasts, which are responsible for bone resorption and apposition, respectively. Bone lining cells may also aid in octeocyte signaling to surface cells during the repair process (Cowin, 2001, pp. 15-22). During formation, osteoblasts lay down osteoid; a collagenous matrix material that will eventually calcify into bone (Bartel, Davy, & Keaveny, 2006, p. 111) (Cowin, 2001, pp. 15-22).

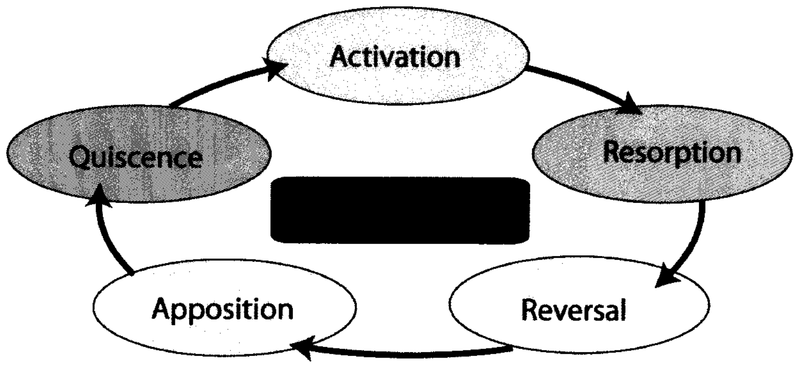

Figure 1: The phases of bone remodeling

Unlike soft biological tissues that can undergo both interstitial and appositional growth, bone, as a hard biological tissue, only experiences resorption and apposition on its free surfaces (Rouhi, Herzog, Sudak, Firoozbakhsh, & Epstein, 2004) (Rouhi, Epstein, Sudak, & Herzog, 2006). Remodeling in trabecular bone is not as organized as it is within cortical (Haversian) bone, however its interconnected plate and rod-like structure provides a greater surface area upon which remodeling occurs. Therefore, remodeling occurs at a generally increased rate for trabecular bone in comparison with that of cortical bone (Cowin, 2001, pp. 28-30).

In an attempt to create a universally accepted model, many remodeling theories have been proposed. Following, the well known hypothesis by Wolff, many researchers attempted to create early simulation models that could test their respective theories. Cowin and Hegedus developed an adaptive elasticity theory involving thermo-mechanical principles of stimulation of bone remodeling (Cowin & Hegedus, 1976). Frost's mechanostat theory later hypothesized that a constant minimum effective strain should be exceeded in order to trigger the adaptive response of bone (Frost, 2001). He also proposed that a difference exists between modeling and remodeling. Commonly accepted today, Huiskes and co-workers proposed the use of strain energy density, a scalar quantity, instead of the originally proposed effective strain as a potential stimulus to initiate the bone remodeling response (Huiskes, Ruimerman, Van Lenthe, & Janssen, 2000) (Huiskes, Weinans, Grootenboer, Dalstra, Fudala, & Slooff, 1987). Continuum theories in which the strain history plays a role in the remodeling rate is representative of the viscoelastic nature of bone, from which a principle of cellular accommodation was recently proposed by Turner (Turner, 2006) (Turner, 1998). He proposed an ever-changing threshold stimulus which is now also incorporated into theories involving stress history that claim microdamage in the form of microcracks and damage accumulation as contributors in the remodeling response. Recently some semi-mechanistic models have been proposed in an effort to include both the mechanical and biological influencing factors affecting the response of bone (Huiskes, Ruimerman, Van Lenthe, & Janssen, 2000) (Ruimerman, Hilbers, Van Rietbergen, & Huiskes, 2005) (Vahdati & Rouhi, 2007). A universally accepted bone remodeling theory does not yet exist, despite many proposed theories.

1.4 Fracture healing

The adaptive nature of bone enables it to repair itself following damage or fracture. Natural fracture healing, also known as secondary-healing, occurs through the development of callus formation and proliferation (see Figure 2) (Einhorn, 1998). Upon fracture, there is an immediate inflammatory phase, followed by a reparative phase. In this phase, the fracture gap is filled by a callus material that develops eventual cartilaginous characteristics in the fracture gap and bony characteristics close to the major fragments (Bartel, Davy, & Keaveny, 2006, p. 262) (Mow & Huiskes, 2005, p. 577). If healing progresses successfully, bone bridges the fracture gap leading to eventual remodeling and an increase in stiffness and strength.

Depending on the nature of the fracture, it may be necessary to provide a treatment method to aid in the natural healing process. In many cases, implants such as plates and screws are used to provide the necessary initial structural support to fractured long bones to ensure successful and rapid healing. This type of fracture healing is denoted as primary fracture healing, as it bypasses the natural callus formation phase (see Figure 2). Inter-compression of the bone fragments allows for direct gap bridging and remodeling that occurs at an increased rate of healing in comparison with natural healing.

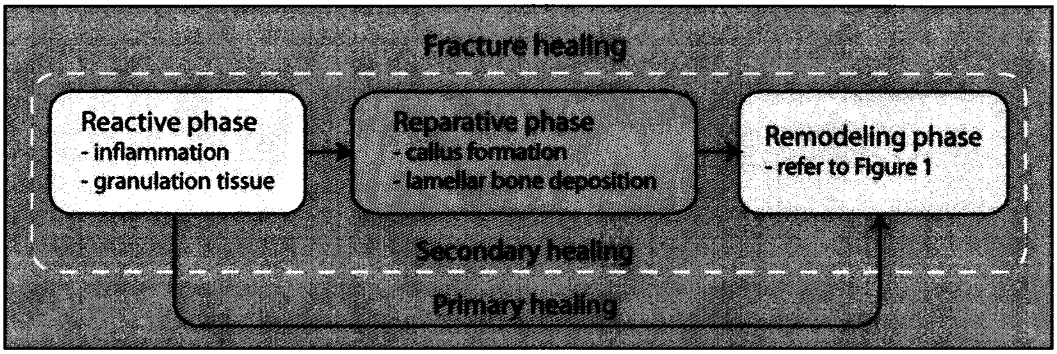

Figure 2: Primary and secondary fracture healing

Failure of both primary and secondary healing can occur as delayed or non-union. In the case of secondary healing, the callus material may not necessarily provide the required clinical stability (i.e. limited micromotion) for union. In the case of primary healing, insufficient clinical stability or stress shielding can lead to improper fracture healing. Primary healing also requires precise alignment of bone fragments, and comes with the risk of infection associated with the surgical inclusion of an implantable device. Although rapid when performed successfully, rigid fixation (which promotes primary healing) is shown to cause bone loss in the vicinity of implants, particularly in bone underlying plates. Bone loss that persists following the normal resorption of necrotic bone is a negative effect usually attributed to stress shielding, and is usually apparent via thinning of the cortices or an increase in internal porosity. According to Perren, poor vascularization, due to the compression of the plate on the bone, may also be a contributing factor in successive bone loss (Perren, 2002). Research has shown that poor blood perfusion alone leads to a decline in the rate of fracture healing (Funsten & Lee, 1945) and therefore may also contribute to decreased rates of remodeling.

Ideally, fracture fixation devices should provide the necessary rigid support to the fractured bone during the initial stages of healing, and gradually allow the bone to share the load during the latter stages of the healing process. Implants made from bioresorbable polymers may potentially eliminate the need for implant removal altogether, in the future (Gogolewski, 2000). If suitably strong material properties are developed, these polymers may also overcome drawbacks such as stress shielding, corrosion, and debris formation, which are associated with metal implant devices.

1.5 Stress shielding

As mentioned in the preceding paragraphs, a common negative effect involved with the use of implants is that of stress shielding (see Figure 3). This stress shielding effect encompasses an adverse adaptation of bone to changes in its normal level of mechanical stress due to the load-sharing associated with any type of implant. For the case of fixation plates, the combined behaviour of bone and plate is generally much stiffer and stronger than the original intact bone. This behaviour causes the bone to fall below its normal range of stress thereby resulting in an excess response of osteoclast activity (bone resorption), and results in subsequent bone loss and implant loosening (Bartel, Davy, & Keaveny, 2006, p. 278) (Brunet, Sarkar, & Uhthoff, 1986).

Through *in vivo* animal experimentation, researchers reveal thinning of bone's cortices during osteosynthesis using compression plating systems (Uhthoff & Dubuc, 1971). Periosteal resorption and localized porosity results directly under the plate in only a couple of weeks (Uhthoff & Dubuc, 1971). With the removal of plates, bone formation again occurs. A similar effect is demonstrated with the use of intramedullary nails, where an increase in the nominal nail size effectively increases the bending stiffness of the implant system, but causes a greater amount of bone resorption (Wang, Brown, Yettram, & Procter, 2000).

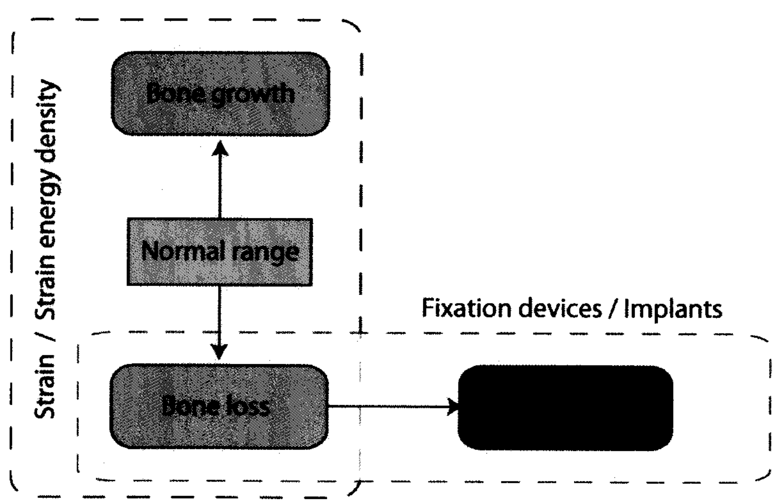

Figure 3: Stress shielding resulting from a reduction in mechanical stimulus

There has been a movement towards the use of more flexible plating techniques, as they prove to dramatically reduce the level of stress shielding resulting in bone (Wenzl, Porte, Fuchs, Faschingbauer, & Jurgens, 2004; Akeson, Woo, Coutts, Matthews, Gonsalves, & Amiel, 1975)

(Uhthoff, Bardos, & Liskova-Kiar, 1981; Woo, et al., 1984) (Uhthoff, Poitras, & Backman, 2006).This is discussed further in section 2.1.

1.6 Computational models and the use of FEA

Due to the complex nature of *in vivo* testing, as well as the high expense, ethical considerations, and elapsed-time constraints involved, developed computational methods identify prosthetic design deficiencies prior to clinical testing.

In order to incorporate a bone adaptation theory into computational models, it is necessary to include feedback from the mechanics responsible for the adaptation. Models incorporating a strain-driven bone remodeling theory assume that the adaptation process is error driven (see Figure 4) (Mullender, Huiskes, & Weinans, 1994). Generally the magnitude of response is a relative measure of the difference between localized strain and a biological attractor state (Beaupre, Orr, & Carter, 1990). Finite element models usually incorporate a range of strains, between which the remodeling rate is quiescent (Carter, 1987). Therefore, when the measured difference exceeds the upper threshold of this limit, the response is a linearly increasing rate of remodeling. The reverse is true for a difference below the lower limit. It should be noted that a universally accepted mechanical stimulus for the initiation of the bone remodeling process does not exist. Some researchers are in favor of strain as the mechanical stimulus for initiating the bone remodeling process (Cowin & Hegedus, 1976), while others are of the notion that strain energy density is a more effective initiator of bone adaptation (Huiskes, Ruimerman, Van Lenthe, & Janssen, 2000).

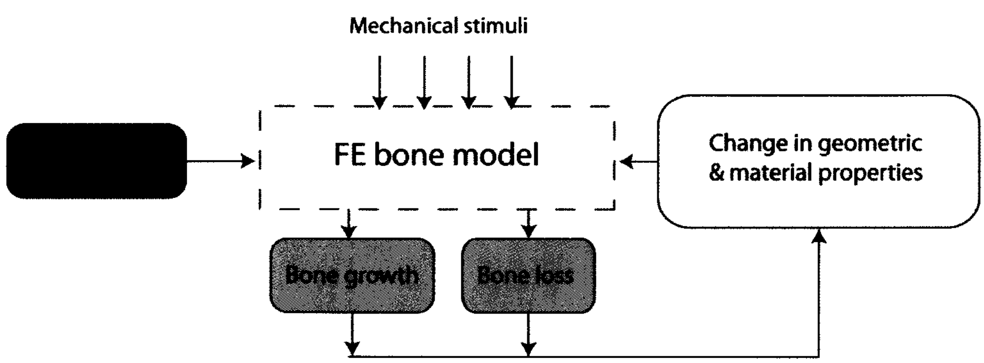

Figure 4: Simplified schematic diagram of FE models incorporating bone remodeling

As mentioned previously, when an implant is introduced, as is the case in fracture fixation or joint replacement, the normal loading condition of the bone in question is altered, subsequently causing localized adaptation and changes in the rate of remodeling. Geometry and material properties of implants play an important role in the level of change that develops upon fixation. A large difference in elastic modulus between a poorly designed implant and the bone can lead to highly altered levels of localized stresses and strains, resulting in bone loss and fixation failure (Miclau & Martin, 1997).

1.7 Thesis objective

Stress shielding associated with the use of fixation devices is a common cause of improper fracture healing. Research has shown that large differences between implant and bone flexural rigidities cause an increase in bone porosity in the vicinity of the implant (Woo, et al., 1984) (McCartney, MacDonald, & Hashmi, 2005). In the case of long bone plate-fixation, screw loosening and/or avulsion can result in a loss of clinical stability and should be avoided.

The main objective of this thesis is to shed some light on the open question of bone remodeling with respect to bone-implant interactions. Although the mechanical stimuli responsible for the initiation of the remodeling response is unknown, from Wolff's law and experimental research of others, we know that limiting stress shielding will lead to a reduction in bone loss and improper fracture healing. Therefore it is possible to correlate a mechanical stimuli distribution to a relative amount of stress shielding, i.e. a higher stimuli transferred to bone should result in less stress shielding. By comparing stimuli distributions (in our case using stress and SED as potential stimuli) we can investigate the nature of fixation plate constructs and orthopaedic screws, and determine whether particular implant design factors influence resultant levels of stress shielding.

Using finite element software, the initial focus involves an analysis of long-bone plating systems; a simple bone-plate model is used to demonstrate stress reductions in underlying bone for various modes of loading; and a parametric model indicates that stress shielding can be reduced through a reduction in plate rigidity through a change in its cross-sectional area (thickness and angle), and a change in screw position.

A subsequent bone-screw model analyzes resulting stress and strain energy density levels from various screw configurations based on parametric changes in geometry and material properties. A reduction in stress shielding is seen as a positive measure of biocompatibility between an implant and bone. Therefore, a previously defined parameter that uses stress and a newly defined parameter that uses SED indicate the relative biocompatibility of the various screw configurations. The influential factors affecting stress shielding and the role of stress or strain energy density as potential stimuli for the initiation of bone remodeling are discussed.

Chapter 2: Internal fixation plates

2.1 The progression of plating techniques

Internal fixation of long bones with plates and screws dates back over a half-century. A researcher, by the name of Danis, was the first person to design and use a rigid longitudinal compression system that led to the healing of fractures without the formation of a visible callus (Allgower, Perren, & Matter, 1970). This type of conventional rigid plating promotes primary healing through the direct compression of the plate to bone with or without a removable compressor and is now known as the AO/ASIF method (Association for the study of internal fixation) (Cheng, Tse, & Chow, 1985). These techniques rely on the axial force generated by the insertion torque of spherical screw heads to compress the plate to the bone (see Figure 5: Conventional compression plates and locking dynamic compression plates

(a)). Not all plating devices rely on this method of compression. For example, in the case of comminuted fractures, lag screws provide the necessary compression through the purchase of the distal bone fragment (Allgower, Perren, & Matter, 1970; Borgeaud, Cordey, Leyvraz, & Perren, 2000).

Although the AO/ASIF method produces rigidly stable fixation which is initially required for the union of fracture segments, disadvantages of these conventional techniques include: unpredictable changes in pressure upon removal of the compressor; the inability to adapt the screw position to an oblique fracture (screws are inserted perpendicularly); and the development of high stress transfer between the screws and plate which can induce corrosion (Allgower, Perren, & Matter, 1970).

In response to these disadvantages, a dynamic compression plate (DCP) is designed including tapered screw holes and non-locking slot-type conical holes. This allows for axial compression caused by physiological loading and compression without an extra compressor (Borgeaud, Cordey, Leyvraz, & Perren, 2000) (Allgower, Perren, & Matter, 1970). Clinical studies demonstrate primary healing in as little as 4 months with the use of DCPs (Allgower, Perren, & Matter, 1970).

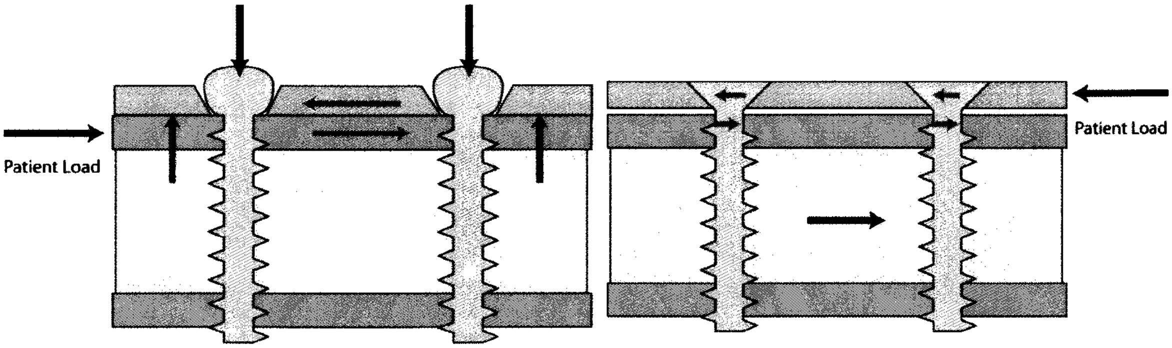

(a) Conventional plating relies on the axial force from the applied screw torque and the friction between the plate and bone to resist loading.

(b) Locked plates do not require compression between the plate and bone due to the locking nature of threads.

Figure 5: Conventional compression plates and locking dynamic compression plates

Although inherently stable, DCPs also exhibit some major disadvantages. These include: the bending required prior to surgical insertion; the damage caused to vascular tissue adjacent to the bone; and most importantly stress shielding in the underlying bone (Wagner, 2003).

Some researchers suggest that vascular insufficiency is the main cause of increased bone porosity, as there is an increase in necrotic bone and subsequent resorption (Klaue, Fengels, & Perren, 2000). Therefore, to alleviate soft tissue damage, researchers sought the use of plating devices which limit the contact area between the plate and bone. A variation of the DCP, known as the LC-DCP or locked-compression DCP systems provides clinical stability through locked tapered screw heads while limiting the plate-bone contact area (see Figure 5 (b)). Other devices which limit the contact between the plate and bone such as the Less Invasive Stabilization System (LISS) and the Point-Contactor Fixator (PC-Fix) promote stable fixation with uni-cortical screws, as opposed to the bi-cortical screws used with DCP (Borgeaud, Cordey, Leyvraz, & Perren, 2000) (Miclau & Martin, 1997) (Wenzl, Porte, Fuchs, Faschingbauer, & Jurgens, 2004). Experimental evidence suggests that these types of devices reduce both the amount of vascular tissue damage and stress shielding that develops post-fixation (Haasnoot, Munch, Matter, & Perren, 1995; Egol, Kubiak, Fulkerson, Kummer, & Koval, 2004).

Another method commonly used to reduce stress shielding is to limit the difference between bone and plate rigidities through the use of more flexible plating materials. Early implants mainly consisted of stainless steel and vitallium alloys (Claes, 1989). There is still much controversy between the use of completely rigid systems and systems with increased material flexibility (Stahl, 1993). Some researchers believe that a small amount of micro-motion at the fracture site promotes more rapid fracture healing, since a combination of primary and secondary healing occurs in this case (Perren, Evolution of the internal fixation of long bone fractures, 2002). As it is a well accepted concept, flexural rigidity is dependent both on the cross-sectional area and material properties of the plating device (Popov, 1990). In terms of materials, less rigid titanium alloy devices with increased resistance to corrosion have proven to be advantageous (Allgower, Perren, & Matter, 1970) and are slowly beginning to replace stainless steel devices that previously dominated the market. Experimental evidence reveals an increasing trend towards the general acceptance of more flexible systems, as the level of stress shielding is reduced (Woo, et al., 1984) (Woo, Simon, Akeson, Gomez, & Seguchi, 1983) (McCartney, MacDonald, & Hashmi, 2005) (Ganesh, Ramakrishna, & Ghista, 2005). Carbon-fiber reinforced polymers have also demonstrated less reduction in stress shielding in comparison to their stainless steel counterparts (Akeson, Woo, Coutts, Matthews, Gonsalves, & Amiel, 1975) (Saidpour, 2006) (Fujihara, Huang, Ramakrishna, Satknanantham, & Hamada, 2003).

As early as 1970, researchers tested the biocompatibility of titanium alloy DCP's and found that, in conjunction with spherical screw holes, they are advantageous in their resistance to corrosion, are more malleable for surgical bending, and have an elastic modulus closer to that of bone (in comparison to stainless steel) which demonstrated a reduction in stress shielding (Allgower, Perren, & Matter, 1970). In a later study, Woo and co-workers proved that decreasing the rigidity alone causes a significant decrease in stress shielding thus more flexible plating materials should be used (Woo, Simon, Akeson, & McCarty, 1977). For example, a graphite fiber reinforced methyl methacrylate resin composite plate that has a Young's modulus approximately 10 times less than that of stainless steel is found to produce significantly less porosity in underlying bone, i.e. 6.8% porosity in comparison to 14% porosity in bone for the composite and stainless steel plates, respectively (Akeson, Woo, Coutts, Matthews, Gonsalves, & Amiel, 1975). Using a less-rigid implant promotes more of the load to be shared by the bone, which causes less bone resorption, since the mechanical stimuli is not reduced as much as it would be with a stiffer implant. However, a balance must still exist between flexibility of the implant and the clinical stability of the system. If the plate does not provide the initial clinical stability, it is likely that bony bridging between fracture gaps will not occur. An ideal system is one that transforms gradually from a rigidly stable system to a more flexible one as fracture healing progresses.

The practice of using internal fixation devices to promote healing of comminuted fractures in long bones is one of continual development. Advancements in the research of internal fixation devices and techniques are the result of continuous studies by many researchers in the field (Prendergast, 1997) (Cegonino, Garcia Aznar, Doblare, Palanca, Seral, & Seral, 2004). These researchers study the bone remodeling process and effects of stress shielding in relation to fixation devices. The use of finite element analysis (FEA) is a well recognized tool for performing *in situ* research in this area and allows researchers to gain further insight into the behaviour of complex nonlinear systems which would otherwise rely on trial-and-error type methods, which are rare and based mostly on rough *in vitro* experiments. Parametric studies using FEA allows us to predict the effects of material properties and device geometry on bone and its surrounding tissue.

The success of fracture fixation is dependent on many factors, some of which include: the proper placement of the device; the quality of bone into which it is inserted; and choosing the most appropriate device, both from the structural and material properties points of view, for a particular type of fracture. From a biomedical engineering standpoint, the first two factors cannot be controlled; however analysis and the design of the fixation device can be controlled prior to implementation. Actually, a momentous shift from mechanical to biological priorities is taking place as more researchers promote the use of micro-motion over completely stable systems. It is widely accepted that using more flexible fixation devices; minimizing contact between devices and bone; long-span bridging, and using fewer screws reduces stress shielding and fixation failure (Perren, 2002) (Ganesh, Ramakrishna, & Ghista, 2005).

In recent years, the age-standardized incidence of bone fracture has increased amongst various populations with unknown cause (Kannus, et al., 2002). The increase of low-impact fractures generally associated with osteoporosis in the elderly, in particular, is a major healthcare burden, particularly due to the difficult nature of fixation in these cases (Kannus, et al., 2002). Although improvements in internal fixation devices have been made over the years, the determination of an optimal device for specific fracture types, including those in low-density bone, remains an elusive goal and an open question. The lack of an optimal method for plating long-bones is evident as an extensive search of related literature, to the best of the author's knowledge, provides minimal information pertaining to a well-accepted fixation method.

2.2 Predicting bone stresses using composite beam theory

In an effort to design implants that reduce stress shielding, some researchers, employ theories, such as composite beam theory, in an attempt to pre-determine the resulting stresses in both the plate and bone of plated-bone constructs prior to development (Cordey, Perren, & Steinemann, 2000; Ramakrishna, Sridhar, & Sivashanker, 2004). As a preliminary theoretical method, composite beam theory is used to predict the stress in bone underlying plates, as modeled in our validation and parametric FE models. In the case of our first model, the plate is rigidly affixed to the bone, so we are able to consider the model as a rough approximation of a two-material composite beam. We are able to predict the stresses in bone at the fracture site using the following equation (Bartel, Davy, & Keaveny, 2006); the derivation for which can be found in Appendix iii:

$$\sigma_b = -\frac{PE_B}{E_B A_B + E_P A_P} - \frac{E_B M t_B}{E_B I_B + E_P I_P} \tag{1}$$

Using Eqn. (1) we can calculate the stresses in bone (σ_B) at a distance (t_b) from the neutral axis of the composite structure. We are interested in the region of bone directly beneath the plate; therefore we calculate the stresses in bone between the range of $r_i \geq t_b \leq r_o$ (where r_i and r_o are the inner and outer radii of bone, respectively). This measure (t_b) is effectively the distance away from the point of application of the load (P), as shown in Fig. 1 (a). The moduli of elasticity of the bone (E_B) and plate (E_P) and their respective second moment of areas (I_B) and (I_P) are calculated using material properties of that of Plexiglas and stainless steel in order to compare with our validation FE model. For the case of our validation model, the cross-sectional area of bone (A_B) remains constant, however, that of the plate (A_P) is changed to reflect a change in plate design; i.e. a change in plate thickness and plate angle, for our parametric model. The moment (M) about the neutral axis, which is caused by the application of the applied load (P), can be calculated as follows:

$$M = P(d - \hat{y}) \tag{2}$$

From Eqn. (2) we can also calculate the moment (M) that develops in the plated-bone construct from an axial and eccentric axial load that is applied at a distance (d) away from the neutral axis of the plated bone construct (where $\hat{y}$ is the composite's neutral axis). The results using this theory are discussed in the following Chapter, 3.

Chapter 3: Three-dimensional FE plated-bone models

In this chapter two FE models of a plated-bone construct (simple representations of a fractured bone in the post-union phase of fracture healing with an applied plate) are discussed. The first model is a geometrically simplified bone-plate construct that allows us to investigate the stress distributions at the bone-plate interface along the fracture site (without a gap). For the simple model we compare stress reductions for a variety of static loading conditions, and compare results to both composite beam theory (as outlined in Section 2.2) and to experimental results of others. The second model discussed is a parametric model that relies on screw tension (instead of a fixed boundary condition) to develop the necessary plate compression to the bone. Comparing the parametric model to the simple model demonstrates the importance of implementing realistic contact conditions between the plate and bone. As well, the parametric model is used to investigate the effects of plate geometry and screw position on the level of stress that results at the fracture site.

3.1 Simple bone-plate model

The purpose of this initial study is to observe a reduction in stress with the application of a plate to a cylinder (representative of bone) under a variety of loading conditions using FEA. Researchers have noted the importance that the bone-plate interface plays in terms of the amount of stress shielding and subsequent bone loss that develops underlying plates. For this reason, we compare the level of resulting reductions in stress at the fracture site with results calculated using beam theory, for a fixed-contact model, which is representative of a compression plate that is rigidly fixed to bone. In addition, a comparison with strain gage results from studies done by Cheal and co-workers (Cheal, Hayes, White, & Perren, 1983) is used as a validation of the FE methods used.

3.1.1 Model geometry and methods

In this study, two models are developed to provide a comparison between simple representations of a fixed bone model to a normal bone model. The fixed bone model is modeled as a direct contact model wherein nodal constraints directly connect the plate surface to the bone surface. The imposition of direct contact between the plate and bone eliminates the possibility of plate-bone separation, allowing the transfer of normal and shear stresses to occur. This type of model is representative of a conventional compression plate system, where clinical stability is its primary role. This approach affords the observation of Von Mises stresses (a conservative failure theory) and allows for a comparison of these values to yield strengths of the respective materials modeled.

The plate and bone geometries are modeled using ANSYS Design Modeler. Specifically, a self-compressing 316L stainless steel plate that measures 10.3 cm long, 1.2 cm wide, and 0.38 cm thick (distributed by Synthes) is centrally located on a 29 cm long Plexiglas tube (representative of bone) having inside and outside diameters of 1.90 and 2.54 cm, respectively (see Figures 12 and 13). The material properties used in this study are as follows: Plexiglas tube: E = 3.1 GPa, and v = 0.2; and stainless steel plate: E = 196 GPa, and v = 0.3. The use of Plexiglas, results in a tendency for higher bending and lower axial rigidities, and is most comparable to the canine femur (Cheal, Hayes, White, & Perren, 1983). These material properties are suitable for low to moderate load under static conditions, such as those used in this study (Cheal, Hayes, & White III, 1985). The use of 316L stainless steel is common in applications requiring superior corrosion resistance (AK Steel Corporation, 2007), as in the case of *in vivo* implantation.

A total of 195 linear isotropic SOLID186 elements make up the mesh of the tube, and 24 of these same elements are used to discretize the plate. The SOLID186 element, available in ANSYS version 11.0, is a higher order 3-D 20 node solid element that employs quadratic displacement interpolation that is well suited to modeling irregular meshes (ANSYS, 2005), and is easiest for the mesh refinement in our model. Specified contact and target elements produce the bonded contact surface between the plate and tube.

Displacement constraints on the nodes maintain symmetry; therefore only one quarter of each model is required for analysis, thereby reducing the solution time (see Figure 6). Upon fracture, the main role of an implant is to supply structural support to the bone. An initial reduction of the load carried by the bone is beneficial in promoting the initial stages of fracture healing, be it, either primary or secondary healing (see Chapter 1.4). As fracture healing progresses, the physiological loads should ideally be transferred gradually from the implant to the bone. For this reason, we are only interested in the stress reduction in bone after initial union of the fracture has occurred. The model, thereby, represents a compressed long-bone fracture in the post-union phase of healing; and so, a fixed boundary is applied to the mid-plane in order to negate any deformation at the fracture site.

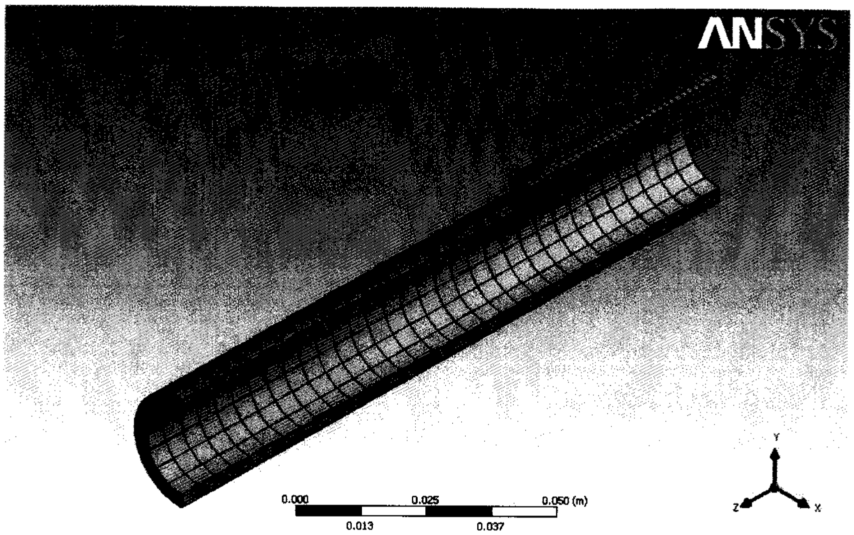

Figure 6: Mesh of ¼ model of plated bone

Three loading conditions are applied to the control and fixed-bone model, consecutively: a compressive axial load of 342 N which is applied as a distributed load to the outer face of the bone cylinder (see Figure 7); a moment of 9.34 Nm is applied to the outer face (see Figure 8); and an eccentric axial load of 342 N is applied as a point load to the mid-point between the outer and inner radii of the cortex opposing the plate (see Figure 9). The applied loads are chosen as a general set of representative loading conditions within the range of normal physiological loading of a femur (Cheal, Hayes, White, & Perren, 1983), and in the model are applied on the surface opposing the fracture site. Although loading conditions in *in-vivo* bone are quite complex, these simplified conditions allow us to compare our results to those of a previous study wherein a physical model using the same geometry is instrumented with strain gauges. We are able to estimate whether failure of either the plate or bone occurs by comparison to known yield stress and strain material properties.

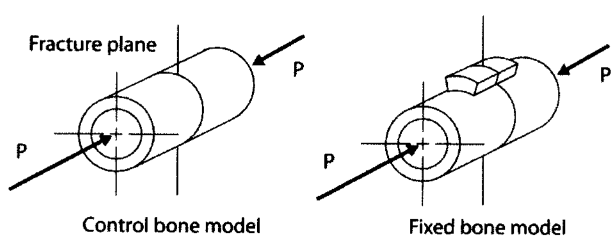

Figure 7: Compressive axial load

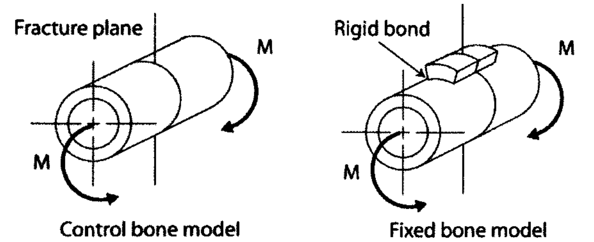

Figure 8: Pure bending moment

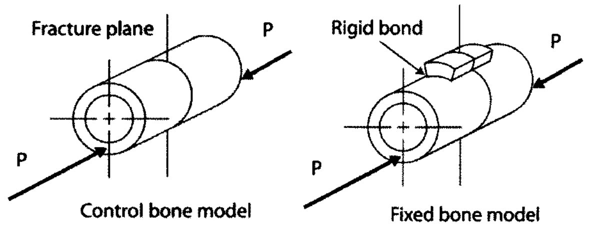

Figure 9: Eccentric axial load

Von Mises effective stress and total deformation results are compared between the control and the fixed-bone model in order to demonstrate the effects of adding a plate to a bone. Particular attention is placed on the plate-bone interface as the occurrence of stress shielding in underlying bone will cause a decrease in bone remodeling and may result in increased porosity (Claes, 1989). Results from the fixed-bone model are also compared to a FE model and to strain gage data from a physical model analyzed by Cheal and co-workers (Cheal, Hayes, White, & Perren, 1983) (Cheal, Hayes, & White III, 1985). As well, theoretical stresses are derived from composite beam theory, as outlined in Appendix iii, wherein the plate is assumed to be rigidly fixed to the bone.

The use of Von Mises failure criterion provides a conservative failure theory that can be used to predict yielding of materials under tri-axial loading. It is applicable for the analysis of plastic deformation for ductile materials, such as metals, and is useful in providing an effective scalar stress value based on the principal stress differences of a material (Benham, Crawford, & Armstrong, 1996).

3.1.2 Simulation results

In order to validate our FE methods, we outline the theoretically predicted bone stresses calculated using composite beam theory and then compare them to our FE model results.

3.1.2.i Theoretically predicted bone stresses

Using Eqn. (1), we calculate the stress in the top cortice of bone, i.e. from just below the plate to the bottom of the cortice. Due to the high flexural rigidity of the modeled plate (plate: EI=2.476 x10^{-6} Nm^2) in comparison to that of modeled bone (bone: EI=1.761 x10^{-7} Nm^2), the neutral axis of our bone-plate system lies in the region of the plate. Since the axial load is applied at the centroid of the bone, below the composites neutral axis, a bending moment is created and the bone below the plate is compressed. From our theoretical calculations, for an axially applied load, a linear decrease in bone stress is predicted, from directly beneath the plate to the outer edge of the top cortice (see Figure 10). A similar behaviour is demonstrated by the application of an eccentric load, wherein the compressive stresses in bone are higher (due to a larger induced bending moment). The bending moments induced by the axial and eccentric axially applied loads, at the centroid of the bone, are 4.73 Nm, and 5.28 Nm, respectively. In the case of pure bending, a 9.34 Nm bending moment is applied, and in the absence of any axial compression there is less total bone stress.

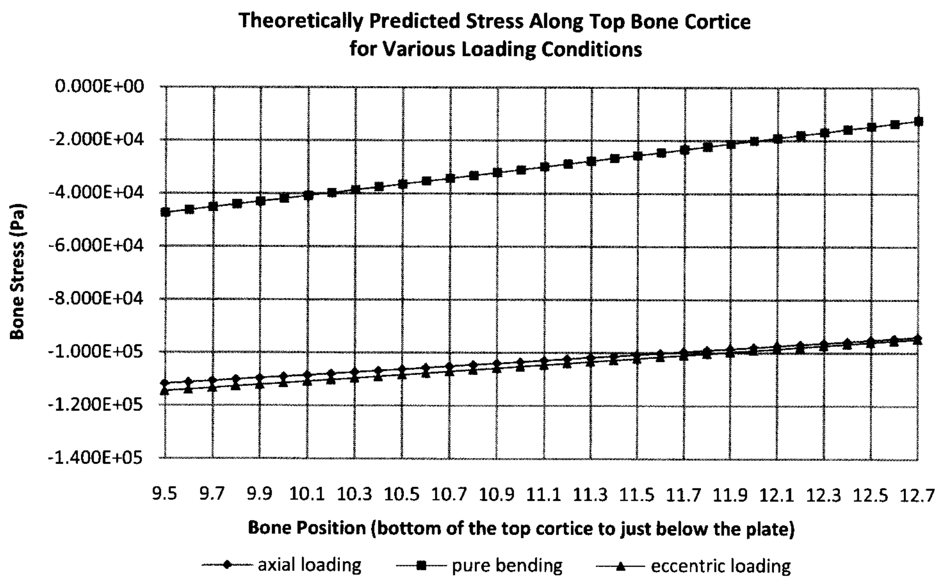

Figure 10: Theoretical prediction of stress in bone below the plate

3.1.2.ii Comparison of predicted bone stresses with FE model results

In Figure 11 we compare the effective stresses resulting from our FE model (along the top cortice of the bone) to our predicted stresses. The results from the FE model produce much larger effective stresses at the bottom of the cortice in comparison to the top, which is expected, however, the stresses are significantly higher than those calculated using composite beam theory.

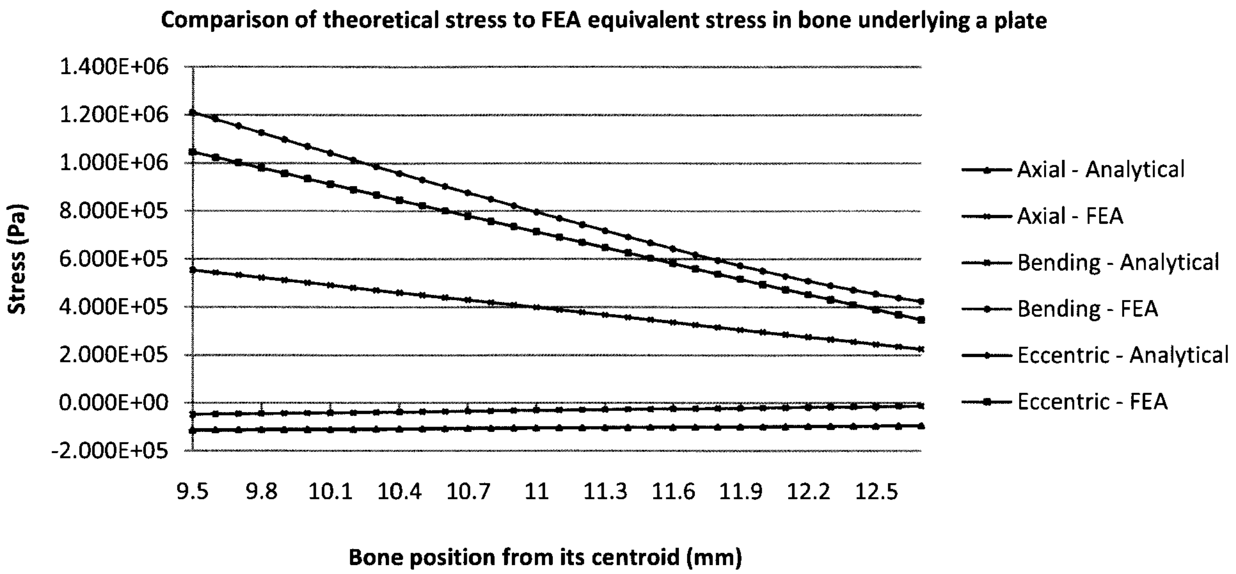

Figure 11: Axial loading of a simple direct contact bone-plate model

With the application of both a compressive axial load and an eccentric axial load to the plated model, a bending moment results (see Figures 15 and 19). This is in agreement with our theoretical prediction wherein a bending moment exists due to the application of compressive axial load at a distance away from the composite's neutral axis. As is intuitively expected, maximum stress levels occur in the proximity of the fracture site. Figure 12 demonstrates a better correlation between theoretical predictions and the stress values from our FE model when comparing with longitudinal principal stresses.

The difference in predicted versus FE model results is due to the simplifying nature of the composite beam theory, which does not account for the sliding contact surfaces between the plate and bone. The theory is only accurate for predicting the axial stress component in the cross section at the center of the plate where little sliding occurs (the smallest difference between predicted and FE results are just below the plate, i.e. at 12.7 mm in Figure 12). The limitations of using composite beam theory to accurately predict the stresses in bone-plate constructs is noted by other researchers (Ganesh, Ramakrishna, & Ghista, 2005) (Cheal, Hayes, White, & Perren, 1983) and demonstrates the usefulness of computational methods for these analyses.

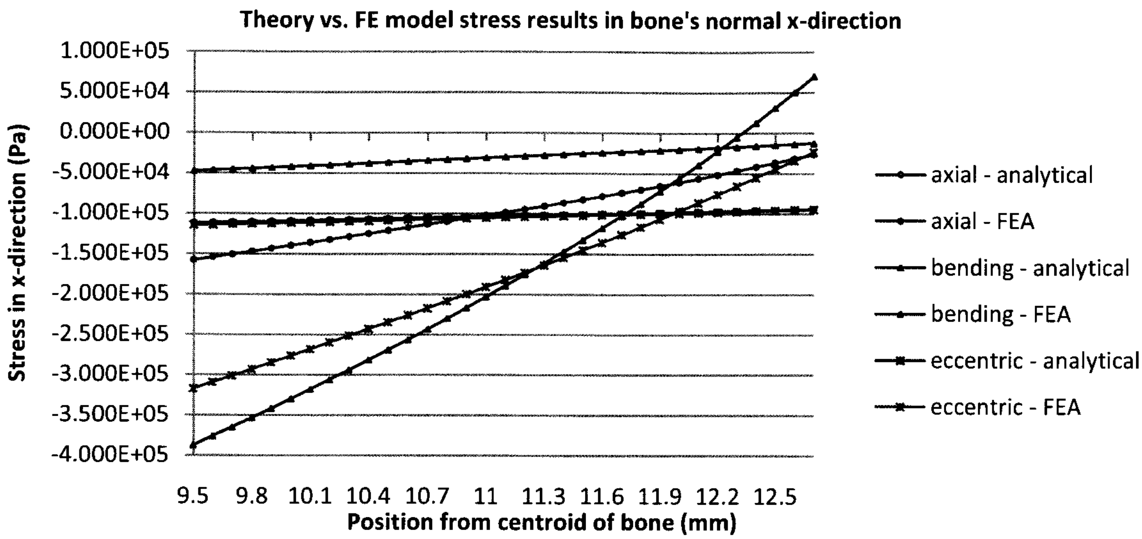

Figure 12: Comparison of theoretical to FE model longitudinal stress values

3.1.2.iii Comparing the plated model to the control

The resulting effective stresses from the inner radius to the outer radius of the top cortice are compared for both the control and plated-bone model (see Figure 13). For all loading scenarios there is a reduction in effective stress along the region analyzed, most notably just below the plate; i.e. at 12.7 mm in Figure 13.

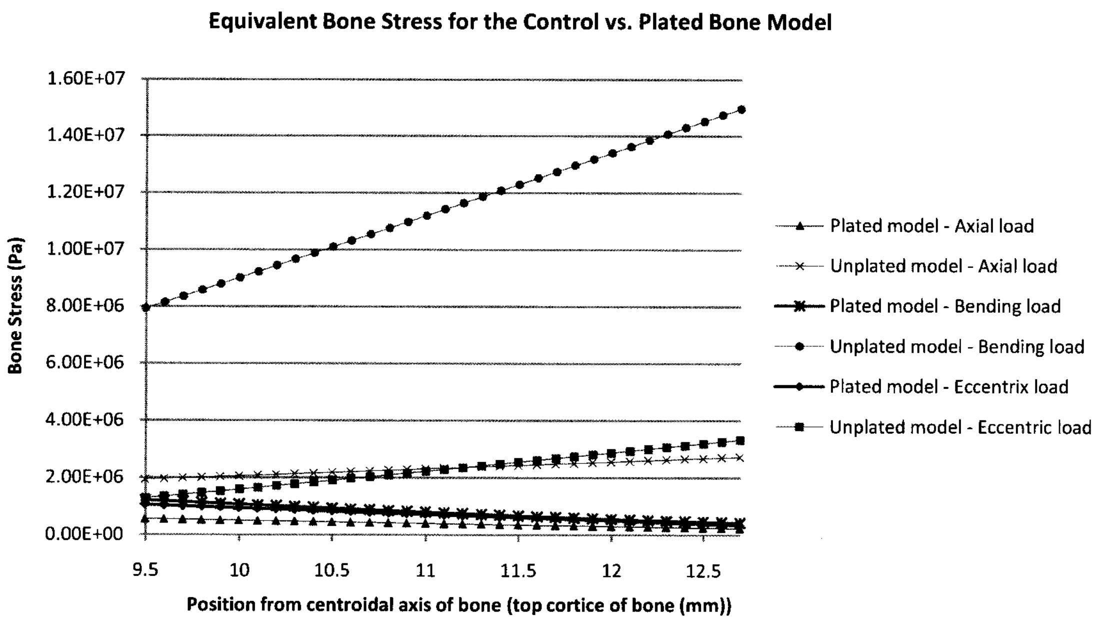

Figure 13: Comparison of bone stresses for the control and the fixed bone model

Figure 13 demonstrates the differences between longitudinal stresses for the control and plated models. Reductions in stress range between 71-92%, 85-95%, and 18-90% for the axial, pure bending, and applied eccentric axial loads. These results correspond well with previous experimental results performed by Cheal et al. (Cheal, Hayes, White, & Perren, 1983) (Cheal, Hayes, & White III, 1985), and demonstrate the effectiveness of plate application in reducing bone strain, and the subsequent reduction in longitudinal bone stresses.

Maximum and minimum equivalent stresses and the mean deformations in bone, resulting from the application of different modes of loading (compressive axial, bending, and eccentrically axial loading), are compared between the control and fixed-bone models (see Table 1) and are discussed further in the subsequent sections.

		Load		
		Compressive Axial	Bending moment	Eccentric Axial
Control model	Maximum Equivalent Stress (MPa)	3.21E+00	1.89E+01	2.58E+01
	Minimum Equivalent Stress (MPa)	2.33E+00	2.87E-03	1.75E-01
	Mean Deformation (mm)	1.44E-01	4.58E+00	5.15E+00
Fixed-bone model	Maximum Equivalent Stress (MPa)	3.61E+01	1.69E+02	1.31E+02
	Minimum Equivalent Stress (MPa)	7.72E-02	9.52E-03	8.91E-02
	Mean Deformation (mm)	3.62E-01	3.30E+00	4.13E+00

Table 1: Resulting stresses and strains resulting from loads applied to the control and fixed-bone models

Compressive axial load

When a compressive axial load is applied to the centroid of the bone cylinder, a symmetric distribution of equivalent stress develops (Figure 14). As expected, the maximum stress occurs on the outer surfaces of the cylinder, whereas the minimum occurs on the inner edges of the cylinder. The bone is effectively shortened along its longitudinal axis and the majority of deformation occurs in the vicinity of the applied load. Upon application of a plate, bending is induced in the composite model even though the load applied on the neutral axis only produces compression in the intact bone (Figure 15). The maximum stresses occur in the plate in proximity to the fracture site, where bone stresses are at a minimum. This result is indicative of stress shielding, as the stress in bone underlying the plate is less than that in the control bone model.

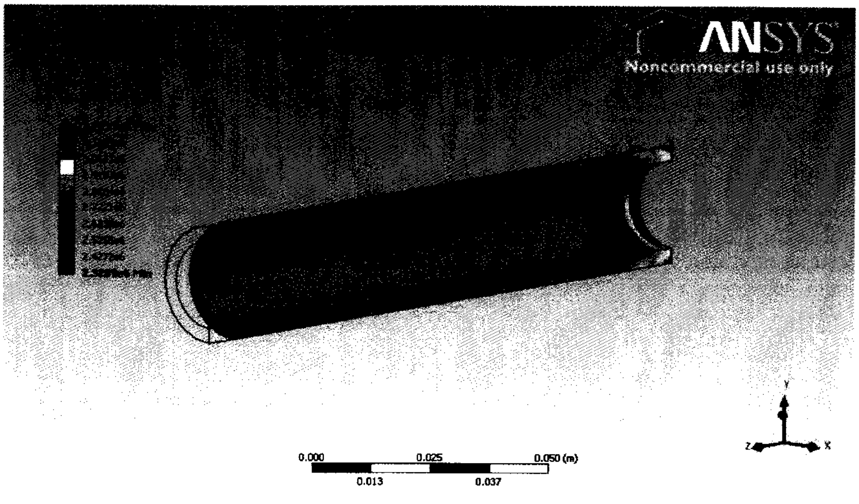

Figure 14: Equivalent stress resulting from an axial compressive load: control bone model

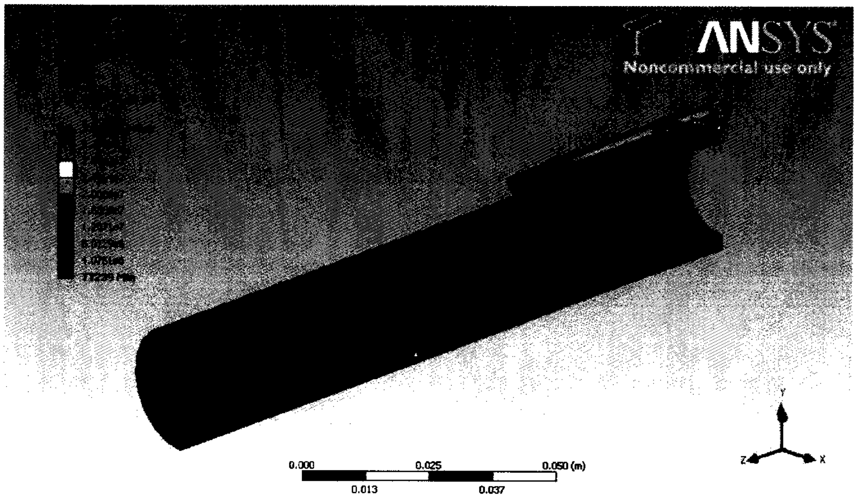

Figure 15: Equivalent stress resulting from an axial compressive load: fixed-bone model

Bending load

Application of a bending load, to the free end of the bone, results in a longitudinally symmetric distribution of equivalent stress in the control model (Figure 16). As seen with the application of a compressive axial load, the highest stresses and the majority of deformation are visible at the region of the bending load, which is to be expected. The bone cylinder deforms in the direction of the applied moment, creating tensile stresses on the upper surface of the cylinder and compressive stresses on the underside. In the case of an applied plate, maximum equivalent stresses develop at the outer edge of the plate end on the cylinder surface (opposite to the fracture site), and again the minimum occurs on the cylinder. There is an increased region of stress on the top edge of the plate as it shares the majority of the load. Similar to the results by Cheal and co-workers, who state that longitudinal stress reductions of 25% or less result in the underlying bone with plate application due to an applied bending moment (Cheal, Hayes, White, & Perren, 1983), our measured results also show a decrease in effective stress in bone under the plate. However, a bending moment tends to increase the equivalent stresses at the outer edge of the plate-bone contact region (Figure 17). This is due to the tendency for the plate to separate from the bone. These high stresses develop in resistance to the fixed contact modeled between the surfaces of the plate and bone.

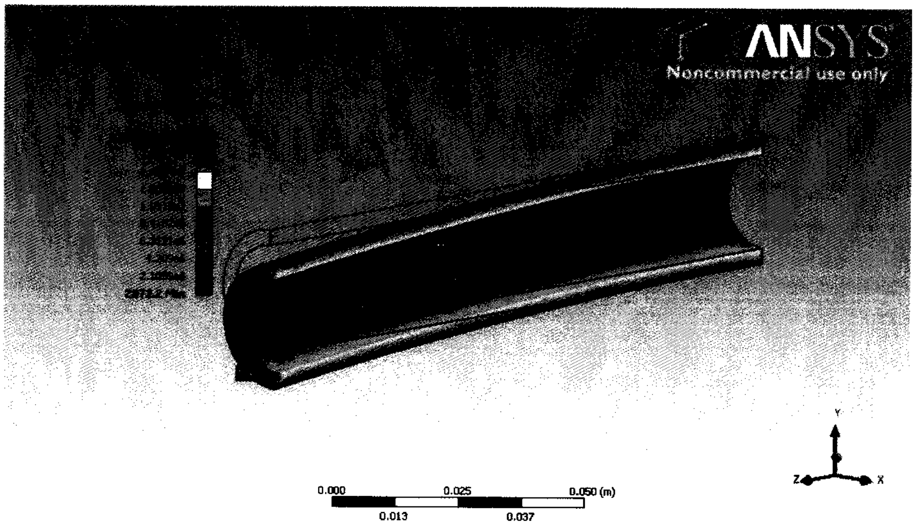

Figure 16: Equivalent stress resulting from a pure bending moment: control bone model

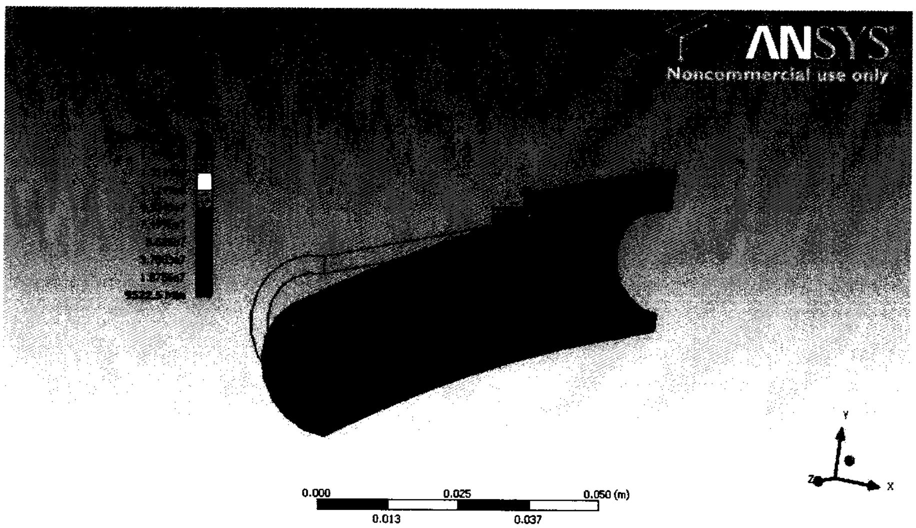

Figure 17: Equivalent stress resulting from a pure bending moment: fixed-bone model

Eccentric axial load

For the control bone, the bone stresses and deformations resulting from an applied eccentric axial load are similar to those demonstrated by an applied bending moment (Figure 18); however the distribution is concentrated closer to the applied load. Higher equivalent stresses and the majority of the bone's deformation occur in the region of loading and along the bottom of the cylinder, which is under compression. For the fixed bone model, equivalent stress increases in the plate and decreases in bone at the fracture site, when an eccentric axially compressive load is applied (Figure 19), however, the increase is not as predominant as for applied bending (Figure 17). With the application of a plate, the highest stresses in the plate occur, again, in proximity to the fracture site and at the distal region where the plate tends to pull away from the bone. The effective stresses in bone are effectively decreased by this uneven load sharing that exists between the plate and bone. Since mechanical stimuli are required to initiate bone remodeling, i.e. a normal rate of bone turnover, efforts should be made to design implants that transfer more of the load to underlying bone.

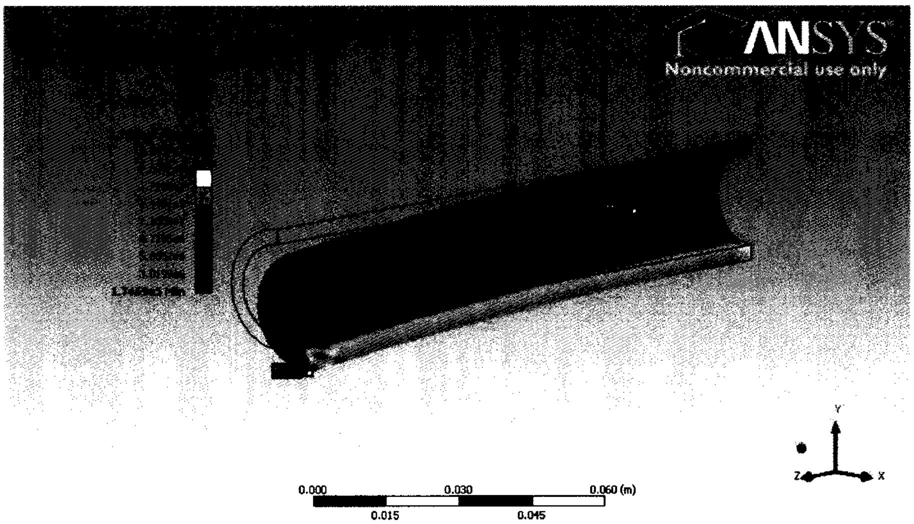

Figure 18: Equivalent stress resulting from an eccentric axial load: control bone model

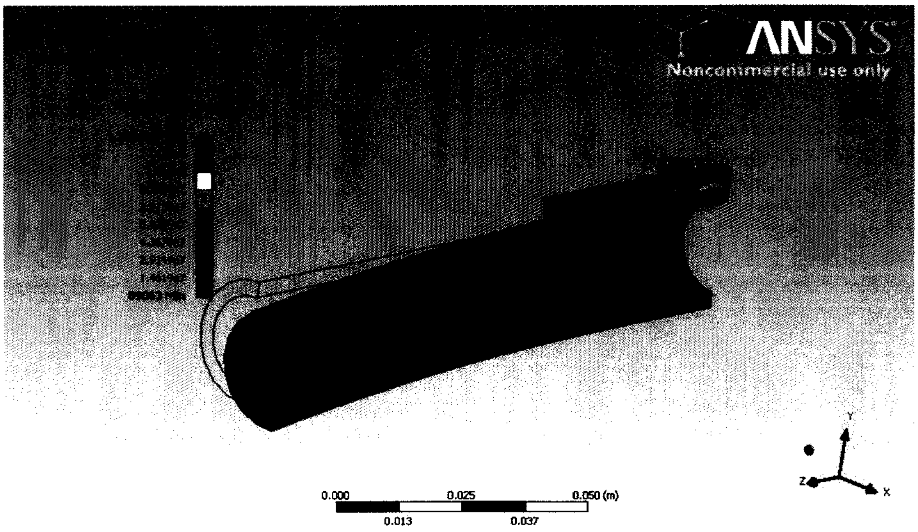

Figure 19: Equivalent stress resulting from an eccentric axial load: fixed-bone model

Bone-plate fixation is shown to result in an uneven load distribution between the plate and bone for all of the modes of loading tested. The maximum stresses that are outlined in Table 1 for the fixed-bone model are all located within the plate, whereas the minimum stresses are located in the bone. The values outlined for the control model, on the other hand, are of course located within bone. From Table 1, we can also see that the maximum stresses increase for all cases employing the fixed-bone model, as the plate undergoes high stresses in resistance to the applied loads.

Although, the plate carries the majority of the load, the maximum stress values do not cause initial yielding of the plate. The range of equivalent stresses, from 36.1 MPa to 169 MPa, that develop in the plate under the three loading conditions fall well below the ultimate tensile strength of 316L stainless steel of 558 MPa (AK Steel Corporation, 2007). The yield stress of Plexiglas is 11,000 psi, which is approximately 76 MPa (Altuglas International, 2006). The range of maximum stresses that develop in the Plexiglas cylinder for the control bone model is between 3.21 MPa and 2.58 MPa, which is significantly lower than the yield stress of the material. Although the use of Plexiglas, also known as poly methyl methacrylate (PMMA), is a rough estimation of bone's material properties, however, it is a commonly used material in arthroplasty and is used as implant surface coatings (Freeman, Bradley, & Revell, 1982).

Moreover, using the ANSYS workbench probe tool, we find that all three loading conditions result in a decrease in longitudinal stresses directly below the plate. This is an indication of stress shielding in underlying bone. From Table 1, we can also calculate the percentage reduction of bone stress at the bone-plate interface at the fracture site. The largest stresses in bone due to bending should be immediately below the plate (Taylor, Tanner, Freeman, & Yettram, 1996). The maximum stresses reported in the table for the control bone model are all approximately located at this site (except for the case of the eccentric axial load, where the highest stresses are at the site of loading), whereas the minimum stresses reported in the table for the fixed bone model correspond to this same location in bone. Therefore, we calculate the percent reduction in bone stresses at the fracture site (just below the plate) to be 97.6%, 99.95%, and 99.22%, for compressive axial, bending, and eccentric axial loading, respectively.

The application of an axially applied load along the centroidal axis of the bone results in a longitudinal deformation in both the control and fixed-bone models. A comparison of the total deformation between the two models demonstrates that the application of a plate reduces the longitudinal deformation of the bone, however, since the applied load is not applied at the centroid of the composite a bending moment is induced (as is also shown using composite beam theory, in Appendix iii) which causes strain in the other two-axes, and results in a higher mean deformation (see Table 1). In comparison to the control bone model, the application of either a bending moment or an eccentric axial load results in a strain reduction with an affixed plate. Knowing that bone is sensitive to the mechanical stimulus, the strain level will, most likely, dictate the rate of bone remodeling on the bone-implant interface (Rouhi, 2006) (Rouhi, Epstein, Sudak, & Herzog, 2007). For this reason, attempts should be made to increase the level of strain in the underlying bone to decrease the stress shielding effect, and subsequently, increase the bone remodeling rate and its apparent density.

A comparison of Von Mises stresses, resulting from FEA, to results calculated using composite beam theory produces a large discrepancy. Based on the geometry and material properties of the model, the stress in bone at the bone-screw interface is calculated using composite beam theory for the combined behaviour of bone and plate and is 116,822 Pa. The stress in bone at the fracture site for the axial compressive loading condition of the fixed-bone model is much less, at only 77,200 Pa. This is due to the bonded contact region between the plate and bone. Composite beam theory is only accurate for predicting the axial stress component in the cross-section at the center of the plate for externally applied axial and bending loads. The determination of static stress fields due to plate and screw pre-tension requires more complex models such as the beam on elastic foundation theory briefly outlined in the previous chapter (Cheal, Hayes, & White III, 1985). The maximum effective stress values obtained in this study could not directly be compared to results by Cheal and co-workers, as only their normal stress values are shown. The stress distributions, however, clearly demonstrate the same type of transition from tensile to compressive loading on bone upon application of the plate and under a compressive axial load (Cheal, Hayes, White, & Perren, 1983).

3.1.3 Conclusions

The most basic conclusion that can be derived from the validation model is the well known fact that the application of a plate to a bone results in a reduction in stress in the underlying bone, which is an indication of stress shielding. This behaviour is demonstrated regardless of the modes of loading, i.e. for a uniform compressive axial load, a pure bending moment, and a highly eccentric axial load. Although total deformation of the fixed-bone constructs are higher than for the control model, it is due to the deformation of the plate which carries almost the entirety of the load. If the stiffness of the plate is increased, the deformation of the underlying bone will be limited.

When compared to the control bone model, the composite plated-bone model experiences (1) An upward shift of the neutral axis towards the plate due to the plate application; (2) A change from a constant stress state to a combination of axial and bending stress (for uniform axial loading); (3) A minimized combination of loading for an off-center axial load, in comparison to pure bending; (4) An increase in stress at the plate/tube interface for a highly eccentric axial load; (5) A reduction of the longitudinal stresses (between 95% and 99%), directly beneath the plate, at the fracture site; (6) A tendency for plate separation with applied bending and eccentric axial loading; and (7) An increase in tensile stresses in the region beneath the outer end of the plate due to the fixed contact conditions used in the model.

The restriction of the bonded contact elements used in this study causes a tendency to develop stresses in resistance to sliding motion between the plate and bone. This indicates that the region of the outermost screw will be the location of highest stress in future models, as it will be the only resistance to plate-tube separation.

Resultant stress distributions of this study are in agreement with the results found by Cheal and co-workers whom also demonstrate very high longitudinal stress reductions in bone (between 80% to 95%) (Cheal, Hayes, & White III, 1985). The results did, however, vary from those of the composite beam theory, demonstrating the importance of accounting for relative motion between the plate and the tube.

3.2 Parametric model

Many researchers claim that a reduction in the stiffness of an implant will reduce the effects of stress shielding in plated long bones. Since the rigidity of an implant can be described by its bending stiffness, i.e. the product of its modulus of elasticity (E) and its area moment of inertia (I), a reduction in implant stiffness can be made by a modification of E, I, or both (Akeson, Woo, Coutts, Matthews, Gonsalves, & Amiel, 1975). Most of the literature surveyed involves a reduction in implant stiffness through a change in material properties. For example, a reduction in the modulus of elasticity through the use of titanium alloy implants instead of stainless steel (Foux, Yeadon, & Uhthoff, 1997) (Uhthoff, Bardos, & Liskova-Kiar, 1981), and new bioresorbable materials (Isaksson & Lerner, Mathematical modeling of stress shielding with bioresorbable materials for internal fracture fixation, 2003) (Hofer, Wildburger, & Szyszkowitz, 2001) (Goldhahn, Seebeck, Frenz, Antoniadis, & Schneider, 2005). In order to shed some light on the role of implant geometry, in relation to its influence on stress shielding, a 3D parametric finite element model is created.

3.2.1 Model geometry and methods

In actuality, fixation plates are not rigidly bonded to bone, as in the simple bone-plate model; rather, they are compressed to the tensile side (or convex side of the diaphysis) (Stoffel, Klaue, & Perren, Functional load of plates in fracture fixation in vivo and its correlate in bone healing, 2000) of one cortical layer by means of screw tensile forces. In an attempt to more accurately predict the stresses that develop in bone due to plate-fixation (in comparison to the simple bone-plate model), this model incorporates a stainless steel plate (E=200 GPa and ν=0.3) and is reliant upon 4 titanium screws (Ti-6Al-4V, E=105 GPa, and ν=0.3) for compression. The plate geometry consists of an inner radius of 7.35 mm, an outer radius that changes as the thickness is increased (one of the parameters), and a constant plate length of 50 mm. The screw is modeled as a simplified version of the standard ASIF 3.5 mm diameter cortical screw with a core diameter of 2.5 mm. The cylinder that is representative of cortical bone has an inner radius of 3.7 mm and an outer radius of 7.35 mm (Wheeless III, Nunley II, & Urbaniak, 2009), with material properties of E=14.5 GPa and ν=0.3 that are within the normal range for cortical bone (Ferguson, Wyss, & Pichora, 1996) (Lawrence, 2000).

In order to generate compression between the plate and bone a 50 N tensile load is applied to each screw and a stress-free (sliding contact) condition is employed between the plate and bone. In reality, this compression will cause friction between the plate and bone (Borgeaud, Cordey, Leyvraz,

& Perren, 2000), but leads to difficulties in analysis. Nunamaker and Perren tested an entire range of screws manufactured by Synthes and found that the maximum axial compression of cortical screws in bovine bone for a 3.5 mm screw is within a range of 49-789 N/m (Nunamaker & Perren, 1976). Although on the lower end of this range, a magnitude of 50 N was chosen for the tensile load on the screws in this model. The single screw thread modeled acts as a geometric anchor and a fixed contact condition is employed between the bottom face of the screw and the neighbouring bone.

The geometry (see Figure 20) is representative of a transverse radius fracture in the post-union phase of fracture healing. In order to simulate this scenario, a fixed boundary condition is implemented at the fracture site (the mid-point of the model). A reduction in computational time is established through the use of symmetry and appropriate boundary conditions; therefore, only a quarter-model is required for the analysis (see Figure 20 (b)). Contact and target elements are used to generate a bonded connection between the screw head and plate and between the screw and bottom cortice of bone in order to simulate a clinically stable screw insertion or locking compression plate (Wagner, 2003).

The effective stress analyses result from varied parameters that include a change in the cross-sectional area of the plate via a change in plate thickness from 3.0 to 4.5 mm analyzed in 1mm increments, and a change in the angular plate contact area from 60° to 90° analyzed in 1° increments. Although a change in plate length would definitely effect the overall stiffness (i.e. a larger length would result in a lowered stiffness) of the construct, it is not included within the scope of this study. In order to investigate the effect of screw placement, an increase in the distance of the distal screw between 15 mm to 30 mm from the fracture site is implemented. The proximal screw is kept at a constant distance of 15 mm from the fracture site for all parametric configurations.

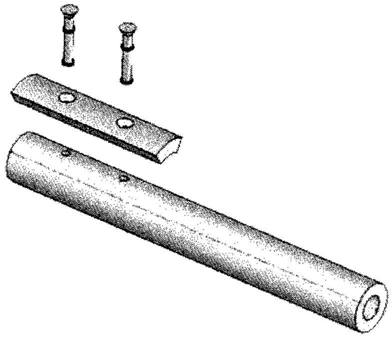

(a) Exploded view of ½ model

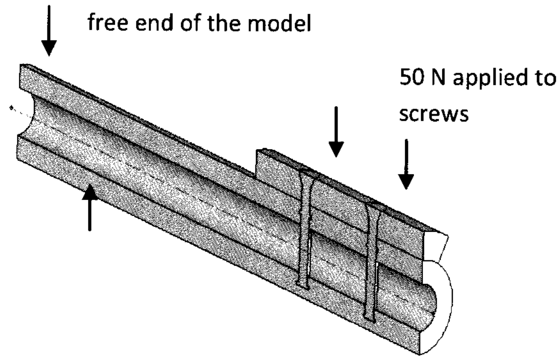

(b) Longitudinal cross-sectional view

Figure 20: 3D parametric bone-plate model

In this study, a 4-point bending moment of 125 Nm is applied to the free end of the model, which is well below the reported failure loads in Myer's study of Colles' fractures (Myers, Hecker, Rooks, Hipp, & Hayes, 1993). The load is applied via point loads aligned with local co-ordinate systems in order to simulate a similar loading scenario to *in vitro* experimentation by (Martens, Van Audekercke, De Meester, & Mulier, 1986). Due to its orthotropic-like behaviour, bone is stronger in a preferred direction of loading, i.e. along its longitudinal axis for long bones. Since it is truly an anisotropic material, the strength of bone is also reliant upon the mode of loading. For example, bone is much stronger in compression than in tension (Bartel, Davy, & Keaveny, 2006, p. 83) (Martens, Van Audekercke, De Meester, & Mulier, 1986). This explains why transverse fractures are often the result of torsion and bending in the case of long bones (Wade & Richardson, 2001). The radial cross-sectional area is highly correlated to the failure load of the forearm (mean failure force of 1780 $\mp$ 650 N in the distal radius) (Myers, Hecker, Rooks, Hipp, & Hayes, 1993)

A patch conforming mesher generates an all-tetrahedral mesh of Solid187 linear isotropic solid elements, a total of 6637 elements for the first configuration (see Figure 21). The region of interest for our equivalent stress comparisons is at the fracture end of the model, therefore an automatic mesh refinement is used along with mapped meshing at the fracture end of the model (see Figure 22). Convergence testing is performed using the equivalent stress tool. Two curve/proximity refinements are necessary to produce convergent results. The number of nodes and elements are increased from 27910 and 8997 to 107790 and 70402, respectively, resulting in a convergent effective stress value (set to 25% change). Finer mesh requirements were deemed unnecessary as the solution time and memory requirements are quite high.

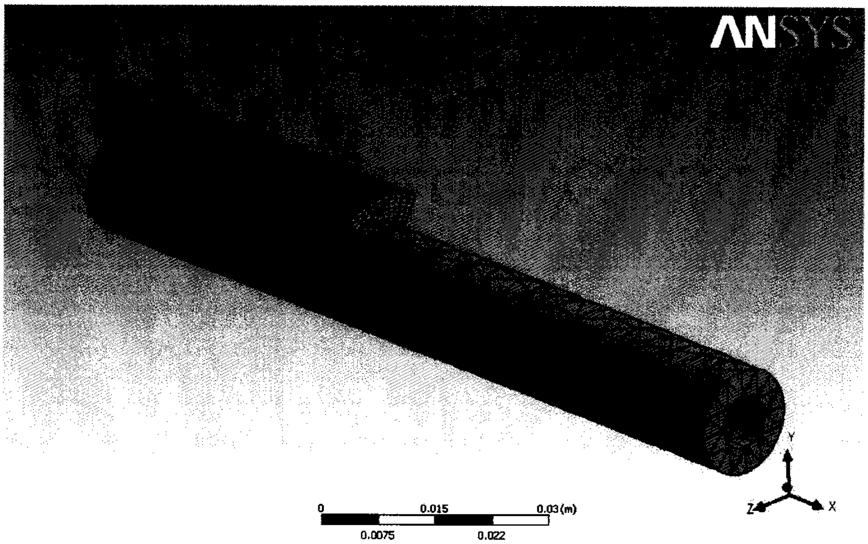

Figure 21: Original mesh of the parametric model

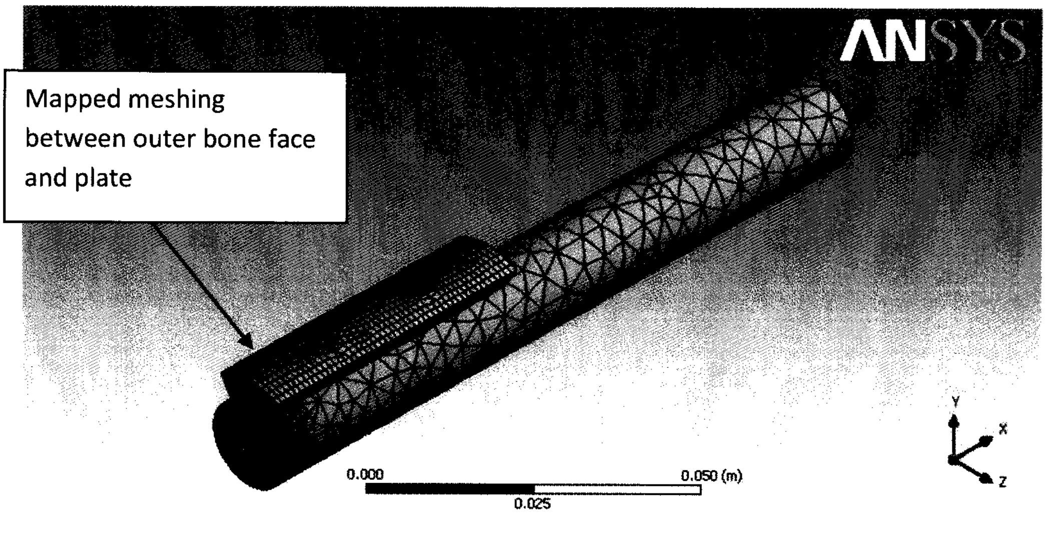

Figure 22: Mesh refinement at the fixed end (representative of the fracture site)

Von Mises equivalent stresses in bone (at the fracture site) are recorded for each of the parametric configurations analyzed under the same loading and boundary conditions. A reduction in the level of stress in bone at the fracture site will indicate the presence of stress shielding, which will affect the rate of bone remodeling and subsequently initiate bone resorption. Comparison of the stresses that develop from the varied parameters will donate valuable insight into their influence on stress shielding.

3.2.2 Simulation results

The parametric study incorporates simplified screws into the model and also allows for sliding to occur at the bone-plate interface. Our theoretical predictions of resultant bone stresses (immediately underlying the plate) are compared to our FE model results below, in order to demonstrate the limitations of using the composite beam theory for predicting stresses in bone-plate constructs. With the addition of a plate, as found by other researchers, the tendency for stress shielding can lead to improper or delayed fracture healing (Uhthoff & Jaworski, 1978; Badke, Hontzsch, Kaps, & Weise, 2005; Borgeaud, Cordey, Leyvraz, & Perren, 2000).

Results of the 3D parametric model, of a plated bone with screws under a pure bending loading condition, is demonstrated in Figure 23. A cross-sectional view of the resulting equivalent stress in the plated bone model is shown. The applied bending moment results in high regions of stress located at the fixed or fracture end, and at the plate-bone contact region most distal from that same end. The stress concentration at the fracture site develops in resistance to the bending load; however, the stress concentration at the outer plate end is due to the plate separation. Stresses between the two screws at the top of the plate are increased by the bending of the plate. This is expected, as the screws resist the separation of the plate from the bone as the load is applied. Upon fixation, the plated-bone composites' neutral axis shifts upwards towards the plate, and the top cortice of the bone experiences tensile stresses while the bottom experiences compressive stresses. The opposite would be true if the direction of the bending moment is reversed.

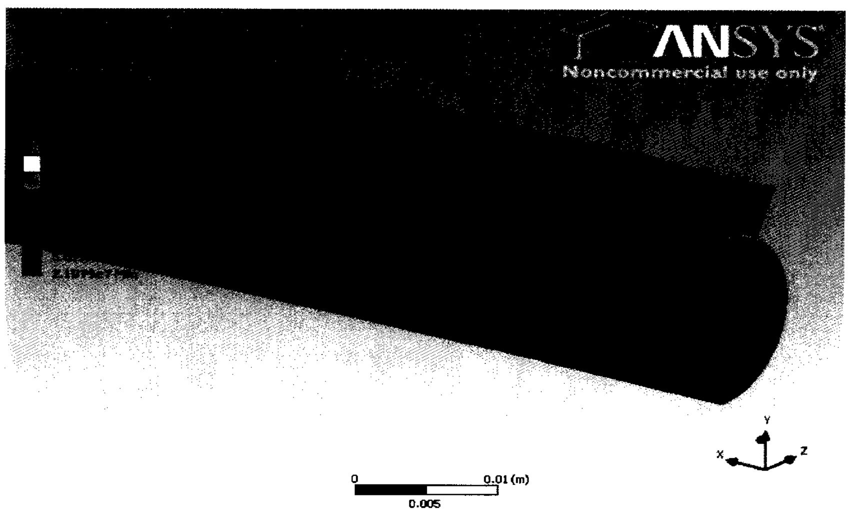

Figure 23: Equivalent stress resulting from an applied bending moment on the 3D model

Results indicate that the distal screw is consistently a region of high concentrated stress. Therefore, particular attention should be placed on ensuring that the pullout strength of the screw is higher than the stresses created under bending loading in order to avoid screw avulsion, and failure of fixation. This result is consistent with the indication of a higher tendency for plate-bone separation at the distal end of the plate (opposite the fracture site/fixed end) seen in the fixed plate validation model and Figure 24.

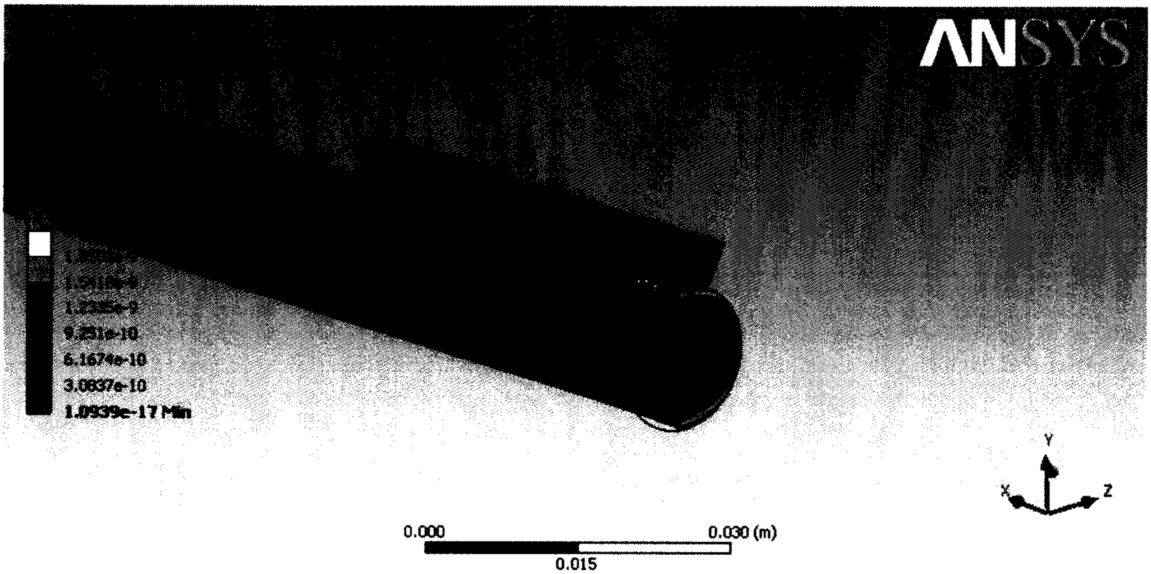

Figure 24: Equivalent strain resulting from an applied bending moment to the 3D model

Upon application of an applied bending moment to the 3D parametric model, certain results are identifiable, as demonstrated by the equivalent elastic strain results in Figure 24. The areas where deformation is most noted are at the fracture site where deformation of bone due to tensile strain directly underneath the plate and where compressive strain occurs at the cortice distally located from the plate. The greatest region of bone deformation, however, occurs at the bone-plate interface most distal from the fracture site. This is the expected result as for this particular model the contact region between the plate and bone are assumed to be rigidly bonded to one another. This is indicative of the tendency for bone-plate separation to occur, as the much more flexible bone undergoes a higher level of deformation by the bending load in comparison to the stiff plate. This result is consistent with previous studies (Ganesh, Ramakrishna, & Ghista, 2005) and indicates the importance of reducing plate stiffness over time during fracture healing.

3.2.2.i The effect of plate thickness on bone stress

Using the geometry and material properties modeled in our parametric study in Eqn. (1), it is predicted that at the smallest plate thickness, i.e. 3.0 mm, the stress in bone just below the plate is tensile (see Figure 25). While maintaining a plate angle of 60˚, as the thickness of the plate increases, the neutral axis of the bone-plate system moves further upward towards the plate causing a decrease in compressive stresses in bone below the plate until a plate thickness of 3.7 mm is used, wherein bone stress then becomes compressive. This compressive stress increases as the thickness of the plate increases from 3.7 to 4.5 mm.

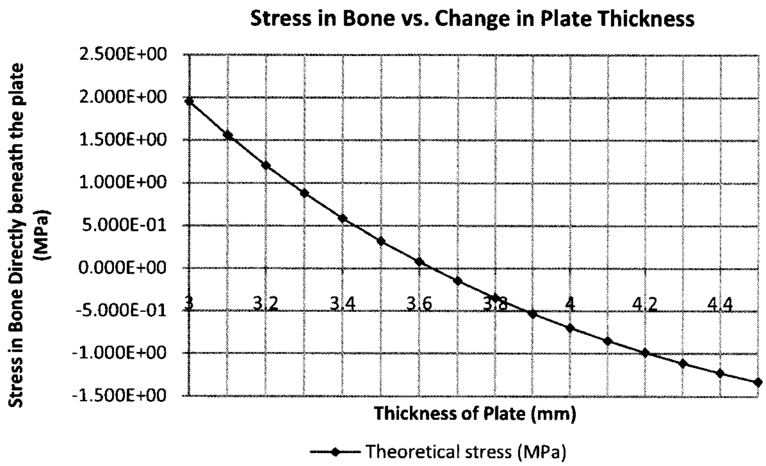

Figure 25: Theoretical predictions of stress in bone underlying a plate of changing thickness

As seen in Figure 26, our FE results demonstrate a decrease in bone stress for an increase in plate thickness. The variation between the theoretical prediction of stress and our FE results can be explained by the boundary conditions used. For our theoretical calculations, it is assumed that the bone and plate are rigidly affixed, which is a poor approximation of the bone-plate interface, where sliding motion exists.

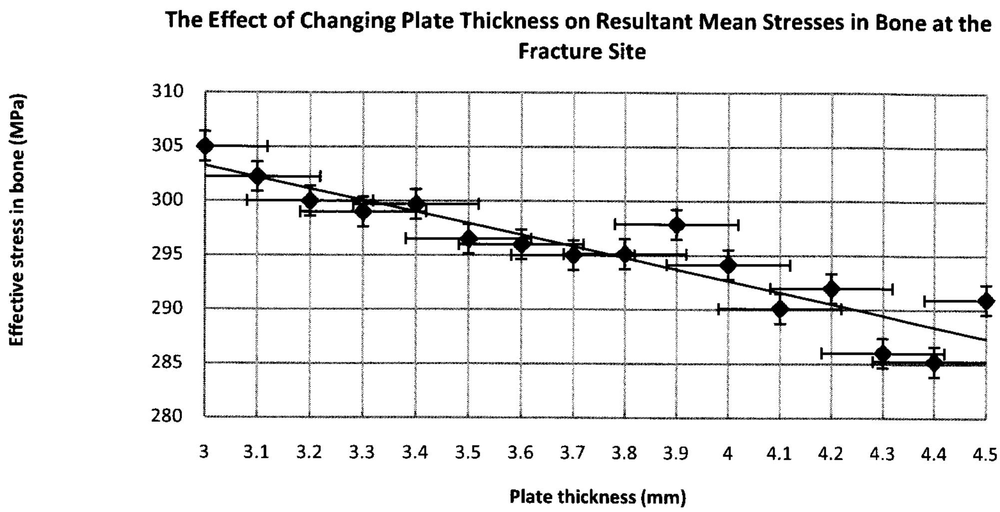

Figure 26: The effect of plate thickness on effective stress at the fracture site

In order to see the effect of changing the plate thickness on the resultant level of stress shielding in bone, the plate thickness is increased from 3 mm to 4.5 mm in increments of 0.1 mm. In Figure 26, we can see that the effective stress in bone at the fracture site decreases linearly as the plate thickness increases. This is the expected result, as an increase in the cross-sectional area of the plate effectively increases the stiffness of the plate (Akeson, Woo, Coutts, Matthews, Gonsalves, & Amiel, 1975). Subsequently, the neutral axis of the system, under a pure bending load, shifts further upwards towards the plate (as in the simple model). The regions of bone above the neutral axis are under a tensile load, where the regions below are under compression, however, the opposite would apply if the direction of the moment is reversed. The tensile stress in the bone at the fracture site and at the plate-bone contact area decreases as the plates' rigidity is effectively increased by an increase in its thickness.

Bradley and co-workers support the claim that a plate with a higher stiffness results in an apparent increase in stress shielding of bone (Bradley, McKenna, Dunn, Daniels, & Statton, 1979). Using a range of fiber-polymer composite plates between a thickness of 2.5 and 6.3 mm, they first calculate the corresponding flexural rigidity for each of the composite plates. Then, after 16 weeks in use with femoral osteotomies, the plates are removed and underlying bone samples are tested for strength against their respective contra lateral bone controls. These researchers find that bone strength increases as the flexural rigidity of the plate decreases (Bradley, McKenna, Dunn, Daniels, & Statton, 1979), thus signifying that stress shielding can be reduced by reducing the rigidity of the implant through either its material or geometric properties.

An optimal plate thickness is dependent on the type of material in question, since both E and I must be considered when determining the rigidity of an implant. Based on our findings, which is in agreement with others (Ramakrishna, Sridhar, & Sivashanker, 2004), a reduced plate thickness will result in a lower level of stress shielding in bone. For a particular material, the optimal thickness is one that is small enough to be surgically inserted and does not interfere with bone's surrounding tissue, and one that is thick enough to withstand high screw insertion torques.

3.2.2.ii The effect of plate angle

The theoretical prediction of bone stress due to an increase in plate area is shown in Figure 27. At a plate angle of 60° the bone is under compressive stress which decreases until the plate angle is modeled as 67°, wherein the bone experiences an increase in tensile stress up to the modeled plate angle of 90°. While maintaining a thickness of 4.5 mm, an increase in the plate angle effectively moves the neutral axis of the bone-plate towards the centre of the bone, thereby creating tensile stresses in the top cortice of the bone when a plate angle of 67° or larger is modeled.

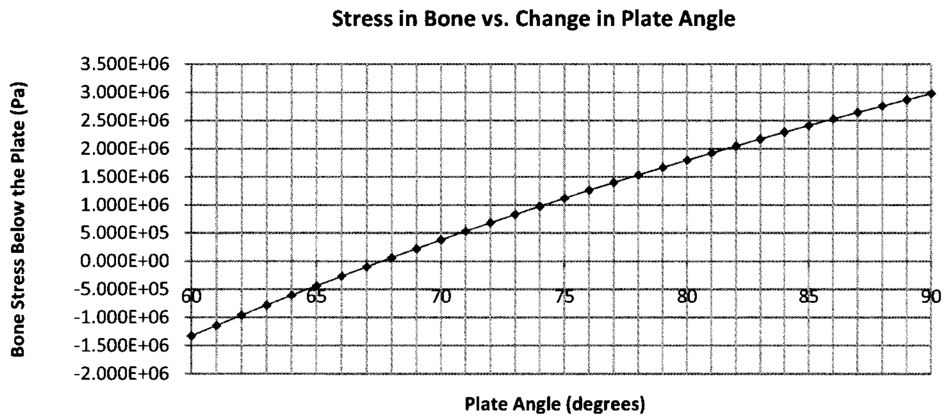

Figure 27: Predicted change in bone stress below the plate with a change in plate angle

Results from our FE model (see Figure 28) indicate that an increase in plate angle will cause a decrease in stress in the underlying bone, i.e. a higher degree of stress shielding develops in the neighbouring bone. The variation between the theoretical prediction of bone stress and our FE results is quite prominent here, and can once again be explained by the assumptions made about the bone-plate interface. In the FE model, because of the sliding contact between the bone and plate, the majority of the bending moment is effectively transferred to the plate.

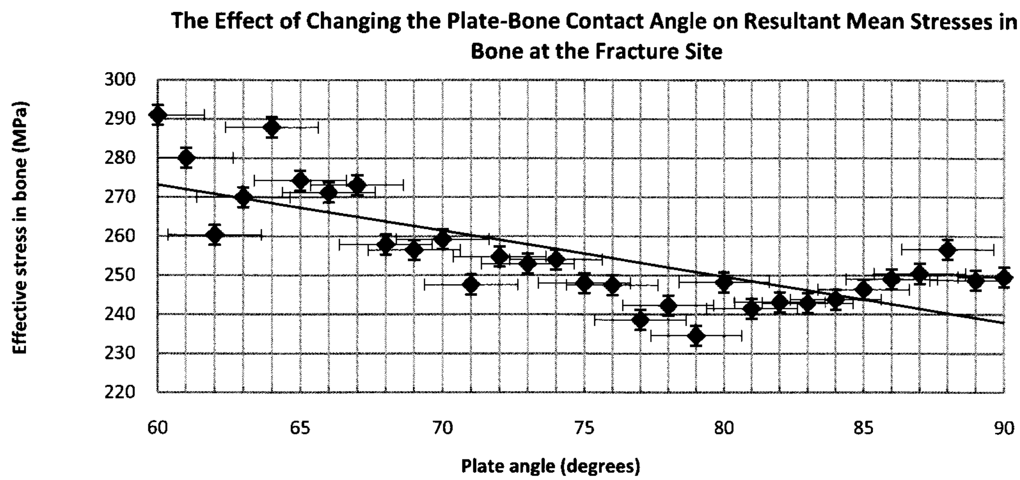

Figure 28: The effect of increasing the plate-bone contact area

Most plates available commercially are pre-bent to a limited degree in order to conform to the curved nature of long bones, however, most conventional plating systems are bent pre-operatively (Wheeless III, Nunley II, & Urbaniak, 2009). The overall decrease in effective stress at the fracture site following an increase in plate angle is to be expected, since an increase in the contact angle, while maintaining a constant thickness, will increase the cross-sectional area of the plate, thereby increasing its flexural rigidity. The plate's maximum allowable contact angle would depend on the size of the long bone in question. However, from our observations, the plate angle should be kept at a minimum in order to reduce the effects of stress shielding in underlying bone. An optimal plate value should be one that: limits the contact angle to reduce stress shielding in bone; yet is wide enough for the inclusion of the appropriate screws without inducing stress concentrations that yield the plate during loading; and provides sufficient strength and clinical stability (i.e. no micromotion) without interfering with the soft tissues surrounding bone.

3.2.2.iii The effect of screw position

Experimental research has highlighted some of the geometric factors responsible for the pullout strength of bone screws (Asnis, et al., 1996) (Lyon, Cochran, & Smith, 1941). However, little information involving the stress distribution between screws and bone exists. Our parametric study reveals an important consideration involving bone screw stresses; the distal screw is the highest region of concentrated stress as it must withstand plate-bone separation, which is in agreement with previous works (Cheal, Hayes, White, & Perren, 1983). Stress and strain reductions in bone are seen to be the most apparent in between the two innermost screws, near the fracture site (see

Figures 23 and 24). This indicates that stress shielding is most prominent in the vicinity of the fracture. According to other researchers (Simon, et al., 1977), this is beneficial upon initial fracture reduction; however, in the post-union phase, the reduction of load will affect the rate of remodeling and can cause subsequent bone loss.

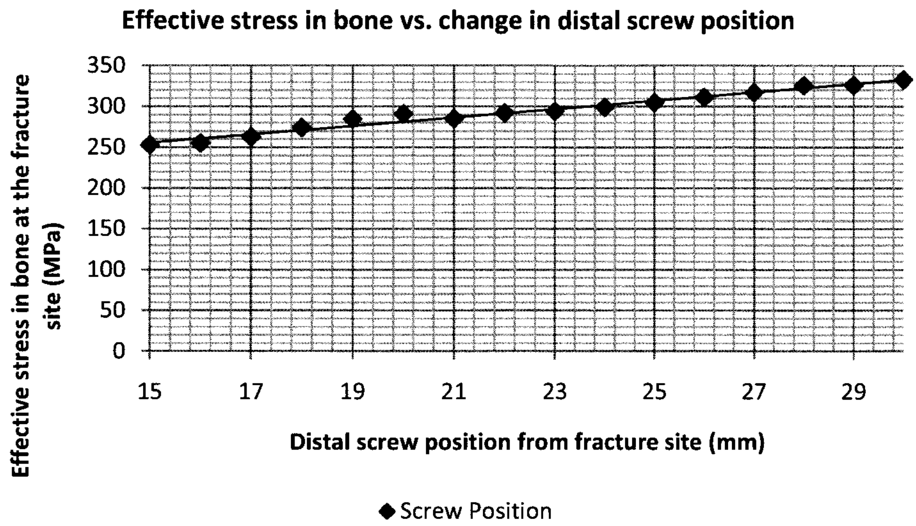

Figure 29: Effect of changing the distal screw position (increased distance from the fracture site)

Based on our results, an optimal screw position may exist. In terms of the outer screw's placement from the fracture site, a further distance is preferred as it reduces stress shielding in bone at the fracture site, however, it is limited by the length of the plate. Wider spaced screws also result in an increase in bending strength, and results in lower strains post fracture reduction (Ellis, Bourgeault, & Kyle, 2001). Alternative screw positions should also be analyzed, since factors such as divergent screw placement can also affect both the holding power of screws and the strength of bone-plate constructs (Robert, Chandler, Baratta, Thomas, & Harris, 2003). The ability of the plated-bone construct to withstand forces is dependent on the length of the plate and the number of screws inserted while the torsional resistance is only affected by the number of screws in place (Törnkvist, Hearn, & Schatzker, 1996). Many combinations involving other parameters such as plate length and alternative screw positions are required before an optimal design can be determined.

3.2.2.iv Simulation using stainless steel screws

The combinatory use of a stainless steel plate with titanium screws was an oversight of the model. In reality the two metals in contact with one another may cause galvanic corrosion if used *in vivo*

(Patterson, Daffner, & Gallo, 2005), and the same material should be implemented for both plate and screw. For this reason, one simulation is run which incorporates the stainless steel material properties for both the screws and plate (for one configuration of the model). Using the same geometry and boundary conditions as described in Section 3.2.1 the 60° angled plate with thickness of 3.0 mm is analyzed.

This configuration results in 27910 nodes and 8997 elements for both analyses (the stainless steel and the titanium screws). Using the stress probe tool in ANSYS Workbench the maximum effective stress at the fracture end is found to be 178.69 Pa, which is very close to the maximum effective stress at the same location for the same configuration using the Ti-6Al-4V screws (179.53 Pa). Figure 30 shows that the stress distributions for the two simulations are quite similar. High stress concentrations develop within the screw proximal to the fracture site under this loading condition. The resulting maximum equivalent stress of the proximal titanium is approximately 1.5 times greater than that of the proximal stainless steel screw. Since the titanium screw has a much lower Young's modulus (105 GPa) in comparison to that of the stainless steel screw (200 GPa), the titanium screw model results in overall larger deflections including larger bone strains, which is favourable if one considers that more mechanical stimuli transferred to bone will likely result in less stress shielding. The maximum magnitude of strain in this simulation is 1.34 $\mu\varepsilon$ for the stainless steel screws and 1.23 $\mu\varepsilon$ for the titanium screws simulation, respectively. This range of bone strain is within the range reported by Beaupre et al. who also demonstrate, in their FE model, that a change in the frictional coefficient between the plate and bone as well as the magnitude of the screw force play a significant role in the level of resulting bone strain (Beaupre, Carter, Orr, & Csongradi, 1988).

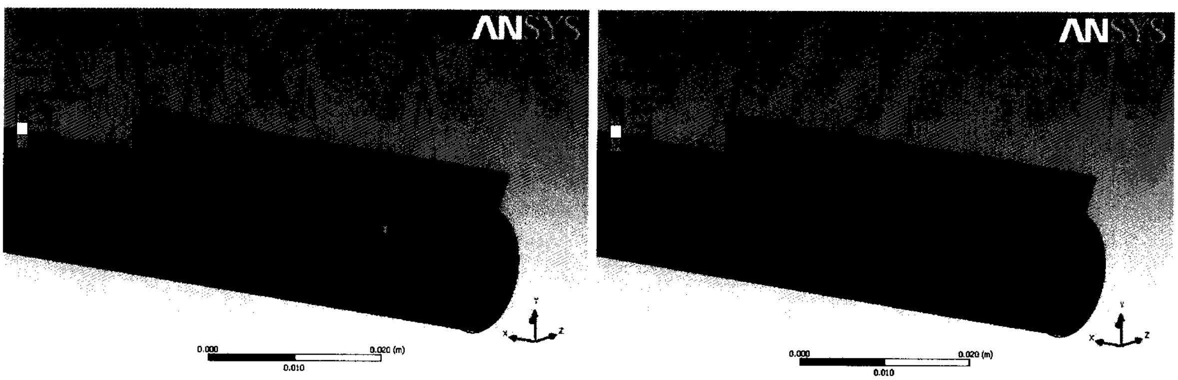

(a) Stainless steel screws (b) Titanium screws

Figure 30: Comparison of stress distribution with stainless steel and titanium screws

Considering that we are only interested in comparing the stresses occurring at the bone-plate interface from a change in plate geometry (plate thickness and angle), the modeling of titanium instead of stainless steel screws does not have a significant effect on our results as they can only be used as rough approximation of the level of stress shielding (due to the simplification of bone as an orthotropic material). Knowing that we cannot generate realistic quantitative results without the use of complex material properties incorporated into the model (Tawara, Sakamoto, & Oda, 2005), there is no concern that the use of a different metal of screws will influence the comparison of biocompatibility of the parametric configurations.

In reference to bi-cortical insertion, researchers such as Battula et al. (Battula S. , Schoenfeld, Vrabec, & Njus, 2006) determine that the holding power of screws is directly related to the depth of insertion, and that the threads should penetrate 1 mm beyond the far cortex for normal bone and 2 mm past for osteoporotic bone. Future models that are concerned with the stress distribution either along the length of the screw or in the cortex opposing the plate should include screws that penetrate beyond the lower cortex. However, in this model only simplified screws are generated, as realistic screw threads, which are computationally difficult to analyze, are beyond the scope of this study.

3.2.3 Conclusions

The theory that a reduction in mechanical loading of bone is the primary cause of increased bone bone resorption in the vicinity of the implants is a topic of much debate amongst researchers (Stahl, 1993) (Uhthoff & Finnegan, 1984) (Cordey, Perren, & Steinemann, 2000). The decrease may also be attributed to vascular insufficiency, also referred to as plate induced osteopenia (Perren, 2002). In order to further investigate the stress shielding developed by plate application a model involving stress-free plate separation using screws is modeled. Stress in the plate-bone contact area is of particular interest as the occurrence of stress shielding in underlying bone will cause a decrease in bone remodeling and may result in increased porosity (Claes, 1989).

Observations reveal that stress reduction in bone at the bone-plate interface is most evident between the innermost screws. The normal stresses in the regions of the middle and outer screws increase with the application of a plate when compared to the control bone model. Previous studies, (Cheal, Hayes, & White III, 1985) (Cegonino, Garcia Aznar, Doblare, Palanca, Seral, & Seral, 2004) (Borgeaud, Cordey, Leyvraz, & Perren, 2000) (Claes, 1989) in correlation with these results, also dictate that the outermost screw should experience the highest level of loading and result in a significant stress concentration.

Results from this study reveal that stresses in the region of contact between the plate and bone depend upon the type of loading condition applied on the geometry. Longitudinal stress reductions of 25% or less result in the underlying bone with plate application due to an applied bending moment, which is consistent with previous research (Cheal, Hayes, & White III, 1985). This is much more realistic than the near 100% reductions demonstrated in the validation fixed-bone model. Upon measuring the reduction of stress in bone in the region below the applied plate under a bending load, the parametric model indicates that stress shielding effects can be reduced by limiting the angular plate contact angle and thickness, which inherently reduces the stiffness of the device.

3.4 Discussion

In order to reduce the likelihood of fracture fixation failure, pre-deterministic failure models must be conceived. An ideal *in situ* model incorporating realistic three-dimensional geometry, anisotropic, and adaptive material properties of bone, is required to quantitatively measure the likelihood of implant failure due to stress shielding.

In an effort to avoid stress shielding and subsequent failure associated with plated long bones, a preliminary three-dimensional model is analyzed using ANSYS FEA software. As a preliminary study, a simplified plated bone model is compared to a bone cylinder under different loading conditions. In coincidence with previous work by other researchers, our results indicate that FE discretization is required to analyze complex systems such as plated-bone models, as analytic methods alone (e.g. composite beam theory) cannot adequately predict the behaviour of bone and plate (Cheal, Hayes, & White III, 1985).

The results stemming from the validation models demonstrate the importance of correctly defining model geometry, material properties, and boundary conditions in an FE model of a plated-bone construct. For example, the validation model showed the limiting behaviour of the direct contact model instead of allowing stress-free separation at the bone-plate interface. Since stress-free plate-tube separation is not represented by the fixed-bone model, high magnitude tensile stresses are present beneath the outer end of the plate. According to Cheal and co-workers this may be the case for a plate that incorporates a porous in-growth surface; however, this is unlikely for other plate types (Cheal, Hayes, & White III, Stress analysis of compression plate fixation and its effects on long bone remodelling, 1985). Depending on the nature of the model and the required accuracy of results, FEA tools must be implemented in a manner that assures convergent data. In the case of modeling bone and implants, results must generally be verified using *in vitro* analyses, due mainly to the complex nature of bone. An extensive search of the literature reveals a lack of information regarding both theoretical and experimental work directly related to fixation plates and stress shielding.

In an effort to produce a stress-free separation model and test various plating parameters, a more realistic model is developed. From this model, we conclude that the plate angle and thickness should be reduced in order to limit stress shielding. Limiting these plate geometric factors effectively reduces the stiffness of the plate without directly changing the material properties. We also note that stress reduction is most evident between the innermost screws under an applied bending moment, whereas the outermost screw experiences high levels of stress. The deviation from normal levels of bone stress in the regions surrounding screws can lead to locally increased rates of formation and absorption (Uhthoff H. , Mechanical factors influencing the holding power of screws in compact bone, 1973). In regions where localized absorption persists, loosening can occur and result in screw pullout. In order to avoid this negative effect, emphasis should be placed on employing screw types that minimize the probability of bone absorption. For this reason, the next part of this thesis focuses on: orthopaedic screws; screw pullout strengths; and a parametric analysis that relates screw geometry and material properties to stress shielding.

Chapter 4: Orthopaedic screws

Orthopaedic screws are a commonly used device for the fixation of bone, and are primarily responsible for maintaining the clinical stability (i.e. limiting micromotion) of plating systems. Although screws are able to adequately provide the necessary compression for the reduction of bone fragments, their inherent strength leads to uneven load sharing between the screw and bone. Many studies have proven the concept of Wolff's law which, roughly speaking, states that bone is adaptive in nature, and that disuse leads to bone atrophy (Carter, 1987) (Duncan & Turner, 1995). Therefore, a difference between the rigidities of the implanted screw and bone develops in locally altered rates of bone remodeling, and thus an abnormal bone density distribution in the vicinity of screws and/or implants, generally speaking. This stress shielding effect in the vicinity of screw threads is a major concern as resulting bone loss can lead to screw avulsion and failure of fixation in the post-union phase of fracture healing (Uhthoff H. , 1973).

Since a significant number of cases of screw loosening have been reported, many researchers have focused their attention on determining those factors which affect the pullout strength of screws. *In vitro* studies that generally involve pullout test methods have provided some insight as to which geometric factors are responsible for the holding power of screws (Lyon, Cochran, & Smith, 1941) (Schatzker, Sanderson, & Murnaghan, 1975) (Hughes & Jordan, 1972). The resistance to screw avulsion is highly dependent on the geometric design of the threads and the properties of the host material. The volume of host material in between the screw's threads must withstand the shear forces during pullout. For this reason, a screw's thread profile shape, thread depth, number of threads, and pitch, all critically affect its holding power in bone. Although pullout testing provides information about factors affecting the holding power of screws, it does not provide sufficient information about the contact conditions between the screw and bone. Currently, FE models are being used as a more feasible alternative to *in vitro* studies for the analysis of these conditions (Zhang, Tan, & Chou, 2004) (Lin, Lin, & Chen, 2006) (Chou, Jagodnik, & Muftu, 2008).

Optimization of screw geometric and material properties in a way that induces and distributes stress evenly across bone between and around screw threads may minimize the risk of loosening. Therefore, in this study, a simplified 2D finite element screw-bone model is generated to test the effect of varying these parameters on the level of resultant stress shielding in adjacent bone. In order to characterize this stress transfer, two pairs of dimensionless parameters are defined. They implement Von Mises stresses and strains from the model to compare and quantitatively measure the biomechanical compatibility of a particular screw with bone.

In this chapter a brief introduction to orthopaedic screws and their specific uses will be outlined involving a discussion on the use of both cortical and cancellous screws, and methods for determining and maximizing their holding power in bone. A theoretical analysis of the prospective holding power for the screw configurations tested in this study is performed prior to outlining the specific methods used for definition of the 2D screw-bone model.

4.1 Employment of screws in bone fixation

Screws are the most common orthopaedic device used for the fixation of bone. They are used as both standalone fixators and in conjunction with other orthopaedic hardware devices, particularly plates. Screws are primarily responsible for retaining the stability of most screw-plate fixation devices and are commonly associated with failure due to pull-out associated with poor screw purchase or bone loss. Therefore, particular attention should be placed on the type of screws in use and their placement in bone.

Orthopaedic screws are based on the design of those screws typically used in industry, the earliest of which is the V-shaped thread form. Initially comprised of sharp points, at both the crest and root, this common thread form is vulnerable to damage and severe stress concentrations (Juvinall & Marshek, 2000). Due to these limitations, both the American and British standards for fasteners were initially modified to a Unifed (inch series) standard, and then later adopted the ISO (International Standards Organization) metric thread standard, now agreed on by all major nations (Juvinall & Marshek, 2000). Both the Unifed and ISO threads are based on a standard geometry as shown in Figure 31 (adapted from (Juvinall & Marshek, 2000)).

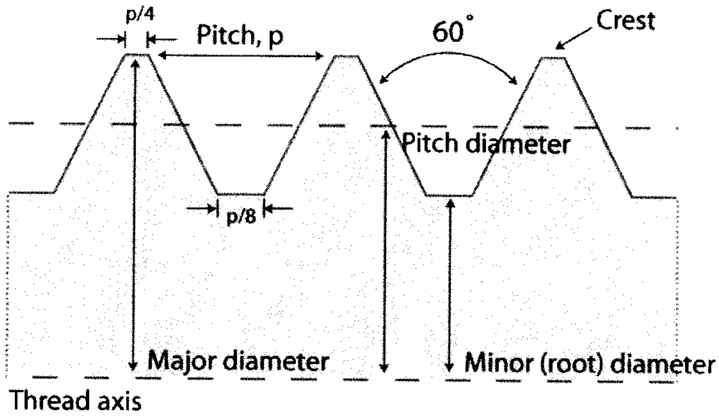

Figure 31: Basic profile for Unified and ISO thread geometry

The basic profile shown in Figure 31 is manufactured according to the level of precision and clearance required for a particular application. When used with a mating threaded member, screws are manufactured to different classes of fit; class 1 representing the loosest fit with greatest tolerances, and class 3 representing the tightest fit and smallest tolerances (Juvinall & Marshek, 2000). In the case of orthopaedic screws, a certain level of precision is necessary when used in conjunction with a locking plate, such as the locking-DCP.

Other geometric variations in screw thread forms exist; these include: trapezoidal, square, and buttressed profile shapes (Figure 32 (adapted from (Juvinall & Marshek, 2000)). The oldest and most common of these types is the Acme thread, which is trapezoidal in profile and is generally used as a power screw (Juvinall & Marshek, 2000). Alternatively, square threads are advantageous as a power screw in that they are slightly more efficient; however, the difficulty in manufacturing a 0° thread angle makes them uncommon. More often, a modified square thread, with a thread angle of 5°, is used as it is less difficult to manufacture (Juvinall & Marshek, 2000). A buttress profile shaped thread is sometimes used in industry when it is necessary to resist large axial forces in the screw's longitudinal direction (Juvinall & Marshek, 2000). This type of thread is also used in orthopaedics.

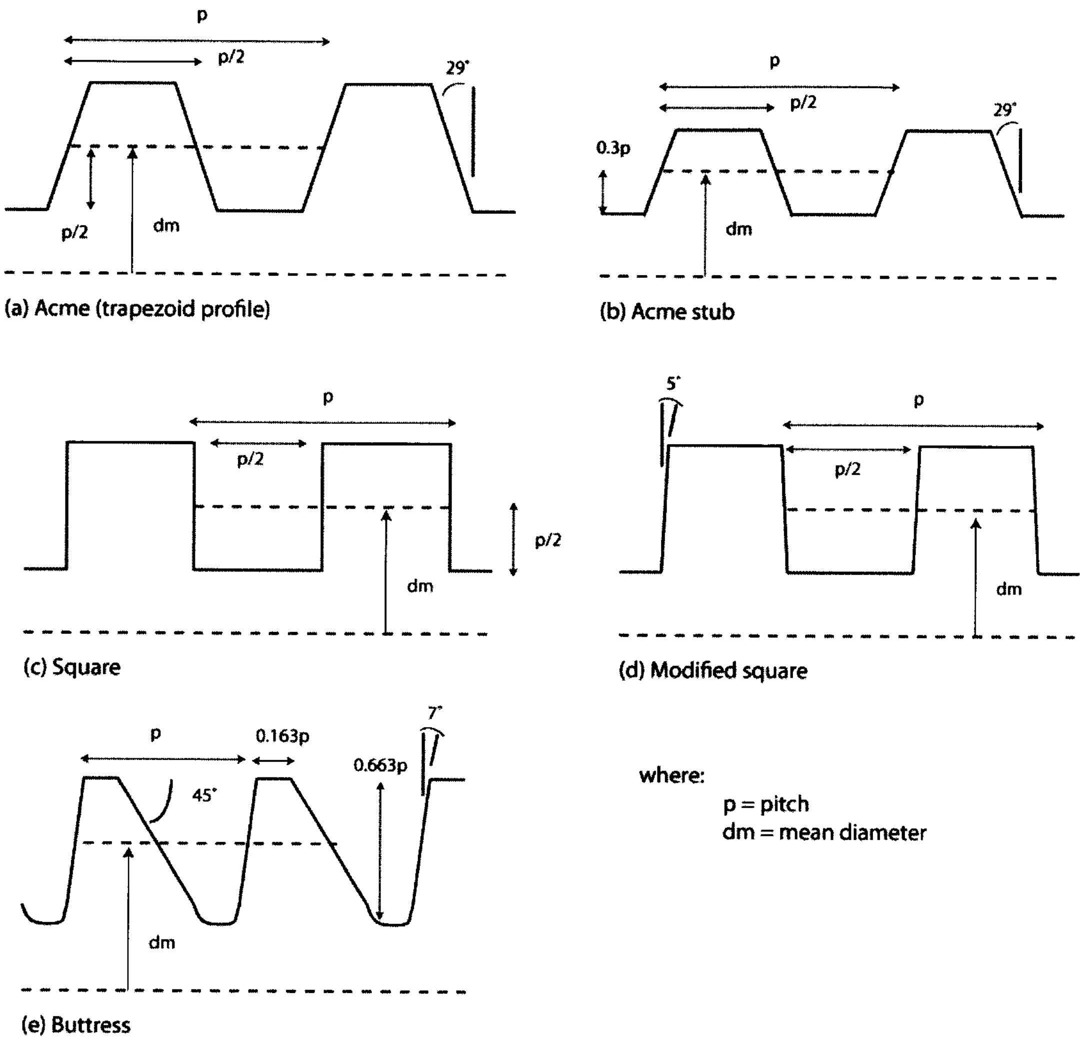

Figure 32: Alternate commercial screw thread profile shapes

The naming convention of Unified threads is based upon the length and number of threads per inch (i.e. 1 in.-12UNF), whereas that of ISO threads are based upon the diameter and pitch (i.e. M8 x 1.25) (Juvinall & Marshek, 2000). Unlike these naming conventions, orthopaedic screws are typically referred to in industry by the outer diameter of the threaded portion; 3.5, 4.5, and 6.5 mm screws being the most common types available (Glowniak & Miller, 2009). In this study, with the exception of the buttress profile shaped thread, the most commonly manufactured shapes are modeled, i.e. triangular, trapezoidal, and rectangular.

Threaded fasteners inherently have high mean stresses as they are initially subject to torsional stresses during tightening (Juvinall & Marshek, 2000). A high insertion torque is beneficial in most cases, as a high initial tension is more resistant to the separation of the adjoined members; the bone and screw, in the case of this study. A higher initial tension also produces greater frictional forces that resist any loading in shear (Juvinall & Marshek, 2000). The basis of bone-plate fixation relies on the compression of the plate to the bone by the induced tensile stresses in the screw (Hughes & Jordan, 1972). An approximately linear relationship exists between the insertion torque applied to the screw and the resulting tension. The screw should be inserted at the highest possible torque (without shearing the bone), in order to induce a desired higher screw tension. A higher screw tension is desirable because a higher frictional force must be overcome in order for loosening to occur, and it will also likely result in an increased transfer of mechanical stimuli to bone, which will reduce stress shielding. Sufficiently high torque is required to induce tension as losses occur to the cutting of host material threads and friction (Hughes & Jordan, 1972).

In terms of industrial applications, an initially high tension should also be considered, since screw loosening generally occurs and relieves most of the torsion during initial use (Juvinall & Marshek, 2000). Generally, all threaded fasteners are designed to be self-locking, meaning that they have a sufficiently small helix angle and a sufficiently high coefficient of friction to withstand loosening under static conditions (Juvinall & Marshek, 2000). Orthopaedic screws and plated-bone constructs are undoubtedly susceptible to this same type of loosening, as complex *in vivo* loading conditions will also tend to relieve some of the initial screw tension. Screw fatigue would involve the fluctuating tension accompanied by a small amount of alternating bending upon physiological loading of a long bone. A high screw tension will also reduce the dynamic load between the screw and bone, as the contact area between the mating surfaces is increased through compression (Juvinall & Marshek, 2000) (Hughes & Jordan, 1972) (Nunamaker & Perren, 1976). The torsional and tensile strengths of a screw are dependent on both its geometry and material properties and both should be considered in determining an appropriate fixator. The ultimate torsional strength of a screw is dependent on the cube of its root diameter, whereas the tensile strength is related to the square of the root diameter (Hughes & Jordan, 1972).

The choice in material is one of the main distinctions between orthopaedic screws and those commonly used in industry. Some of the factors considered in material selection of threaded fasteners within industrial applications include the required strength, weight, corrosion resistance, and cost (Juvinall & Marshek, 2000). In the case of orthopaedic devices, body tissue interactions must be taken into consideration. Most fasteners used for mechanical assemblies are made from steel of specific standards. Although stainless steels do provide the initial strength and corrosion resistance required for screws used in fracture fixation, titanium alloys are more ductile, are lighter in weight, and have proven to induce less stress shielding (Nazzal, Lozano-Calderon, Jupiter, Rosenzweig, Randolph, & Lee, 2006) (Niinomi, 2003) (Woo, et al., 1984). Ductility of screw materials is important so that localized yielding can occur in areas of stress concentration, such as near the ends of the loaded portion, where distribution of the axial stress is far from uniform (Juvinall & Marshek, 2000). The greatest portion of the load is carried by the first thread, since it is the shortest (and stiffest) path. Therefore the material chosen should be ductile enough to withstand some distortion of the first thread.

Hughes and co-workers tested orthopaedic screws of different materials in a synthetic bone substitute, Delron (a laminated phenolic resin), in both tensile and torsional loading conditions (Hughes & Jordan, 1972). They found that an approximately linear relationship exists between the core diameter and ultimate tensile and torsional strength, which in their experiments, they found is highest for EN58J stainless steel, followed by cast Co-Cr-Mo, and lastly titanium (Hughes & Jordan, 1972). From this relationship, one can deduce that a small increase in core diameter will produce a considerable increase in strength. A titanium alloy, Ti-6A1-4V, tested early on by Hughes and co-workers is found to be comparable in strength to a stainless screw steel of the same core diameter and has become a commonly used material for orthopaedic devices (Hughes & Jordan, 1972). The manufacturing methods of screws play a significant role in the resulting material characteristics. For example, annealing demonstrates a reduction in strength of a stainless steel screw by up to 40% in comparison to a cold-worked screw (Hughes & Jordan, 1972).

Besides variations in materials, many geometric screw variations exist in correspondence to their specific requirements. Some of the distinguishing characteristics of common orthopaedic screws are discussed in the following sections.

4.2 Common Orthopaedic Screw Types

Many variations in screw properties exist. Two classifications, cortical and cancellous bone screws, encompass these variations which commonly include differences in pitch, core diameter, and tip design (either self-tapping or non-tapping). Self-tapping bone screws are an essential component of both cortical and cancellous bone screws. They are manufactured as having either cannulated or solid central axes, and can be fully or partially threaded. Cannulated screws have the advantage of being easily insertable over a guide wire or pin, thereby reducing the chance of misalignment

(Wheeless III, Nunley II, & Urbaniak, 2009). As noted by Cleek and co-workers the extraction strength of these screws is not significantly affected by the cannulation (Cleek, Reynolds, & Hearn, 2007). A discussion involving the variances between cortical, cancellous, and lag screws is discussed below.

4.2.1 Cortical Screws

Cortical screws, developed for placement into cortical bone, are generally comprised of closely-spaced shallow threads that have a larger difference between the thread and core diameters than that of cancellous screws (Glowniak & Miller, 2009). Examples of each screw type are shown in Figure 33. Higher in strength than cancellous screws of corresponding diameter, cortical screws are used primarily in conjunction with plates for the fixation of long bones. Bi-cortical insertion is common to achieve maximal clinical stability. Cortical screws are usually comprised of blunt tips, and should not pass further than 2 mm beyond the distal cortice as to reduce any ensuing soft tissue damage (Glowniak & Miller, 2009). A common example is the 3.5 mm cortex screw which is commonly used for fixation of small bones including the forearm, fibula, and clavicle (Wheeless III, Nunley II, & Urbaniak, 2009).

2.0 mm diameter cortical screw

4.0 mm diameter cancellous screw

Figure 33: Examples of commercially available cortical and cancellous bone screws (New Life Surgical Works)

4.2.2 Cancellous Screws

Cancellous screws, designed for the fixation of cancellous bone, are most commonly used in the metaphyses of long bones. In comparison with their cortical screw counterparts, they generally include a wider pitch, and deeper cut threads (see Figure 33) (Gausepohl, Mohring, Pennig, & Koebke, 2001). These geometric variations are correspondent to the lowered density and mechanical properties of cancellous bone. These screw types are generally self-tapping, fully threaded screws, and therefore must avoid excessive damage of the already thin connectivity of cancellous trabeculae (Glowniak & Miller, 2009). Examples of these screw types are the 6.5 mm and 4.5 mm diameter types used for metaphyseal fractures, and as malleolar screws, respectively (Wheeless III, Nunley II, & Urbaniak, 2009). Tapping of these screws is common, as screw purchase is gained by the compression of trabeculae under the driving force of non-self-tapping screws.

Partially threaded cancellous screws are sometimes used as lag screws for metaphyseal fractures (Glowniak & Miller, 2009). In cancellous bone, the maximum pullout strength of large screws occurs when the pilot-hole diameter is nearly equal to the root diameter and drops off as the diameter increases (Tencer & Johnson, 1994).

4.2.3 Lag Screws

Not in reference to any particular screw type but rather to the method of insertion, lag screws are used to compress the bony segments of fractures. Their functionality relies on the inherent purchase of the distal portion of the screw into bone. The proximal part of the screw merely slides through the proximal part of the fracture. As the screw is tightened, the head forces the fracture gap to close; this is commonly denoted as interfragmentary fixation. Both cortical and cancellous bone screws can be used as lag screws (with or without plates), for long bone and metaphyseal fractures, respectively. Placement of these screws must be perpendicular to the axis of the fracture surface otherwise the fracture segments will not be compressed. Inadvertent angled paths can be cut if self-tapping screws are not placed correctly during insertion, and therefore should not be used as lag screws (Glowniak & Miller, 2009).

4.3 Stress shielding in the vicinity of screws

4.3.1 Stress concentrations caused by screw removal

Theoretical analysis suggests that introducing holes into bones for the insertion of orthopaedic screws causes a reduction in the local strength of bone by a factor of 3 (Tencer & Johnson, 1994). Bone strength is reduced as the stresses imposed by normal loading conditions are concentrated around the defect, namely the screw holes. Resistance to torsional loading in particular is affected by holes, and experimental evidence suggests that as a hole's diameter is increased upwards of 50% of the bone's diameter, the torsional strength decreases linearly by approximately 40% (Bartel, Davy, & Keaveny, 2006, p. 285). This reduction in strength is caused by the altered pattern of resistance to torsion, which is limited to the shear force at the periphery of the bone (Nordin & Frankel, 2008). The inclusion of a pin or screw in the hole does little to improve the strength of the bone. Overtime, however, as the fracture heals, callus fills the gaps adjacent to the screws, which eventually causes a significant increase in strength (Bartel, Davy, & Keaveny, 2006, p. 285). *In vivo* animal experimentation by Burnstein and co-workers reveal insignificant differences between energy ratios observed for holes drilled with and without screws two weeks after screw removal;

however, at eight weeks a significant increase in overall strength is observed with a retained screw (Burnstein, Currey, Frankel, Heiple, Lunseth, & Vessely, 1972). Histological examination reveals that woven bone builds up under the screw head and extends into the medullary space between four and six threads in as little as four weeks (Burnstein, Currey, Frankel, Heiple, Lunseth, & Vessely, 1972). This is in agreement with histological evidence from Uhthoff's work that reveals cell migration within two weeks post implantation and subsequent callus formation at four weeks (Uhthoff H. , 1973). Considering the aforementioned research, one might think it best to leave screws *in vivo*, however, sufficient levels of mechanical stimuli must be present in order to stimulate bone remodeling, and therefore this phenomenon of increased strength may only be temporary. If stress shielding affects the bone in the vicinity of screws, the already weak callus-filled gap will eventually be resorbed and the screws will ultimately loosen. This is not only a matter of resorption around the implant over time, but also a question of timing implant or screw removal.

4.3.2 Bone atrophy or hypertrophy?

An extensive search of the literature relating to histological evaluations of implanted orthopaedic screws results in very few articles directly pertaining to bone loss, or conversely hypertrophy, in the vicinity of bone screws. It is possible that where physiological loading is mainly cyclic and weight bearing in nature, bone hypertrophy in the vicinity of the screws may occur, if it is assumed that micromotion at the bone-screw interface exists (Nordin & Frankel, 2008). In the case of a plated femur or tibia, a large portion of the load would be carried by the plate and screws, and the cyclic nature of loading of the lower extremities would assumedly promote bone formation around the screws in the cortex opposing the plate due to the constant delivery of mechanical stimuli to the surrounding bone. This is in agreement with Wolff's law that states bone formation and bone loss are directly related to use and disuse, respectively.

In order for the hypothesis, that bone hypertrophy will occur in the vicinity of screws, to be true we must consider both Wolff's law and the mechanisms of fracture healing. Although an increase in mechanical stimuli (above bone's normal threshold) will promote bone remodeling, in the case of fracture or bone trauma healing must take place before remodeling can occur. As seen with many cases of fracture healing with plates and screws, initial rigidity must exist following implantation in order to promote boney bridging at the fracture site. This same principle is true for the trauma caused by screw insertion, where new bone formation around screws has been shown to take place independently of bone remodeling (Uhthoff H. K., 1973). The holding power of screws in bone is undoubtedly affected by the trauma of insertion, the reaction of bone to the implant, and on the resorption and remodeling of bone as a result of healing (Schatzker, Sanderson, & Murnaghan, 1975).

Loss of pullout strength of bone screws has been noted as early as 1941, where *in vivo* experimentation performed by Lyon et al. demonstrated losses of 34% for stainless steel, 27% for vitallium, and 74% for vanadium steel screws, in only ten weeks following insertion (Lyon, Cochran, & Smith, 1941). The authors claim that the reduction in holding power for both the stainless steel and vitallium screws is too small to be considered clinically significant, considering that most fractures exhibit bony union in eight weeks. However, the authors do not consider the cause of this loss in holding power or the implications of an implant remaining *in vivo* beyond their assumed eight-week window of fracture healing.

According to Uhthoff, careful radiologic examination has shown bone loss around screws prior to their avulsion (Uhthoff H. K., 1973). Direct observation of screw loosening due to bone loss has also been observed by radiolucency at the bone-screw interface during histological examinations of others (Okuyama, Abe, Suzuki, Tamura, Chiba, & Sato, 2000). For example, histological evaluations by Schuller-Gotzburg et al. of two lag screws implanted in the mandible of two patients were retrieved at 12 weeks and 19 months post-operatively. From their evaluation, microcrack formation can be seen following screw insertion, which is then followed by minimal resorption of necrotic bone and eventual remodeling. The authors observe stable osteosynthesis of the fracture in only 12 weeks, and consistent remodeling at the fracture site after 19 months, however, they also observed a decrease in remodeling around the screws at the 19 month mark, leading the authors to suggest that implants should be removed as early as three to four months after the surgery (Schuller-Gotzburg, Krenkel, Reiter, & Plenk Jr., 1999).

Here we examine three possible scenarios that could transpire when rigid fixation is employed; the first scenario maintains rigidity throughout implantation, the second involves some relative motion that occurs over time, and the third involves relative motion at the bone-screw interface for the entirety of implant implementation.

4.3.2.i No relative motion at the bone-screw interface throughout implantation

As in fracture healing, a certain level of rigid compression between fracture segments is required in order to allow for boney bridging and osteonal migration across the fracture gap. The removal and compaction of bone due to screw insertion causes a similar level of trauma to the bone, wherein rigidity is required initially to promote healing. Therefore, in this first scenario, we postulate that the stability of the implant will at first result in the resorption of necrotic bone and its eventual replacement by new bone, but ultimately there will be a reduction in the rate of remodeling due to low levels of mechanical stimuli. This is in agreement with Schatzker et al., that demonstrate that if rigid fixation is maintained, then the holding power of screws in bone reaches a maximum between four and six weeks following insertion (Schatzker, Sanderson, & Murnaghan, 1975). This peak in maximum holding power is followed by slight weakening, up until the end of their 12 week experimentation period, due to the resorption of the necrotic bone due to the trauma of insertion. The researchers state that the overall tissue reaction, regardless of the use of tapped or untapped screws, is not deleterious to the holding power of screws *in vivo*; the pullout strength never falls below the original pullout strength (Schatzker, Sanderson, & Murnaghan, The holding power of orthopaedic screw in vivo, 1975). We must keep in mind that their experiment only lasted 12 weeks, and that prolonged implantation leads to stress shielding.

It has been observed that active compression of the bone-screw interface results in little activity at the site of compression, whereas neutral regions, wherein a gap exists between the screw and bone, are areas of high activity, i.e. resorption of necrotic bone and formation of new bone (Schatzker, Horne, & Sumner-Smith, 1975). According to histological evidence, once the necrotic bone surrounding the screw threads is absorbed and replaced by new bone, the compression at the interface falls to zero (Schatzker, Horne, & Sumner-Smith, 1975), as hypothesized by Perren et al. (Perren & al., The reaction of cortical bone to compression by screw threads, 1969)to be a result of remodeling. From these statements, one may elucidate that bone remodeling will only persist if there is a constant supply of compression. A loss of compression between the screw and bone is inevitable, particularly in the case of lag screws (Schatzker, Horne, & Sumner-Smith, 1975). However, results from *in vitro* analysis of bovine bone samples reveals that axial compression of the bone screw is correlated to the screw size and insertion torque (Nunamaker & Perren, 1976) (Johnson & Smith, 2003).

One method of fixation in which little or no relative motion may occur is that of locking plates and screws. Bekler and co-workers also determine that micromotion and resistance to pullout is also limited by placing screws at divergent angles (Bekler, Bulut, Usta, Gokce, Okyar, & T., 2008). Although this may be a good method for creating rigidly stable fixation with plates, Kearny et al., determine that, on their own, screws placed at divergent angles of insertion progressively reduce the resistance to pullout (Robert, Chandler, Baratta, Thomas, & Harris, 2003).

4.3.2.ii Initially rigid fixation followed by some relative motion over time

If sufficient stability is maintained immediately following the insertion of bone screws, then new bone should occur between and around screw threads followed by eventual remodeling. Remodeling should persist if sufficient mechanical stimuli are present at the bone-screw interface.

Considering the magnitude of the physiological loads that are placed upon the implant-bone structure, post implantation, it is highly improbable that there will be no relative motion between the bone and screw, particularly for cases of implantation within the lower extremities. Researchers such as Zindrick et al. note that cyclic loading, of pedicle screws in vertebrae, leads to screw loosening (Zindrick, et al., 1986). This is in correspondence with Okuyama et al. whom reference works that relate screw loosening of pedicle screws mainly to cyclic toggling at the bone-screw interface (Okuyama, Abe, Suzuki, Tamura, Chiba, & Sato, 2000). In the case where new bone has formed, this type of cyclic micromotion may provide the mechanical stimuli (transferred from the screw to the adjacent bone) required for remodeling. It is proposed that remodeling will occur particularly in regions of stress concentrations, for example at the tips of threads for V-shaped threads.

The results of a study by Inceoglu et al. also suggests that loading rate has an influence on the mechanics of the bone-screw interface (Inceoglua, Ehlert, Akbayb, & McLainc, 2006). Even after a significant amount of compression trabecular bone can regain the majority of its initial undeformed height. The observation of load-deformation hysteresis during cyclic axial loading is therefore resolved to be due to the compression and subsequent decompression of trabeculae during each of the tensile and compressive phases of axial loading (Inceoglua, Ehlert, Akbayb, & McLainc, 2006). If this type of cyclical axial loading occurs *in vivo*, then sufficient mechanical stimuli should cause a remodeling response. In the case where the mechanical stimulation is much higher than the normal threshold level of bone, bone hypertrophy may occur in localized regions of high stress (or strain energy density).

4.3.2.iii Relative motion occurs at the bone-screw interface for the entirety of implementation

If relative motion occurs at the bone-screw interface before remodeling begins then the dead tissue will be resorbed and only fibrous tissue, not new bone, will fill its place leading to eventual screw loosening. This is demonstrated by *in vivo* studies performed by Schatzker et al. whom compared the difference between the reaction of bone to implanted screws under immediate physiological loading, and comparatively no loading (Schatzker, Horne, & Sumner-Smith, 1975). For all cases where relative motion existed between the screw and bone, the gaps at the bone-screw interface were filled with dense connective tissue. These regions of fibrous tissue, due to extensive osteoclastic activity (bone resorption), were observed to be larger than the initial hole size. The necrotic bone that existed in the vicinity of the screw threads from insertion is fully resorbed rendering the pullout strength of the screw inadequate. The motionless control models, on the other hand, lead to extensive osteoblastic activity adjacent to the threads. An overall conclusion that can be drawn from Schatzker et al.'s work is that motion at the bone-screw interface should be limited until new bone formation takes place.

One reason that rigidity may not be retained immediately following screw insertion is due to micro-cracking of bone. Researchers, such as Vangsness et al., suggest that microcracks, formed at the bone-screw interface at the time of insertion, may propagate during physiologic loading, and if the micro-damage accumulates faster than the rate of biological repair, screw loosening will occur (Vangsness, Carter, & Frankel, 1981). Using scanning electron microscopes they investigate the influence of repeated loading on the pullout strength of self-tapped and non-self tapped cortical bone screws. Results from their study reveal that regardless of the use of tapping or non-self-tapping screws, microcracks exist and propagate during cyclic loading producing measureable loosening and screw head migration, more so for the case of tapped screws (Vangsness, Carter, & Frankel, 1981).

Although significant relative motion at the bone-screw interface immediately following implantation will cause eventual loosening, resorption occurs gradually over time, and there remains a period following insertion where the screw may not readily pullout of the bone without a significant axially applied tensile load. This is particularly noted with trabecular bone, where a significant amount of compaction of trabeculae occurs, lending to the holding power of the screw in bone. This is exemplified by pullout studies in bovine and synthetic bone, wherein the holding power of fine threaded cancellous bone screws is superior to coarse threaded screws, partially due to the impaction of drilling debris (Gausepohl, Mohring, Pennig, & Koebke, 2001).

4.3.3 Resorption may be critical in osteoporotic bone

Research related to bone loss around screw threads is an under-studied topic. A great deal of consideration must go into the design of implants in order to reduce this pitfall. Cancellous bone screws are commonly used alone for the fracture treatment of small bones, or in the epiphyseal regions of long bones, where plates are either unnecessary or cannot be easily implemented. The difficulty in securing a rigid hold of screws in cancellous bone is much greater than in cortical bone, and is magnified in low density osteoporotic bone, wherein fracture healing is prolonged (Kawagoe, Saito, Shibuya, Nakashima, Hino, & Yoshikawa, 2000) (Stromsoe, 2004). Okuyuma et al. exemplify this problem by demonstrating the direct correlation between bone's mineral density and the stability of pedicle screws *in vivo* (Okuyama, Abe, Suzuki, Tamura, Chiba, & Sato, 2000). Considering that the rate of bone resorption in osteoporotic bone is increased (Manolagas & Jilka, 1995), it is probable that overall resorption around implants will be higher than that observed in healthy bone, due to its already weakened state. Since 1 in 4 Canadians develop osteoporosis during their lifetime, efforts should be directed towards the study of reducing implant related stress shielding (Minister of Public Works and Government Services Canada, 2002). Due to ethical considerations, costliness, and the invasively difficult nature in studying resorption in and around screw threads *in vivo, in situ* studies are gaining popularity (Gefen, 2002) (Zhang, Tan, & Chou, 2004). Since the complex nature of screw-bone systems is difficult to model many assumptions and simplifications are presently incorporated into models. Therefore experimental evidence is still necessary to validate results. Advancements in computational methods and accuracy in modeling may, in the future, cast *in vivo* research as a secondary method to *in situ* studies.

4.4 Screw Pullout Strength

Although bone resorption and implant fatigue may be an issue in the later stages of fracture healing, the bone-screw interface strength is initially the limiting factor in the overall strength of a stabilizing implant (Krag, Beynnon, Pope, Frymoyer, Haugh, & Weaver, 1986). Upon pullout, the volume of bone contained between screw threads fails under shear forces, as bone is the weakest in this mode of loading. Considered as a two-phase porous material, consisting of a solid phase (mineralized bone) and a fluid phase (soft-tissue and interstitial fluids), bone's apparent density is the most influential factor affecting its material properties which can be determined empirically from a power law equation of the form (Carter & Hayes, 1977):

$$\gamma = A\rho^B \tag{3}$$

Where:

γ *is a material property (i.e. strength, Young's modulus),*
ρ *is the apparent density,*
and A *and* B *are experimentally determined constants.*

Carter et al. determine the effects of strain rate and density on test specimens in order to approximate the compressive strength of bone to be:

$$S = S_c\dot{\epsilon}^{0.06}\left(\frac{\rho}{\rho_c}\right)^2 \tag{4}$$

Where:

S *is the compressive strength*
ρ *is the apparent density*
$\dot{\epsilon}$ *is the strain rate (per second)*
and S_c *is the compressive strength of compact bone with apparent density* ρ_c.

At a strain rate of 1.0 per second, the researchers found the compressive strength of bone to be approximately 221 MN/m^2 with an apparent density of 1.8 g/cm^3 (Carter & Hayes, 1977). This allows for a simplification of Eqn. (4):

$$S = 68\dot{\epsilon}^{0.06}\rho^2 \tag{5}$$

The average anisotropic and asymmetric ultimate stress properties of human femoral cortical bone are higher in the longitudinal direction (133 MPa tensile and 193 MPa compressive) in comparison to the transverse direction (51 MPa tensile and 133 MPa compression), and is weak in shear (68 MPa) (Reilly & Burstein, 1975). Not only is bone weak under shear loading, but it is also more flexible in the shear direction, i.e. 3,300 MPa in comparison to 17,000 MPa and 11,500 MPa in the longitudinal and transversely loaded directions (Reilly & Burstein, 1975) (Fyhrie & Vashishth, 2000). The asymmetry and anisotropy of bone's strength is caused by its transversely isotropic nature, which is due to the directionally aligned lacunae and architecture of cortical and trabecular bone, respectively (Turner, 2006). Knowing that host material density is a key factor in maintaining the holding power of screws (Asnis, et al., 1996), researchers have focused their attention on determining other geometric factors affecting the holding power, thread spacing and pilot holes, some of which are discussed in this section.

4.4.1 Pullout strength test methods

Screw pullout tests performed either through *in vitro* experiments using animal and human cadaveric bone have shed some light on factors influencing the holding power of screws (Schatzker, Sanderson, & Murnaghan, 1975) (Zindrick, et al., 1986) (Hearn, Schatzker, & Wolfson, 1993). However, variability in the quality of bone used has led to a wide variation of results. According to De Coster and co-workers a standard deviation between 30-50% has been noted between pullout strengths resulting in the inability of most studies to demonstrate a correlation between strength and screw parameters (DeCoster, Heetderks, Downey, Ferries, & Jones, 1990). Variability may also be caused by differences in loading rates. Axial cyclic tests also suggest that the loading rate significantly affects the strength and stiffness of the bone-screw interface (Inceoglua, Ehlert, Akbayb, & McLainc, 2006). Therefore, pullout rates should be matched in order to compare the results of these tests. To eliminate the variability of bone density in testing, researchers have sought a homogenous synthetic material with similar material properties to bone; rigid polyurethane (PU) foam having a trabecular-like structure is commonly used in these cases (DeCoster, Heetderks, Downey, Ferries, & Jones, 1990) (Asnis, et al., 1996) (Chapman, Harrington, Lee, Anderson, Tencer, & Kowalski, 1996). This homogenous foam allows for the testing of isolated screw parameters and their effects on holding power. Research using both bone and PU foam experiments donate valuable insight into which factors can greatly influence the strength of screws in bone. These factors are discussed below.

4.4.2 Host material density

Host material density is of particular importance in retaining the holding power of screws (Asnis, et al., 1996). Schatzker and co-workers also made this correlation between pullout strength and host material density, but instead reported an increase in strength to a relative increase in the thickness of the cortical layer (Schatzker, Sanderson, & Murnaghan, 1975). Therefore, the difference between densities of cancellous and cortical bone must be considered when choosing particular screw designs. Even within a particular bone, local variations in density result in variations in strength. For example, the shear strength of trabecular bone decreases with an increase in distance from the cortico-cancellous junction (Halawa, Lee, Ling, & Vangala, 1978). In some cases where trabecular bone density is particularly low, such as with osteoporotic bone, polymethyl methacrylate (PMMA), also known as bone cement, is used to fill voids in an effort to gain screw purchase (Halawa, Lee, Ling, & Vangala, 1978). The thinning and weakening in the cortex of osteoporotic bone is due to a decrease in osteoblast activity (bone formation) (Mullender, Van Der Meer, Huiskes, & Lips, 1996) which results in less material for the screw threads to grip.

Lyon and co-workers demonstrated a striking loss of holding power when performing pullout tests in cancellous bone and suggested the use of the coarsest possible threads to insure appreciable engagement (Lyon, Cochran, & Smith, 1941). They also found that holding strength nearly doubled if drilling was not performed past the cortical layer. Based on their tests in different densities of polyurethane foam, Lyon and co-workers claim that there is a linear relationship between bone density and the pullout strength of screws (Lyon, Cochran, & Smith, 1941).

With the use of cortical bone screws, a slight variation in the thickness of the cortex makes a significant variation in the holding power of screws. This is demonstrated by Lyon and co-workers who showed that when screws are extracted from animal, cadaver, and human bones, a small amount of bone is also removed in some cases (Lyon, Cochran, & Smith, 1941). The same type of fracture behaviour is demonstrated in polyurethane foam tests (DeCoster, Heetderks, Downey, Ferries, & Jones, 1990).

4.4.3 Screw design factors

Many geometric screw design factors have been tested in relation to their effect on the pullout strength of screws. Experimentally tested parameters include: the major diameter, minor diameter, thread pitch, length of engagement, and thread profile shape. A discussion on the various findings pertaining to each of these parameters is described below.

4.4.3.i Major & minor diameter

An approximately linear relationship between the major thread diameter and pullout strength exists as is shown by testing of a variety of screw types in synthetic foam blocks of varying densities (DeCoster, Heetderks, Downey, Ferries, & Jones, 1990) which demonstrate results within a clinical range of similar testing done in cadaveric bone of human radii (Trader, Johnson, & Kalbfleisch, 1979). DeCoster and co-workers demonstrate a mean increase in pullout strength from 469 N to 1360 N by increasing the major diameter of their custom designed screws from 3 to 6 mm. On the other hand, a small decrease in strength is reflective of an increase in the minor diameter from 4 to 5 mm (DeCoster, Heetderks, Downey, Ferries, & Jones, 1990). This is effectively a decrease in the major/minor diameter ratio, which would decrease the volume of bone contained between each thread.

4.4.3.ii Pitch & length of engagement

Some researchers have demonstrated that coarser threaded screws with a longer engagement demonstrate a better holding power in bone (Lyon, Cochran, & Smith, 1941) (Nunamaker & Perren, 1976). This design approach is commonly used in low density cancellous bone in order to gain a stronger hold through the penetration of a greater volume of bone. However, a comparison of commercial screws by DeCoster and co-workers (1.2 mm pitch with a 3.5 mm major diameter versus a 1.75 mm pitch with a 4.5 mm major diameter) shows that the finer threaded screw demonstrates a greater purchase in polyurethane foam tests (DeCoster, Heetderks, Downey, Ferries, & Jones, 1990). This not only suggests that a finer thread may actually promote a stronger hold in cancellous bone, but that pitch may actually be more influential than the outer diameter. This claim is supported by tests in both foam and bovine bone that demonstrated superior strength of fine threaded screws relative to their diameter in comparison with conventional cancellous and cortical screws (Gausepohl, Mohring, Pennig, & Koebke, 2001). This gain in holding power is thought to be in part due to the impaction effect of the drilling debris between the thread and bone, thereby countering the notion of pre-drilling.

Pullout testing performed with pedicle screws revealed that pitch alone does not have a significant effect on pull-out strength as long as the length of engagement is kept at a constant (Krag, Beynnon, Pope, Frymoyer, Haugh, & Weaver, 1986). Research has shown an approximate 30% gain in screw placement strength by increasing the depth of penetration from 50 to 80% (Krag, Beynnon, Pope, Frymoyer, Haugh, & Weaver, 1986). This linear correlation between an increase in the number of threads (while maintaining a constant pitch) and pullout strength is supported by other researchers (Zhang, Tan, & Chou, 2004).

4.4.3.iii Thread profile shape

Although many surgeons and researchers promote the use of buttress shaped profile threads over the use of V-shaped threads (see Figure 25), no evidence has been provided stating that one is more effective than the other. Isolating these two profile thread shapes, Krag and co-workers found no significant difference in pullout strengths, as is expected since the shear cylindrical area of bone is the same when the outer thread diameter remains unchanged (Krag, Beynnon, Pope, Frymoyer, Haugh, & Weaver, 1986). The only advantage of using the buttress shaped profile threads is an apparent ease of insertion. The lack of information regarding thread profile shape stems from the difficulty in re-producing alternative shape designs. Even with the use of commercially available screws, there are undoubtedly variations in size from screw to screw.

4.4.4 Pilot-hole size

Performance of screws is also dependent on pilot-hole size in the initial period following insertion. Cortical bone screws are generally placed into pre-drilled holes, whereas cancellous screws are generally self-tapping. An experimental study performed by Batulla and co-workers determined that the insertion torque of self-tapping screws is higher than that of screws inserted into pre-drilled pilot holes (S. Battula, 2008). However, the study also demonstrated that pullout strength decreases for pilot holes in excess of 71.5% of the screw outer diameter. Theoretically, the ideal drill size should be equal to the root diameter, as any larger hole would cause a loss in thread engagement. However, insertion of most screws in this condition is difficult and can result in the stripping of bone (Lyon, Cochran, & Smith, 1941). Based on experimental findings, bi-cortical insertion of surgical screws 2 mm beyond the distal cortex is generally recommended in order to increase the pullout strength and loading energy, regardless of pilot-hole size (Battula S. , Schoenfeld, Sahai, Vrabec, Tank, & Njus, 2008).

4.4.5 Screw insertion angle

The angle of insertion of screws also plays a role in the pullout strength of screws. In most instances screws are inserted perpendicularly to plates. However, with modified locking compression plates this angle can be varied. A study by Bekler and co-workers tests screws inserted through a locking compression plate attached to a bi-cortical PU model. They conclude that screws placed in divergent orientations have higher strengths and fail by bone breakage, as opposed to failure by screw pullout as seen with convergent and vertical screw configurations (Bekler, Bulut, Usta, Gokce, Okyar, & T., 2008). This conclusion is logical since there is a greater shear area when employing screws on an angle which would require a greater pullout force.

The opposite finding has been reported for the engagement of screws in bone without plating devices. This is demonstrated by Patel and co-workers who vary the insertion angle of screws by up to 40° in different densities of PU foam, and find that the 0° and 10° configurations produce higher pullout strengths than placement at 20°, 30°, and 40° orientations (Patel, Shepherd, & Hukins, 2008). This result, however, does not consider the purpose of the implanted screw or the angle of the pullout force. Where interfragmentary compression is required, cancellous screws should be inserted perpendicularly to the fracture regardless of orientation to the longitudinal axis of the bone.

The individual screw forces in a bone-plate system are difficult to predict. They are dependent upon their position on the plate, the local bone properties, the insertion torque, and the pilot-hole size, amongst other factors (Bartel, Davy, & Keaveny, 2006, p. 285). The tensile strength of the screw, itself, is dependent on the root diameter, whereas the pull-out strength is dependent on the outer thread diameter (in relation to the shear area of bone) (Nunamaker & Perren, 1976). Correspondingly, shear strength is proportional to the cube of the root diameter, whereas the torsional strength is proportional to the square (Wheeless III, Nunley II, & Urbaniak, 2009). The next section describes two methods that are commonly used to theoretically predict the shear failure force of screws in bone.

4.5 Theoretical analysis of shear failure force

As described in the previous section, clinical failure due to screw pullout generally occurs by stripping of the host material threads. Therefore, the holding power of the screws is reliant upon the shear strength of the host material and the shear area of the threads (Asnis, et al., 1996). Two methods for calculating the shear failure force exist: one which neglects any effects of profile shape; and one which takes the effects of profile shape into account. Both methods, based on ASTM (American Society for Testing Materials) factors, are outlined in order to predict the shear failure force of the screw configurations used in this study.

The first method directly relates the shear failure force to the density of the host material and to the outer diameter of the thread. Measured experimentally, the predicted shear stress failure of the screws is equal to the product of the shear strength of the host material and the area of the threads (Asnis, et al., 1996):

$$F_s = S \times (L \times \pi D) \tag{6}$$

Where:

$$S = shear\ strength\ of\ host\ material$$
$$L = length\ of\ engagement\ of\ the\ screw$$
$$D = outer\ diameter\ of\ the\ screw's\ threads$$

This theory predicts that, for screws of the same outer diameter, the shear strength will be consistent and will change only with a change in bone density.

On the other hand, the second method considers that thread depth and pitch are significant in determining the screw pullout strength, which has been proven experimentally (DeCoster, Heetderks, Downey, Ferries, & Jones, 1990). In order to account for these effects, a dimensionless thread shape factor (TSF) is defined by ASTM as follows (Asnis, et al., 1996):

$$TSF = \left(0.5 + 0.57735 * \frac{d}{p}\right) \tag{7}$$

Where:

$$d = thread\ depth\ (mm) = \left(D_{major} - D_{minor}\right)/2$$
$$D_{major} = major\ (thread) diameter\ (mm)$$
$$D_{minor} = minor\ (root) diameter\ (mm)$$
$$p = thread\ pitch\ (mm)$$

The TSF is calculated for the various screw shape parameters involved in this study and are listed in Table 2 below. This factor is used in conjunction with the previous method's formula to predict the shear failure force, introduced by ASTM as follows:

$$F_s = S \times A_s = S \times \{L \times \pi \times D_{major}\} \times TSF \tag{8}$$

Where:

$$F_s = predicted\ shear\ failure\ force\ (N)$$
$$S = material\ ultimate\ shear\ stress\ (MPa)$$
$$A_s = thread\ shear\ area\ (mm^2)$$
$$L = length\ (mm)$$

The formula predicts that if pullout failure occurs along the interface between screw and bone, then the strength of the interface is determined by the product of the shear area and bone's maximum shear strength. Although the TSF accounts for the screw thread geometry, a high level of importance is placed on the host material shear strength.

Depending on the bone sample in question, variations in density will lead to variations in shear strengths. A power-law can be used to describe this behaviour (Carter & Hayes, 1977) as seen earlier in Section 4.4. Through experimental research, Asnis and co-workers develop a power-law relationship between the apparent density and shear strength of bovine trabecular bone (Asnis, et al., 1996):

$$S = 21.6p^{1.65} \tag{9}$$

This relationship demonstrates that as the density of the bone increases, there is a corresponding increase in shear strength. Experimental evidence from the same researchers results in a similar power-law equation for unicellular polyurethane foam (Asnis, et al., 1996):

$$S = 23.9p^{1.54} \tag{10}$$

This similarity supports the use of unicellular polyurethane foam (also known as pedilen) as a good representative material of cancellous bone. With a similar trabecular-like structure as in cancellous bone, pedilen is a good substitute for pullout tests as the foam can be blown with different porosities.

To demonstrate the effects of density on shear strength, we represent low and moderate density cancellous by pedilen having densities of 0.15 g/cm^3 and 0.22 g/cm^3, respectively. Using the above power-law equations, we can compare the shear strengths with those measured experimentally by Asnis and co-workers in the following table:

	ρ (g/cm^3)	
	0.150	0.220
S (bovine bone) (Mpa)	0.944	1.776
S (pedilen) (Mpa)	1.287	2.321
S (experimental) (Mpa) (Asnis, et al., 1996)	1.330	1.900

Table 2: Predicted shear strength(s) of bovine bone, pedilen, and experimental bovine bone results

The values calculated in Table 2 demonstrate the significance of bone density in relation to shear strength; a small increase in density of cancellous bone will result in a significant increase in shear strength. Therefore, obtaining appropriate material properties of both trabecular and cortical bone should be noted when determining the screw pullout force during *in vitro* tests. In particular, site-specific average values should be considered for trabecular bone, as its mechanical properties vary greatly between anatomic sites (Einhorn, 1998).

Using the experimentally derived shear strength of cancellous bone with a moderate density (0.22 g/cm^3), the pullout forces are calculated using both the simple and TSF methods. The effects of increasing the outer thread diameter and the length of engagement for the screw configurations used in this study are demonstrated in Table 3.

Shear strength of bone (N/mm2)	1.9	1.9	1.9	1.9	1.9	1.9
L (length of thread engagement in material (mm))	9	9	15	15	17	17
Do (outer diameter (mm))	4	6	4	6	4	6
Di (inner diameter (mm))	2	2	2	2	2	2
p (pitch (mm))	2	2	2	2	2	2
d (screw depth (mm))	1	2	1	2	1	2
TSF (thread shape factor)	0.789	1.077	0.789	1.077	0.789	1.077
F (N) Calculated using Eqn. (8)	169.47	347.26	282.46	578.77	320.12	655.93
F (N) Calculated using Eqn. (6)	214.88	322.33	358.14	537.21	405.89	608.84

Table 3: Shear force calculations for screw configurations tested in 2D bone-screw model

It is clear that an increase in the outer diameter results in an increase in the predicted shear force for both methods of calculation. In terms of the TSF, the theoretical prediction is one where holding power is directly proportional to an increase in thread depth, and inversely proportional to an increase in pitch. The effects of which are more pronounced in less dense host materials (Asnis, et al., 1996). However, for the larger diameter thread configurations used in our model, the thread depth is equal to the pitch, thus resulting in a TSF greater than 1. This explains the large discrepancy between the predicted shear force values for the 2 mm thread depth configurations wherein the simple method predicts a lower value than when the screw geometry is accounted for.

The thread shape factor employed in these calculations does not provide an accurate representation of the thread profile shapes employed in this study. The calculations using the TSF performed by Asnis and co-workers are used to represent commercially available screw designs which generally include beveled profile shaped threads. Since many variations exist, there is a need for the theoretical development of an appropriate thread shape factor to be used in predicting the shear pullout force of varied thread profile shape designs. The inclusion of an appropriate geometric factor is important in accurately predicting the pullout strength of new and existing thread designs. An accurate description of the interface between the screw's thread profile and bone is also necessary in determining a relationship between a particular screw design and the level of resultant stress shielding. Information regarding stress shielding around screws, which would donate valuable information into the prevention of screw and implant loosening, is limited. It is for this reason that our 2D screw-bone model is developed, as outlined, in the following chapter.

Chapter 5: Two-dimensional FE screw-bone model

As detailed in Section 4.3, the biological reaction of bone to screws is quite complex and depends on both the initial healing ability and the eventual remodeling of bone in and around screw threads over time. If we consider prolonged rigid fixation without any micromotion, stress shielding of bone will result do to the lack of mechanical stimuli supplied to the bone. Schatzker et al. state that the application and maintenance of compression between screw threads and bone are the most important factors in attaining rigid internal fixation (Schatzker, Horne, & Sumner-Smith, 1975). Since a rapid loss of compression will result in loss of fixation rigidity, it is likely that movement, non-union and overall failure of the fixation may occur. The exact cause of bone loss surrounding screws remains an open question. Regardless of whether bone loss around screw threads is caused by movement and loosening, or resorption, it is still commonly associated with failure of fixation.

In light of this potential problem, a 2D screw-bone model is developed to ascertain the effect of screw geometry and material properties on the distribution of mechanical stimuli in neighbouring bone. Since, our model is not time-dependent; we are only interested in the immediate load distribution within bone that results from varying the geometric and material properties of the screw. Considering that the mechanical stimuli for the initiation of bone remodeling is unknown, and that higher levels of stimuli transferred to the bone will hypothetically promote bone remodeling, we are able to compare the effectiveness of transfer by the different parametric configurations. Both results pertaining to stress and strain energy density are compared as possible stimuli for mechanical adaptation. Although our model is a rough approximation of the three dimensional geometry we can still observe that manipulations in the thread contour will result in a definite change in the stress transfer and distribution to adjacent bone. Details of the 2D model are outlined below.

5.0 Model overview

Screw configurations that maximize mechanical stimuli transfer to bone adjacent to screw threads are sought. A 2D axisymmetric idealization of a long bone shaft which includes a cortical bone layer, trabecular bone region and a perpendicularly inserted screw is analyzed in a pullout scenario (Figure 34). The application of a tensile force on the screw allows for the analysis of isolated geometric and material screw parameters and their respective abilities to transfer stress to bone. The finite element modeling, control of the screw parameters, and analyses are effectively performed through the execution of code, designed using ANSYS Parametric Design Language (APDL).

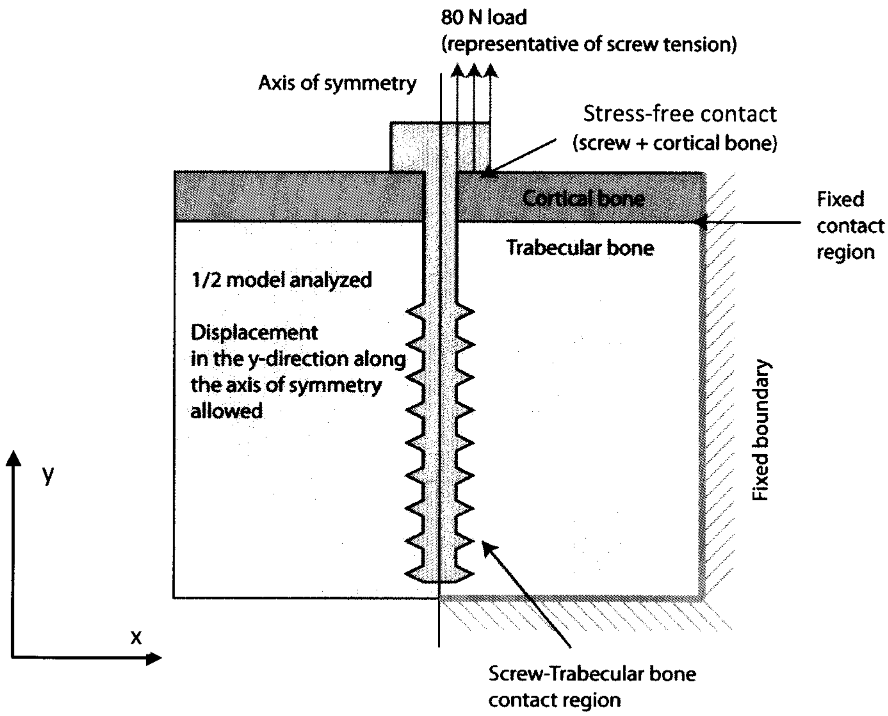

Figure 34: 2D screw-bone model

5.1 Bone screw parameters

The principal screw dimensions modeled for this study are based on commercially available designs. The screw head and inner shaft diameters are both kept constant at 6.0 mm and 2.0 mm respectively, for the initial five parameters tested. The initial parameters tested include varying geometrical and material properties of the screws in a similar manner to those modeled in a previous study by Gefen (Gefen, 2002). Our results, which are quantifications of stress shielding are calculated using a previously defined parameter and a newly proposed parameter, and are compared to results from Gefen's study. The parameters include a change in profile shape between a triangular, rectangular, and trapezoidal shaped screw thread; a change in the shaft length from the bottom of the screw head to the first screw thread between 1 and 5 mm; a change in the outer thread diameter between 4 and 6 mm; and altering the screw's elastic modulus from 105 GPa to 40 GPa. The two moduli of elasticity tested are representative of a regular titanium alloy screw (Ti-6Al-4V) with a Poisson's ratio of 0.35 and a treated titanium alloy screw with a reduced stiffness. This new type of titanium alloy, known as Gum metal, is a super elastic β-type titanium alloy that is similar in composition to Ti-Nb-Ta-Zr alloys that are used in the biomedical industry (Niinomi, 2003). A newly tested parameter involves a change in the inner shaft diameter from 2.0 mm to 6.0 mm.

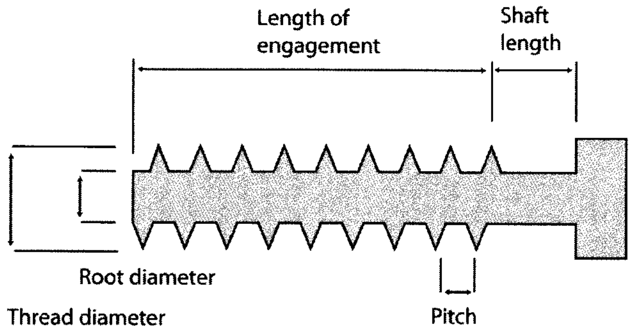

Figure 35: Screw geometry

5.2 Finite element analyses methods

In order to compare the biocompatibility of the screw configurations for the varied parameters described above, an axisymmetric idealized screw-bone model is generated using ANSYS APDL. The components of the model are generated as follows: a 3 mm thick homogeneous cortical bone layer, an underlying volume of trabecular bone, and a screw with variable geometric and material properties (see Figure 35). The thickness of the cortical bone layer is typical of a femur, while the trabecular region is bounded at a reasonable distance from the screw as to not greatly affect the stress distributions resultant of the loading condition. As in Gefen's model (Gefen, 2002), the cortical and cancellous bone regions are modeled as having homogeneous and linearly elastic isotropic material properties with Young's moduli of 20 GPa and 1 GPa, respectively, each with a Poisson's ratio of 0.35. These material properties correlate to those specified in the literature (Rice, S.C., & J.A., 1988). This is a simplification of the true nature of cortical and cancellous bone, which are both well known to be inhomogeneous anisotropic materials (Cowin, 2001, p. 151).

Fixed boundary conditions are implemented within the model to refrain from any displacement of the outer boundaries of cortical and trabecular bone (see Figure 34). However, the symmetric axis that lies along the mid-plane of the screw is restrained only in the horizontal direction, allowing for vertical displacement upon loading. Instead of applying a force to simulate a screw's insertion torque, as in previous models (Gefen, 2002), an 80 N tensile distributed force is applied to the top of the screw head (1/2 of the model) in an effort to simulate a pullout scenario. The magnitude of this pullout force is the same as that in Gefen's study in order to compare results between a screw tightening and a screw pullout scenario. A force of 160 N (along the bottom of the screw) is generated for axial tension in a study by Schuller-Götzburg and co-workers wherein the stress distributions of lag screws with and without a biconcave washer are compared using 2D FE models and histomorphological data (Schuller-Gotzburg, Krenkel, Reiter, & Plenk Jr., 1999). Predicted shear failure forces using equations such as (6) and (8) in Section 4.5 will likely produce higher values than what would be demonstrated experimentally, as is the case in a study by Patel et al. (Patel, Shepherd, & Hukins, 2008), and as seen in Table 2 where we compare the predicted values of shear failure force to those found experimentally by Asnis and co-workers (Asnis, et al., 1996). The range of expected shear failure forces for the geometry in the screw-bone model lies between 169 N and 608 N, as predicted by the aforementioned equations in Table 3 (Section 4.5). Considering that this range of values may over-predict that failure force, a total pullout force of 80 N (160 N in total) is reasonable for our analysis. The effect of load magnitude is further examined in Section 5.4.2. Analysis of Von Mises stresses and strains under this condition reveals the relative stress distributions between screw and bone for the various configurations.

5.3 Simulation and evaluation of biocompatibility

The discretization of elements is performed using the automatic mesh capability of ANSYS (see Figure 36). Quadrilateral 4-node elements (Plane82) are created, and a mesh refinement is specified along the bone-screw interface regions in order to improve the accuracy of the numerical solution in these regions. The SMRTSIZE command is used and set to 1 (fine) in order to implement a more refined mesh for the screw area. A mesh refinement is performed using the LREFINE command in the APDL code. Although no significant differences exist between resulting stresses and strains for the trabecular bulk, a refinement of 3 is required for convergence of results in the screw threads.

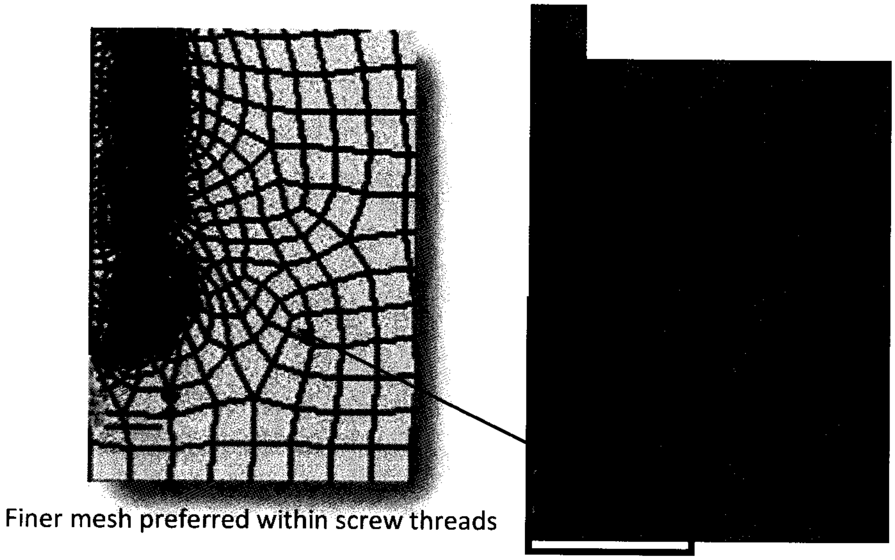

Figure 36: Mesh of 2D screw-bone model with mesh refinement along screw threads

Both tensile and compressive stress and strain distributions are represented by Von Mises equivalent stress and strain; which are calculated based on the difference in principal stresses (Benham, Crawford, & Armstrong, 1996):

$$\sigma_e = \frac{1}{\sqrt{2}}[(\sigma_1 - \sigma_2)^2 + (\sigma_2 - \sigma_3)^2 + (\sigma_3 - \sigma_1)^2]^{1/2} \tag{11}$$

Where:

σ_e *is the Von Mises equivalent stress;*
and $\sigma_1, \sigma_2,$ *and* σ_3 *are the principal stresses.*

The measured equivalent stresses and strains are recorded along a defined path in the post-processor for each parametric configuration. These measurements correspond to the points outlined in Figure 37, and are stored in a table for calculation purposes.

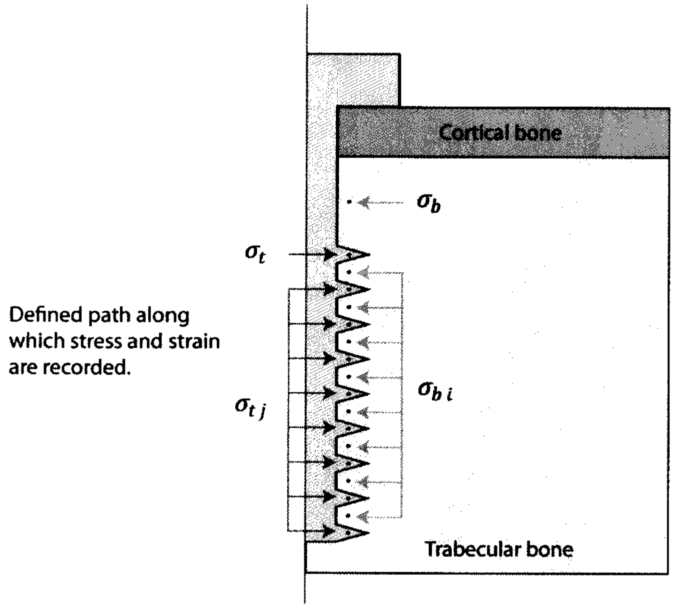

Figure 37: Stress and strain path defined in ANSYS

In order to characterize the stress transfer between the screw threads and the bone two pairs of dimensionless parameters are defined. These parameters known as stress transfer parameters (STPs – introduced by Gefen (Gefen, 2002)) and strain energy density parameters (SEDTPs – introduced in this research) are a measure of the biocompatibility of the various screw configurations tested. The parameters allow us to not only compare the various screw configurations previously mentioned, but also to demonstrate the difference between using stresses or strain energy densities as mechanical stimuli responsible for changes in the rate of remodeling. The parameters are defined below.

5.3.1 Stress transfer parameters (STPs)

Using the effective stresses located at the defined points in the trabecular bone and screw threads allows for calculation of STPs as previously defined (Gefen, 2002). The level of stress shielding is effectively measured as a ratio between the stress in bone and that of the underlying thread(s). Low STP results will indicate poor stress transfer between the screw and bone which is a sign of stress shielding. An ideal system would result in a near homogeneous stress transfer between the screw and bone. Ideally, a screw embodying the identical material properties of bone would produce this result, therefore STP results approaching unity are sought to eliminate stress shielding existent in bone.

$$STP\ \alpha = \frac{\sigma_b}{\sigma_t} \tag{12}$$

Where:

$\sigma_b = stress\ in\ the\ bone\ between\ the\ bottom\ of\ the\ screw\ head\ and\ the\ first\ thread$
$and\ \sigma_t = stress\ in\ the\ midpoint\ of\ the\ first\ screw\ thread$

And:

$$STP\ \beta = \sum_{i=j=2}^{i=j=N} \frac{\sigma_{bi}}{\sigma_{tj}} \tag{13}$$

Where:

$\sigma_{bi} = stress\ in\ the\ bone\ between\ consequtive\ screw\ threads$
$and\ \sigma_{ti} = stress\ in\ the\ midpoint\ of\ screw\ threads$

A distinction is made between these two α and β parameters, in order to observe the effect of the first screw thread in relation to the remaining threads. The first thread is generally the location where the highest stress concentrations occur, and therefore is the most likely location of failure. In order to generalize an overall STP value for comparison between the various screw configurations, we define the STP total as:

$$STP\ total = \sum STP\ \alpha + STP\ \beta \tag{14}$$

It is this value that we define as the ranking factor in deeming a particular screw configuration as a more negative or positive stress shielding contributor.

5.3.2 Strain energy density transfer parameters (SEDTPs)

The strain energy density function is a scalar valued function that relates the strain energy density (SED) of the material in question to its deformation gradient.

$$U = \frac{1}{2}\sigma \cdot \varepsilon \tag{1}$$

Recent bone remodeling theories hypothesize that SED, not stress, may be a more suitable mechanical stimulus responsible for osteocyte response, and consequently for the bone remodeling process (Huiskes, Ruimerman, Van Lenthe, & Janssen, 2000) (Vahdati & Rouhi, 2007). Recent theoretical predictions (Rouhi, Theoretical aspects of bone remodelling and resorption processes, 2006) indicate that SED may be a potential candidate for initiating the bone remodeling process, and although experimental research is needed, *in situ* testing of SEDTP criterion will provide some insight into the behaviour of its distribution with respect to the STP criterion (Haase & Rouhi, FEA orthopaedic screw optimization to reduce stress shielding, 2009). In order to compare the use of strain energy density as a prospective stimuli for bone remodeling strain energy density transfer parameters (SEDTPs) are defined as follows:

$$SEDTP\ \alpha = \frac{\sigma_b \varepsilon_b}{\sigma_t \varepsilon_t} \tag{16}$$

Where:

σ_b *and* σ_t *are defined as in the definition of STPs*
and ε_b
$=$ *strain in the bone between the bottom of the screw head and the first thread*
and $\varepsilon_t =$ *strain in the midpoint of the first screw thread*

And:

$$SEDTP\ \beta = \sum_{i=j=2}^{i=j=N} \frac{\sigma_{bi}\,\varepsilon_{bi}}{\sigma_{tj}\,\varepsilon_{tj}} \tag{17}$$

Where:

$\varepsilon_{bi} =$ *strain in the bone between consequtive screw threads*
and $\varepsilon_{tj} =$ *strain in the midpoint of screw threads*

A distinction is made again between the first thread and the remaining threads, as in the case of the STPs. The total SEDTP value, used to compare the level of stress shielding resulting from the various screw configurations, is defined as follows:

$$SEDTP\ total = \sum SEDTP\ \alpha + SEDTP\ \beta \tag{18}$$

Results pertaining to the STP and SEDTP calculations performed for each of the parametric screw configurations will be presented in the following section.

5.4 Verification of the model

5.4.1 Testing the validity of quantifying parameters

To validate the ideal values of the defined parameters, i.e. STPs and SEDTPs, one sample set of screw configurations is tested with the screw's modulus of elasticity modeled as 1 GPa (the same as that of the trabecular bulk (Gefen, 2002)). In theory, when the screw's modulus of elasticity is the same as that of the host material density, the STP α and β values should approach values of unity as the stress transfer should be evenly distributed between the screw threads to the bone. The result should be the same when calculating SEDTP α and β values under this condition, as both the stress and strain that develop should be even between both the screw and bulk, as they act as a single material (not including the cortical layer).

Upon simulation, it is noted that the trabecular bone bulk carries the majority of the load due to the definition of the model and boundary conditions. The stress concentrations from the tensile load on the top of the screw head decreases linearly down the shaft of the screw, however there are higher stress concentrations, as expected, at the interface of the bottom of the screw head and shaft, as well as the region where the cortical bone ends and cancellous bone begins. Since both the screw and trabecular bone region share the same material properties and share a fixed contact region they now act as one continuous material. For each of the configurations analyzed, the stresses obtained along the defined path are slightly higher in bone than for its corresponding thread(s), except between bone and the first thread of the larger diameter screw with a short shaft (i.e. the triangular, 6 mm thread diameter, 1 mm shaft length configurations). This anomaly is due to the definition of the path which is farther from the shaft for a larger diameter thread, and is therefore further from the stress concentration. These effects are demonstrated in Figure 38: a-d, where it is clear that despite the difference in shaft length, the stress distribution decreases outwardly from the shaft-trabecular bone interface. Stresses are higher in the larger thread diameter cases, as is expected due to the increased holding power of the larger host diameter threads.

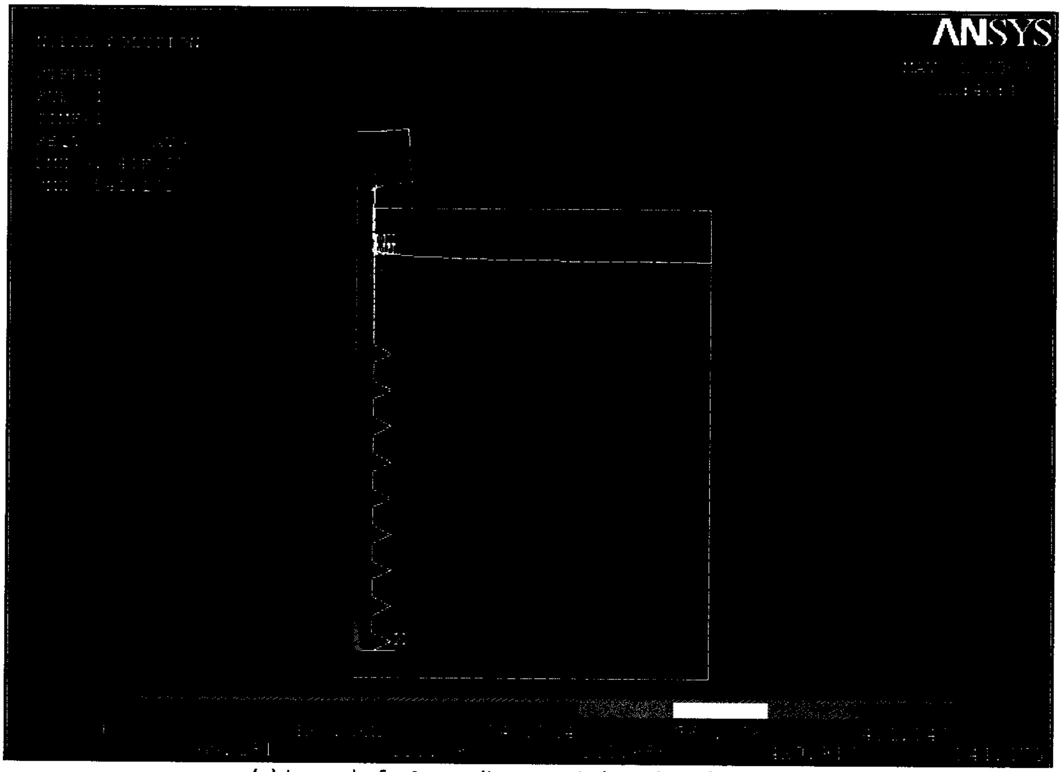

(a) Long shaft, 4 mm diameter 9 thread configuration

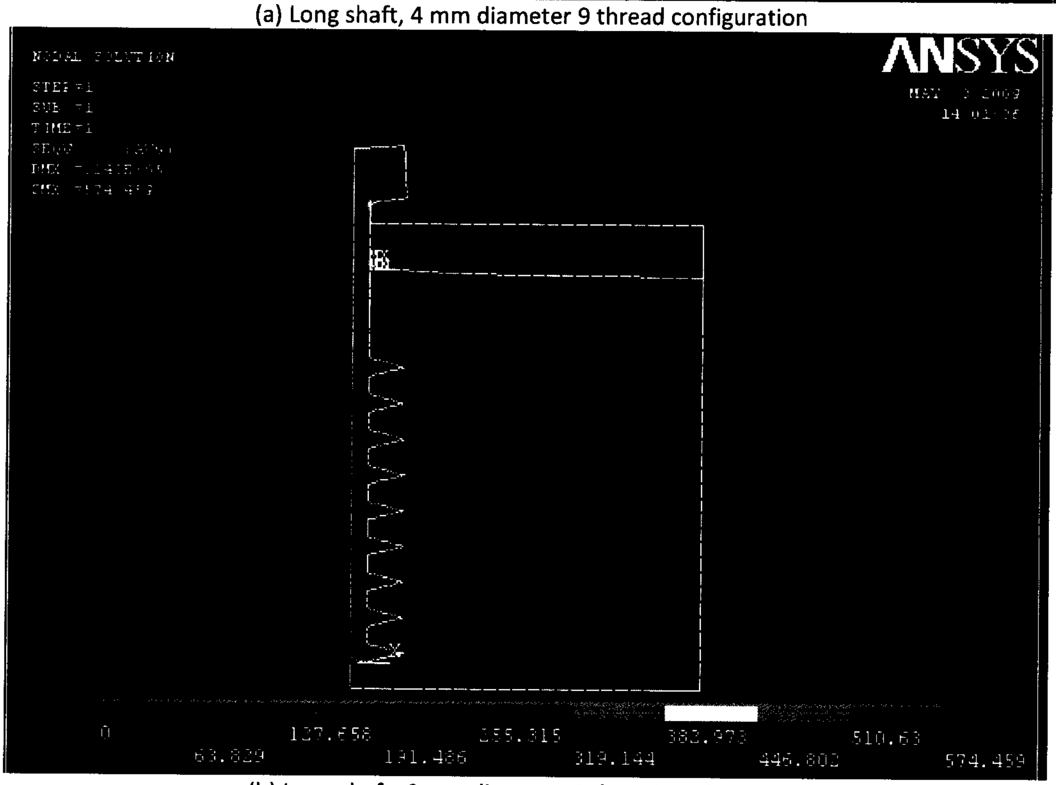

(b) Long shaft, 6 mm diameter 9 thread configuration

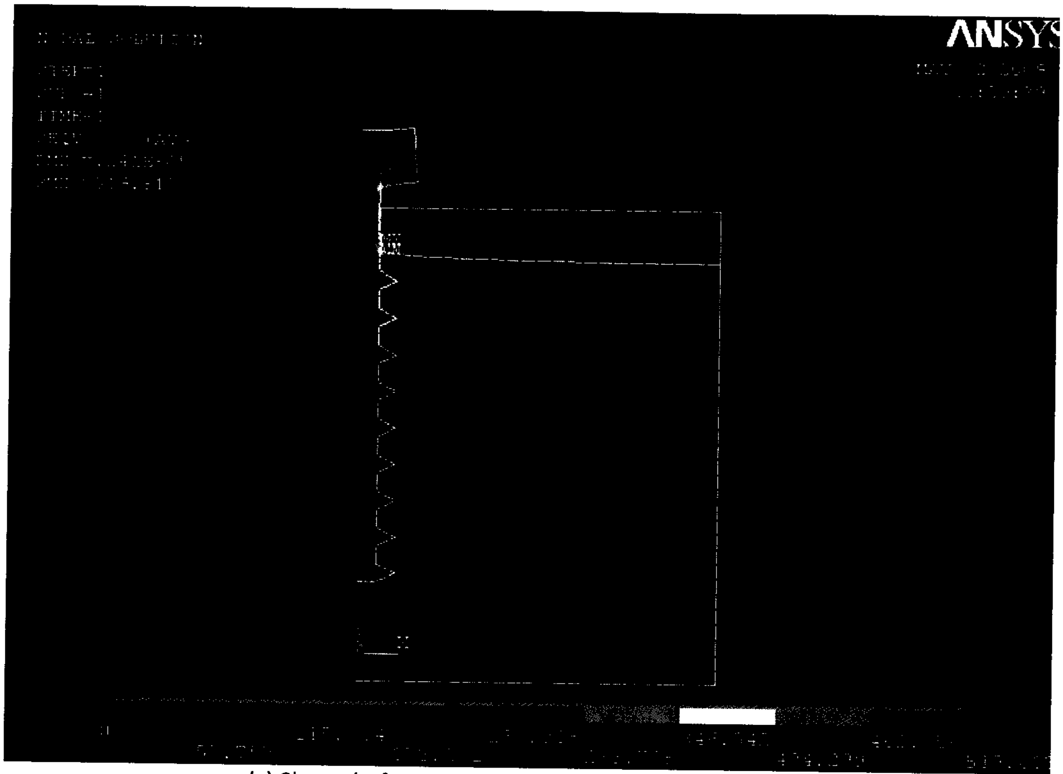

(c) Short shaft, 4 mm diameter 9 thread configuration

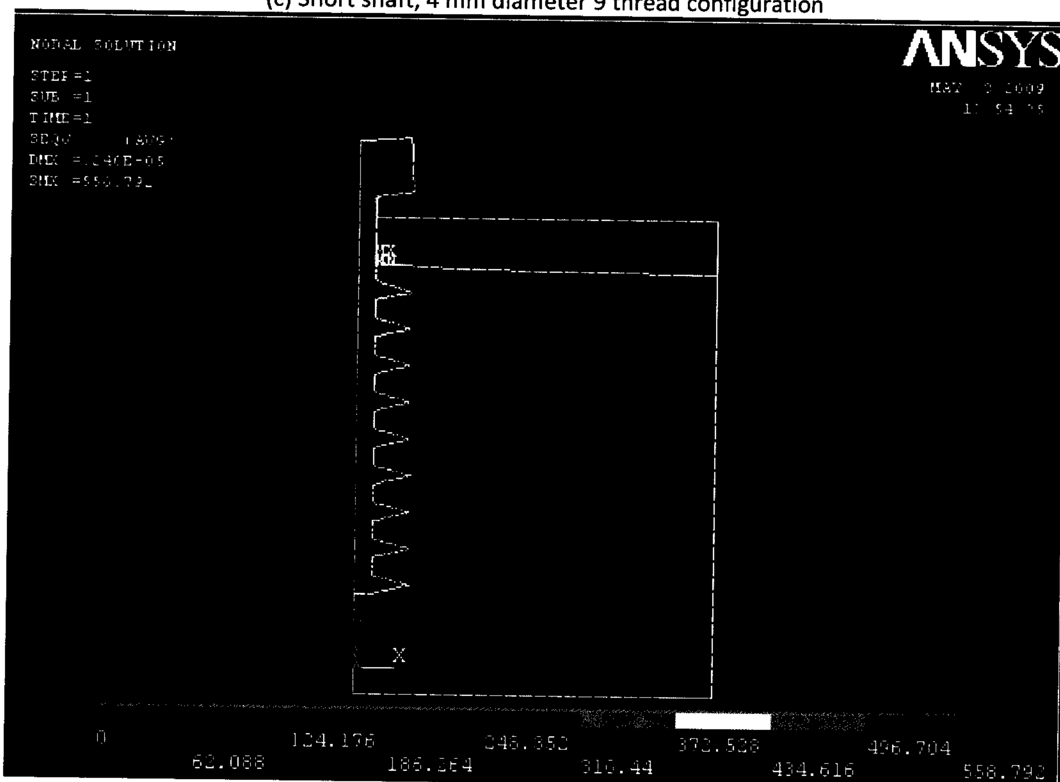

(d) Short shaft, 6 mm diameter 9 thread configuration

Figure 38: (a-d) Examples of 1 GPa screw configurations under tensile loading

The STP and SEDTP values are essentially representative of a ratio of the difference in stress and strain energy density between the screw threads and adjacent bone, respectively. Therefore in the cases where resulting stresses are higher in bone, the ratio of stress transferred between the bone and screw, the parameters are calculated as the inverse ratios of what has been previously defined. For example, the STP α value for this analysis is calculated as follows:

$$STP\ \alpha = \sum \frac{\sigma_t}{\sigma_b} \tag{19}$$

A similar approach is executed for the calculation of the SEDTP values. Both sets of values are outlined in the following table. For the purpose of comparison in the following tables, the SEDTP values were reduced by a factor of 10.

Thread diameter	4						6					
Shaft length	long			short			long			short		
No. of threads	5	8	9	5	8	9	5	8	9	5	8	9
STP α =	0.610	0.610	0.610	0.816	0.942	0.734	0.670	0.670	0.672	0.717	0.682	0.691
STP β =	0.781	0.850	0.923	0.763	0.826	0.884	0.783	0.852	0.926	0.777	0.841	0.902
Total	1.391	1.460	1.533	1.579	1.767	1.619	1.453	1.522	1.598	1.494	1.523	1.593
SEDTP α =	0.372	0.372	0.372	0.649	0.877	0.533	0.449	0.449	0.450	0.519	0.477	0.489
SEDTP β =	0.743	0.799	0.838	0.689	0.729	0.751	0.748	0.805	0.845	0.726	0.771	0.796
Total	1.114	1.171	1.209	1.338	1.606	1.284	1.197	1.254	1.295	1.246	1.248	1.285

Table 4: STP and SEDTP values for the 1 GPa screw configurations

In most cases the STP and SEDTP α parameters result in values lower than the corresponding β parameters, indicating a more even transfer of load between the bone and distal portion of the screw. This is correspondent to the linearly decreasing stress concentrations as seen in Table 4 and the definition of the parameters. Since the stress in the trabecular bone contained between the cortical layer and the first thread experiences the highest levels of stress and the distance between the path points for the STP α parameter is the largest, it is expected that the ratio will be higher than for the remaining trabecular bone and thread stress points. A comparison between total results obtained from STP and SEDTP values is shown below (see Figure 39). The figure demonstrates a direct correlation between results calculated by both methods, i.e. STP and SEDTP criteria.

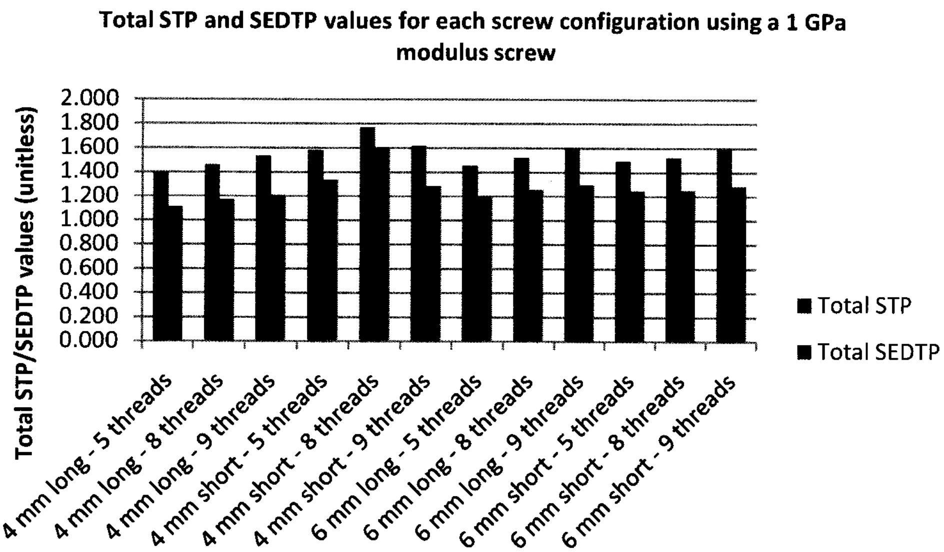

Figure 39: Comparison of STP and SEDTP total values for a screw with modulus of elasticity of 1 GPa

Although the values do not reach the optimal value of unity, they are higher in comparison to the same configurations analyzed with moduli of elasticity of 40 and 105 GPa. This is demonstrated in Figures 40 and 41.

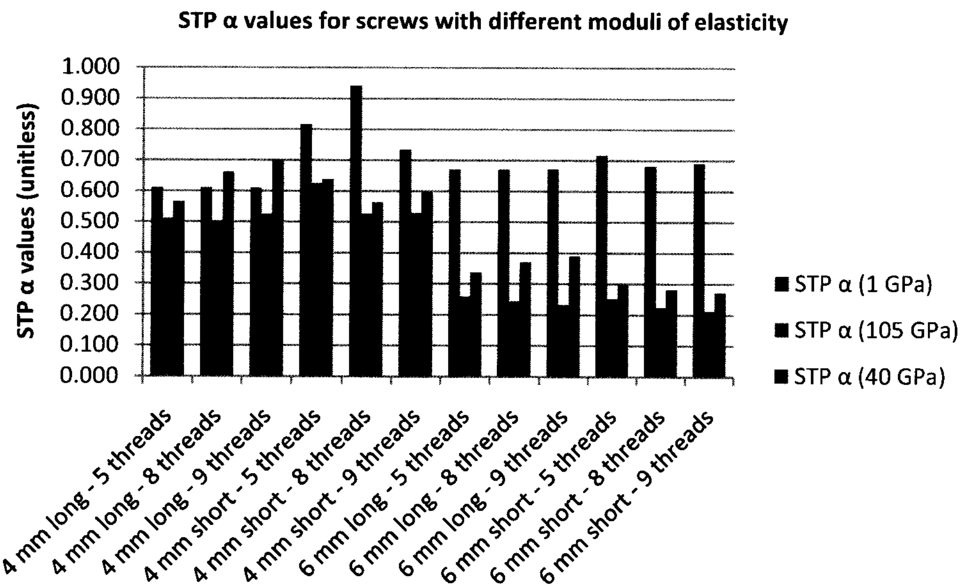

Figure 40: Difference between STP α values for screws with different moduli of elasticity

The difference between the STP α values using a 1 GPa screw and that of 105 GPa is evident. In all cases, the ratio of stress between the bone and screw is closer to unity when the screw is modeled as having the same elastic modulus as the trabecular bone. However, in the case of screws with 4 mm diameter threads and long shafts, this ratio is higher for the 8 and 9 threaded 40 GPa configurations which produces a seemingly better stress transfer between the first screw thread and bone. This discrepancy is caused by the nature of the defined path wherein the path point, along which the effective stress is recorded, is at the midpoint between the cortical layer and the first thread. When the 1 GPa screw is employed the difference between the stress in the screw thread and bone is greater than for the 40 GPa screw because of the difference in the stress distributions (see Figure 42). As described previously, due to the definition of the path along which stress values are taken, the values reveal a large difference between the results of the 1 GPa screw modulus to that of the higher moduli for the 6 mm diameter screw thread configurations.

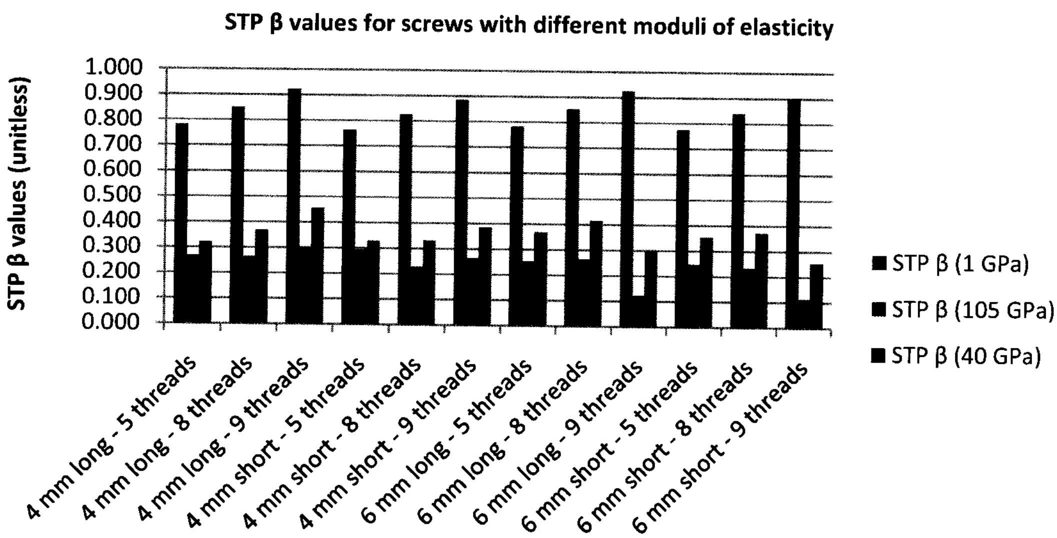

Figure 41: Difference between STP β values for screws with different moduli of elasticity

Results from a comparison between the STP β values reveals that for all configurations, the use of a screw with an elastic modulus of 1 GPa results in much higher values of STPs than those resulting from the 40 and 105 GPa screws. These values also increase with an increase in the number of threads, for the ideal case using a 1 GPa screw. Again, this is due to the fact that the stress decreases linearly away from the concentration at the top of the screw head. Increasing the number of threads results in stresses being recorded more distally away from the concentrated region, therefore resulting in a higher average ratio for the screws below the first thread. Similar stress distributions along the length of the screw are demonstrated in a 3D FE analysis of bone-screw pullout modeled by Zhang and co-workers where peak Von Mises stresses occur at the thread root in both screw and bone (Zhang, Tan, & Chou, 2004).

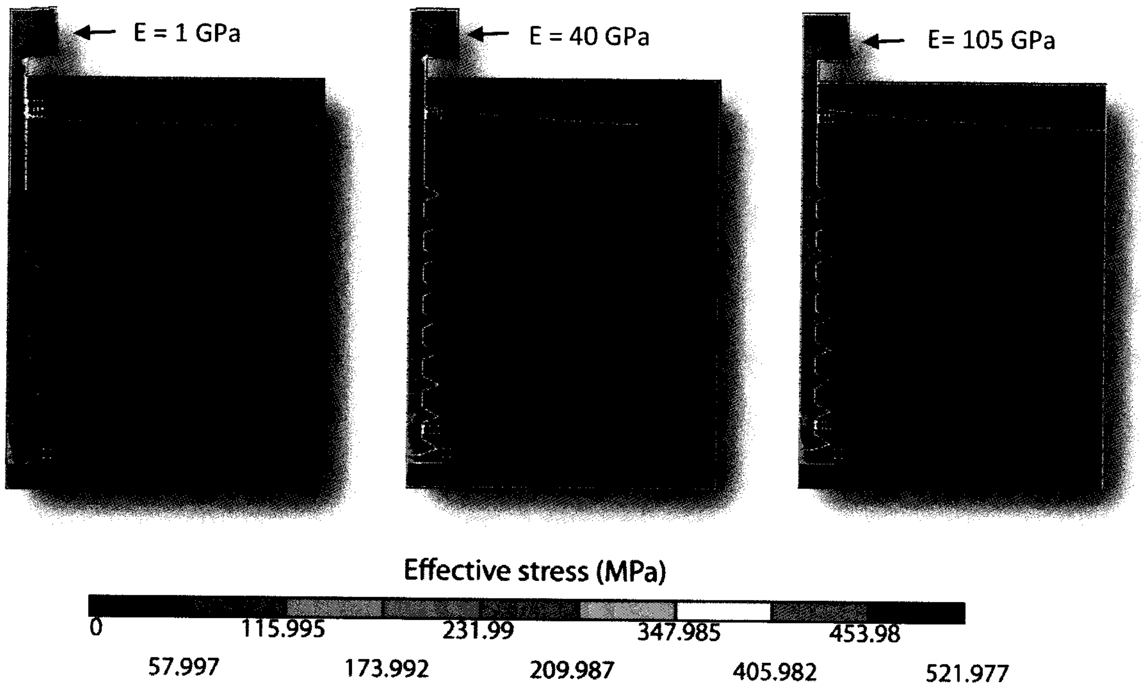

Figure 42: Example of stress distribution for the long shaft, 4 mm diameter, 9 thread configurations

Although neither the STP α nor β values result in the theoretically optimal value of unity, the results are consistent with the resulting stress distribution as shown in Figure 42. Since the interface between the screw and trabecular bone region is modeled as a fixed contact region, a distinction in material properties must be made between the two areas in order to demonstrate the results of the two separate entities.

If we model the screw as having a slightly higher modulus of elasticity than 1 GPa, then we should encounter a similar stress distribution, as seen for both the 40 and 105 GPa cases. Therefore, as demonstrated in Figure 43, as the stiffness of the screw and subsequently the difference between the moduli of bone increases, the stress in the screw increases. This effectively causes stress shielding in neighbouring bone.

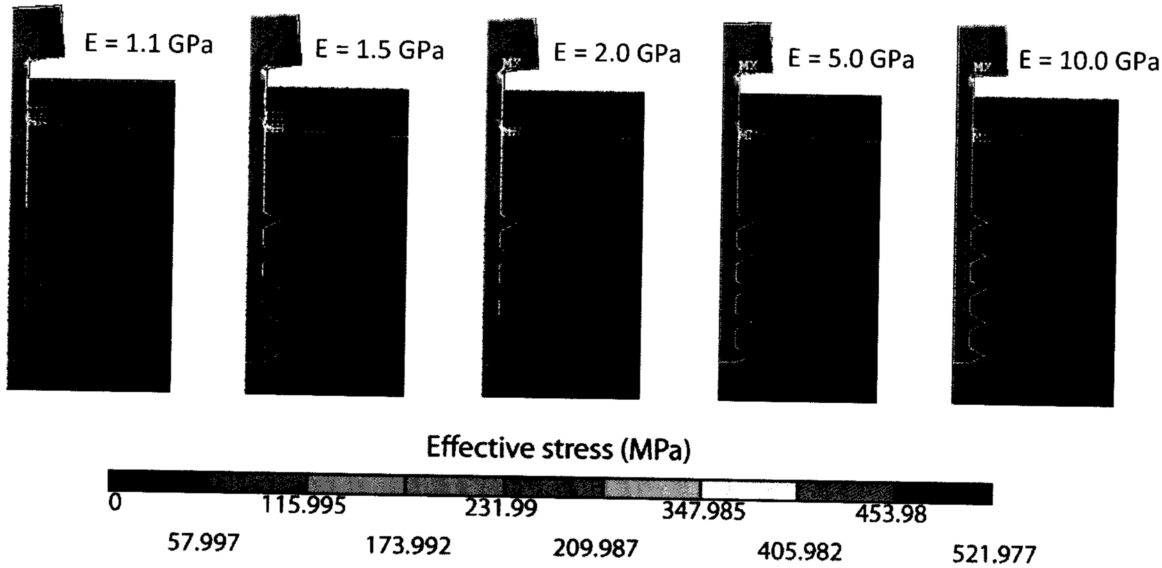

Figure 43: Change in load distribution as the screw's elastic modulus increases

5.4.2 Testing the effect of load magnitude

In order to test the effect of varying the magnitude of the tensile load, a range of loads between 25% higher and lower than the original loading condition (80 N) is applied to the top of the screw head for the configuration resulting in highest STP (triangular shape, 4 mm diameter threads with a long shaft and 9 threads in total). An example of the stress and strain plots obtained from ANSYS for the original 80 N load is shown in Figure 44.

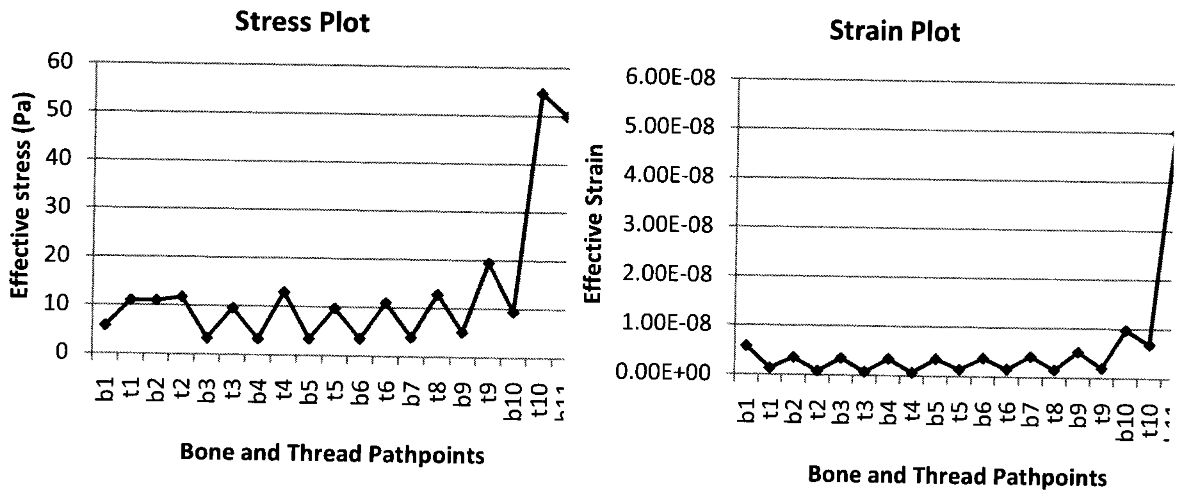

Figure 44: Stress and strain plot for 80 N tensile load

From the above figure it is noted that the stress within the proximal region of bone and screw is higher and more evenly distributed between the two components than in the medial region, where both stress and strain peaks alternate. This is due to the higher stress carried by the threads of the screw, and consequently the higher levels of strain seen in adjacent bone. An increase in both stress and strain occurs in the distal region. This is caused by the nature of the fixed interface and the attempt of the screw to pull away from the bone. As all screw parameters are kept constant, an increase in the magnitude of the load between the aforementioned range does reflect an increased magnitude of the resulting effective stresses and strains, however their distribution between the screw and bone is not affected. This is demonstrated by the results for the extremes of the range of loads analyzed (see Figure 45). For all points along the bone and thread path points the larger tensile force of 100 N results in higher effective stresses than when a tensile force of only 60 N is applied. This difference is more evident beyond the 7th path points in both the bone and screw and is caused by the stress concentration in the distal region of the screw (induced by the fixed contact between the screw and trabecular bulk) as can be seen in the 40 and 105 GPa screw configurations of Figure 45.

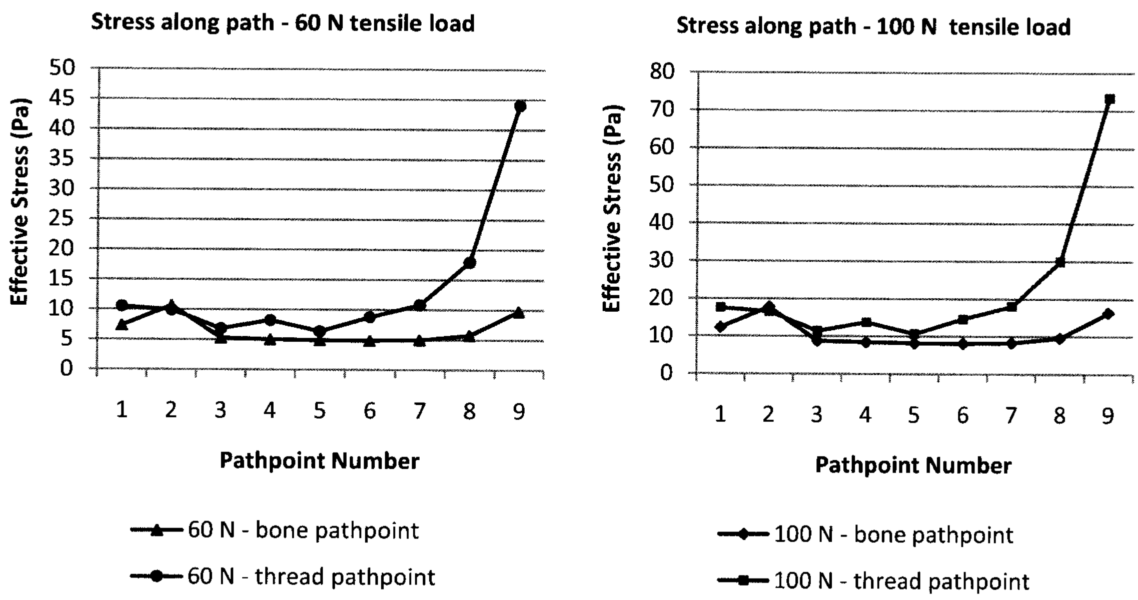

Figure 45: Stresses in bone and threads along the defined path

The resulting effective stresses recorded along the defined path in ANSYS demonstrate a linear increase with an increase in the applied tensile load. This linear relationship is demonstrated in Figure 46 which shows a linear increase for the stress in the bone located between the cortical layer and first thread (path point #1 – see Figure 37), as well as a slightly higher linear increase in stress in the first screw thread (path point #2 – see Figure 37).

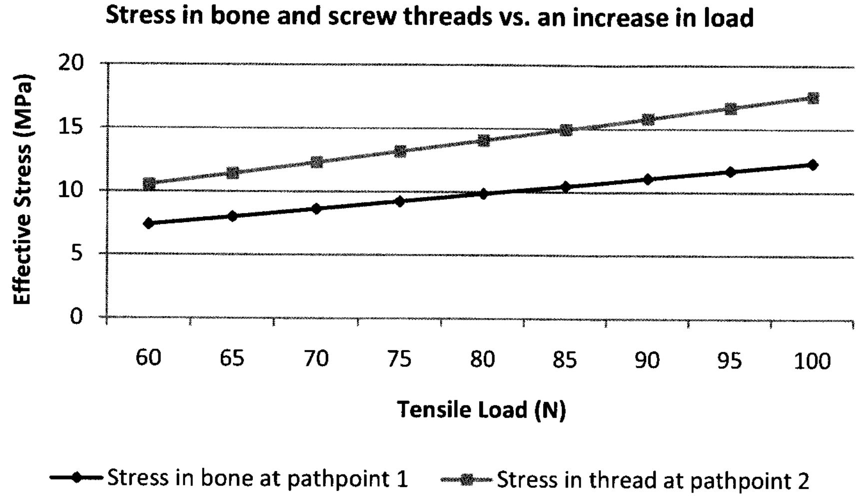

Figure 46: Stress in bone and screw versus an increase in load

Due to this linear relationship between the load and resulting stresses, there is no significant difference between calculated STP and SEDTP results for each of the loading cases. This justifies the use of the original load magnitude, as it does not influence the resulting measures of biocompatibility amongst those configurations varied. Of course, in reality the mechanical stimulus required to initiate the remodeling response operates at a threshold stimulus level. This should be considered in future models wherein a bone remodeling theory would be required. Pull-out testing is utilized, since this load type is the most sensitive to thread design variations, as suggested by Krag et al. (Krag, Beynnon, Pope, Frymoyer, Haugh, & Weaver, 1986). However, this is a simplification as pure pullout loads are not likely to occur *in vivo*, since bending and shearing would occur simultaneously.

5.4.3 Testing the model under a compressive axial load

In order to determine whether the mode of loading has a large effect on the distribution of mechanical stimuli in bone, we test one configuration of the model under a compressive load of 80 N. For this case we removed the fixed constraint from the upper cortical layer of bone, so that the screw head will displace the cortical layer in the negative y-direction, similarly to that of Gefen's study (Gefen, 2002). In Figure 47 the total deformation of the screw-bone model is shown under a compressive load of 80 N and is a similar deformation as seen in previous models (Gefen, 2002).

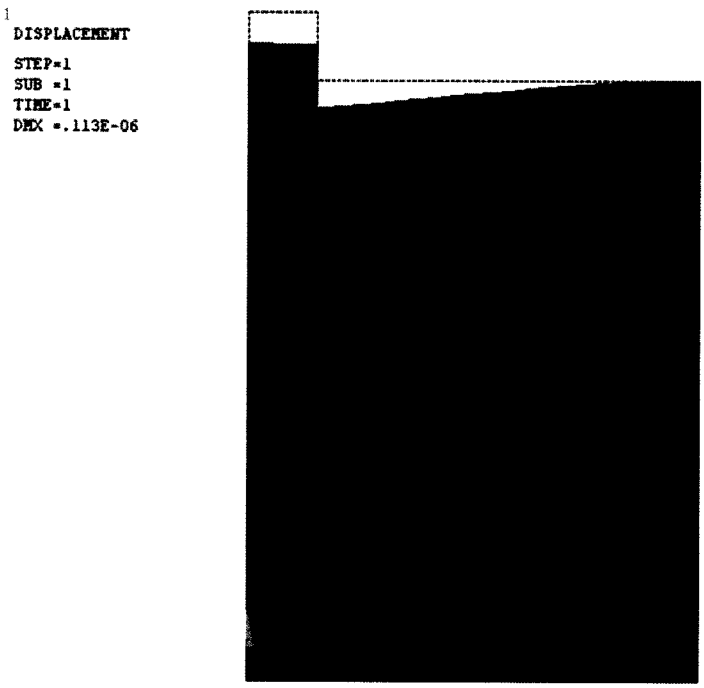

Figure 47: The total deformation of the 2D bone-screw model under a compressive load of 80 N

The results of this simulation are compared to an identical simulation having the same boundary conditions and screw parameters, the only difference being that the 80 N load is applied in the tensile direction. Equivalent stresses and strains are recorded along the defined path as is performed for all other simulations. Results from a comparison of the two loading scenarios reveal identical values at all path-points, for which the nodal equivalent stress distributions for both cases are seen in Figure 48.

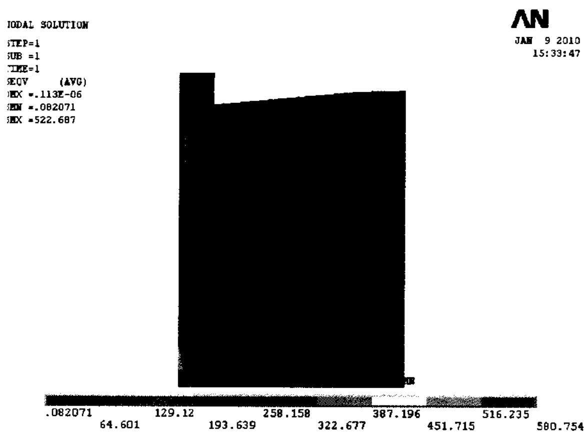

(a) Compressive load of 80 N

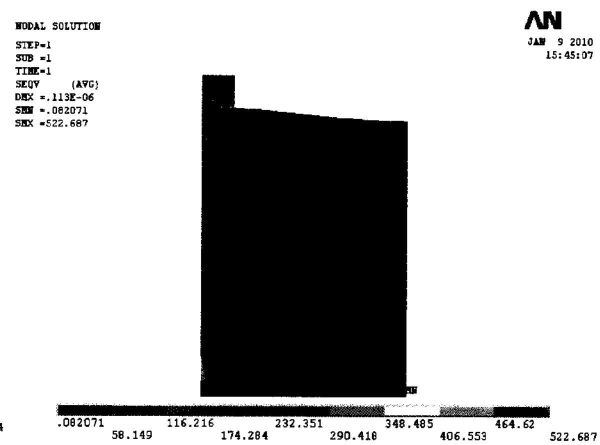

(b) Tensile load of 80 N

Figure 48: Comparison of nodal solutions of equivalent stress for (a) compressive and (b) tensile loading.

Results from this simulation tells us that if all of the model's geometry and boundary conditions are maintained, then an axial force applied to the screw head will result in the same equivalent stress and strain distributions regardless of the direction of the load, i.e. axial or compressive. This may not be the case for all scenarios, for example, when the screw does not share a fixed boundary along all points of contact with the trabecular bulk and cortical region. Calculating STP values for a screw configuration having a triangular profile shape, short shaft, 9 threads, 105 GPa elastic modulus, under this loading scenario and with the altered boundary condition, results in an STP α of 0.316 and an STP β value of 0.159. STP values reported in Gefen's study for the same screw configuration under a tensile load are an STP α of 0.231 and an STP β of 0.082 (Gefen, Computational simulation of stress shielding and bone resorption around existing and computer-designed orthopaedic screws, 2002), which suggests that the two model's boundary conditions must differ. Boundary conditions play a significant role in the accuracy of a model, and future studies should implement contact elements allowing frictional relative movement between the screw and bone interfaces. The bone-screw interface is highly complex *in vivo* and it is unlikely that there would not be any relative motion between the two geometrical bodies (Uhthoff H. K., 1973), as we know from earlier an earlier discussion involving the topic of bone resorption in the vicinity of screws (see Section 4.3).

5.5 Simulation results

The nodal solutions for the equivalent stresses, along with the stress and strain plots for each of the configurations tested can be found in Appendices A-G. The idealized axisymmetric screw-bone model is analyzed as detailed in section 5.2. Resulting STP α, β, and total values are compared in Tables 5 and 6, followed by the corresponding SEDTP values in Tables 7 and 8. Differences resulting between α and β parameters are discussed, followed by detailed results of the effects of changing the initial five screw parameters, i.e. a change in: profile shape, shaft length, thread diameter, number of threads, and elastic modulus. Results for a newly defined and tested parameter, i.e. a change in the screw's root diameter, are then discussed. In order to evaluate strain energy density as a possible measure of biocompatibility, comparisons between STP and SEDTP values are made in each case. The two sets of quantifying parameters cannot be directly compared, as the scale of the SED based values are higher in magnitude by definition; stress multiplied by strain. However, the various screw configurations can be compared based on their relative increase or decrease in resulting biocompatibility. In both cases, higher values are sought as they are, roughly speaking, representative of a higher degree of biocompatibility between the screw and bone.

5.5.1 The difference between α & β values

5.5.1. I STP results

A distinction is made between α and β values in order to demonstrate the importance of the first screw thread, as it is nearest the applied load and therefore experiences higher stresses. Tabulated simulation results using STP α and β calculated values are shown in Table 5 (see Appendix ii: SEDTP results). The highest values for each particular screw configuration in relation to the number of threads modeled are highlighted, which indicates that for the majority of screw configurations α and β values are not always proportional. The values highlighted in red in Table 5 indicate the maximum STP α and β values calculated for all tested screw configurations and reveal the most biocompatible screw, based on the total STP values, as that which has a 5 mm shaft, 4 mm thread diameter, triangular thread profile shape, and a modulus of elasticity of 40 GPa.

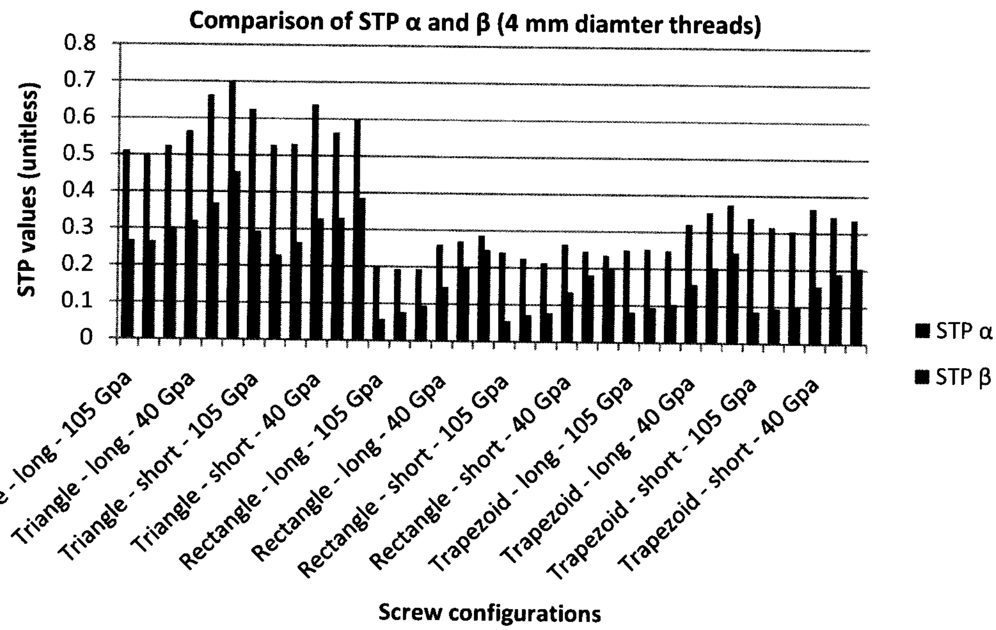

Figure 49: Comparison of STP α and β values for 4 mm diameter thread

From Figure 49, it can be seen that the STP α values are higher than those of the STP β calculations for all cases where the smaller diameter screw thread is employed. Each x-axis label corresponds to a 5, 8, and 9 thread configuration, as represented consecutively by the three pairs of data for each label. A higher STP value indicates a better stress transfer between the screw threads and bone. Therefore, when a smaller diameter screw thread is used the stress transfer between the first thread and the volume of bone above it is better than the average stress transfer between the remaining threads and bone below. On average, for the smaller diameter thread configurations, the STP α values are 18% greater than corresponding STP β values, which is indicative of greater stress shielding in the most distal portion of the screw. A significant difference between these average values is also noticed for the different thread profile shapes tested; specifically differences of 26.1%, 17.4%, and 10.7%, for the triangular, trapezoidal, and rectangular shaped threads, respectively. The thread profile shape clearly has an effect on the stress transfer between the screw and bone and will be discussed further below.

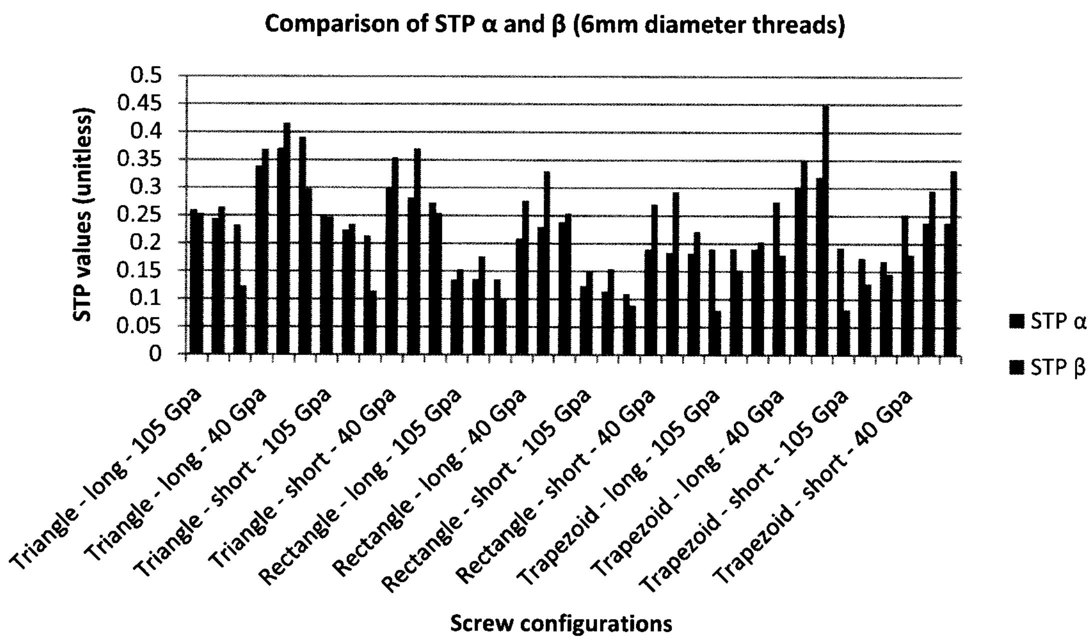

Figure 50: Comparison of STP α and β values for 6 mm diameter thread

The opposite trend is demonstrated in Figure 50 for the majority of cases involving the larger diameter screw threads, where 21 out of 36 cases denote the STP β value as higher than its corresponding STP α value. This indicates a poor stress transfer between the first thread and the volume of bone above it in comparison to the remaining threads, in these cases. However, the average difference between STP α and β values is much smaller, at only 5.6% compared to 18% for the smaller diameter screws. The differences between thread profile shapes are much smaller as well, with differences of 4.8%, 5.0%, and 7.0%, for triangular, rectangular, and trapezoidal shaped threads, respectively, compared to 26.1%, 17.4%, and 10.7%, for the smaller diameter screws. Not only are the differences between α and β values smaller for the larger diameter screws, but in some cases the STP α value was higher than that of the STP β value. This suggests that there is a more even load distribution throughout the length of the screw.

When a larger diameter thread is used the volume of bone between the threads is increased, therefore resistance to screw pullout should be increased. There should also be a more even stress transfer that develops between the screw and bone since the tensile load remains constant as the surface area between the screw threads and bone is increased. The stress concentrations developing at the thread and inner shaft intersecting area, however, may increase. This is discussed further in Section 5.5.5.

5.5.1. II SEDTP results

In order to investigate the differences between using stress and strain energy density as mechanical stimuli responsible for the initiation of bone remodeling, SEDTP calculations are compared to the results obtained using STP values (see Appendix ii: SEDTP results). Since both STP and SEDTP values are measures of the biocompatibility of screw configurations in bone, they should yield similar results. Tabulated simulation results calculated using SEDTP α and β values can be seen in Table 7. The highest SEDTP values for each particular screw configuration, in relation to the number of threads modeled, are highlighted. The values shown in Table 7 highlighted in red, represent the maximum SEDTP α and β values calculated for all tested screw configurations (see Appendix ii: SEDTP results). The best parametric configuration based on the values obtained using total SEDTPs (see Table 8), is the trapezoidal, short-shafted, higher modulus, smaller diameter thread, screw having only 5 threads.

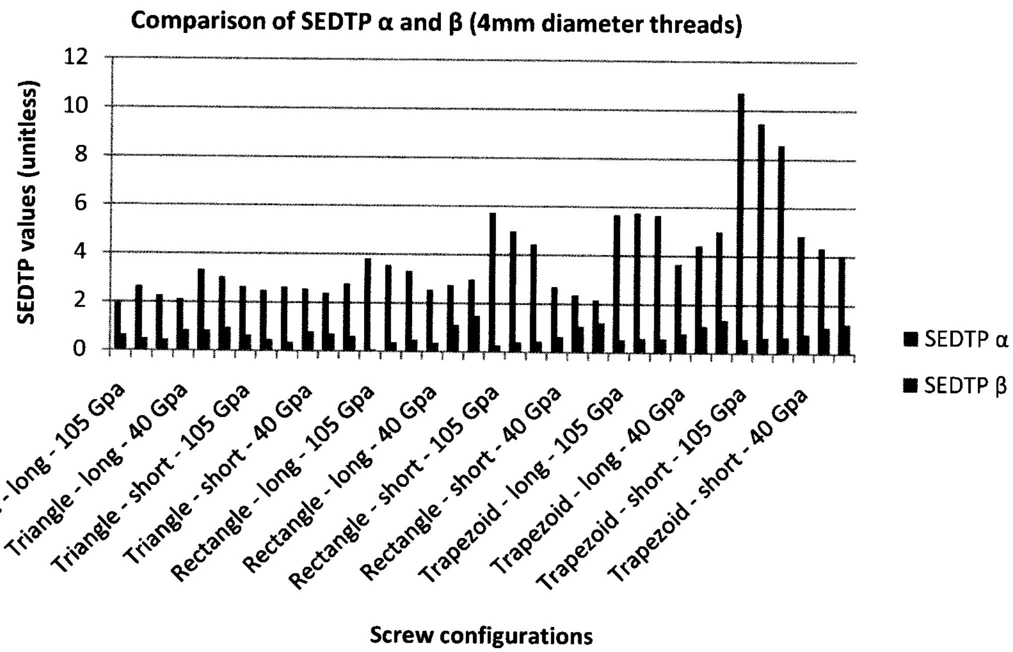

Figure 51: Comparison of SEDTP α and β values for 4 mm thread diameter

From Figure 51, it is noted that the SEDTP α values are higher than those of the SEDTP β calculations for all of the 4 mm thread diameter configurations, as previously demonstrated by the STP α and β values. Since, by definition, SEDTP values are unitless and cannot be related in terms of percentages of a total value. Therefore, the average SEDTP α value is 3.29 unitless measures higher than its corresponding SEDTP β value. Due to the definition of SEDTPs, the optimal magnitude is no longer 1; however, higher values are still indicative of increased biocompatibility of screws. Therefore comparisons are made between the relative differences of SEDTP values. This result indicates that for a smaller diameter screw thread less stress shielding occurs (SEDTP values are higher) near the first screw thread with respect to the other screw threads. There is also a significant difference between the SEDTP α and β values for the different profile shapes tested: 1.91 for triangular; 2.77 for rectangular; and 5.18 for the trapezoidal profile shaped threads. Profile shape, therefore, has a definite effect on the stress transfer between the threads and surrounding bony tissue, as well as, on the local strain.

A larger diameter screw thread results in higher levels of stress shielding nearest the first screw thread, as opposed to subsequent threads in the majority of cases (see Figure 52). As in the case of STPs, a similar percentage of the larger diameter (6 mm) configurations demonstrates that the

SEDTP β value is higher than the corresponding SEDTP α value (in 22 out of 36 cases). However, the configurations that demonstrate this behaviour are different between the two quantifiers.

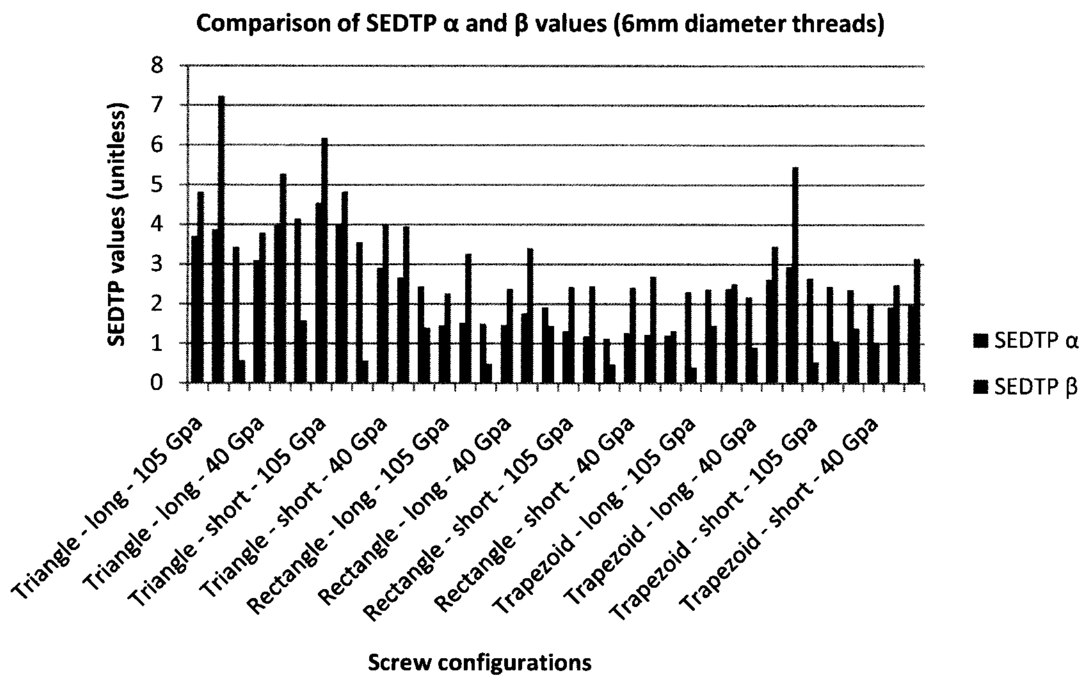

Figure 52: Comparison of SEDTP α and β values for 6 mm diameter thread

The average difference between SEDTP α and β values is 1.33 for the 6.0 mm thread diameter cases as opposed to a difference of 3.29 for the 4.0 mm configurations, which is 57.6% below and 142.4% higher than the total average difference for all configurations, respectively. The differences between thread profile shapes are much smaller as well with differences of 1.73 for triangular, 1.03 for rectangular, and 1.23 for trapezoidal shaped threads. These differences include the 14 cases where the STP α value was higher than that of the STP β value, yet suggests that there is a more even load distribution throughout the length of the screw.

As demonstrated previously with STP measures, the use of a larger diameter thread increases the resistance to screw pullout. A change in profile shape and number of threads also has an effect on the biocompatibility of a screw. A definite decrease in stress shielding is noted with a reduction in elastic modulus. Most of these results are in agreement with results obtained by previous researchers, who suggest that a critical magnitude of screw stiffness exists (Gefen, 2002; Nunamaker & Perren, 1976).

5.5.2 The effect of varying thread profile shape

5.5.2.1 STP results

The triangular shaped profile threads produce an average total STP value that is 35.8% higher than a rectangular shaped profile thread, and 27.4% higher than that of the trapezoidal shaped profile thread. This result suggests that the triangular profile shape is more biocompatible in terms of stress transfer between the screw and adjacent trabecular bone. There are some exceptions, however, (i.e. the long-shafted 6 mm diameter thread configurations with 9 threads) where the trapezoidal profile shaped thread results in the highest STP value. This discrepancy may be due to the nature of the discretized model, as an average value for effective stress is measured across the element where the path point is located. The rectangular profile is the least biocompatible thread shape in this sample set, except in the case of the larger diameter, where only 5 threads are used. The difference in STP values between the triangular shaped profile thread and the rectangular and trapezoidal shapes is much more pronounced for the smaller diameter threads. For example, the average triangular STP value is 53.1% higher than the average rectangular STP value for a 4 mm screw thread diameter, and 18.5% higher than the 6 mm diameter configuration. This demonstrates the interdependent nature of the profile shape with the thread diameter, which is logical as they both critically alter the thread shape and volume of the bounded host material. For each of the isolated thread profile shapes the STP α values are consistently higher than the STP β values. These differences are 13.4%, 3.4%, and 9.3% for the triangular, rectangular, and trapezoidal profile shaped threads, respectively. This suggests that a change in profile thread shape does affect the stress distribution along the length of the screw shaft. Previous analysis by others, under compressive loading, concluded that better biocompatibility results from using a trapezoidal shaped profile thread (Gefen, 2002). Therefore, a comparison of the two loading conditions should be made in a future study to determine if a particular thread shape is more susceptible to stress shielding under tensile or compressive loading. From our analysis in Section 5.4.3 it is clear that differences between our reported results and those of Gefen's study are influenced by differences in our boundary conditions more so than the direction of loading. Although both studies are simplistic in geometry and material properties, it is arguable, that our boundary condition maintaining zero displacement on the upper cortice is more realistic than a severe displacement of the bone, as is seen in Gefen's model.

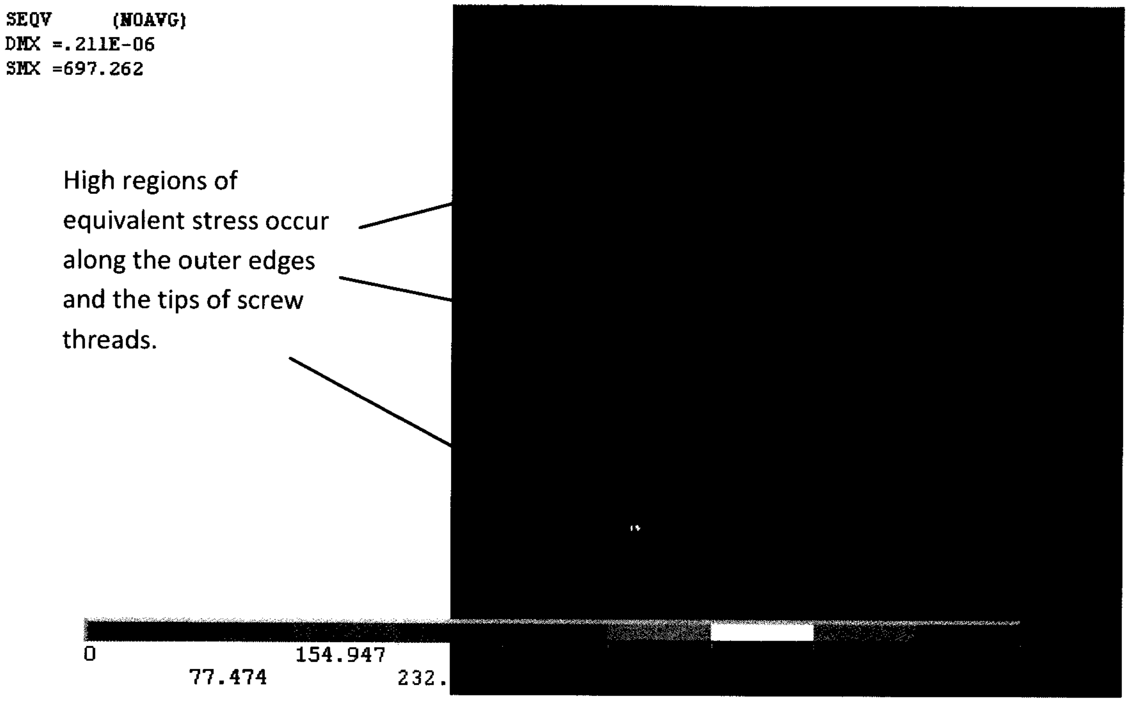

Figure 53: Detail of nodal average solution of equivalent stress along thread contour

A study by King and Cebon involving pullout tests *in vitro* using human bone samples reveals that the mode of failure of bone occurs in fractured layers one pitch in thickness (King & Cebon, 1992). The fractures stemmed radially from the major diameter of each screw thread, which is suggestive that the highest stress transfer occurs at the tip of the V-shaped threads. This result corresponds well with results from this study for the triangular threaded configurations (as seen in Figure 53) that suggest a higher biocompatibility with this type of profile head based on STP results. Similar distributions are seen in a 2D FE model that analyzes the effects of size and contour shape with respect to peak stresses in bone (Hansson & Werkeb, 2003). A 3D FE model of a solid screw dental implant (Eraslan & İnan, 2009) also shows a similar dependence between the screw contour and the resulting stress distribution, suggesting that although our 2D model, although geometrically simplistic, may be able to predict trends on a qualitative level.

5.5.2. II SEDTP results

The highest resulting average total SEDTP value is the trapezoidal shaped profile thread at 5.58, followed by the triangularly shaped profile thread at 5.21, and then the rectangular shaped profile thread with an average value of 3.80. Unlike results calculated using STP values, the SEDTPs reveal that the trapezoid is the preferred thread profile shape when used in conjunction with a smaller diameter screw thread. For the larger diameter screw thread, i.e. 6 mm, the triangular shape results in higher SEDTP values, except for the case of 9 threads, where the trapezoidal shape is again preferred in all but one case. Although, the average results from both the STP and SEDTP calculations yield the rectangular profile shaped thread as the least favorable in terms of biocompatibility, in some of the configurations for the SEDTP, they are actually better than corresponding trapezoidal threads (i.e. in those cases of a smaller number of screw threads and a larger thread diameter). There exists an interdependent nature between the choice of thread profile shape and the thread diameter which is demonstrated in the above in Figures 47 and 48 and through a calculation of the averages between thread diameters. For example, the trapezoidal shaped threads demonstrate a significantly higher average SEDTP value for the smaller diameter thread, i.e. 4 mm, with 2.52 dimensionless units above the larger diameter configuration. The opposite is true for the triangular configuration, which demonstrates on average a difference of 3.99 measures higher than the small thread diameter configurations. The rectangular configuration demonstrates a much smaller average difference of only 0.62 higher for its smaller diameter cases. For each isolated shape the total average STP α values are consistently higher than the STP β values, the most influential being that of the trapezoidal profile shaped threads. This suggests that a change in profile thread shape does affect the stress distribution along the length of the screw shaft. This result is in agreement with the analysis performed by Gefen, who concluded that under compressive loads, better biocompatibility results from using a trapezoidal shaped profile thread (Gefen, 2002).

5.5.3 The effect of varying the number of screw threads

5.5.3. I STP results

Isolating for a change in the number of screw threads reveals an average STP value of 0.499 with the use of 5 threads, 0.526 for 8 threads, and 0.521 for 9 threads. This demonstrates that there is no significant difference in altering the threads between 8 and 9 threads; however there is a small increase in average STP values between the use of 5 and 8 threads. When comparing between average values relating to the thread profile shapes, no direct conclusion can be drawn. For example, the average values decrease slightly for the triangular profile shape, and increase using the trapezoidal profile shape. Therefore, increasing the number of threads does not seem to have an independent effect on biocompatibility, but rather is dependent on those other parameters tested. Results from the compressive load study done by Gefen demonstrated that an increase in the number of screw threads yielded a more continuous stress transfer between the screw and bone; a 21% increase when increasing the threads from 5 to 9 (Gefen, 2002). Considering that the increase between 5 and 9 threads is only 4.4% in this study, the difference in results is significant and should be explored with further testing to determine whether the behavioral differences is due to the nature of loading or other boundary conditions. Future studies should include a deeper trabecular bulk, as the results using 9 threaded configurations are affected by the proximity of the most distal path points to the fixed boundary layer. Differences in results also stem from the fact that previous studies kept the overall length of the screw constant, whereas an increase in threads count in this study effectively increases the length of the screw's engagement into bone (Gefen, 2002). In other words pitch, which is kept constant in this study, should be varied and decoupled from other parameters in a future study.

5.5.3. II SEDTP results

The average values associated with an increase in the number of threads, are as follows; 4.83 for 5 threads, 5.35 for 8 threads, and 4.41 for 9 threaded configurations. This result demonstrates that there is a slight increase in biocompatibility between the use of 5 and 8 threads and there exists an average peak value with the use of 8 threads, which is in accordance with the result demonstrated by the use of STP values. The anomaly in results is, again, due to the proximity of the fixed boundary layer to the path points when testing the 9 threaded screws. There is no significant difference between the 4 mm and 6 mm diameter thread averages. When isolating for the three thread profile shapes, we find that the average total SEDTP values vary for each shape. For example, the triangular and rectangular shaped threads result in a peak average value with the use of 8 threads, whereas the average trapezoidal shaped thread values increase linearly with increasing number of threads. Overall, increasing the number of threads does not seem to have an independent effect on biocompatibility, but rather is dependent on those other parameters tested.

5.5.4 The effect of varying the shaft length

5.5.4. I STP results

The shaft length between the cortical layer and first screw thread, referred to as the shaft length, is altered between 1 and 5 mm. From Figures 42 and 43 one can see that there is little difference between the long shaft configurations which generally demonstrate higher STP values than their corresponding short shaft configurations. The longer shaft length results in an average value that is

3.5% higher than the short shaft configurations. Comparison between average values resulting from the 4 mm and 6 mm diameter screw threads reveals that there is not a significant difference between STP values for a change in the shaft length for the shorter diameter, however there was an increase of almost 7% for the larger diameter. Overall, isolating for shaft length does not demonstrate a distinct change in biocompatibility. This result is to be expected, as varying the shaft length does not affect the shape of the screw thread or the volume of bone compressed between the threads and there is no stress transfer directly between the shaft and the bone. For results pertaining to compressive loading, previous studies found that the short shaft models produce significantly higher STP values (32% higher on average) and that local internal stresses within the first thread were greater (Gefen, 2002). This would be the expected result, since the first thread is under the greatest amount of stress, as it is closest to the applied load. As well, stress is transferred through the threads of the screw to the bone and not through the shaft, indicating that a longer shaft length will transfer less stress in the proximal region of the screw. This should be avoided, as less mechanical stress transferred to the bone will lead to more bone resorption over time. This discrepancy between our results and those of previous studies is due to the definition of the path points. In the previous study, Gefen does not specify whether or not the path points are at a fixed distance from the screw threads (Gefen, 2002). In this study, the first path point in bone is located at the mid-point between the cortical region and the first thread, which changes in correspondence to the specified shaft length, i.e. 1 or 5 mm.

5.5.4. II SEDTP results

When isolating for the effect of varying the shaft length between the cortical layer and the first thread between 1 and 5 mm, no significant difference between the average values results. Upon averaging these totals, with respect to the thread diameter, it is noted that there is a slight decrease in SEDTPs for the small thread diameter, i.e. from 5.14 to 4.86, and a slight increase in SEDTPs for the larger diameter thread, i.e. from 4.61 to 5.40. When comparing the shaft length values in terms of α and β, the result appears to be relative to the volume of bone bound between the cortical layer and the first screw thread, in which case the shorter shaft tends to result in better SEDTP values, signifying a better strain energy density transfer between the thread and bone. Overall, isolating for the effects of an increase in shaft length does not demonstrate a significant change in biocompatibility but it does indicate a dependency on the other parameters, as is also demonstrated using STP values.

5.5.5 The effect of varying the screw thread diameter

5.5.5. I STP results

The screw thread diameter is tested for 4 mm and 6 mm configurations, for which all configurations employing the smaller screw thread diameter demonstrate a higher STP value than their corresponding larger thread diameter configurations. The average STP value for the 4 mm configurations is 11.7% higher than for the 6 mm average value. This suggests that the use of a smaller diameter screw promotes a more even stress transfer between the threads to the bone which results in less stress shielding and subsequent bone loss. Upon closer inspection, average values in relation to respective profile shapes reveal that a significant difference does not exist between the smaller and larger diameter averages for the rectangular and trapezoidal shaped profile threads. On the other hand, there is a 33% higher average STP value for the triangular 4 mm configurations in comparison with the 6 mm configurations. Therefore, it seems as though the effect of the thread diameter is largely dependent on profile shape. As previously mentioned, the effect of thread diameter is also more apparent for the STP α values in comparison to the β values, for all of the profile shapes analyzed. When comparing the average values in relation to an increase in the number of threads employed, the 4 mm screw diameter configurations all reveal a higher average value; however there was no significant difference with a change in the number of threads. These results indicate that an increase in thread diameter generally increases STP results; however there is a general dependence on the other parameters, particularly the profile shape which is effectively changed when increasing the outer diameter, in our case. Results from previous studies demonstrate a similar interdependent nature, yet the biocompatibility contrarily decreased for the case of the trapezoidal shaped threads (Gefen, 2002). This is due to the differences in loading and boundary conditions between the studies.

5.5.5. II SEDTP results

An increase in the thread diameter, between 4 and 6 mm results in a more varied effect than demonstrated for STP values. The total average value of the 6 mm thread diameter is higher than the 4 mm thread diameter, but overall, this trend is highly dependent on profile shape. For instance, in the case of triangular shaped threads, the larger diameter configurations produce higher SEDTP values, whereas the trapezoidal shaped threads result in the opposite trend (however, to a lesser degree). Rectangular shaped threads demonstrate the least amount of change between thread diameter configurations. This result is similar to the results gained from STP values, where there is no significant difference between the smaller and larger diameter averages for the rectangular and trapezoidal shaped profile threads. On the other hand, the large increase in STP value between when the thread diameter is decreased from 6 to 4 mm is the opposite of what is demonstrated for the SEDTP results, where there is a large increase in average values for an increase in thread diameter (average values range from 3.22 to 7.21 for 4 and 6 mm configurations, respectively). As previously mentioned, the differences between SEDTP α and β values are greater for the smaller diameter threads in comparison to the larger cases, signifying better conditions for the first thread with a smaller diameter. Increasing the outer screw thread diameter effectively changes the profile shape of the screw and increases the contact area shared between the screw and bone, which is why there is high dependence on profile shape for this parameter. In a future study the pitch angle should be decoupled from the outer diameter parameter in order to gain a better idea as to which factor has more of an influence in the mechanical stimuli distribution.

5.5.6 The effect of varying the screw's modulus of elasticity

5.5.6. I STP results

For all of the screw configurations analyzed, a reduction in the modulus of elasticity of the screw from 105 GPa to 40 GPa results in an increase in total STP value. The average total STP value calculated for the 40 GPa screw is 20% higher than the average value calculated for the 105 GPa screw. Therefore, using a screw with a lower elastic modulus results in a better stress transfer between the screw and bone, thereby reducing stress shielding. This result is in agreement with the results found by Gefen, who demonstrates an average increase of 35 % in STP values obtained for a similar decrease in stiffness (Gefen, 2002). Our average value is 15% lower, however, mainly due to the differences in path points, loading, and that our length of engagement changes for an increase in the number of threads. Reducing the screw's elastic modulus also tends to have a lower influence on the STP values of screws having a smaller diameter in comparison with the larger diameter. The average increase in STP for the 4 mm diameter screw threads is 16.9% as opposed to a 23.1% increase for the 6 mm diameter screws. Previous work demonstrates similar reductions in stress shielding under compressive loading (Gefen, 2002) (Goel, et al., 1991). These results indicate that the structural stiffness of bone screws, which is defined as the product of the elastic modulus multiplied by the cross-sectional area, is a critical magnitude in determining the level of resultant stress shielding under both tensile and compressive loading.

5.5.6. II SEDTP results

When decreasing the screw's elastic modulus between 105 GPa and 40 GPa, the higher modulus screw actually produces a higher average total SEDTP value. This result is not expected, as it is demonstrated by the STP results and from previous research, that a decrease in the difference between stiffnesses will reduce the level of resultant stress shielding (Gefen, 2002). For the case of SEDTPs, the effects of this parameter tend to be interrelated to other parameters. For example, in the case of the triangular profile shaped threads having an outer thread diameter of 4 mm, the 40 GPa screws produce higher SEDTP values than the 105 GPa screws. The opposite is demonstrated by the same configurations with a larger diameter thread for the case of 5 and 8 screw threads. This discrepancy is due to the nature of the defined path points. The effective strain values are smaller when bound within a larger volume, i.e. when using the 6 mm diameter threads. Considering that the materials are simplified as isotropic homogenous materials, then, according to Hooke's law, when the modulus of elasticity of the screw is increased the resulting strain will decrease under a constant stress state. Considering that, when testing with a 1 GPa screw (the same modulus of elasticity as that of the trabecular bulk), both the screw and bone act as a single material, the optimal value is close to unity. Measurements of effective strain within the model may not accurately represent the deflections of the geometry as discontinuities in the model may affect the average nodal values recorded. Measurements of the differences in strain (a scalar value) or direct measurement of strain energy would eliminate this type of behaviour and should be considered in future studies.

5.5.6 The effect of varying the screw shaft diameter

As a newly defined and tested parameter, a change in the screw's shaft diameter is analyzed. In order to determine the effects of this parameter on the level of resultant stress shielding, the shaft diameter of the most biocompatible configuration based on STPs is altered. The triangular configuration incorporating the long shaft, 40 GPa elastic modulus, the 4 mm smaller diameter thread, having 9 threads in total results in the highest total STP value. This configuration is subsequently representative of having the lowest level of stress shielding under the applied tensile loading condition. The radius of the screw shaft ranges between 1.0 mm and 4.0 mm in the half-model analyzed. Results are calculated using both STP and SEDTP parameters and are compared in the following figures.

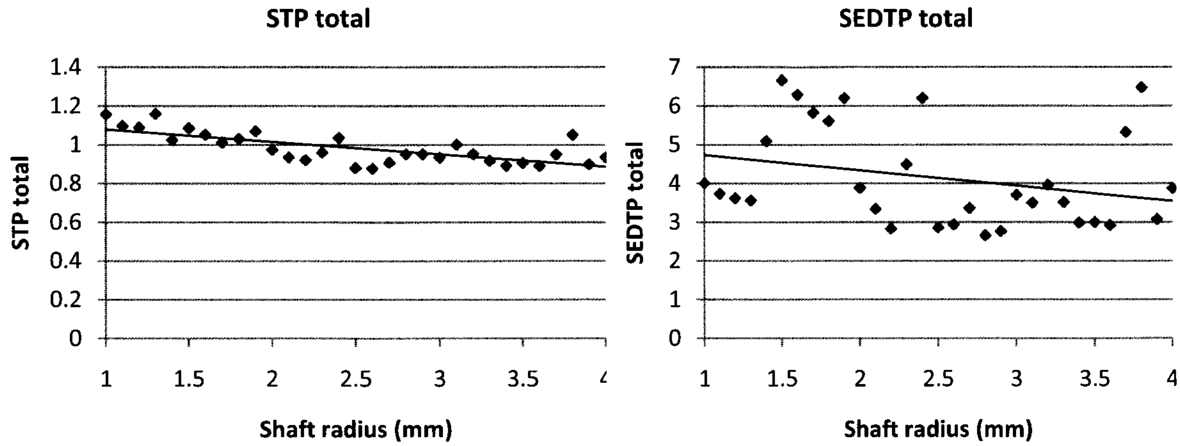

Figure 54: Total STP and SEDTP values for a change in shaft radius

As seen in Figure 54 increasing the screw's shaft radius results in an overall decreasing trend in STP values. A decrease is also seen using SEDTP values, however, there is much greater deviation in these results, possibly due to the nature of using strain as a quantifier, since it can lead to singularities in a static analysis. From the STP results we can conclude that a greater shaft radius causes an increase in the level of stress shielding. This is demonstrated by both STP α and β values as seen in Figure 55. Since the STP β values are lower than the STP α values, stress shielding is more apparent in the distal portion of the screw.

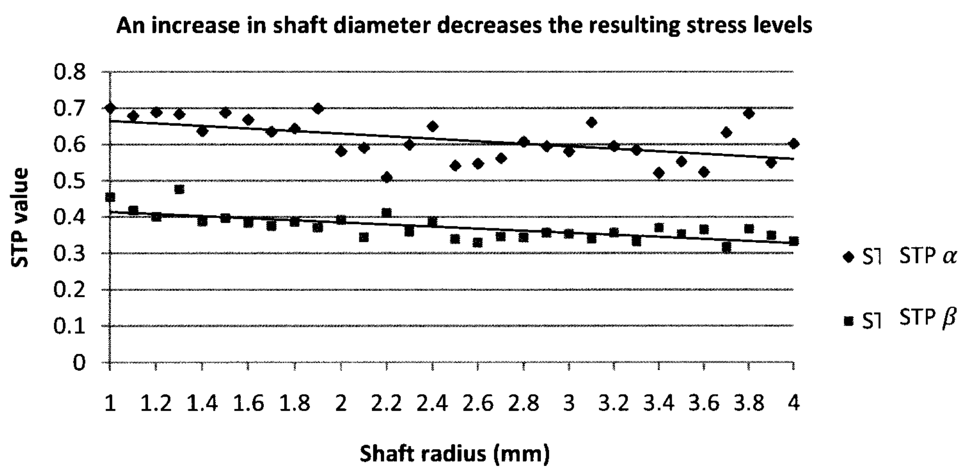

Figure 55: STP trends for an increase in shaft diameter

The use of a larger diameter screw shaft results in a greater level of stress shielding and therefore should be avoided. However, a balance between the screw's root diameter and its required resistance to bending must exist.

5.6 Conclusions

The bottom line of this research is to gain insight into the open question of bone-implant interactions. A general conclusion that can be derived from the results obtained using STP and SEDTP as quantifying measures of biocompatibility is that changing the screw parameters has a definite effect on the relative level of resulting stress shielding in bone. In all cases where the smaller diameter screw thread is modeled and for the majority of larger diameter cases, resulting STP and SEDTP α values are larger than the corresponding STP and SEDTP β values, respectively. This demonstrates the importance of the holding power of the first thread in cancellous bone.

From the observations of STPs discussed, we can conclude that in order to minimize the effects of stress shielding in bone adjacent to the screw: (a) a triangular profile shaped thread is preferred over a trapezoidal or rectangular shaped thread; (b) the number of threads should be increased in order to promote a more even stress transfer between the screw and bone; (c) a longer shaft length (from the screw head to the first thread) should be used; (d) a smaller diameter thread should be used; (e) and most influentially a screw with a reduced modulus of elasticity should be used.

Results from the SEDTP calculations did not reveal any independent parameter trends. However, based on SEDTP results, stress shielding can be limited by: (a) implementing a trapezoidal profile shaped thread when used with a smaller diameter screw thread or a triangular shaped profile thread when used with a larger diameter screw thread; (b) increasing the number of threads if a smaller diameter screw thread is used; (c) using a short-shaft and a larger diameter if using rectangular or triangular shaped profile threads.

Further investigation into this distinct difference between the strain energy density and stress-based results is ongoing; however this result may suggest that all parameters are dependent which is sensible from the bone remodeling point of view. Similar trends do result from average values (for 5, 8, and 9 threads) between STPs and SEDTP, suggesting that the variation due to strain may play a role in the individual discrepancies. Due to the scale and nature of testing screws *in vivo*, current reviews of related literature reveals little information directly related to quantifying stress shielding in the vicinity of bone screws. Future experimental testing of our parameters in relation to stress shielding is necessary to verify our theoretical results and would be a good basis for creating experimental methods.

The newly tested parameter involving an increase in the inner screw shaft diameter produces a decrease in both STP and SEDTP values. This indicates an increase in stress shielding when a larger screw shaft diameter is used. Since a larger screw shaft would effectively remove more bone upon insertion, the minimum screw shaft size that supports the required strength of the screw should be used. Cadaveric pullout tests by Krag and co-workers suggest that the minor diameter is a significant variable influencing pullout strength, but that it is also dependent on the outer thread diameter (Krag, Beynnon, Pope, Frymoyer, Haugh, & Weaver, 1986). According to our STP results, a smaller outer thread diameter results in less stress shielding. Therefore both the inner and outer diameters should be limited, however, not to a size that would also affect the pullout strength. A future directive of this work should be to optimize the screw parameters in order to minimize stress shielding and maximize the holding power.

Consistency in the modeling approach must be obtained in order to use comparative evaluation measures such as STP and SEDTP. In this way, parameters can be isolated and rated based on their respective biocompatibility. These dimensionless parameters may be a good approach for universally rating the design of bone screws. Ultimately, this type of comparative approach can be transferred to a more complex three-dimensional model which will eventually provide more realistic predictions of resultant stress and strain, and quantitative predictions of stress shielding.

5.7 Discussion

Although it is a good indicator of the holding power of screws, pullout testing does not provide information about the stress distributions in adjacent bone, and so cannot be considered as a determining factor for the altered bone remodeling in the vicinity of an implant. The problem of fixation failure due to loss of clinical stability via screw avulsion is well known, and according to some researchers is greatly attributed to stress shielding (Be'ery-Lipperman & Gefen, 2006). As discussed in Section 4.3 excessive bone resorption in the vicinity of an implant may occur if following the initial resorption of necrotic bone, insufficient mechanical stimuli exists to stimulate a bone remodeling response. Therefore, it seems necessary and crucial to analyze the transfer of mechanical stimuli along the bone-screw interface and to determine which factors are greatly attributed to bone loss in the vicinity of screw threads. For this reason, a variety of screw configurations are compared in this study by their level of biocompatibility as measured by the two defined criteria: stress and strain energy density transfer parameters.

Unlike some previous models, our model applies a tensile load to the screw in a simulated pullout scenario. Peak stress regions are located in the distal third of the screw for tensile loading, as the screw threads tempt to displace vertically upward subsequently causing larger stresses in those regions of adjacent bone (see Figure 53) (Schuller-Gotzburg, Krenkel, Reiter, & Plenk Jr., 1999). Three-dimensional simulations by Zhang and co-workers reveal that the pullout force is nearly evenly distributed throughout the bone, whereas peak stresses in the screw are at a maximum in the first two threads closest to the head (Zhang, Tan, & Chou, 2004). This result is not intuitive, since some of the load should be transferred through the screw threads to the bone, which should result in a linear decrease along the longitudinal direction of the screw and applied load. The study performed by Gefen, under a compressive axial loading condition, demonstrated peak stresses within or immediately above the first bone thread, which is logical as the stresses would be closest to the applied loading area (Gefen, 2002). These stresses tend to increase as the length of the screw's shaft is decreased, which is also intuitive, as the inclusion of a thread closer to the cortical bone layer compresses the volume of trabecular bone and develops stress concentrations in the region. Documented clinical failures have reported screw failure occurring in the screw shaft proximal to the head (Chen, Chang, & Lin, 2001). However, failure is generally caused by bone shearing with little or no damage to the screw (Zhang, Tan, & Chou, 2004).

Although the magnitude of the load applied to the screw in this study seems arbitrary, it is within the range of physiologically applied screw loads, as is discussed in Section 5.2. The aim is to demonstrate the nature of stress transfer between the screw and bone during axial tensile loading, opposed to previous studies that focus on compressive loading (e.g. (Gefen, 2002) (Zhang, Tan, & Chou, 2004)). A sensitivity analysis that test the effect of varying the magnitude of the pullout force by up to 25% results in negligible changes in STP and SEDTP results.

For all of the screw configurations tested in this study, the general pattern of stress that results is one linearly decreasing distribution from the screw head down the shaft (see Figure 42). However, with the use of 8 and 9 screw threads in particular there is a tendency for the stresses to be highest in the most distal region due to the nature of the fixed boundary condition between the bone-screw interface and due to the proximity of the boundary of the trabecular bulk. Future studies should include a larger trabecular bulk as to not interfere with the stress distribution in the distal portion of the screws. As well, in order to simulate more realistic strain in bone and relative motion between the screw and bone, a layer of gap elements should be generated at the interface.

Evidence from histomorphological data collected by Schuller-Gotzburg and co-workers during the re-operative retrieval of screws from the mandible of two patients presents valuable information regarding stress shielding in bone at only 3 months post-implantation (Schuller-Gotzburg, Krenkel, Reiter, & Plenk Jr., 1999). Images presented by these researchers show that the majority of bone resorption takes place around the tip of the triangularly shaped screw threads and that there is a distinct gap between the screw and bone in the distal third. The images also showed little resorption directly under the screw heads, which is in agreement with the findings of this study, which suggest that the stress transfer between the first thread and bone is generally better than the more distal screws. Results from other studies also demonstrate the highest regions of stress in the most proximal region of the first screw thread (Gefen, 2002). These findings suggest that the majority of the mechanical stress is transferred to the bone volume compressed between the first thread and the cortical layer, and that the remaining threads only carry a small portion of the load leaving the distal portion of bone susceptible to excessive resorption, and possibly subsequent screw loosening.

Our results, using STPs and SEDTPs as quantifying measures of biocompatibility, demonstrate the interdependent nature of most of the screw parameters tested. The only independent parameter tested is that of a change in modulus of elasticity, where a decrease in the screw's modulus of elasticity results in less stress shielding. This result is to be expected since a smaller difference between the moduli of elasticity of bone and screw results in a more evenly shared load. A comparison to results obtained from previous work (Gefen, 2002) demonstrates a good correlation between results using STP values (see 5.5.6. I).

According to researchers, an increase in thread number and density (reduced pitch) reduces the stress concentrations in the region of the first thread (Zhang, Tan, & Chou, 2004). According to our results, increasing the number of screws between 5 and 9 generates a slight increase in the biocompatibility of the screw, but the effect is highly dependent on other parameters. It is noted that the stress distribution between the screw threads and bone are more evenly distributed and that the peak stresses in the screw tips (particularly for the triangularly shaped profile threads) decrease with a longer screw containing more threads. Additional evidence is provided by Gefen's results that demonstrate a similar reduction in peak stresses and a distinctly better stress transfer to bone when eight or more threads are employed (Gefen, 2002). The more pronounced biocompatibility shown in previous works, for instance, (Gefen, 2002), is a result of the compressive loading and boundary conditions used, therefore future testing under a variety of loading conditions should be performed in order to substantiate that these findings are valid under more realistic loading scenarios.

Comparing the ratio between the stress in bone and screw under the applied loading condition is an effective method for comparing the biocompatibility of various screw parameters. The ability to easily change and isolate design parameters in a FE model allows for the prediction of relative stress transfer behaviours when tested within a controlled manner. However, the results indicated by the stress transfer parameters can only be used for qualitative analysis purposes. This is demonstrated in Gefen's model where the effects of varying screw parameters are compared between an idealized model and a femoral head model through which the relative rating system remains unchanged. The femoral head model produces significantly larger STP values indicating that a more realistic model actually indicates greater biocompatibility between the screws and bone than for an idealized model (Gefen, 2002). Since the nature of loading in bone is quite complex, it is expected that *in vivo* conditions would generate higher stress transfer between the screws and bone. When loading is restricted to the screw's longitudinal axis stress is generally transferred laterally through the screw threads. However, when complex loading is involved, stress transfer will most likely occur not only through the thread tips but throughout the entire thread profile. Future *in vivo* testing is necessary to provide experimental validation of predicted stress shielding for the various screw types.

The use of ANSYS APDL and the simplified two-dimensional nature of the model allows for ease in the alteration of the parameters tested. Since the boundary and loading conditions are kept constant, the results obtained can be used to compare the relative biocompatibility between screw configurations. However, in order to produce quantitative results, future models should include more realistic geometry, material properties and boundary conditions; i.e. 3D geometry and anisotropic material properties of bone.

Screw-bone implant systems are three-dimensional in nature, and the spiral nature of screw threads will definitely result in more complex stress distributions than those resulting from our current model. Uhthoff concluded in his study that bone formation, which acts independently of bone remodeling, proceeds centripetally around screws and that it is in the direction of load transmission from the screw (Uhthoff H. , 1973). Therefore, in order to accurately determine the stress transfer between screws and bone, more complex, 3D geometry should be modeled in future studies.

Another limitation of this study is the use of homogeneous isotropic material properties as representative bone material properties. This is a simplification of the true anisotropic properties of both bone types; however, neglecting to include the natural trabecular architecture of the cancellous bone particularly affects the results of this study. In order to relate the distribution of mechanical stimuli in bone to the rate of bone remodeling, it seems necessary to consider the stress (or any other mechanical stimulus as an initiator of the bone remodeling process, i.e. strain energy density) transfer between local threads and individual trabeculae, in future models.

Along with the design of a more realistic model, other important screw parameters should be tested. Cancellous bone screws are generally designed to have greater thread depth and decreased thread cross-sectional thickness in comparison to cortical bone screws, to provide more holding power in porous materials (Chapman, Harrington, Lee, Anderson, Tencer, & Kowalski, 1996). Although this study did measure the effects of varying thread depth by changing the outer thread diameter, the model did not test variations in thread thickness. Varying the thickness of threads effectively changes the pitch. Since the distance between the threads in this study is kept at a constant 1 mm for each case, future models should test the effects of thread pitch while maintaining a constant length.

Alternative screw designs have also been tested in a similar manner under a compressive load and have led to promising results (Gefen, 2002). The newly designed graded-stiffness screw, comprised of a stiff core and more elastic outer threads, significantly increased STP values approaching an optimal level of unity when very low modulus of elasticity threads were analyzed (Gefen, 2002). This result also supports the theory that a reduction in the stiffness of the implant leads to a reduction in stress shielding. Also, the design of screws which apply compressive forces to bone near the tip of the screws result in STP β values close to unity, thus the likelihood of bone resorption in the distal region is reduced (Gefen, 2002).

The use of FEA allows for effective comparison of isolated parameters, in this case for comparison of screw geometry and material properties. More realistic 3D geometries, non-homogeneous material properties, and an adaptive bone remodeling theory, incorporated into the model will result in an increased accuracy in predictions of stress shielding around screw threads. Since stress shielding in the vicinity of threads affects the long-term holding power of screws in bone, a consideration of the most influential factors should be weighed with those factors that have been noted to affect holding power by pullout test methods; Holding power is mainly dependent on host material density, outer diameter, pitch, length of engagement and root diameter (Asnis, et al., 1996). Therefore, a balance must exist between these parameters in order to ensure sufficient pullout strength while limiting the effects of stress shielding. The eventual optimization of these parameters in a simulation model that includes a remodeling theory will donate valuable insight into the reduction of bone loss that leads to screw loosening and eventual plate avulsion in internal fixation.

Chapter 6: Concluding summary & suggestions for future work

6.1 Three-dimensional FE plated-bone model

In cases of long bone fracture, implants of plates and screws are often used to promote quick healing and the early return to use of the limb in question. Clinical reports of mal-union and non-union are associated with bone resorption due to what some researchers believe is insufficient vascularity (Perren, 2002) and more notably stress shielding (Uhthoff, Boisvert, & Finnegan, 1994). Failure often involves the loss of clinical stability of the plated bone construct, caused by localized regions of bone resorption occurring in underlying bone and in the vicinity of screws. Although some research into various geometric and material plate and screw systems have been studied experimentally *in vivo* and *in vitro*, a universally optimized plate design or set of guidelines to reduce stress shielding is yet to be determined. In order to do so, we must first accurately determine the distribution of mechanical stimuli to bone as a result of a particular implant, and second we must be able to relate this to a universally accepted bone remodeling theory. To avoid the ethical, cost, and equipment-associated limitations of these types of experiments, many researchers have turned to computational models in order to develop pre-determinate measures of the effects of particular plate and screw designs.

In an effort to gain further insight into the factors that influence stress shielding two FE models are developed in this study. An initial simplified bone-plate model is used as a validation of the use of FEA. Through a comparison of the stresses in the plate and bone under purely axial, bending, and eccentric axial loading conditions to a non-plated model, it can be concluded that plate fixation causes a shift in the neutral axis of the bone-plate system and that stress shielding develops in underlying bone. A discrepancy between the simulation and theoretical results from composite beam theory demonstrates the inability of the theory to predict the complex nature of a plated bone system. The simple model resulted in large decreases in stress below the plate near the fracture site and an increase in stress at the opposite end due to the tendency for plate separation and the fixed boundary condition used in the model. This demonstrated the need for stress-free separation of the bone-plate interface in the subsequent parametric model. With the inclusion of geometrically simplified screws, this new model demonstrates more realistic levels of stress shielding in underlying bone (reductions of 25% or less, which is in good agreement with other models (Gefen, 2002)). Parametric analyses using this model indicate that stress shielding can be reduced by limiting: the plate thickness; and bone-contact angle, which effectively reduce the stiffness of the plate. We hypothesize that an optimal value (i.e. one that minimizes stress shielding) for both parameters exists, however, many factors must be considered in deeming a particular set of parameters optimized. As a fairly good indication of an optimal value, a future model should include the minimum strength requirement of the plate, along with a maximum plate thickness and angle that will not interfere with the bone's vascularity, and then optimize the parameters within those particular constraints. In terms of screw position, the screws nearest the fracture site experiences the highest levels of loading, thereby producing large stress concentrations. Under the same applied bending load, re-locating the distal screws further from the fracture site demonstrates a reduction in the level of stress in the plate and generates a more even stress distribution in bone. An optimal screw configuration must also exist for the specified plate geometry. One must consider that the proximal screw should remain a nominal distance away from the fracture site, whereas the distal screw should be placed far enough away from the fracture site to reduce the stress concentration in the proximal screw, yet still far enough from the outer plate end to reduce the likelihood of failure due to a resulting stress concentration. The role of screw position in the plated-bone construct significantly influences the stress distribution, predominantly at the fracture site, therefore a variety of screw configurations should be tested.

Many attributes of the parametric 3D model must be improved upon to obtain accurate results pertaining to the quantification of stress shielding resulting from varying implant parameters. These include: geometry, material properties, and boundary conditions. In terms of geometric and material properties, modeling the bone as a cylinder and as an isotropic material is a great simplification of its irregular form and anisotropic behaviour, respectively. Although these simplifications are useful for comparison to composite beam theory and can shed some light on the stress shielding problem, they do not provide realistic results. Orthotropic and eventually anisotropic material properties should be included in the model along with more realistic geometries, for instance 3D geometries resulting from CT scan images.

This model assumes a transverse fracture in the post-union phase of fracture healing, thereby limiting the need to impose a fracture gap in the model. However, future analyses should involve a fracture gap as to demonstrate the nature of remodeling that takes place during the initial stages of fracture healing. This would also allow one to observe the effects of varying implant parameters for a variety fracture types, i.e. transverse, oblique, and spiral, which will undoubtedly produce varied results.

Although the model does include stress-free separation of the plate from bone and is reliant upon the geometry of the simplified screws to fix the plate to the bone, future studies must include the application of pre-tensioned screws, which significantly raise stress in the geometry. Moreover, the screws are simplified for computational purposes, and it is important to include threads into the model to compare the stresses generated in the adjacent bone in relation to those resulting in the 2D screw-bone model.

The use of less rigid plates has been proven by many researchers to reduce the negative effects of stress shielding (Foux, Yeadon, & Uhthoff, 1997) (Goel, et al., 1991) (Uhthoff, Bardos, & Liskova-Kiar, 1981) (Woo, et al., 1984) (Claes, 1989). One way to reduce the stiffness of a fixation plate is to effectively reduce its cross-sectional area, which is demonstrated in our 3D model. Another way to reduce stiffness is to choose a more flexible material, i.e. a titanium alloy instead of stainless steel. Future investigations should include a range of less-rigid plate materials along with the use of composite plates that could account for the orthotropic-like behaviour of cancellous bone. An ideal plate would provide initial clinical stability in order to support the majority of the load during the initial phases of fracture healing and then become increasingly less rigid over time. This would allow for the bone to regain a portion of its load-sharing capabilities as it heals and would reduce the likelihood of stress shielding through the stimulation of the rate of remodeling. New resorbable bio-materials may provide a more appealing plating solution in comparison to the traditional metal plating options still currently in use.

Other parameters associated with the positioning of screws and the effects of pre-operative plate bending should also be analyzed. However, until an adaptive remodeling theory, as demonstrated in Figure 51, is introduced into the model which simulates the changing nature of bone over the course of healing, the current quasi-static type of analysis can only give us a very narrow view of the stress shielding that might result in the post-union phase of fracture healing. If a model follows the schematic diagram in Figure 51, with each iteration (or solution) the mechanical stimuli delivered to the bone would either result in bone formation or bone resorption, depending on a threshold level of stimuli that is inherent to initiating bone's remodeling response. Resorption and formation of bone are usually modeled by cortical thinning or thickening and by a decrease or increase in density of cancellous bone, respectively (Beaupre, Orr, & Carter, 1990).

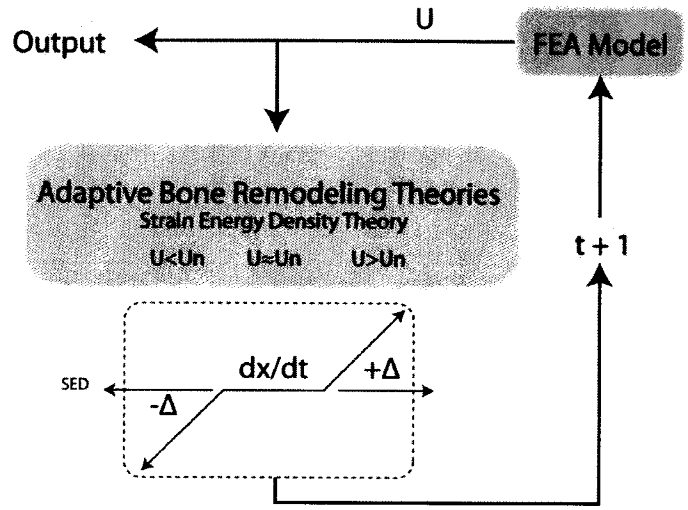

Figure 56: The inclusion of an adaptive bone remodeling theory

Ideally, experimental models under the same simplified loading conditions as in the validation and parametric models should be tested for verification of our theoretical results, as this is the only method to verify results.

6.2 Two-dimensional FE screw-bone model

In order to avoid pullout-failure many researchers have focused on determining the factors that critically affect the holding power of screws in bone. Experimental pullout test methods are able to predict the holding power of a variety of screw parameters in bone. Several researchers suggest that besides the host material density, the major thread diameter is the most influential screw design parameter in determining a screw's holding power in bone (Asnis, et al., 1996). Decreasing the inner thread diameter and pitch also increases the holding power, however, to a less significant degree (Zhang, Tan, & Chou, 2004). A linear correlation between the pullout strength and thread count, which effectively increases the length of a screw's engagement, is also noted (Krag, Beynnon, Pope, Frymoyer, Haugh, & Weaver, 1986). However, this claim has been disputed by others through experimental evidence that found no difference in pullout strength with a change in screw length (Zindrick, et al., 1986). These differences may be the result of variances in host material properties or loading rates used during testing. Benefits of using polyurethane foam as a test material, as well as FE models, where consistency in the model can be controlled are revealed by these discrepancies.

Although this information is useful in the initial stages of implantation, little information pertaining to the long-term effects of stress shielding in the vicinity of screws exists. Therefore, in order to investigate the geometric and material properties of screws that influence the resulting level of stress shielding in surrounding bone, a two-dimensional screw-bone system is modeled in this study. Two parameters are defined in order to quantify stress shielding as a measure of the biocompatibility of the various screw configurations with bone; one that employs effective stress (STP), which was introduced by other researchers (Gefen, 2002), and the other that uses strain energy density (SEDTP), which is defined in this research.

The model, which is representative of a cancellous bone screw in a pull-out scenario, sheds some light on particular screw parameters that contribute to the level of resultant stress shielding in adjacent bone. Based on our results, in particular, the screw's modulus of elasticity should be reduced in order to obtain a more even stress distribution between screw threads and bone. A general conclusion that can be derived from the results obtained using both STP and SEDTP values, is that changing the screw parameters has a definite effect on the resulting stress distribution, and also it is understood that most geometrical parameters are interrelated. Greater attention should be placed on limiting the effects of bone resorption in the distal portion of the screw, as results indicate a greater level of stress shielding (which is in agreement with other work, i.e. (Harnroongroj & Techataweewan, 1999)), despite the increased levels in stress at the screw tip due to the simplified fixed boundary condition.

We can draw some overall conclusions based on both our *in situ* results and observation of experimental screw pullout of others. In order to increase the biocompatibility of screws or in other words, to minimize the likelihood of initial pullout and long-term effects of stress shielding, one can: reduce the screw's modulus of elasticity (Gefen, 2002) (Lin, Chuang, Lin, Lee, Ju, & Yin, 2007) (Woo, et al., 1984) (Uhthoff, Boisvert, & Finnegan, 1994); employ triangular or trapezoidal profile shaped threads (Gefen, 2002) (Eraslan & İnan, 2009) (Hansson & Werkeb, 2003); choose a thread diameter based on the density of bone (i.e. a smaller thread is suitable for dense cortical bone, however, larger threads may be more suitable for less dense cancellous bone); increase the depth of penetration (i.e. decrease pitch while increasing shaft length) (Hughes & Jordan, 1972) (Gausepohl, Mohring, Pennig, & Koebke, 2001); limit the root diameter of the screw, while maintaining appropriate screw tensile and torsional strengths which are dependent on the square and cube of the root diameter, respectively (Nunamaker & Perren, 1976).

Whether or not stress or SED is a good candidate for representing the effects of stress shielding remains an open question, because experimental evidence in relation to the bone remodeling response is necessary. Comparing STP and SEDTP results demonstrates that different mechanical stimuli are distributed differently within a given model. Results from the SEDTP calculations reveal a more dependent nature between the varied screw parameters than is demonstrated by the use of STPs. A comparison between the results averaging from tests using 5, 8, and 9 threaded configurations reveals similar trends in relative measures of biocompatibility (see Figure 57). Further investigation between the use of SED and stress-based results is ongoing; however this result may suggest that all parameters are dependent which is physically sensible if one considers the bone remodeling process. Future experimental testing of such parameters in relation to stress shielding is necessary to verify theoretical results.

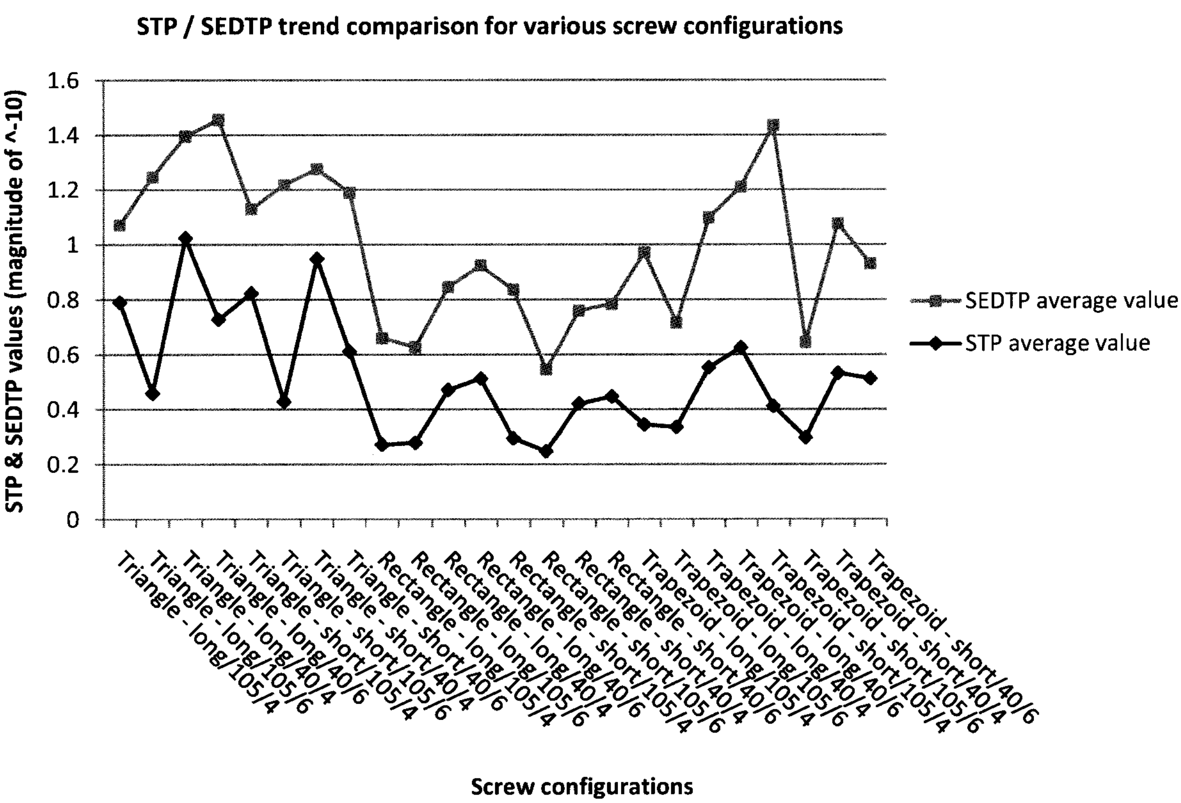

Figure 57: STP/SEDTP average trend comparison

A major disadvantage of this model lies in its two-dimensional geometry and simplified boundary conditions. Therefore, resulting data can only be compared in a qualitative manner. Future 3D models such as that modeled by Zhang and co-workers may lead to a more accurate prediction of the stress distribution (Zhang, Tan, & Chou, 2004). In their model, a 6.5 mm cancellous bone screw with spherical under-surfaces and asymmetrical thread are used to test the strength and stress distribution that arises in bone and screw from a simulated pullout load (Zhang, Tan, & Chou, 2004). The model uses a rigid to flexible contact surface along the trailing edge of the screw threads, with no direct contact between the other screw-bone junctions. Although this is a more realistic approach, to modeling the screw-bone interface, it is still a simplification of actual conditions. In a period of about 6 to 12 weeks post-implantation there is no gap between the bone and screw threads due to callus formation and eventual remodeling (Uhthoff, Poitras, & Backman, 2006). However, Zhang and co-workers 3D analysis does produce results consistent with experimental studies (Zhang, Tan, & Chou, 2004).

In this study, we did not consider dynamic modes of loading as static analyses are used to determine the level of biocompatibility of the various screws tested. Upon the inclusion of a bone remodeling algorithm into the model, in a future study, dynamic modes of loading should be considered. Axial cyclic tests suggest that the loading rate influences the mechanics of the bone-screw interface (Inceoglua, Ehlert, Akbayb, & McLainc, 2006). Therefore the biocompatibility of the same parameters may change over time under dynamic loads. Based on unexpected hysteresis-like behaviour, these same authors hypothesize that under a periodic axial load the bottom layer of bone beneath the screw thread compresses, while the initially compressed top layer springs back to fill the gap. If the opposite occurs during unloading, wherein the displacement of the screw moves upwards and re-compresses the top layer of bone, this type of non-destructive micro-motion of screws (less than 0.2 mm displacement) may be beneficial in terms of initiating a bone remodeling response (Chao & Inoue, 2003).

The inclusion of more realistic material properties for both cancellous and cortical bone should have a significant effect on the level of stress shielding adjacent to the screws, even in two-dimensions. There is a definite non-uniformity in the density of cancellous bone, particularly upon insertion where a significant amount of compression of the underlying trabeculae occurs. Unlike cortical bone screws, it is common for cancellous bone screws to employ self-tapping tips and rely in-part on the compression of these trabeculae to gain further hold in the porous material. Compression of the trabeculae in the vicinity of screws creates a non-uniform distribution of cancellous bone, which in turn results in non-uniform distributions of mechanical stress and altered local rates of remodeling.

As a suggestion for future research, the varied screw parameters should be tested in a bi-cortical model such as the one shown in Figure 58. It is recently reported that the preferred method to ensure clinical stability and increase screw pullout strength is through insertion 2mm beyond the second cortex (Harnroongroj & Techataweewan, 1999) (Battula S. , Schoenfeld, Sahai, Vrabec, Tank, & Njus, 2008). It is hypothesized that a change in screw parameters will have less of an effect on the initial holding power in this type of arrangement, since the length of engagement and the shear strength of cortical bone is increased. However, the effects of load distribution at the screw-bone interface should be determined in an effort to limit eventual bone loss due to stress shielding.

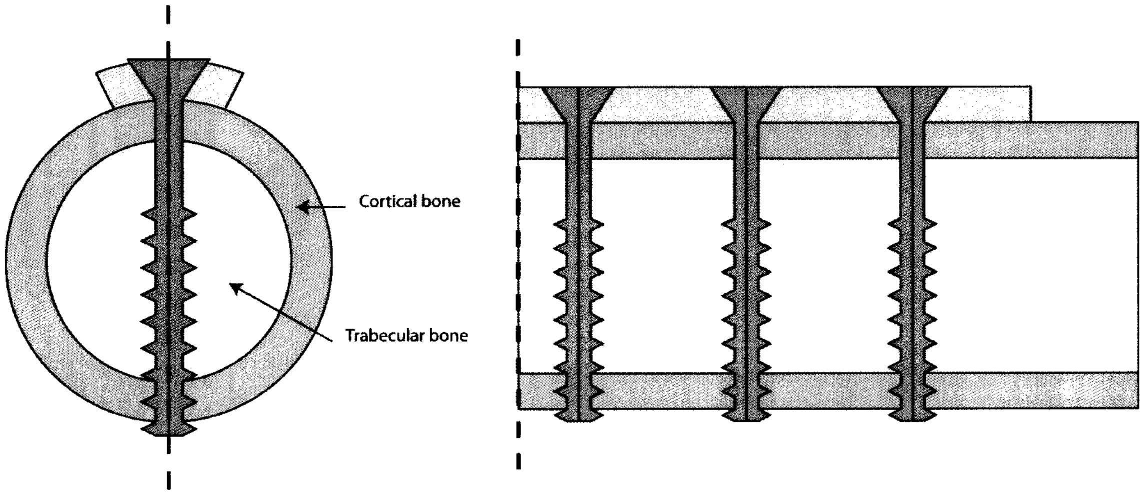

Figure 58: A 2D bi-cortical screw-bone model

The long-term goal is to incorporate an adaptive remodeling theory into the model. An example of this type of model is performed by Gefen in response to his initial parametric bone-screw analysis (Gefen, 2002). With the inclusion of a SED threshold-type bone remodeling algorithm, Gefen's results predict the order in which screw loosening first occurs: the triangular profile, followed by the trapezoidal, and finally the rectangular shaped profile threaded screws (Gefen, 2002). For each case the wider shaped thread designs demonstrate a longer period until loosening. These results however, do not account for all of the geometric variations initially analyzed. The predicted time to loosening for a triangular profile shaped thread is approximately 70 weeks, however, histomorphological results from a study by Schuller-Götzburg and co-workers demonstrates loosening at only 12 weeks (Schuller-Gotzburg, Krenkel, Reiter, & Plenk Jr., 1999). The difference in time to loosening may be due to the fact that Gefen uses a static load, while the mechanosensory function of osteocytes is generally thought to respond to the strain energy density rate as produced by dynamic loading of bone (Ruimerman, Huiskes, Van Lenthe, & Jansshen, 2001). Along with 3D realistic geometry, that can accurately predict the mechanical stimuli distribution within bone, a suitable algorithm, based on a universally accepted bone remodeling theory, must be incorporated to accurately mimic the adaptation of bone. Therefore, we propose that future model should use modified SEDTPs as an indicator of biocompatibility under dynamic loading conditions.

The use of consistent FE models allows for the effective comparison of isolated screw and plate parameters. More realistic 3D geometries, non-homogeneous material properties, and the inclusion of an adaptive bone remodeling theory incorporated into the model will result in increased accuracy in the prediction of stress shielding in the vicinity of implants. Eventual optimization of these parameters in a more realistic model will donate valuable insight into the reduction of stress shielding. Through optimizing the design of implants, we can reduce the likelihood of failure of fixation, which is the ultimate goal.

6.3 A brief discussion on the use of FEA

The direction of this research is a step towards the ultimate goal, which is to create a finite element model that can accurately predict the nature of bone adaptation in response to implants, specifically plated long bones in the post-union phase of fracture healing. A model that incorporates non-symmetric bone geometry, anisotropic material properties, and an adaptive bone remodeling theory, along with appropriate boundary conditions, will substantiate this goal. However, certain obstacles must be overcome, some of which involve the difficulty in modeling complex geometries, contact conditions, and lack of a universally and comprehensive, mechanistic bone remodeling theory.

In terms of modeling complex geometries, CT scans are useful in providing geometric data to generate realistic bone models. However, the difficulty lies in the discretization of such complex geometries into a manageable number of nodes and elements. Mesh refinement must be used in regions of abrupt changes in geometry and/or material properties, as well as in the locations of applied loading in order to avoid inherent problems associated with computational requirements (Fischer, Jacobs, Levenston, & Carter, 1997).

Another limitation involves assigning element material properties to the model. For the sake of simplification, many computational models use constant mechanical properties. This is common for models that include adaptive remodeling, where elements are initially assigned as isotropic materials with uniform density distributions (Garcia, Doblare, & Cegonino, 2002). Large scale FEA systems, such as the "Adventure System", may aid in the application of inhomogeneous material properties to bone problems. Based on the premise that bone mass density distributions can be obtained from CT images, the system is able to assign a Young's modulus to the elements, one by one (Tawara, Sakamoto, & Oda, 2005).

Stress analysis of bodies in contact, such as in plated long bones, presents a complex problem. Hertz theory can be used to approximate stresses that develop between two contacting bodies with similar elastic moduli (Benham, Crawford, & Armstrong, 1996). However, in order to investigate the behavior of dissimilar materials, one must use complex theories of elasticity or results from finite element analysis. Depending on the loading conditions, material properties and boundary conditions, the modeled geometries can come in and out of contact in a rather abrupt manner. Due to their highly non-linear nature, and costly computing power, the development of efficient models which incorporate realistic contact analyses presents a difficult task. The inclusion of friction into a model (through the use of contact and target elements), alone, produces such chaotic behaviour and results in difficulties in developing a convergent solution (Egol, Kubiak, Fulkerson, Kummer, & Koval, 2004).

Although a variety of contact elements are available, the current model produces the most convergent results when fixed contact between the screw and bone is assumed. Since the 2D geometry is modeled from coincident points, the generated areas representative of the screw and bone regions inherently share a boundary, eliminating the need to create separate contact elements. For future models, it is recommended that contact elements are used at the bone-implant interface. The contact problem should be classified as rigid-to-flexible, as the screw is considered to have a much higher flexural rigidity than that of the neighbouring bony material.

ANSYS supports both rigid-to-flexible and flexible-to-flexible types of contact problems by definition of a contact pair including contact and target elements. For surface-to-surface contact in 2D a target 169 and a contact element of either 171 or 172 must be defined and they must share a defined real constant number (ANSYS help files, v.11.0). These elements have several advantages over the node-to-node element, including: that they support both lower and higher order elements, while providing better contact results for normal pressure and friction stress contour plots; and they have no restrictions on the shape discontinuities of the target surface, be it physical or due to mesh discretization. Node-to-surface contact elements can be used near contact corners in conjunction with the defined surface-to-surface elements which support general static analyses if the contacting surface is defined by a group of nodes. The advantage of using this type of element over the node-to-node type is that the knowledge of the exact location of the contacting area is unnecessary. The contact components in question do not require a compatible mesh, and large deformation and relative sliding are allowed. Node-to-node contact elements, on the other hand, are typically used to model point-to-point contact applications and require the location of contact to analyze small relative sliding. Further exploration of the bone-plate interface, which plays an important role in fracture healing (Cheal, Hayes, & White III, 1985), should involve the contact elements available in ANSYS.

In an effort to simulate the bone remodeling response to implants, researchers have incorporated different bone adaptation theories into their models (Jacobs, Levenston, Beaupre, Simo, & Carter, 1995) (Beaupre, Orr, & Carter, 1990) (Huiskes, On the modelling of long bones in structural analyses, 1982). However, all of the employed theories are based on many simplified assumptions and mostly phenomenological in nature, and so no universally accepted theory of bone remodeling exists to date. The loading conditions of long bones are also complex in nature and are difficult to model. Simplifying assumptions must account for factors, such as, in the case of bone loads, muscle forces arising from different physical activities. The validity of FE models is therefore reliant upon *in vitro* and *in vivo* experimental testing. Simplified models, however, such as the ones proposed in this study, can provide a useful starting point for analysis and predict the necessary attributes for inclusion in more complex models in the future. This will lead to beneficial insight into the mechanical stimuli distributions that develop from implants, which will subsequently donate insight into the negative effects of stress shielding.

References

AK Steel Corporation. (2007). *Product data bulletin: 316/316L stainless steel.* Retrieved from AK Steel: www.aksteel.com

Akeson, W., Woo, S.-Y., Coutts, R., Matthews, J., Gonsalves, M., & Amiel, D. (1975). Quantitative histological evaluation of early fracture healing of cortical bones immobilized by stainless steel and composite plates. *Calcified Tissue Research , 19*, 27-37.

Alho, A., Stromsoe, K., & Hoiseth, A. (1995). Pairwise strength relationships of cortical and cancellous bone in human femur: an autopsy study. *Archives of Orthopaedic and Traumatic Surgery , 114*, 211-214.

Allgower, M., Perren, S., & Matter, P. (1970). A new plate for internal fixation - The dynamic compression plate (DCP). *Injury, The British J. of Accident Surgery , 2* (1), 40-47.

Altuglas International. (2006). *Plexiglas.* Retrieved from Altuglas International: www.altuglasint.com

Ang, K., Das De, S., Goh, J., Low, S., & Bose, K. (1997). Periprosthetic bone remodeling after cementless total hip replacement. *J. Bone and Joint Surgery , 79B* (4), 675-679.

ANSYS, I. (2005). ANSYS Release Notes 10.0. SAS IP, Inc.

Ashman, R., Cowin, S., Van Buskirk, W., & Rice, J. (1984). A continuous wave technique for the measurement of the elastic properties of cortical bone. *J. Biomechanics , 1* (5), 349-361.

Asnis, S., Ernberg, J., Bostrom, M., Wright, T., Harrington, R., Tencer, A., et al. (1996). Cancellous bone screw thread design and holding power. *J. Orthopaedic Trauma , 10* (7), 462-469.

Badke, A., Hontzsch, D., Kaps, H.-P., & Weise, K. (2005). Treatment of distal femoral fractures with the less invasive stabilization system (LISS) in paraplegics. *European J. of Trauma , 31* (5), 499-502.

Bartel, D., Davy, D., & Keaveny, T. (2006). *Orthopaedic Biomechanics.* New Jersey: Pearson Prentice Hall.

Battula, S., Schoenfeld, A., Sahai, V., Vrabec, G., Tank, J., & Njus, G. (2008). The effect of pilot hole size on the insertion torque and pullout strength of self-tapping cortical bone screws in osteoporotic bone. *J. Trauma Injury Infection and Critical Care , 64* (4), 990-995.

Battula, S., Schoenfeld, A., Vrabec, G., & Njus, G. O. (2006). Experimental evaluation of the holding power/stiffness of the self-tapping bone screws in normal and osteoporotic bone material. *Clinical Biomechanics , 21*, 533–537.

Beaupre, G., Carter, D., Orr, T., & Csongradi, J. (1988). Stresses in plated long-bones: The role of screw tightness and interface slipping. *J. Orthopaedic Research , 6* (1), 39-50.

Beaupre, G., Orr, T., & Carter, D. (1990). An approach for time-dependent bone modeling and remodelling - application: A preliminary remodelling situation. *J. Orthopaedic Research*, *8* (5), 662-670.

Be'ery-Lipperman, M., & Gefen, A. (2006). A method of quantification of stress shielding in the proximal femur using hierarchical computational modeling. *Computer Methods in Biomechanics and Biomedical Engineering*, *9* (1), 35-44.

Bekler, H., Bulut, G., Usta, M., Gokce, A., Okyar, F., & T., B. (2008). The contribution of locked screw-plate fixation with varying angle configurations to stability of osteoporotic fractures: an experimental study. *ACTA Orthopaedica Traumatologica Turcica*, *42* (2), 125-129.

Benham, P., Crawford, R., & Armstrong, C. (1996). *Mechanics of engineering materials, second edition.* Essex, England: Pearson Education Limited.

Bona, M., Martin, L., & Fischer, K. (2003). Joint load estimation based on bone density and a contact model applied to the proximal femur of a chimp. *Summer Bioengineering Conference*, (pp. 0877-0878). Florida.

Bonnaire, F., Zenker, H., Lill, C., Weber, A., & Linke, B. (2005). Treatment strategies for proximal femur fractures in osteoporotic patients. *Osteoporosis International*, *16*, S93-S102.

Borgeaud, M., Cordey, J., Leyvraz, P., & Perren, S. (2000). Mechanical analysis of the bone to plate interface of the LC-DCP and of the PC-Fix on human femora. *Injury, International J. for Care of the Injured*, *31*, SC29-SC36.

Boyce, T., Fyhrie, D., Glotkowski, M., Radin, E., & Schaffler, M. (1998). Damage type and strain mode associations in human compact bone bending fatigue. *J. Orthopaedic Research*, *16* (3), 322-329.

Bradley, G., McKenna, G., Dunn, H., Daniels, A., & Statton, W. (1979). Effects of flexural rigidity of plates on bone healing. *Journal of bone and joint surgery*, *61*, 866-872.

Brunet, J., Sarkar, K., & Uhthoff, H. (1986). Ultrastructure of the fibrous tissue surrounding internal fixation devices. *Clinical Orthopaedics and Related Research* (208), 84-94.

Burnstein, A., Currey, J., Frankel, V., Heiple, K., Lunseth, P., & Vessely, J. (1972). Bone Strength The Effect of Screw Holes. *J. Bone and Joint Surgery*, *54-A* (6), 1143-1156.

Burr, D., Forwood, M., Fyhrie, D., Martin, R., Schaffler, M., & Turner, C. (1997). Bone microdamage and skeletal fragility in osteoporotic and stress fractures. *J. Bone and Mineral Research*, *12* (1).

Burr, D., Martin, R., Schaffler, M., & Radin, E. (1985). Bone remodelling in response to in vivo fatigue microdamage. *J. Biomechanics*, *18* (3), 189-200.

Burstein, A., & Wright, T. (1994). *Fundamentals of Orthopaedic Biomechanics.* Baltimore: Williams and Wilkins.

Carter, D. (1984). Mechanical loading histories and cortical bone remodelling. *Calcified Tissue International, 36,* S19-S24.

Carter, D. (1987). Mechanical loading history and skeletal biology. *J. Biomechanics, 20,* 11-12.

Carter, D., & Caler, W. (1985). A cummulative damage model for bone fracture. *J. Orthopaedic Research, 3* (1), 84-90.

Carter, D., & Hayes, W. (1977). The compressive behavior of bone as a two-phase porous structure. *J Bone Joint Surg Am., 59-A* (7), 954-962.

Cegonino, J., Garcia Aznar, J., Doblare, M., Palanca, D., Seral, B., & Seral, F. (2004). A comparative analysis of different treatments for distal femur fractures using the finite element method. *Computer Methods in Biomechanics and Biomdical Engineering, 7* (5), 245-256.

Chao, E., & Inoue, N. (2003). Biophysical stimulation of bone fracture repair regeneration and remodelling. *European Cells and Materials, 6,* 72-85.

Chapman, J., Harrington, R., Lee, K., Anderson, P., Tencer, A., & Kowalski, D. (1996). Factors affecting the pullout strength of cancellous bone screws. *J. Biomechanical Engineering, 118,* 391-398.

Cheal, E., Hayes, W., & White III, A. (1985). Stress analysis of compression plate fixation and its effects on long bone remodelling. *J. Biomechanics, 18* (2), 141-150.

Cheal, E., Hayes, W., White, A., & Perren, S. (1983). Stress analysis of a simplified compression plate system for fractured bones. *Computers & Structures, 17* (5-6), 845-855.

Chen, S., Chang, C., & Lin, R. (2001). The effect of the pedicle screw length within the vertebral body. *Proceedings of the Summer Bioengineering Conference of the ASME Bioengineering Division,* (pp. 263-4).

Cheng, J., Tse, P., & Chow, Y. (1985). The place of the dynamic compression plate in femoral shaft fractures. *Injury, 16* (8), 529-534.

Cheung, G., Zalzal, P., Bhandari, M., Spelt, J., & Papini, M. (2004). Finite element analysis of a femoral retrograde intramedullary nail subject to gait loading. *Medical Engineering & Physics, 26,* 93-108.

Chou, H.-Y., Jagodnik, J., & Muftu, S. (2008). Predictions of bone remodelling around dental implant systems. *J. Biomechanics, 41,* 1365-1373.

Chow, J., Wilson, A., Chambers, T., & Fox, S. (1998). Mechanical loading stimulates bone formation by reactiviation of bone lining cells in 13-week-old-rats. *J. Bone and Mineral Research, 13* (11).

Claes, L. (1989). The mechanical and morphological properties of bone beneath internal fixation plates of differing rigidity. *J. Orthopaedic Research, 7* (2), 170-177.

Cleek, T., Reynolds, K., & Hearn, T. (2007). Effect of screw torque level on cortical bone pullout strength. *J. Orthopaedic Trauma , 2*, 117-123.

Cordey, J., Borgeaud, M., & Perren, S. (2000). Force transfer between the plate the bone: relative importance of the bending stiffness of the screws and the friction between plate and bone. *Injury, International J. for Care of the Injured , 31* (3), SC21-SC28.

Cordey, J., Perren, S., & Steinemann, S. (2000). Stress protection due to plates: Myth or reality? A parametric analysis made using the composite beam theory. *Injury, International J. for Care of the Injured , 31*, SC1-SC13.

Cornell, C. (2003). Internal fracture fixation in patients with osteoporosis. *J. American Society of Orthopaedic Surgeons , 11* (2), 109-119.

Cowin, S. (Ed.). (2001). *Bone Mechanics Handbook, 2nd Edition* (Vol. 2). CRC Press.

Cowin, S. (1978). Bone remodelling 3: uniqueness and stability in adaptive elasticity theory. *J. Elasticity , 8* (3), 285-295.

Cowin, S., & Firoozbakhsh, K. (1981). Bone remodelling of diaphyseal surfaces under constant load: thoeretical predictions. *J. Biomechanics* (7), 471-484.

Cowin, S., & Hegedus, D. (1976). Bone remodelling 1: thoery of adaptive elasticity. *J. Elasticity , 6* (3), 313-326.

Currey, J. (1988). The effect of porosity and mineral content on the Young's modulus of elasticity of compact bone. *Biomechanics , 21* (2), 131-139.

Currey, J. (1999). What determines the bending strength of compact bone? *The Journal of Experimental Biology , 202*, 2495–2503.

Curtis, R., Goldhahn, J., Schwyn, R., Regazzoni, P., & Suhm, N. (2005). Fixation principles in metaphyseal bone - a patent based review. *Osteoporosis International , 16*, S54-S64.

D'Amelio, P., Grimaldi, A., Pescarmona, G., Tamone, C., Roato, I., & Isaia, G. (2004). Spontaneous osteoclast formation from peripheral blood mononuclear cells in postmenopausal osteoporosis. *J. FASEB* .

Dammak, M., Shirazi-Adl, A., Schwartz Jr., M., & Gustavson, L. (1997). Friction properties at the bone-metal interface: comparison of four different porous metal surfaces. *J. Biomedical Materials Research , 35*, 329-336.

DeCoster, T., Heetderks, D., Downey, D., Ferries, J., & Jones, W. (1990). Optimizing bone screw pullout force. *J. Orthopaedic Trauma , 4* (2), 169-174.

Dendorfer, S., & Maier H.J.Hammer, J. (2009). Fatigue damage in cancellous bone: An experimental approach from continuum to micro scale. *Journal of the Mechanical Behavior of Biomedical Materials*, *2* (1), 113-119 .

Duma, S., Schreiber, P., McMaster, J., Crandall, J., Bass, C., & Pilkey, W. (1999). Dynamic injury tolerances for long bones of the female upper extremity. *J. Anatomy*, *194*, 463-471.

Duncan, R., & Turner, C. (1995). Mechanotransduction and the functional response of bone to mechanical strain. *Calcified Tissue International*, *57*, 344-358.

Egol, K., Kubiak, E., Fulkerson, E., Kummer, F., & Koval, K. (2004). Biomechanics of locked plates and screws. *J. Orthopaedic Trauma*, *18* (8), 488-493.

Einhorn, T. (1998). The Cell and Molecular Biology of Fracture Healing. *Clinical Orthopaedics and Related Research*, *355*, S7-S21.

Ellis, T., Bourgeault, C., & Kyle, R. (2001). Screw Position Affects Dynamic Compression Plate Strain in an In Vitro Fracture Model. *Journal of Orthopaedic Trauma*, *15* (5), 333–337.

Eraslan, O., & İnan, Ö. (2009). The effect of thread design on stress distribution in a solid screw implant: a 3D finite element analysis. *Clin Oral Invest* .

Ferguson, S., Wyss, U., & Pichora, D. (1996). Finite element stress analysis of a hybrid fracture fixation plate. *Medical and Engineering Physics*, *18* (3), 241-250.

Fischer, K., Jacobs, C., Levenston, M., & Carter, D. (1997). Observations of convergence and uniqueness of node-based bone remodelling simulations. *Annals of Biomedical Engineering*, *25*, 261-268.

Foux, A., Yeadon, A., & Uhthoff, H. (1997). Improved fracture healing with less rigid plates. *Clinical Orthopaedics and Related Research* (339), 232-245.

Freeman, M., Bradley, J., & Revell, P. (1982). Observations upon the interface between bone and PMMA cement. *The Journal of Bone and Joint Surgery*, *64-B* (4), 489-493.

Frigg, R. (2001). Locking compression plate (LCP). An osteosynthesis plate based on the dynamic compression plate and the point contact fixator (PC-Fix). *Injury, International J. for Care of the Injured*, *32*, SB63-SB66.

Frosch, K.-H., & Sturmer, K. (2006). Metallic biomaterials in skeletal repair. *European J. of Trauma*, *32* (2), 149-159.

Frost, H. (2001). From Wolff's law to the Utah paradigm: Insights about bone physiology and its clinical applications. *The Anatomical Record*, *262*, 398-419.

Frost, H. (1992). Perspectives: bone's mechanical usage windows. *J. Bone and Mineral*, *19*, 257-271.

Fujihara, K., Huang, Z.-M., Ramakrishna, S., Satknanantham, K., & Hamada, H. (2003). Performance study of braided carbon/PEEK composite comression bone plates. *Biomaterials , 24*, 2661-2667.

Funsten, R., & Lee, R. (1945). Healing time in fractures of the shafts of the tibia and femur. *27* (3), 395-400.

Fyhrie, D., & Vashishth, D. (2000). Bone Stiffness Predicts Strength Similarly for Human Vertebral Cancellous Bone in Compression and for Cortical Bone in Tension. *Bone , 26* (2), 169-173.

Ganesh, V., Ramakrishna, K., & Ghista, D. (2005). Biomechanics of bone-fracture fixation by stiffness-graded plates in comparison with stainless-steel plates. *Biomedical Engineering Online , 4* (46).

Garcia, J., Doblare, M., & Cegonino, J. (2002). Bone remodelling simulation: a tool for implant design. *Computational Materials Sceince , 25*, 100-114.

Garcia-Aznar, J., Rueberg, T., & Doblare, M. (2005). A bone remodelling model coupling microdamage growth and repair by 3D BMU-activity. *J. Biomechanical Modeling & Mechanobiology , 4*, 147-167.

Gausepohl, T., Mohring, R., Pennig, D., & Koebke, J. (2001). Fine thread versus coarse thread A comparison of the maximum holding power. *Injury, Int. J. Care Injured* (32), S-D-1-S-D-7.

Gautier, E., Perren, S., & Cordey, J. (2000). Strain distribution in plated and unplated sheep tibia: An in vivo experiment. *Injury, International J. for Care of the Injured , 31*, SC37-SC44.

Gefen, A. (2002). Computational simulation of stress shielding and bone resorption around existing and computer-designed orthopaedic screws. *J. Medical and Biological Engineering and Computing , 40*, 311-322.

Gefen, A. (2002). Optimizing the biomechanical compatibility of orthopaedic screws for bone fracture fixation. *J. Medical Engineering &Physics , 24*, 337-347.

Gibson, L. (1985). The mechanical behaviour of cancellous bone. *J Biomech. , 18* (5), 317-328.

Glowniak, J. V., & Miller, P. R. (2009). *Orthopaedic Hardware Atlas*. Retrieved from Orthopedic Hardware: A teaching program and atlas of orthopaedic hardware: http://www.med.wayne.edu/diagradiology/RSNA2003/screws_atlas.htm

Goel, V., Lim, T.-H., Gwon, J., Chen, J.-Y., Winterbottom, J., Park, J., et al. (1991). Effects of rigidity on an internal fixation device. *SPINE , 16* (3).

Gogolewski, S. (2000). Bioresorbable polymers in trauma and bone surgery. *Injury , 31* (4), D28-D32.

Goldhahn, J., Seebeck, J., Frenz, M., Antoniadis, I., & Schneider, E. (2005). New implant designs for fracture fixation in osteoporotic bone. *Osteoporosis International , 16*, S112-S119.

Goodacre, C., Kan, J., & Rungcharassaeng, K. (1999). Clinical complications of osseointegrated implants. *J. Prosthetic Dentistry, 81* (5), 537-552.

Goodship, A., & Kenwright, J. (1985). The influence of induced micromovement upon the healing of experimental tibial fractures. *J. Bone and Joint Surgery, 67B* (4), 650-655.

Gray, C., Boyde, A., & Jones, S. (1996). Topographically induced bone formation in vitro: Implications for bone implants and bone grafts. *J. Bone, 18* (2), 115-123.

Haase, K., & Rouhi, G. (2009). FEA orthopaedic screw optimization to reduce stress shielding. *CANCAM.* Halifax.

Haase, K., & Rouhi, G. (2008). Finite element analysis of a fracture fixation plate. *CSME Forum.* Ottawa.

Haase, K., & Rouhi, G. (2008). Finite element analysis of a fracture fixation plate: A parametric study. *CMBES Conference.* Montreal.

Haasnoot, E. F., Munch, T., Matter, P., & Perren, P. (1995). Radiological sequences of healing in internal plate and splints of different contact surface to bone. *Journal*, B28-SB36.

Halawa, M., Lee, A., Ling, R., & Vangala, S. (1978). The shear strength of trabecular bone from the femur,and some factors affecting the shear strength of the cement-bone interface. *Archives of Orthopaedic & Traumatic Surgery*, 19-30.

Hammel, S., Pluhar, G., Novo, R., Bourgeault, C., & Wallace, L. (2006). Fatigue analysis of plates used for fracture stabilization in small dogs and cats. *Veterinary Surgery, 35*, 573-578.

Hansson, S., & Werkeb, M. (2003). The implant thread as a retention element in cortical bone: the effect of thread size and thread profile: a finite element study. *Journal of Biomechanics, 36*, 1247–1258.

Harnroongroj, T., & Techataweewan, A. (1999). Determination of the role of the cancellous bone in generation of screw holding power at metaphysis. *Clinical Biomechanics, 14*, 364-366.

Harrigan, T., & Hamilton, J. (1993). Bone strain sensation via transmembrane potential changes in surface osteoblasts: loading rate and microstructural implications. *J. Biomechanics, 26* (2), 183-200.

Harrington, K. (1975). The use of methylmethacrylate as an adjunct in the internal fixation of unstable intertrochanteric fractures in osteoporotic patients. *J. Bone and Joint Surgery, 57A* (6).

Hart, R., Davy, D., & Heiple, K. (1984). Mathematical modeling and numerical solutions for functionally dependent bone remodelling. *Calcified Tissue International, 36*, 104-109.

Hart, R., Oden, Z., Parrish, S., & Burr, D. (1992). Computational methods for bone mechanics studies. *International J. Supercomputer Applications, 6* (2), 164-174.

Hawkins, R., Bell, R., & Gurr, K. (1986). The three-part fracture of the proximal part of the humerus. Operative treatment. *J. Bone and Joint Surgery , 68*, 1410-1414.

Haynes, R., Poll, R., Miles, A., & Weston, R. (1997). An experimental study of the failure modes of the Gamma locking nail and AO dynamic hip screw under static loading: a cadaveric study. *Medical Engineering & Physics , 19* (5), 446-453.

Hearn, T., Schatzker, J., & Wolfson, N. (1993). Extraction strenght of cannulated cancellous bone screws. *J. Orthopaedic Trauma* , 138-141.

Hegedus, D., & Cowin, S. (1976). Bone remodelling 2: small strain adaptive elasticity. *J. Elasticity , 6* (4), 337-352.

Hente, R., Cordey, J., & Perren, S. (2003). In vivo measurement of bending stiffness in fracture healing. *Biomedical Engineering Online , 2*.

Higgins, T. (2007). "Shimming" a locking plate with washers to correct axial alignment. *J. Orthopaedic Trauma , 21* (6).

Hofer, H., Wildburger, R., & Szyszkowitz, R. (2001). Observations concerning different patterns of bone healing using the point contact fixator (PC-Fix) as a new technique for fracture fixation. *Injury, International J. for the Care of the Injured , 32*, SB15-SB25.

Hughes, A., & Jordan, B. (1972). The mechanical properties of surgical bone screws and some aspects of insertion practice. *Injury , 4*, 25-38.

Huiskes, R. (1982). On the modelling of long bones in structural analyses. *J. Biomechanics , 15* (1), 65-69.

Huiskes, R., Ruimerman, R., Van Lenthe, G., & Janssen, J. (2000). Effects of mechanical forces on maintenance and adaptation of form in trabecular bone. *Nature , 405*, 704-706.

Huiskes, R., Weinans, H., Grootenboer, H., Dalstra, M., Fudala, B., & Slooff, T. (1987). Adaptive bone-remodelling theory applied to prosthetic-design analysis. *J. Biomechanics , 20* (11-12), 1135-1150.

Inceoglua, S., Ehlert, M., Akbayb, A., & McLainc, R. (2006). Axial cyclic behaviourof the bone-screw interface. *Medical Engineering & Physics , 28*, 888-893.

Isaksson, H., & Lerner, A. (2003). Mathematical modeling of stress shielding with bioresorbable materials for internal fracture fixation. *Summer Bioengineering Conference.* Florida.

Isaksson, H., Comas, O., Van Donkelaar, C., Mediavilla, J., Wilson, W., Huiskes, R., et al. (2006). Bone regeneration during distraction osteogenesis: Mechano-regulation by shear strain and fluid velocity. *J. Biomechanics* .

Jacobs, C., Levenston, M., Beaupre, G., Simo, J., & Carter, D. (1995). Numerical instabilities in bone remodelling simulations: the advantages of a node-based finite element approach. *J. Biomechanics , 28* (4), 449-459.

Johnson, K., & Smith, F. (2003). Axial compression generated by cortical and cancellous lag screws in the equine distal phalanx. *The Veterinary Journal , 166*, 159–163.

Jung, D.-Y., Kang, Y.-B., Tsutsumi, S., & Nakai, R. (2006). Computational evaluation of the effects of bone ingrowth on bone resorptive remodelling after a cementless total hip arthroplasty. *JSME International , 49* (1), 135-143.

Jung, D.-Y., Tsutsumi, S., Nakai, R., Ikeuchi, K., & Sekel, R. (2004). Uncemented total hip replacement stem loosening after long term compressive stress application: a simulated FEA study of cortical bone remodelling. *JSME International , 47* (4).

Juvinall, R., & Marshek, K. (2000). *Fundamentals of Machine Component Design.* USA: John Wiley & Sons, Inc.

Kanchanomai, C., Phiphobmongkol, V., & Muanjan, P. (2007). Fatigue failure of an orthopaedic implant - A locking compression plate. *Engineering Failure Analysis , 04* (01).

Kannus, P., Niemi, S., Parkkari, J., Palvanen, M., Heinonon, A., Sievanen, H., et al. (2002). Perspective: Why is the age-standardized incidence of low-trauma fractures rising in many elderly populations? *J. Bone and Mineral Research , 17* (8), 1363-1367.

Kawagoe, K., Saito, M., Shibuya, T., Nakashima, T., Hino, K., & Yoshikawa, H. (2000). Augmentation of cancellous screw fixation with hydroxyapatite composite resin (CAP) in vivo.

Kawashima, T., & Uhthoff, H. (1991). Pattern of bone loss of the proximal femur: a radiologic, densitometric, and histomorphometric study. *J. Orthopaedic Research , 9* (5), 634-640.

Kim, W.-Y., Han, C.-H., Park, J.-I., & Kim, J.-Y. (2001). Failure of intertrochanteric fracture fixation with a dynamic hip screw in relation to pre-operative fracture stability and osteoporosis. *International Orthopaedics , 25*, 360-362.

King, J. (1986). Stiffness variation in semi-rigid plate fixation. *Clinical Materials , 1*, 221-224.

King, T., & Cebon, D. (1992). An alternative to screws for plating osteoporotic bone. *J. Biomedical Engineering , 15*, 79-82.

Klaue, K., Fengels, I., & Perren, S. (2000). Long-term effects of plate osteosynthesis: Comparison of four different plates. *Injury, International J. for Care of the Injuredq , 31* (2), SB51-SB62.

Kotha, S., Hsieh, Y., Strigel, R., Muller, R., & Silva, M. (2004). Experimental and finite element analysis of the rat ulnar loading model - correlations between strain and bone formation following fatigue loading. *J. Biomechanics , 37*, 541-548.

Krag, M., Beynnon, B., Pope, M., Frymoyer, J., Haugh, L., & Weaver, D. (1986). An internal fixator for posterior application to short segments of the thoracic lumbar, or lumbosacral spine. Design and testing. *Clinical Orthopaedics and Related Research* (203), 75-98.

Kubiak, E., Fulkerson, E., Strauss, E., & Egol, K. (2006). The evolution of locked plates. *J. Bone and Joint Surgery, 88-A* (4), 189-200.

Lawrence, J. (2000). Mechanics of Hard Tissue. In J. Bronzino, *The Biomedical Engineering Handbook.* CRC Press.

Lin, C.-L., Lin, Y.-H., & Chen, C.-Y. (2006). Buttressing angle of the double-plating fixation of a distal radius fracture: a finite element study. *Medical & Biological Engineering & Computing, 44*, 665-673.

Lin, D.-J., Chuang, C.-C., Lin, J.-H., Lee, J.-W., Ju, C.-P., & Yin, H.-S. (2007). Bone formation at the surface of low modulus Ti-7.5Mo implants in rabbit femur. *Biomaterials, 28*, 2582-2589.

Lindsey, R., Leggon, R., & Panjabi, M. (1991). Biomechanics of healed experimental fractures. *Clinical Biomechanics, 6* (2), 83-87.

Lyon, W., Cochran, J., & Smith, L. (1941). Actual holding power of various screws in bone. *Annals of Surgery, 114* (3), 376-384.

Manolagas, S., & Jilka, R. (1995). Bone marrow, cytokines, and bone remodeling - Emerging Insights into the Pathophysiology of Osteoporosis. *The New England Journal of Medicine, 332* (5), 305-311.

Martens, M., Van Audekercke, R., De Meester, P., & Mulier, J. (1986). Mechanical behaviour of femoral bones in bending loading. *J. Biomechanics, 19* (6), 443-454.

Martens, M., Van Audekercke, R., De Meester, P., & Mulier, J. (1980). The mechanical characteristics of the long bones of the lower extremity in torsional loading. *J. Biomechanics, 13*, 667-676.

Martin, R. (1991). Determinants of the mechanical properties of bones. *J. Biomechanics, 24*, 79-88.

Martin, R. (1972). The effects of geometric feedback in the development of osteoporosis. *J. Biomechanics, 5*, 447-455.

Martin, R. (2000). Toward a unifying theory of bone remodelling. *J. Bone, 26* (1), 1-6.

Martinez, G., Aznar, J., Doblare, M., & Cerrolaza, M. (2006). External bone remodelling through boundary elements and damage mechanics. *Mathematics and Computers in Simulation, 73*, 183-199.

Maurer, P., Holweg, S., & Schubert, J. (1999). Finite-element-analysis of different screw-diamters in the sagittal split osteotomy of the mandible. *J. Cranio-Maxillofacial Surgery, 27*, 365-372.

McCartney, W., MacDonald, B., & Hashmi, M. (2005). Comparative performance of a flexible fixation implant to a rigid implant in static and repetitive incremental loading. *J. Materials Processing Technology , 169*, 476-484.

McCullen, G., & Garfin, S. (2000). Cervical spine internal fixation using screw and screw-plate constructs. *SPINE , 25* (5), 643-652.

Miclau, T., & Martin, R. (1997). The evolution of modern plate osteosynthesis. *Injury , 28* (1), SA3-SA6.

Miller, D., & Goswami, T. (2007). A review of locking compression plate biomechanics and their advantages as internal fixators in fracture healing. *Clinical Biomechanics , 22*, 1049-1062.

Minister of Public Works and Government Services Canada. (2002). *Canada's aging population.* Ottawa: Division of Aging and Health Services.

Mori, S., & Burr, D. (1993). Increased intracortical remodelling following fatigue damage. *J. Bone , 14*, 103-109.

Moroni, A., Faldini, C., Marchetti, S., Manca, M., Consoli, V., & Giannini, S. (2001). Osteoporotic bone with use of hydroxyapatite-coated tapered external-fixation pins. *J. Bone and Joint Surgery , 83-A* (5), 717-721.

Mosley, J., & Lanyon, L. (1998). Strain rate as a controlling influence on adaptive modeling in response to dynamic loading of the ulna in growing male rats. *J. Bone , 23* (4), 313-318.

Mow, V., & Huiskes, R. (2005). *Basic Orthopaedic Biomechanics and Mechano-Biology* (3rd Edition ed.). Lippincott Williams & WilKins.

Mullender, M., & Huiskes, R. (1995). Proposal for the regulatory mechanism of Wolff's law. *J. Orthopaedic Research , 13* (4), 503-512.

Mullender, M., Huiskes, R., & Weinans, H. (1994). A physiological approach to the simulation of bone remodelling as a self-organizational control process. *J. Biomechanics , 27* (11), 1389-1394.

Mullender, M., Van Der Meer, D., Huiskes, R., & Lips, P. (1996). Osteocyte density changes in aging and osteoporosis. *J. Bone , 18* (2), 109-113.

Myers, E., Hecker, A., Rooks, D., Hipp, J., & Hayes, W. (1993). Geometric Variables from DXA of the Radius Predict Forearm Fracture Load In Vitro. *Calcif Tissue Int , 52*, 199-204.

Nalla, R., Kinney, J., & Ritchie, R. (2002). Mechanistic fracture criteria for the failure of human cortical bone. *Nature Materials* .

Namazi, H., & Mozaffarian, K. (2007). Awful considerations with LCP instrumentation: a new pitfall. *Archives of Orthopaedic Trauma Surgery , 127*, 573-575.

Nazzal, A., Lozano-Calderon, S., Jupiter, J., Rosenzweig, J., Randolph, M., & Lee, S. (2006). A histological analysis of the effects of stainless steel and titanium implants adjacent to tendons: An experimental rabbit study. *J. of Hand Surgery, 31A* (7).

New Life Surgical Works, C. (n.d.). *New Life Surgical Works.* (New Life Surgical Works) Retrieved from New Life Surgical Works: http://www.orthopaedicimplants.com/cancellous-screws.html

Niinomi, M. (2003). Recent research and development in titanium alloys for biomedical applications and healthcare goods. *Science and Technology of Advanced Materials, 4,* 445–454.

Nordin, M., & Frankel, V. (2008). *Basic biomechanics of the musculoskeletal system.*

Norman, T., & Wang, Z. (1997). Microdamage of human cortical bone: Incidence and morphology in long bones. *J. Bone, 20* (4), 375-379.

Nunamaker, D., & Perren, S. (1976). Force measurements in screw fixation. *J. Biomechanics, 9,* 669-675.

Okuyama, K., Abe, E., Suzuki, T., Tamura, Y., Chiba, M., & Sato, K. (2000). Can insertional torque predict screw loosening and related failures? *SPINE, 25* (7), 858–864.

Panagiotopoulus, E., Fortis, A., Millis, Z., Lambiris, E., Kostopoulos, V., & Vellios, L. (1994). Pattern of screw loosening in fractures fixed with conventional and functional plates. *Injury, 25* (8), 515-517.

Patel, P., Shepherd, D., & Hukins, D. (2008). Axial and angled pullout strength of bone screws in normal and osteoporotic bone material. *ICBME 2008 Conference Proceedings,* (pp. 1619-1622). Singapore.

Patterson, S., Daffner, R., & Gallo, R. (2005). Electrochemical Corrosion of Metal Implants. *American Journal of Roentgenology, 184,* 1219-1222.

Pattin, C., Caler, W., & Carter, D. (1996). Cyclic mechanical property degradation during fatigue loading of cortical bone. *J. Biomechanics, 29* (1), 69-79.

Perren, S. (2002). Evolution of the internal fixation of long bone fractures. *J. Bone and Joint Surgery, 84-B* (8), 1093-1110.

Perren, S., & al., e. (1969). The reaction of cortical bone to compression by screw threads. *Acta Orthopaedics, 125* (17).

Pilliar, R. (1979). Bone ingrowth and stress shielding with a porous surface coated fracture fixation plate. *Biomedical Materials Research, 13,* 799-810.

Popov, E. (1990). *Strength of Materials.* Englewood Cliffs, N. J.: Prentice Hall.

Prendergast, P. (1997). Review paper: Finite element models in tissue mechanics and orthopaedic implant design. *Clinical Biomechanics, 12* (6), 343-366.

Prendergast, P., & Taylor, D. (1994). Prediction of bone adaptation using damage accumulation. *J. Biomechanics , 27* (8), 1067-1076.

Ramakrishna, K., Sridhar, I., & Sivashanker, S. (2004). Design of fracture fixation plate for necessary and sufficient bone stress shielding. *JSME International J. , 47* (4).

Reilly, D., & Burstein, A. (1975). The elastic and ultimate properties of compact bone tissue. *J. Biomechanics , 8* (6), 393-405.

Reschauer, R., & Seggl, W. (1983). Results of AO plate fixation of forearm shaft fractures in adults. *Injury , 15* (1), 44-52.

Rho, J., Ashman, R., & Turner, C. (1993). Young's modulus of trabecular and cortical bone material: ultrasonic and microtensile measurements. *J. Biomechanics , 26* (2), 111-119.

Rice, J., S.C., C., & J.A., B. (1988). On the dependence of the elasticity and strength of cancellous bone on apparent density. *Journal of Biomechanics , 21*, 155-168.

Robert, K., Chandler, R., Baratta, R., Thomas, K., & Harris, M. (2003). The effect of divergent screw placement on the initial strength of plate-to-bone fixation. *J. Trauma , 55* (6), 1139-1144.

Roberts, J., Grindel, S., Rebholz, B., & Wang, M. (2007). Biomechanical evaluation of locking plate radial shaft fixation: Unicortical locking fixation versus mixed bicortical and unicortical fixation in a sawbone model. *J. Hand Surgery , 32A* (7), 971-975.

Rogmark, C., Carlsson, A., Johnell, O., & Sernbo, I. (2002). A prospective randomized trial of internal fixation versus arthroplasty for displaced fractures of the neck of the femur. *J. Bone and Joint Surgery , 84-B* (2), 183-188.

Rouhi, G. (2006, March). Theoretical aspects of bone remodelling and resorption processes. *PhD dissertation* . University of Calgary.

Rouhi, G., Epstein, M., Sudak, L., & Herzog, W. (2006). Free surface density and microdamage in the bone remodelling equation: Theoretical considerations. *International J. Engineering Science , 44*, 456-469.

Rouhi, G., Epstein, M., Sudak, L., & Herzog, W. (2007). Modeling bone resorption using mixture theory with chemical reactions. *J. Mechanics of Materials and Structures , 2* (6), 1141-1155.

Rouhi, G., Herzog, W., Sudak, L., Firoozbakhsh, K., & Epstein, M. (2004). Free surface density instead of volume fraction in the bone remodelling equation: Theoretical considerations. *Forma , 19*, 165-182.

Ruimerman, R., Hilbers, P., Van Rietbergen, B., & Huiskes, R. (2005). A theoretical framework for strain-related trabecular bone maintenance and adaptation. *J. Biomechanics , 38*, 931-941.

Ruimerman, R., Huiskes, R., Van Lenthe, G., & Janssen, J. (2001). A computer-simulation model relating bone-cell metabolism to mechanical adaptation of trabecular architecture. *Computational Methods in Biomechanics and Biomedical Engineeering , 4*, 433-448.

Rybicki, E., Simonen, F., & Weis Jr., E. (1972). On the mathematical analysis of stress in the human femur. *J. Biomechanics , 5*, 203-215.

Saidpour, S. (2006). Assessment of carbon fibre composite fracture fixation plate using finite element analysis. *Annals of Biomedical Engineering , 34* (7), 1157-1163.

Scannell, P., & Prendergast, P. (2006). Influence of stem stiffness of bone adaptation around cementless hip replacements using a strain & damage stimulus. *Bioenginnering in Ireland Conference.* Galway.

Schaffler, M., Radin, E., & Burr, D. (1989). Mechanical and morphological effects of strain rate on fatigue of compact bone. *Bone , 10*, 207-214.

Schatzker, J. (1996). Osteosynthesis in trauma. *International Orthopaedics , 20*, 244-252.

Schatzker, J., Horne, J., & Sumner-Smith, G. (1975). The effect of movement on the holding power of screws in bone. *Clinical Orthopaedics and Related Research , 111*, 257-262.

Schatzker, J., Horne, J., & Sumner-Smith, G. (1975). The reaction of cortical bone to compression by screw threads. (111), 263-265.

Schatzker, J., Sanderson, R., & Murnaghan, P. (1975). The holding power of orthopaedic screw in vivo. *Clinical orthopaedics and related research* , 115-126.

Schuller-Gotzburg, P., Krenkel, C., Reiter, T., & Plenk Jr., H. (1999). 2D-finite element analysis and histomorphology of lag screws with and without a biconcave washer. *J. Biomechanics , 32*, 511-520.

Schutz, M., & Sudkamp, N. (2003). Revolution in plate osteosynthesis: new internal fixator systems. *J. Orthopaedic Science , 8*, 252-258.

Simon, B., Woo, S.-Y., Stanley, G., Olmstead, S., McCarty, M., Jemmot, G., et al. (1977). Evaluation of one-, two-, and three-dimensional finite element models and experimental models of internal fixation plates. *J. Biomechanics , 10*, 79-86.

Sod, G., Mitchell, C., Hubert, J., Martin, G., & Gill, M. (2008). In vitro biomechanical comparison of locking compression plate fixation and limited-contact dynamic compression plate fixation of osteotomized equine third metacarpal bones. *Veterinary Surgery , 37*, 283-288.

Sommer, C., Babst, R., Muller, M., & Hanson, B. (2004). Locking compression plate loosening and plate breakage: a report of four cases. *J. Orthopaedic Trauma , 18* (8).

Stahl, E. (1993). Internal fixation of long bone fractures: concepts, controversies, debates. *J. Canadian Medical Association , 149* (6), 837-841.

Stankewich, C., Swiontkowski, M., Tencer, A., Yetkinler, D., & Poser, R. (1996). Augmentation of femoral neck fracture fixation with an injectable calcium-phosphate bone mineral cement. *J. Orthopaedic Research*, *14*, 786-793.

Stoffel, K., Dieter, U., Stachowiak, G., Gachter, A., & Kuster, M. (2003). Biomechanical testing of the LCP - how can stability in locked internal fixators be controlled? *Injury International J. for Care of the Injured*, *34*, SB11-SB19.

Stoffel, K., Klaue, K., & Perren, S. (. (2000). Functional load of plates in fracture fixation in vivo and its correlate in bone healing. *31* (2), S-B37–50.

Stoffel, K., Lorenz, K.-U., & Kuster, M. (2007). Biomechanical considerations in plate osteosynthesis: the effect of plate-to-bone compression with and without angular screw stability. *J. Orthopaedic Trauma*, *21* (6).

Stromsoe, K. (2004). Review: Fracture fixation problems in osteoporosis. *Injury, International J. for Care of the Injured*, *35*, 107-113.

Stromsoe, K., Kok, W., Hoiseth, A., & Alho, A. (1993). Holding power of the 4.5 mm AO/ASIF cortex screw in cortical bone in relation to bone mineral. *Injury, International J. for Care of the Injured*, *24* (10), 656-659.

Sugiura, T., Horiuchi, K., Sugimura, M., & Tsutsumi, S. (2000). Evaluation of threshold stress for bone resorption around screws based on in vivo strain measurement of miniplate. *J. Musculoskeletal Neuron Interactions*, *1* (2), 165-170.

Talaia, P., Ramos, A., Abe, I., Schiller, M., Lopes, P., Nogueria, R., et al. (2007). Plated and intact femur strains in fracture fixation using fiber bragg gratings and strain gauges. *Experimental Mechanics*, *47*, 355-363.

Tawara, D., Sakamoto, J., & Oda, J. (2005). Finite elment analysis considering material inhomogeneousness of bone using "Adventure system". *JSME International*, *48* (2), 292-298.

Taylor, M., Tanner, K., Freeman, M., & Yettram, A. (1996). Stress and strain distribution within the intact femur: compression or bending? *Medical and Engineering Physics*, *18* (2), 122-131.

Tencer, A., & Johnson, K. (1994). *Biomechanics in Orthopedic Trauma.* London: Martin Duntz, Ltd.

Tidermark, J., Ponzer, S., Svensson, O., Soderqvist, A., & Tornkvist, H. (2003). Internal fixation compared with total hip replacement for displaced femoral neck fractures in the elderly. *J. Bone and Joint Surgery*, *85-B* (3), 380-388.

Törnkvist, H., Hearn, T. C., & Schatzker, J. (1996). The Strength of Plate Fixation in Relation to the Number and Spacing of Bone Screws. *Journal of Orthopaedic Trauma*, *10* (3), 204-208.

Trader, J., Johnson, R., & Kalbfleisch, J. (1979). Bone mineral content, surface hardness and mechanical fixation in the human radius. *J Bone and Joint Surgery , 61A*, 1217-1220.

Turner, C. (2006). Bone strength - Current concepts. *Ann. N.Y. Acad. Sci. , 1068*, 429–446.

Turner, C. (1998). Three rules for bone adaptation to mechanical stimuli. *J. Bone , 23* (5), 399-407.

Uhthoff, H. (1973). Mechanical factors influencing the holding power of screws in compact bone. *J. Bone and Joint Surgery , 55B* (3), 633-639.

Uhthoff, H., & Dubuc, F. (1971). Bone structure changes in the dog under rigid internal fixation. *Clinical Orthopaedics and Related Research* (81), 165-170.

Uhthoff, H., & Finnegan, M. (1983). The effects of metal plates on post-traumatic remodelling and bone mass. *J. Bone and Joint Surgery , 65B* (1), 66-71.

Uhthoff, H., & Finnegan, M. (1984). The role of rigidity in fracture fixation: An overview. *Archives of Orthopaedic and Traumatic Surgery , 102*, 163-166.

Uhthoff, H., & Jaworski, Z. (1978). Bone loss in response to long-term immobilisation. *J. Bone and Joint Surgery , 60B* (3).

Uhthoff, H., Bardos, D., & Liskova-Kiar, M. (1981). The advantages of titanium alloy over stainless steel plates for the internal fixation of fractures: An experimental study in dogs. *J. Bone and Joint Surgery , 63B* (3), 427-434.

Uhthoff, H., Boisvert, D., & Finnegan, M. (1994). Cortical porosis under plates. Reaction to unloading or to necrosis? *J. Bone and Joint Surgery , 76A* (10), 1507-1512.

Uhthoff, H., Foux, A., Yeadon, A., McAuley, J., & Black, R. (1993). Two processes of bone remodelling in plated intact femora: an experimental study in dogs. *J. Orthopaedic Research , 11* (1), 78-91.

Uhthoff, H., Goto, S., & Cerckel, P.-H. (1987). Influence of stable fixation on trabecular bone healing: a morphologic assessment in dogs. *J. Orthopaedic Research , 5* (1), 14-22.

Uhthoff, H., Poitras, P., & Backman, D. (2006). Internal plate fixation of fractures: short history and recent developments. *J. Orthopaedic Science , 11*, 118-126.

Usui, Y., Zerwekh, J., Vanharanta, H., Ashman, R., & Mooney, V. (1989). Different effects of mechanical vibration on bone ingrowth into porous hydroxyapatite and fracture healing in a rabbit model. *J. Orthopaedic Research , 7*, 559-567.

Vahdati, A., & Rouhi, G. (2007). A model for mechanical adaptation of trabecular bone incorporating cellular accomodation and effects of microdamage and disuse.

Vahdati, A., Rouhi, G., Ghalichi, & Tahani, M. (2008). Mechanically induced trabecular bone remodeling including cellular accomodation effect: a computer simulation. *The CSME Transactions.*

Valliappan, S., Svensson, N., & Wood, R. (1977). Three dimensional stress analysis of the human femur. *Computational Biological Medicine*, *7*, 253-264.

Van Frank Haasnoot, E., Munch, T., Matter, P., & Perren, S. (1995). Radiological sequences of healing in internal plates and splints of different contact surface to bone. (DCP, LC-DCP and PC-Fix). *Injury*, *26* (2), SB28-SB37.

Van Lenthe, G., de Waal Malefijt, M., & Huiskes, R. (1997). Stress shielding after total knee replacement may cause bone resorption in the distal femur. *Bone and Joint Surgery*, *79-B* (1), 117-122.

Van Rietbergen, B., Weinans, H., Huiskes, R., & Odgaard, A. (1995). A new method to determine trabecular bone elastic properties and loading using micromechanical finite-element models. *J. Biomechanics*, *28* (1), 69-81.

Van Sickels, J., Peterson, G., Holms, S., & Haug, R. (2005). An in vitro comparison of an adjustable bone fixation system. *J. Oral and Maxillofacial Surgery*, *63* (11), 1620-1625.

Vangsness, C. T., Carter, D. R., & Frankel, V. H. (1981). In vitro evaluation of the loosening characteristics of self-tapped and non-self-tapped cortical bone screws. (151), 279-286.

Veerabagu, S., Fujihara, K., Dasari, G., & Ramakrishna, S. (2003). Strain distribution analysis of braided composite bone plates. *Composites Science and Technology*, *62*, 427-435.

Viceconti, M., Bellingeri, L., Crstofolini, L., & Toni, A. (1998). A comparitive study on different methods of automatic mesh generation of human femurs. *Medical Engineering & Physics*, *20*, 1-10.

Wade, R., & Richardson, J. (2001). Outcome in fracture healing: a review. *Injury, International J. for Care of the Injured*, *32*, 109-114.

Wagner, M. (2003). General principles for the clinical use of the LCP. *Injury, International J. for Care of the Injured*, *34*, SB31-SB42.

Wang, C., Brown, C., Yettram, A., & Procter, P. (2000). Intramedullary femoral nails: one or two lag screws? A preliminary study. *Medical Engineering & Physics*, *22*, 613-624.

Wang, C., Yettram, A., Yao, M., & Procter, P. (1998). Finite element analysis of a Gamma nail within a fractured femur. *Medical Engineering & Physics*, *20*, 677-683.

Weinans, H., Huiskes, R., & Grootenboer, H. (1992). The behaviour of adaptive bone-remodelling simulation models. *J. Biomechanics*, *25* (12), 1425-1441.

Weinbaum, S., Cowin, S., & Zeng, Y. (1994). A model for the excitation of osteocytes by mechanical loading-induced bone fluid shear stresses. *J. Biomechanics*, *27* (3), 339-360.

Wenda, K., Runkel, M., Degreif, J., & Rudig, L. (1997). Minimally invasive plate fixation in femoral shaft fractures. *Injury*, *28* (1), SA13-SA19.

Wenzl, M., Porte, T., Fuchs, S., Faschingbauer, M., & Jurgens, C. (2004). Delayed and non-union of the humeral diaphysis - compression plate or internal fixator? *Injury, International J. for Care of the Injured*, *35*, 55-60.

Whalen, R., & Carter, D. (1988). Influence of physical activity on the regulation of bone density. *J. Biomechanics*, *21* (10), 825-837.

Wheeless III, C. R., Nunley II, J. A., & Urbaniak, J. R. (2009, January 23). *Wheeless' Textbook of Orthopaedics*. Retrieved from http://www.wheelessonline.com/

Wolff, J. (1892). Das Gesetz der Transformation der Knochen. *A. Hirschwald, Berlin* .

Wong, C., Gehrchen, P., Darvann, T., & Kiaer, T. (2003). Nonlinear finite-element analysis and biomechanical evalutation of the lumbar spine. *IEEE Transactions on Medical Imaging*, *22* (6).

Woo, S.-Y., Lothringer, K., Akeson, W., Coutts, R., Woo, Y., Simon, B., et al. (1984). Less rigid internal fixation plates: historical perspectives and new concepts. *J. Orthopaedic Research*, *1*, 431-449.

Woo, S.-Y., Simon, B., Akeson, W., & McCarty, M. (1977). An interdisciplinary approach to evaluate the effect of internal fixation plate on long bone remodelling. *J. Biomechanics*, *10*, 87-95.

Woo, S.-Y., Simon, B., Akeson, W., Gomez, M., & Seguchi, Y. (1983). A new approach to the design of internal fixation plates. *J. Biomedical Materials Research*, *17*, 427-439.

Zhang, Q., Tan, S., & Chou, S. (2004). Investigation of fixation screw pull-out strength on human spine. *Journal of Biomechanics*, *37*, 479-485.

Zimmermann, R., Gabl, M., Lutz, M., Angermann, P., Gschwentner, M., & Pechlaner, S. (2003). Injectable calcium phosphate bone cement Norian SRS for the treatment of intra-articular compression fractures of the distal radius in osteoporotic women. *Archives of Orthopaedic and Traumatic Surgery*, *123*, 22-27.

Zindrick, M., Wiltse, L., Widell, E., Thomas, J., Holland, W., Field, B., et al. (1986). A biomechanical study of intrapeduncular screw fixation in the lumbosacral spine. *Clinical Orthopaedics and Related Research* (203), 99-112.

Publications Arising from This Research

Journal Papers

Haase K., Rouhi G., "A Discussion on Plating Factors that Affect Stress Shielding Using Finite Element Analysis", JSME, *accepted November 2009*.

Haase K., Rouhi G., "An Evolution in Thinking: Adaptive Remodelling Theories and Bone-Plate Fixation – A Review Paper", *Currently under review*.

Conference Papers

Haase K., Rouhi G., "Reducing Stress Shielding: FEA of Orthopaedic Screws", CANCAM Conference, Dalhousie University, Halifax, May 2009.

Haase K., Rouhi G., "Finite Element Analysis of a Fracture Fixation Plate", Canadian Society for Mechanical Engineering Forum, Ottawa, June 2008.

Haase K., Rouhi G., "Finite Element Analysis of a Fracture Fixation Plate: A Parametric Study", Canadian Medical and Biological Engineering Society 31st Annual Conference, Montreal, June 2008.

Posters

Haase K., Rouhi G., "Finite Element Analysis of a Fracture Fixation Plate: A Parametric Study", University of Ottawa, February 2008.

Haase K., Rouhi G., "Stress or Strain Energy Density as Osteogenesis Stimuli? A FEA Comparing Orthopaedic screws", University of Ottawa, February 2009.

Appendix i: STP results

Table 5: STP parametric results

Profile Shape	Shaft Length (mm)	Screw Elastic Modulus (Pa)		Diameter of Threads (mm): 4 — Number of Threads: 5	8	9	Diameter of Threads (mm): 6 — Number of Threads: 5	8	9
Triangle	5	1.05E+11	α	0.510636	0.499648	0.524506	0.259745	0.243821	0.233067
			β	0.267574	0.264421	0.302244	0.253433	0.264646	0.1229156
		4.00E+10	α	0.564808	0.662463	[redacted]	0.338086	0.370867	0.3907423
			β	0.320419	0.368844	[redacted]	0.368365	0.416032	0.2972144
	1	1.05E+11	α	0.624785	0.526757	0.530097	0.251659	0.224032	0.2130784
			β	0.293104	0.229228	0.263625	0.247151	0.234164	0.1146121
		4.00E+10	α	0.637825	0.563431	0.597075	0.298157	0.282194	0.2724136
			β	0.328164	0.331019	0.385599	0.353726	0.370277	0.2539633
Rectangle	5	1.05E+11	α	0.199001	0.193738	0.19329	0.134025	0.136023	0.1353428
			β	0.057362	0.075544	0.094667	0.153744	0.176794	0.0995761
		4.00E+10	α	0.260835	0.271381	0.286208	0.20885	0.229146	0.2386064
			β	0.1463	0.199817	0.248571	0.276824	0.329883	0.2536258
	1	1.05E+11	α	0.240616	0.225776	0.213378	0.12387	0.113976	0.1100777
			β	0.055064	0.071347	0.077325	0.151043	0.154034	0.0889965
		4.00E+10	α	0.264126	0.247048	0.235119	0.189364	0.183879	0.1820808
			β	0.134729	0.181942	0.199198	0.270356	0.293225	0.2212263
Trapezoid	5	1.05E+11	α	0.250005	0.25262	0.249387	0.190647	0.190931	0.1897928
			β	0.08229	0.094153	0.103949	0.080322	0.152117	0.2030143
		4.00E+10	α	0.320794	0.35447	0.375482	0.275484	0.302219	0.31944
			β	0.158101	0.204324	0.245287	0.179952	0.350728	0.4493206
	1	1.05E+11	α	0.339268	0.314984	0.304326	0.192826	0.173626	0.1688981
			β	0.085973	0.094347	0.098331	0.082075	0.128397	0.1456863
		4.00E+10	α	0.365915	0.343998	0.336037	0.252207	0.237895	0.2380254
			β	0.155866	0.18982	0.20535	0.180243	0.295352	0.3326877

Table 6: Total STP values

Profile shape/ shaft length/ elastic modulus/ diameter of thread	*Number of Threads* 5	8	9	*Profile shape/ shaft length/ elastic modulus/ diameter of thread*	*Number of Threads* 5	8	9
Triangle - long/105/4	0.78	0.76	0.83	Triangle - long/105/6	0.51	0.51	0.36
Triangle - long/40/4	0.89	1.03	1.16	Triangle - long/40/6	0.71	0.79	0.69
Triangle - short/105/4	0.92	0.76	0.79	Triangle - short/105/6	0.50	0.46	0.33
Triangle - short/40/4	0.97	0.89	0.98	Triangle - short/40/6	0.65	0.65	0.53
Rectangle - long/105/4	0.26	0.27	0.29	Rectangle - long/105/6	0.29	0.31	0.23
Rectangle - long/40/4	0.41	0.47	0.53	Rectangle - long/40/6	0.49	0.56	0.49
Rectangle - short/105/4	0.30	0.30	0.29	Rectangle - short/105/6	0.27	0.27	0.20
Rectangle - short/40/4	0.40	0.43	0.43	Rectangle - short/40/6	0.46	0.48	0.40
Trapezoid - long/105/4	0.33	0.35	0.35	Trapezoid - long/105/6	0.27	0.34	0.39
Trapezoid - long/40/4	0.48	0.56	0.62	Trapezoid - long/40/6	0.46	0.65	0.77
Trapezoid - short/105/4	0.43	0.41	0.40	Trapezoid - short/105/6	0.27	0.30	0.31
Trapezoid - short/40/4	0.52	0.53	0.54	Trapezoid - short/40/6	0.43	0.53	0.57

Appendix ii: SEDTP results

Table 7: SEDTP parametric results

Profile Shape	Shaft Length (mm)	Screw Elastic Modulus (Pa)		Diameter of Threads (mm): 4			6		
				Number of Threads			Number of Threads		
				5	8	9	5	8	9
Triangle	5	1.05E+11	α	1.94891	2.645391	2.276138	3.701594	3.872183	3.4244118
			β	0.641181	0.497352	0.451364	4.815611	[redacted]	0.5656097
		4.00E+10	α	2.121765	3.332359	3.033031	3.102142	3.96767	4.1509289
			β	0.835729	0.83749	0.971043	3.781378	5.282764	1.5758312
	1	1.05E+11	α	2.630102	2.474043	2.631866	4.543223	3.998681	3.5487176
			β	0.644155	0.473197	0.361625	6.172945	4.83789	0.571692
		4.00E+10	α	2.543486	2.382992	2.764291	2.905031	2.654278	2.4308925
			β	0.804788	0.71662	0.61018	4.00618	3.953774	1.3976318
Rectangle	5	1.05E+11	α	3.819496	3.54923	3.310283	1.454534	1.512708	1.4941756
			β	0.080633	0.383033	0.484727	2.261597	3.267608	0.4822504
		4.00E+10	α	2.545762	2.7447	2.971872	1.458579	1.758647	1.9072268
			β	0.370633	1.112513	1.48526	2.377303	3.401357	1.448916
	1	1.05E+11	α	5.737314	4.967549	4.428468	1.308091	1.178796	1.1091854
			β	0.271113	0.410771	0.446324	2.423011	2.439073	0.4751228
		4.00E+10	α	2.699153	2.358947	2.155852	1.258336	1.221455	1.2062824
			β	0.642839	1.077993	1.225426	2.405379	2.699645	1.317036
Trapezoid	5	1.05E+11	α	5.671982	5.752286	5.665703	2.294886	2.361422	2.3739038
			β	0.53788	0.583678	0.590745	0.399105	1.451026	2.5117797
		4.00E+10	α	3.656383	4.41686	5.002592	2.172091	2.619421	2.9329614
			β	0.805029	1.112288	1.366013	0.906506	3.449548	5.4635012
	1	1.05E+11	α	[redacted]	9.460934	8.573011	2.638795	2.441954	2.3585146
			β	0.586438	0.649364	0.674113	0.528105	1.056996	1.3807453
		4.00E+10	α	4.850963	4.343556	4.040091	2.015077	1.922397	1.9547541
			β	0.797331	1.079131	1.210667	1.0381	2.477271	3.1470283

Table 8: Total SEDTP values

Profile shape/ shaft length/ elastic modulus/ diameter of thread	*Number of Threads*			*Profile shape/ shaft length/ elastic modulus/ diameter of thread*	*Number of Threads*		
	5	8	9		5	8	9
Triangle - long/40/4	2.96	4.17	4.00	Triangle - long/40/6	6.88	9.25	5.73
Triangle - short/105/4	3.27	2.95	2.99	Triangle - short/105/6	10.72	8.84	4.12
Triangle - short/40/4	3.35	3.10	3.37	Triangle - short/40/6	6.91	6.61	3.83
Rectangle - long/105/4	3.90	3.93	3.80	Rectangle - long/105/6	3.72	4.78	1.98
Rectangle - long/40/4	2.92	3.86	4.46	Rectangle - long/40/6	3.84	5.16	3.36
Rectangle - short/105/4	6.01	5.38	4.87	Rectangle - short/105/6	3.73	3.62	1.58
Rectangle - short/40/4	3.34	3.44	3.38	Rectangle - short/40/6	3.66	3.92	2.52
Trapezoid - long/105/4	6.21	6.34	6.26	Trapezoid - long/105/6	2.69	3.81	4.89
Trapezoid - long/40/4	4.46	5.53	6.37	Trapezoid - long/40/6	3.08	6.07	8.40
Trapezoid - short/105/4	11.31	10.11	9.25	Trapezoid - short/105/6	3.17	3.50	3.74
Trapezoid - short/40/4	5.65	5.42	5.25	Trapezoid - short/40/6	3.05	4.40	5.10

Appendix iii: Theoretical analysis

An overview of composite beam theory, in relation to the simplified plated-bone construct used in this study, followed by a brief introduction to beam on elastic foundation theory will be outlined in this section.

Composite beam theory

Considered to be a structural element that is able to withstand loads, beams are primarily resistant to bending modes of loading. Single-phase beams, comprised of a single material, are commonly used in industry, and are generally characterized by their cross-sectional profile, length, and material. Composite beams, on the other hand, are comprised of two or more dissimilar materials (usually metals), and are usually designed to be stronger as a whole than the sum of its parts. From this definition, bone, itself, can be considered a composite beam. Bone consists of two cortices of dense lamellar bone and a medullary canal mainly comprised of cancellous bone that, as a whole, acts to resist physiological loading, the majority of which is bending.

As a simplification of the linear theory of elasticity, the Euler-Bernoulli beam theory provides a means for determining the load-carrying and deflection characteristics of beams, both single-phase and composite. This theory is useful in the case of analyzing bone and bone-plate constructs, as in this study, where the bone and plate are considered to act as a two-material composite beam. This is an accepted form of analysis when the plated-bone construct is considered after union of the fracture has occurred (Bartel, Davy, & Keaveny, 2006, pp. 168-169). This theory can be used to predict stresses and strains in both the bone and plate prior to the development of an implant, as well as validate those regions in a finite element model where beam theory applies, i.e. in sections away from regions of an applied load or abrupt changes in geometry. The calculations involved in determining the stresses in the plate and bone as functions of the geometry, loads, and material properties of the structure, are outlined in this chapter.

Axial loading

Beam theory is developed using a strain-displacement relationship, equilibrium relationships, and material behaviours (Bartel, Davy, & Keaveny, 2006, pp. 168-169). The theory is based on the assumption that plane sections remain plane after loading, therefore it results in constant strain over a cross-section for an axially loaded beam (see Figure 54 (adapted from (Bartel, Davy, &

Keaveny, 2006, p. 170)), and strain that varies linearly from the neutral axis for a beam in bending (see Figure 55).

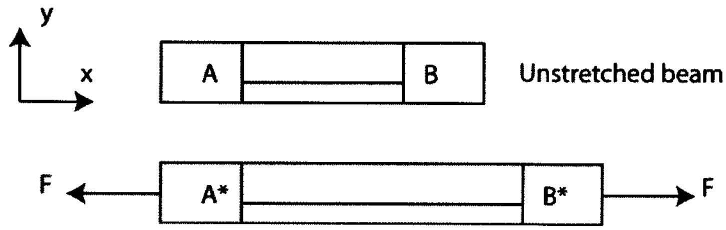

Figure 59: Axial loading of a single-material beam

Based on this assumption and a second one that states that the only stress is the longitudinal stress (σ_x) during axial loading, the strain may be defined as follows (Bartel, Davy, & Keaveny, 2006, p. 170):

$$\varepsilon_x = \lim_{AB \to 0} \frac{A^*B^* - AB}{AB} \tag{2}$$

Where:

$A, and\ B\ are\ the\ location\ of\ the\ original\ points\ on\ the\ unstretched\ beam,$
$and\ A^*\ and\ B^* are\ the\ location\ of\ the\ points\ after\ the\ tensile\ load\ is\ applied\ to\ the\ beam.$

Since the strain is constant over the entire cross-section for uni-axial loading, then for elastic behaviour, and from Hooke's law, the stress can be written as:

$$\sigma_x = E\varepsilon_x = EC$$

Where:

$\sigma_x\ is\ the\ stress\ in\ the\ direction\ of\ the\ applied\ load;$
$E\ is\ the\ material's\ modulus\ of\ elasticity;$
$and\ C\ is\ a\ constant.$

(3)

From equilibrium, we know that the stress must be equal to the applied load, F:

$$F = \int_A \sigma_x dA$$

Where:

$A\ is\ the\ cross-sectional\ area\ of\ the\ beam.$

(4)

Substitution of stress into the equilibrium equation, and integration with respect to the cross-sectional area, simply results in the commonly recognized stress-load relationship:

$$\sigma_x = \frac{F}{A} \tag{5}$$

For the case of a composite beam the resultant load is given as:

$$F = \sum_{i=1}^{n} \int_{A_i} \sigma_x dA \tag{6}$$

In the case of a single material beam, the material's modulus of elasticity does not have an effect on the stress that develops from the uni-axial load as the stress is only dependent on the force applied to its cross-sectional area (Cowin, 2001, p. 234). On the other hand, the various moduli of elasticity of the materials in a composite beam do play a significant role in the resulting stress distribution, as can be seen in Figure 55.

$$F = C(E_i A_i) \tag{7}$$

The stress-load relationship then becomes:

$$\sigma_j = \frac{E_j}{\sum_{i=1}^{n} E_i A_i} F \tag{8}$$

where:

σ_j *is the normal stress in the x direction in the* j^{th} *material, for an* $n-$*material beam.*

Bending

In the case of bending about an axis perpendicular to the plane of symmetry, the deformation of a symmetric beam varies linearly from the neutral axis (Figure 55 (adapted from (Bartel, Davy, & Keaveny, 2006, p. 171)).

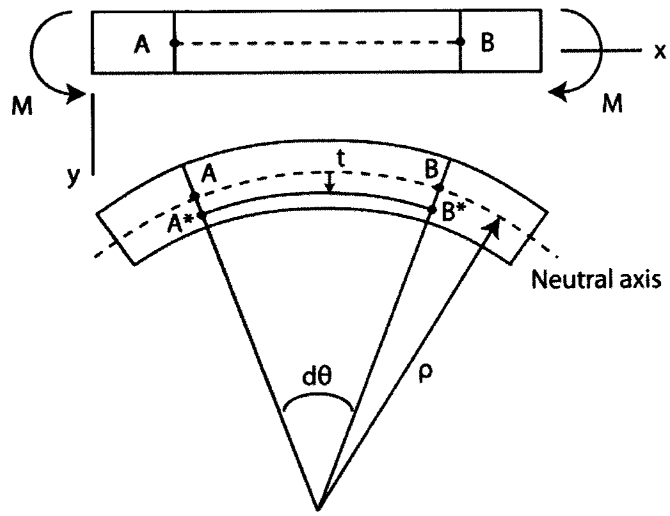

Figure 60: Single material beam under bending load

When represented by a short distance, t, from the neutral axis, the strain relationship reduces to (Bartel, Davy, & Keaveny, 2006):

$$\varepsilon_x = -\frac{t}{\rho} \tag{9}$$

Where:

ρ *represents the radius of curvature of the neutral axis;*

and t is the distance from the neutral axis as shown in Figure 55.

Once again, for elastic behaviour, Hooke's law applies, and the resultant moment at a cross section can be written as:

$$M_z = \frac{E}{\rho}\int_A t^2 dA \tag{10}$$

Solving the integral results in the equation for bending (in one axis) of a one-material beam:

$$\sigma_x = -\frac{Mt}{I}$$

Where:

I is the second moment of inertia.

(11)

Since no axial forces exist during bending, the location of the neutral axis can then be found by equating the axial force to zero:

$$F = \int_A \sigma_x dA = 0 \tag{12}$$

For the case of a composite beam of two or more materials, the resultant moment is as follows:

$$M_z = -\sum_{i=1}^{n} \int_{A_i} \sigma_x \, tdA \tag{13}$$

Since there are no axial forces, the resultant force is again zero, therefore the bending stress in the j^{th} material becomes:

$$\sigma_j = \sum_{i=1}^{n} \frac{-E_j M t}{E_i I_i}$$

Where:

E_i *is the modulus of elasticity of the* i^{th} *material;*
I_i *is the second moment of area of the* i^{th} *material;*
and M *is the applied moment at a distance* t *from the neutral axis.*

(14)

The second moments of area, I_i, are calculated with respect to the neutral axis, $\hat{y}$, which is calculated as follows:

$$\hat{y} = \sum_{i=1}^{n} \frac{\bar{y}_i E_i A_i}{E_i A_i}$$

Where:

$\bar{y}_i$ *is the centroid of the* i^{th} *material;*
E_i *is the modulus of elasticity of the* i^{th} *material;*
and A_i *is the cross – sectional area of the* i^{th} *material.*

(15)

Combined behaviour of bone and plate

The complex nature of *in vivo* loading conditions in bone-plate systems generally involves a combination of axial, bending, torsional, and shear loads. Coupled with plates that are bent pre-operatively to conform to the already complex geometry of bones, these complexities create an incredibly difficult structural system to analyze.

As mentioned previously, it is essential that the plate carries most of the load during the initial stages of fracture healing, however, in the latter stages, when the structural stiffness and strength of bone returns the load sharing should ideally shift from the plate to the bone. In some cases the difference in stiffness between the plate and bone causes stress shielding that leads to bone loss and a further decrease in the structural rigidity of the bone. At the extreme of this negative cycle, the plate may carry the entirety of the load and may be at risk of failure (Cordey, Perren, & Steinemann, 2000).

Our focus is on the load sharing between the plate and bone just following healing (i.e. no fracture gap exists). Some of the assumptions that must be made in order to analyze this simplified bone-plate system include: the plate is firmly attached to the bone and behaves as a composite beam; both the plate and bone exhibit elastic behavior, so Hooke's law for a linear elastic material can be applied for both plate and bone; bone is generalized as a homogeneous material having the properties of intact bone; the system is symmetric and therefore can be described by bending in the plane of symmetry and the plane perpendicular to this plane; and any stresses due to torsion are neglected.

In order to determine the stress in the bone at a distance $t_b$from the neutral axis of the composite structure, we can use the following equation which is derived from equations (7) and (13) (Bartel, Davy, & Keaveny, 2006, pp. 274-275):

$$\sigma_B = -\frac{FE_B}{E_B A_B + E_P A_P} - \frac{E_B M t_B}{E_B I_B + E_P I_P}$$

Where:

F *is the applied load;*
E_B *and* E_P *are the moduli of elasticity of the bone and plate, respectively;*
I_B *and* I_P *are the second moment of areas of the bone and plate, respectively;*
A_B *and* A_P *are the cross – sectional areas of the bone and plate, respectively;*
M *is the moment about the neutral axis caused by the application of the applied load,* F*, a distance* t_B *away from the centroidal axis.*

(16)

The first term of the equation represents the compressive stress due to the axial compressive load, while the second term represents the bending that arises from the load being applied at a point away from the centroidal axis of the bone.

The moment about the neutral axis can be calculated as follows:

$$M = F(\alpha r_o - \hat{y})$$

Where:

αr_o *is the distance from the centroidal axis of the bone.*
and $\hat{y}$ *is the composite's neutral axis.*

(17)

The composite neutral axis, $\hat{y}$, which is calculated in equation (14), can be represented by normalized structural stiffnesses and geometries:

$$\hat{y} = \frac{\rho_A}{1 + \rho_A} \gamma r_o$$

(18)

Where the normalized structural stiffnesses and geometries are defined as:

$$\rho_I = \frac{E_P \bar{I}_P}{E_B \bar{I}_B} \tag{19}$$

$$\rho_A = \frac{E_P A_P}{E_B A_B} \tag{20}$$

$$\beta = \frac{r_m}{r_o} \tag{21}$$

$$\gamma = \frac{\bar{y}_P}{r_o} \tag{22}$$

Where:

r_m *is the radius of the medullary cavity;*
r_o *is the outside radius of the bone;*
$\bar{y}_p$ *is the centroid of the plate.*
$\bar{I}_P$ *and* $\bar{I}_B$ *are the moments of inertia of the plate and bone, respectively;*
A_P *and* A_B *are the cross –*
sectional areas of the device and bone, respectively;
E_P *and* E_B *are the moduli of elasticity of the device and bone, respectively.*

Plates are usually applied to the bone on the side where tensile stresses are the highest, i.e. the convex side of the diaphysis indicates the tension side of a long bone. Application of either a plate or banding wire in this manner is known as the tension band principle (Stoffel, Klaue, & Perren, 2000). Clinically, surgeons insert plates where the least amount of muscle damage occurs; however, when possible this principle should be adhered to as the application of a plate to tensile side of long bones promotes compression between bone segments, whereas the converse is true when applied on the compressive side or where an angular deformity occurs at the fracture site.

Although an axially applied load along the plane of symmetry only produces compression in the intact bone, bending is induced after adding the plate to the system, so changing the location of neutral plane and axis. The stress is very sensitive to the relative axial stiffness between the plate and bone, as this determines the location of the neutral axis (Cordey, Perren, & Steinemann, 2000) (Ramakrishna, Sridhar, & Sivashanker, 2004). With the application of a plate, the neutral axis shifts from the centroid of the bone up towards the plate, thus creating a bending moment, even when one applies an axial load through the centroid of the bone, with respect to the neutral axis of the bone-plate composite. The above equations are only dependent on the location of the centroids, cross-sectional areas, and the moments of inertia of the bone and plate. Therefore, using equation (15) one is able to theoretically predict the stress in bone for a variety of plating geometries, such as those in this study.

Beam on elastic foundation theory

Although beam theory is often used to calculate the load shared between components of composite beams, more complex methods must be used for determining stress and strain distributions near areas of abrupt changes in material properties, geometry, or loading. For instance, beam on an elastic foundation theory can be used to determine how the loads are shared among the components of the composite structure. In using this theory, the components are deemed a composite of beam(s) and elastic foundation, where loads applied to beams are a function of the displacement of the beam. In order to analyze the behavior of the structure, the stiffness of the composite beam is the sum of the individual components' stiffness (Bartel, Davy, & Keaveny, 2006, pp. 204-206):

$$EI = \sum_{i=1}^{n} E_i I_i \tag{23}$$

The governing equation of the system wherein the displacement of both the beam and foundation is related to the applied load corresponds to the following equation:

$$EI\frac{d^4v}{dx^4} + kv(x) = p(x) \tag{24}$$

Where:

$v(x)$ *is the displacement of the beam in the y direction;*
$p(x)$ *is a distributed load applied to the beam;*
$kv(x)$*is the distributed load applied to the beam by the foundation;*
and k *is the foundation modulus of elasticity.*

Solving the above equation for the displacement of the beam, $v(x)$, we can then find the loading on the beam due to the foundation:

$$q(x) = kv(x) \tag{25}$$

The bending moment is then calculated as:

$$M(x) = EI\frac{d^2v}{dx^2} \tag{26}$$

Finally, the stress can be determined using the flexural formula, i.e.:

$$\sigma = -\frac{My}{I} \tag{27}$$

The preceding calculations are applicable only for the idealized model, where the bone is represented by a concentric cylinder. In a study by Huiskes, experimental strain gauge results correlate well with theoretical stress analysis, suggesting that bone can be reasonably approximated by an axisymmetric model (Huiskes, 1982). However, in reality bones are not cylinders and do not have an axis of symmetry. Approximations of non-symmetric cross-sections can be used if the bone is modeled as a straight beam; however, the calculations are considerably more complicated.

Appendix A-H

Appendix A: Triangular 4 mm thread diameter screw configurations

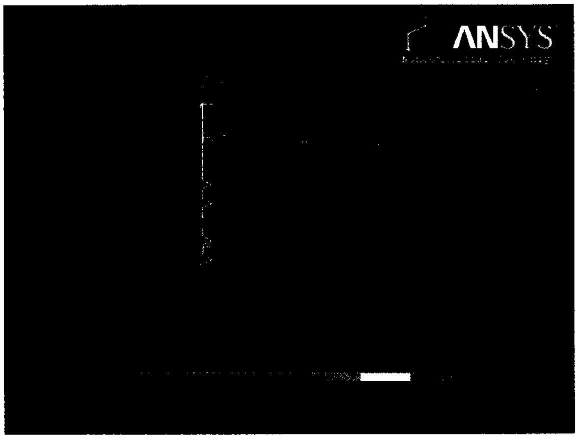

(a) Long shaft, 40 GPa Elastic modulus

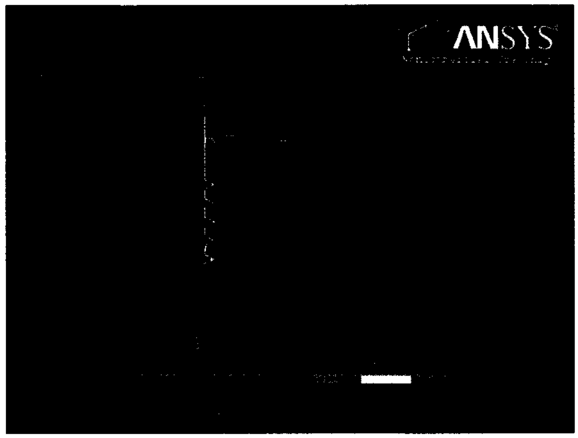

(b) Long shaft, 105 GPa Elastic modulus

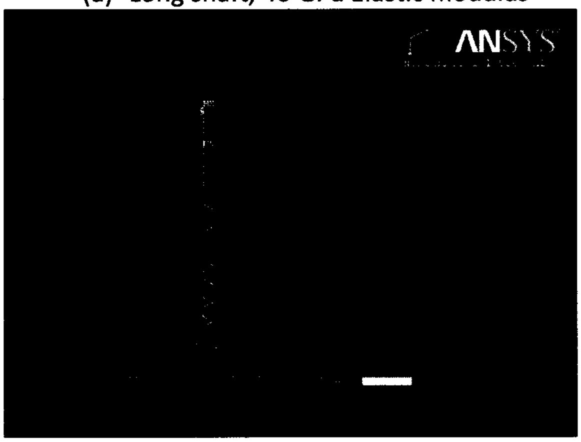

(c) Long shaft, 40 GPa Elastic modulus

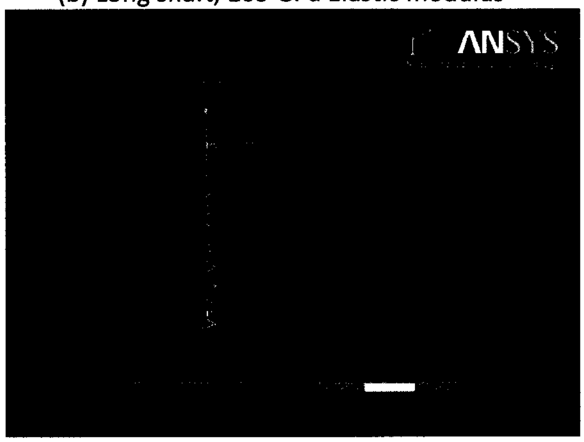

(d) Long shaft, 105 GPa Elastic modulus

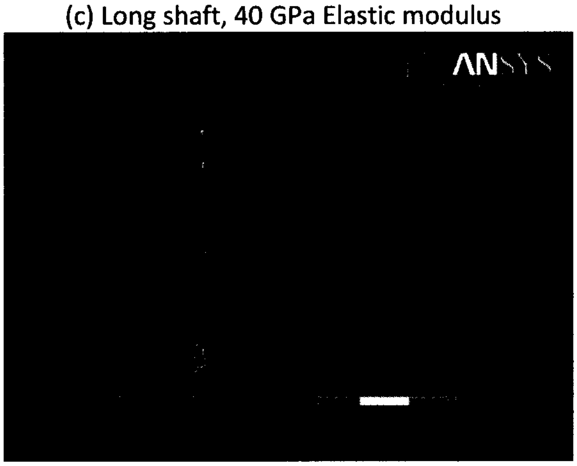

(e) Long shaft, 40 GPa Elastic Modulus

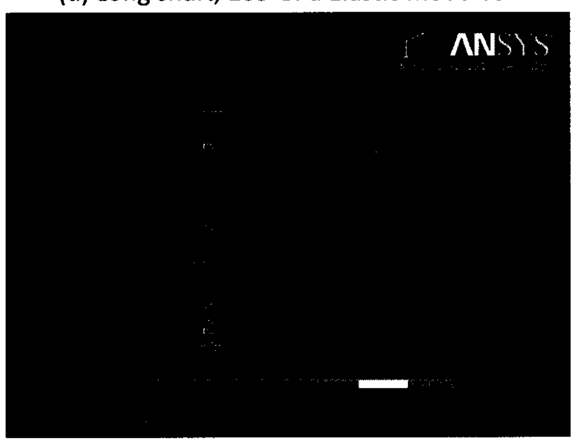

(f) Long shaft, 105 GPa Elastic modulus

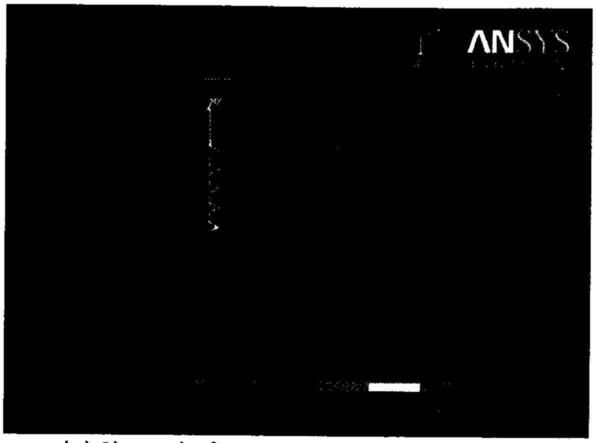

(a) Short shaft, 40 GPa Elastic modulus

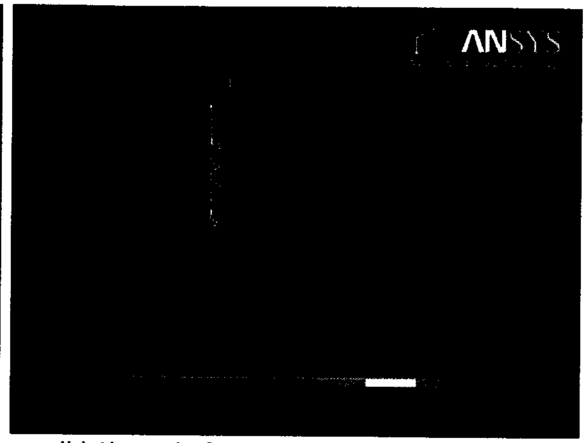

(b) Short shaft, 105 GPa Elastic modulus

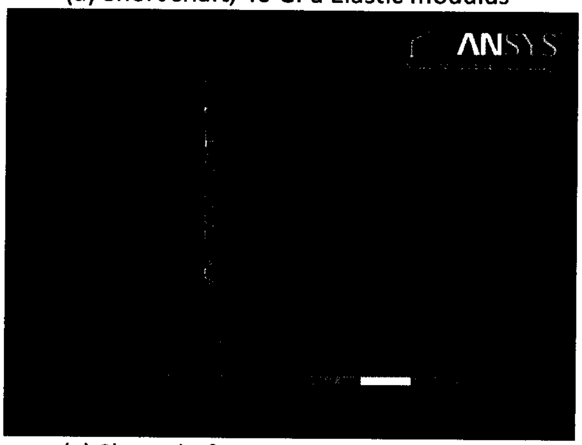

(c) Short shaft, 40 GPa Elastic modulus

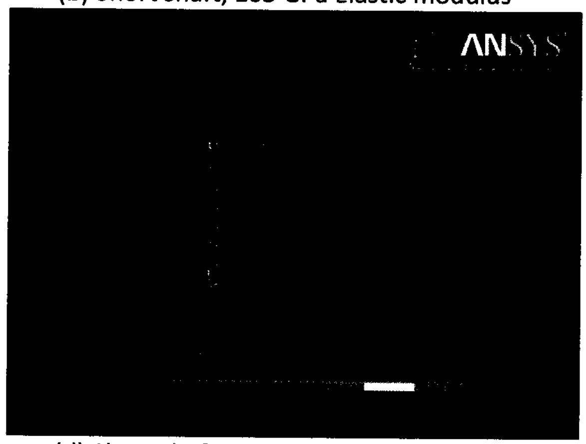

(d) Short shaft, 105 GPa Elastic modulus

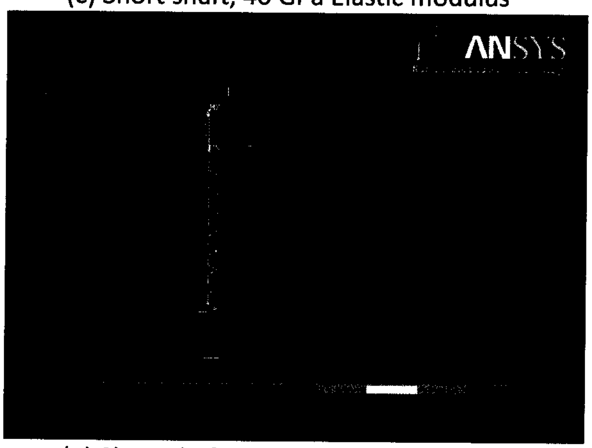

(e) Short shaft, 40 GPa Elastic modulus

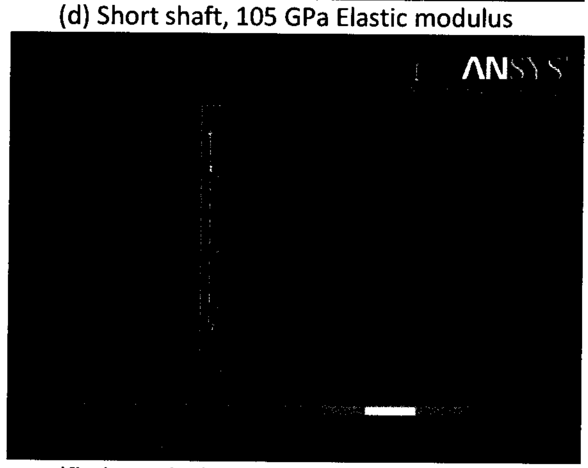

(f) Short shaft, 105 GPa Elastic modulus

Appendix B: Triangular 6 mm thread diameter screw configurations

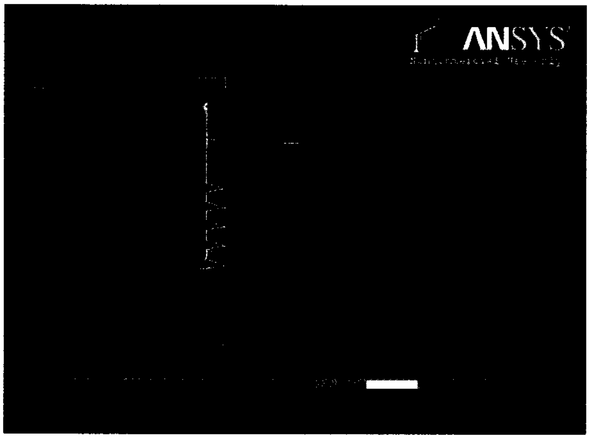

(a) Long shaft, 40 GPa Elastic modulus

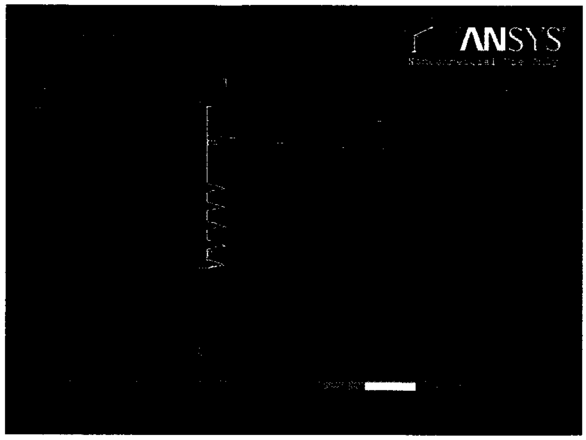

(b) Long shaft, 105 GPa Elastic modulus

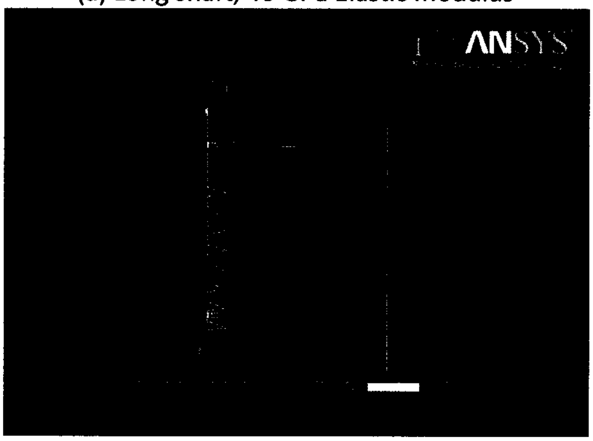

(c) Long shaft, 40 GPa Elastic modulus

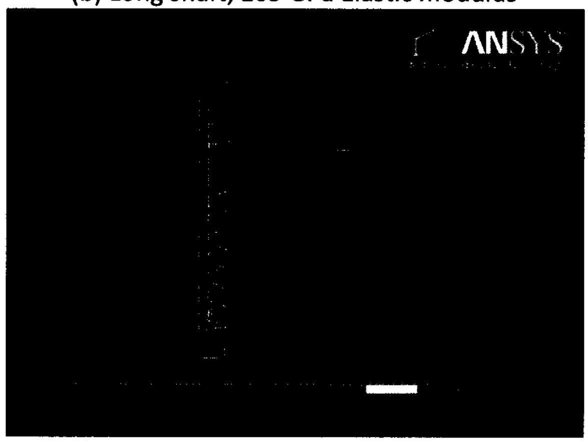

(d) Long shaft, 105 GPa Elastic modulus

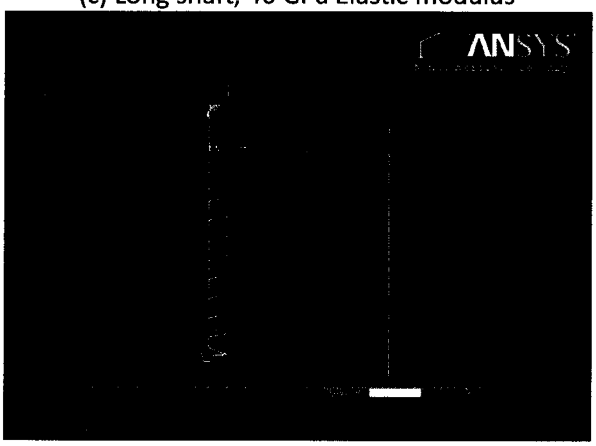

(e) Long shaft, 40 GPa Elastic modulus

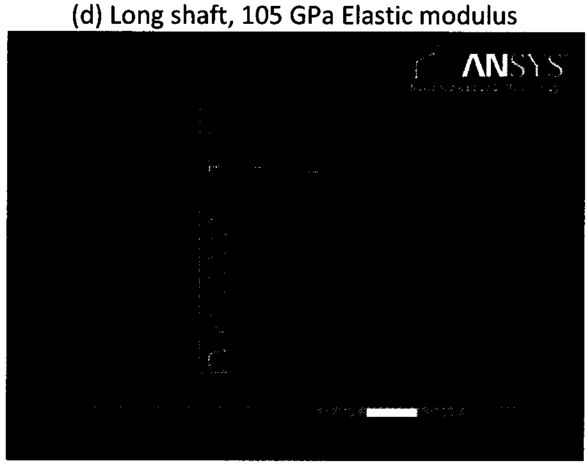

(f) Long shaft, 105 GPa Elastic modulus

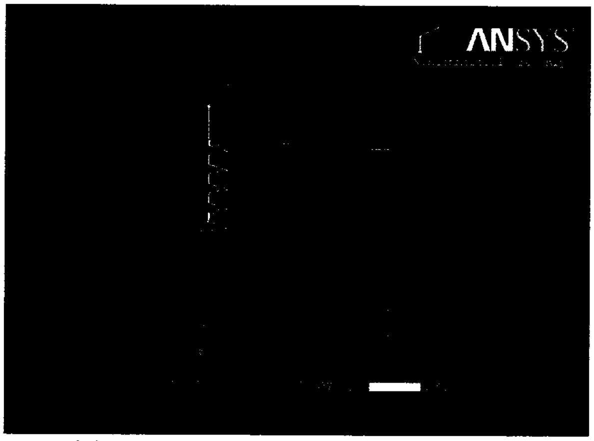

(a) Short shaft, 40 GPa Elastic modulus

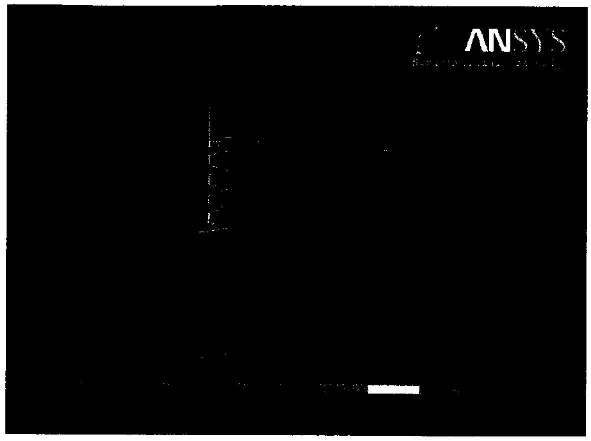

(b) Short shaft, 105 GPa Elastic modulus

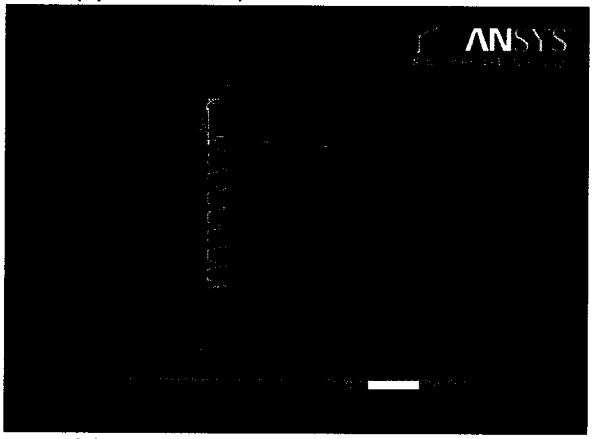

(c) Short shaft, 40 GPa Elastic modulus

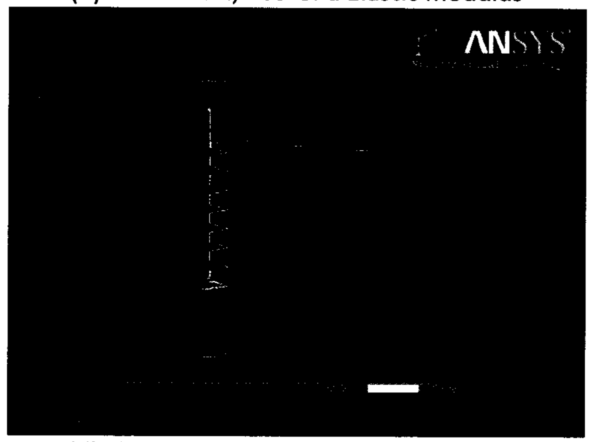

(d) Short shaft, 105 GPa Elastic modulus

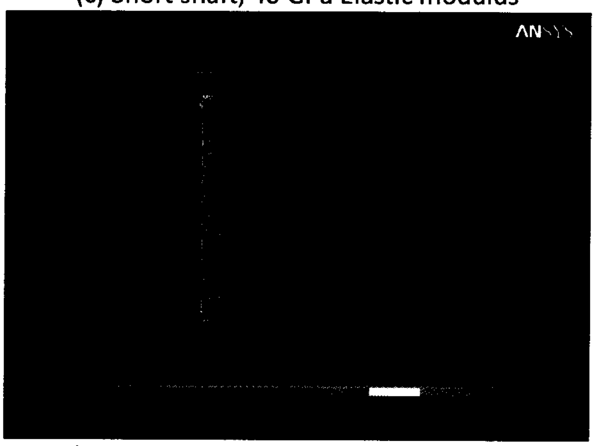

(e) Short shaft, 40 GPa Elastic modulus

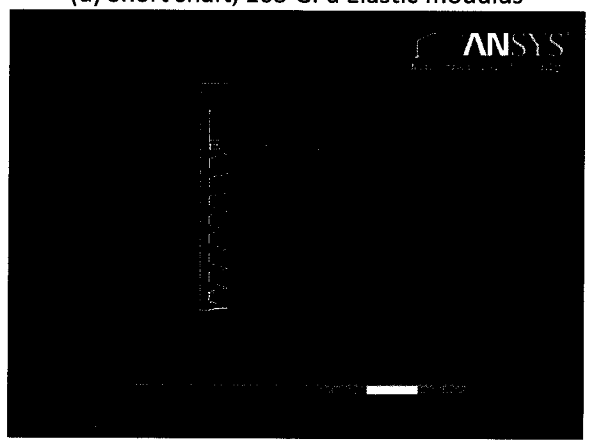

(f) Short shaft, 105 GPa Elastic modulus

Appendix C: Rectangular 4 mm thread diameter screw configurations

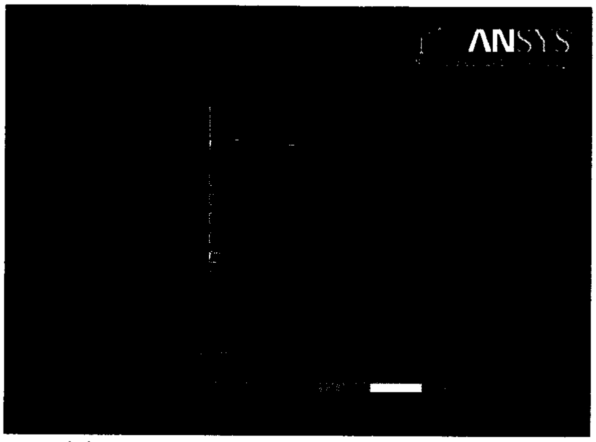

(a) Long shaft, 40 GPa Elastic modulus

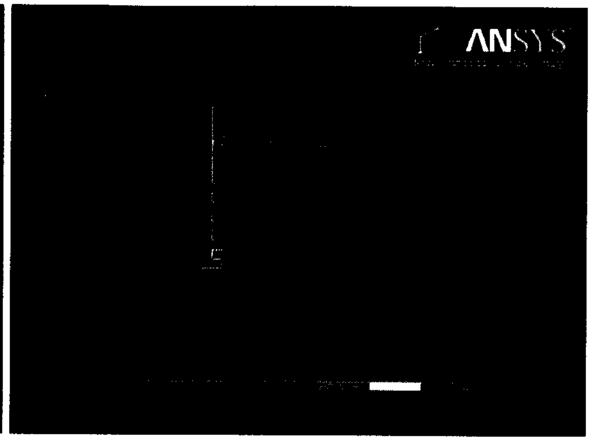

(b) Long shaft, 105 GPa Elastic modulus

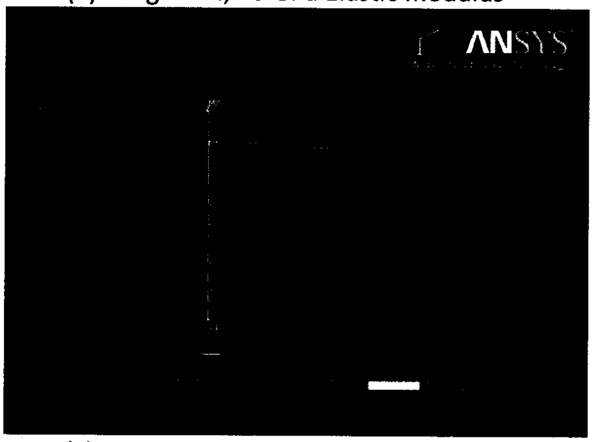

(c) Long shaft, 40 GPa Elastic modulus

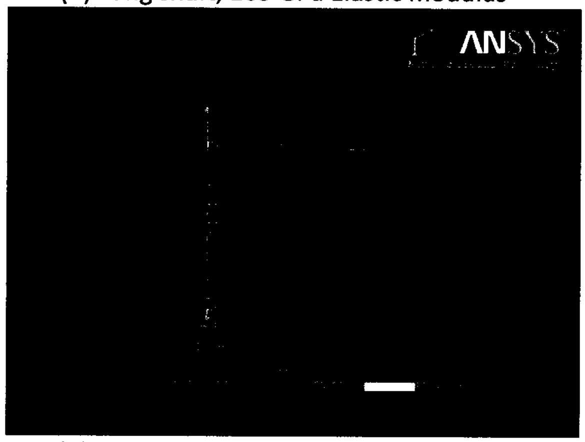

(d) Long shaft, 105 GPa Elastic modulus

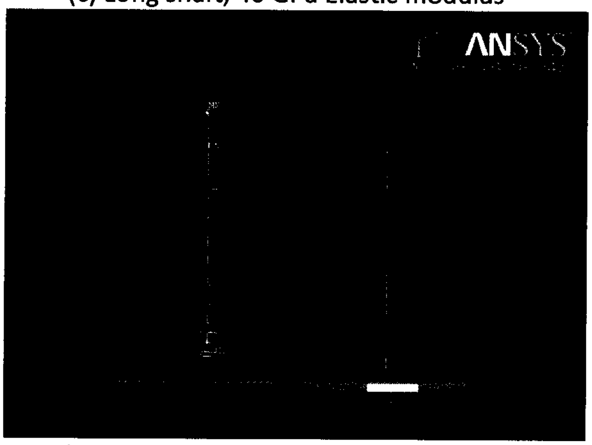

(e) Long shaft, 40 GPa Elastic modulus

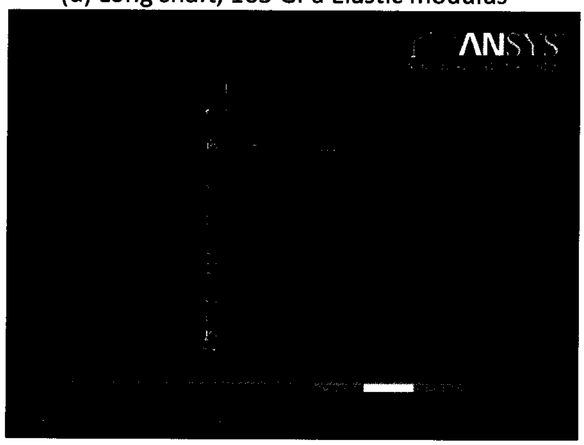

(f) Long shaft, 105 GPa Elastic modulus

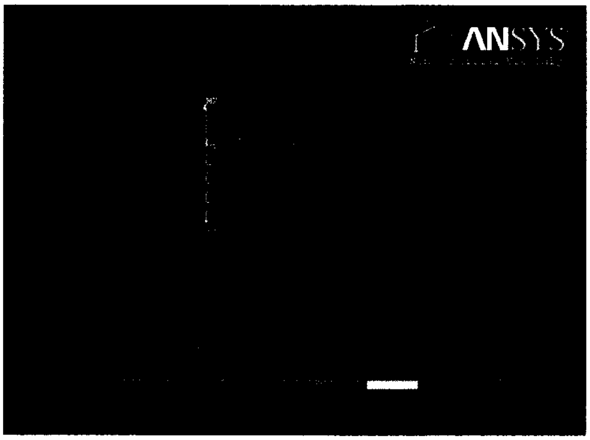

(a) Short shaft, 40 GPa Elastic modulus

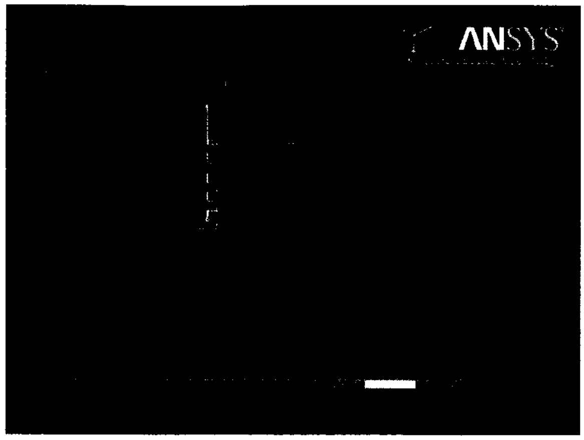

(b) Short shaft, 105 GPa Elastic modulus

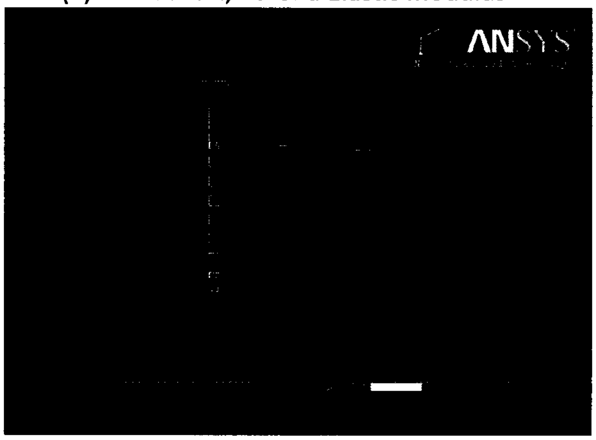

(c) Short shaft, 40 GPa Elastic modulus

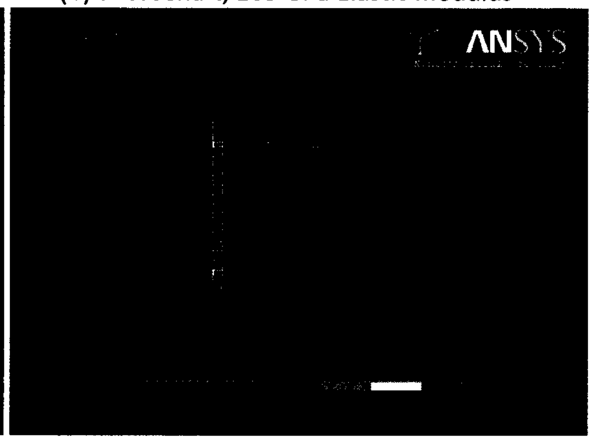

(d) Short shaft, 105 GPa Elastic modulus

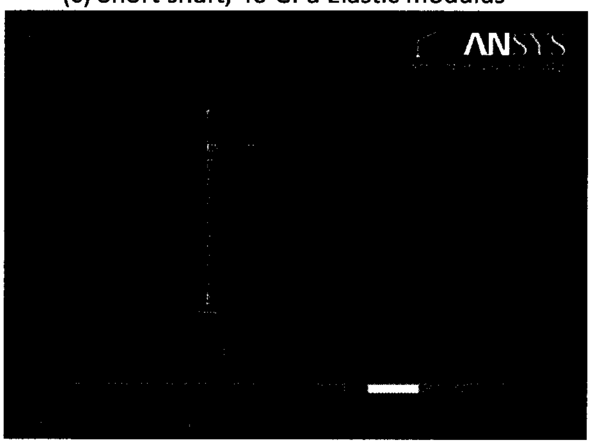

(e) Short shaft, 40 GPa Elastic modulus

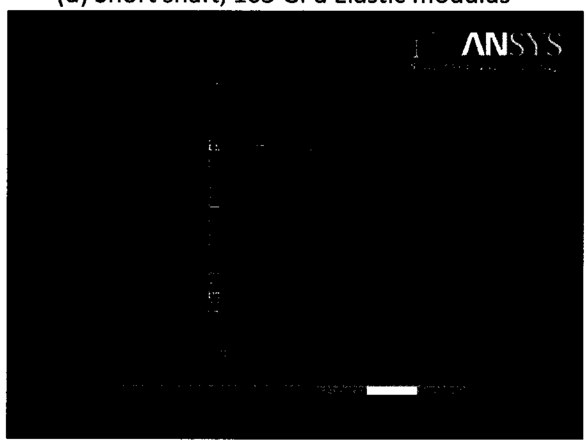

(f) Short shaft, 105 GPa Elastic modulus

Appendix D: Rectangular 6 mm thread diameter screw configurations

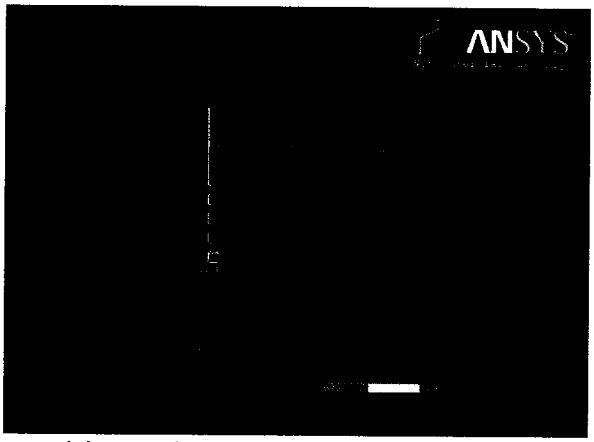

(a) Long shaft, 40 GPa Elastic modulus

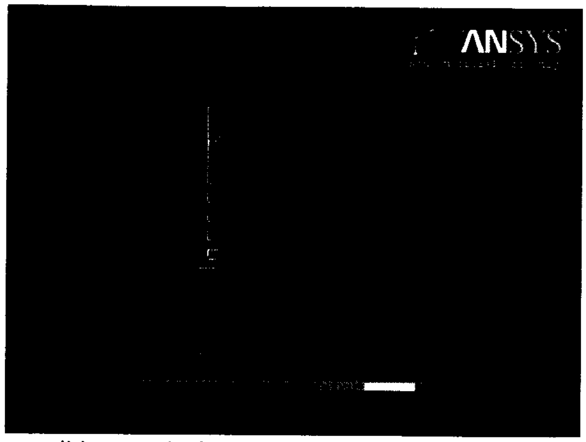

(b) Long shaft, 105 GPa Elastic modulus

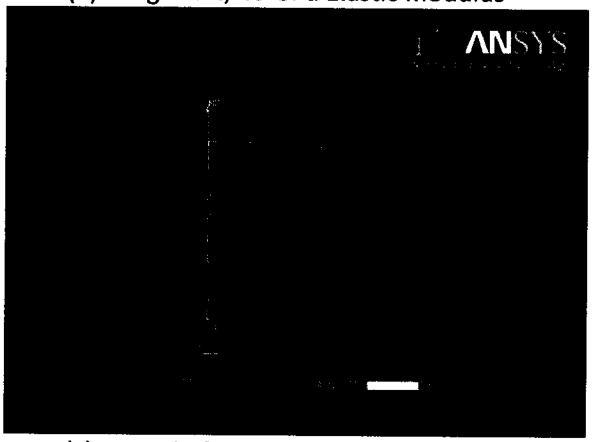

(c) Long shaft, 40 GPa Elastic modulus

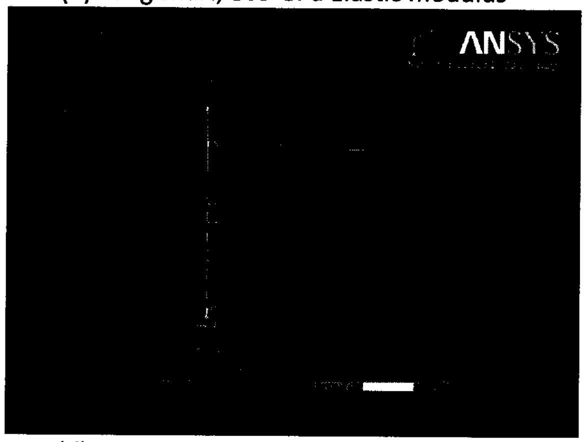

(d) Long shaft, 105 GPa Elastic modulus

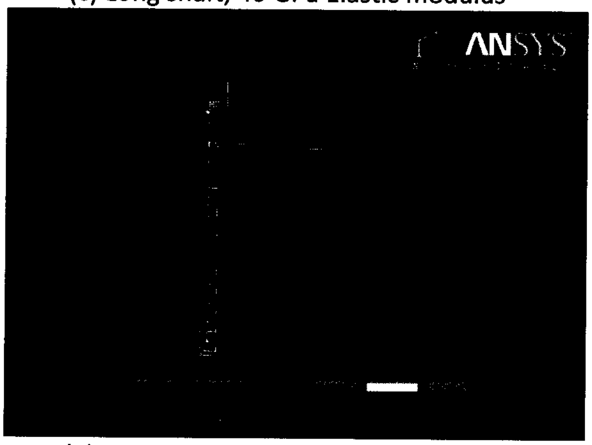

(e) Long shaft, 40 GPa Elastic modulus

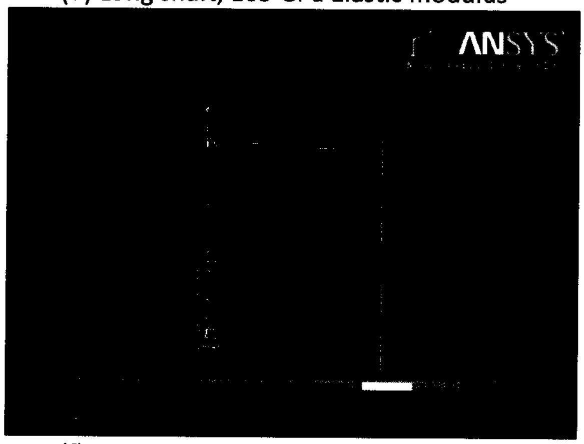

(f) Long shaft, 105 GPa Elastic modulus

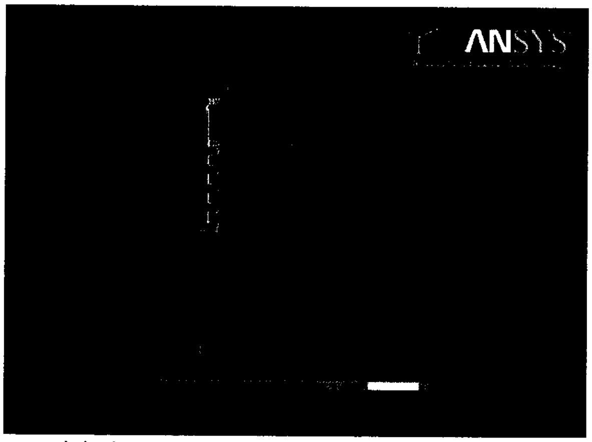

(a) Short shaft, 40 GPa Elastic modulus

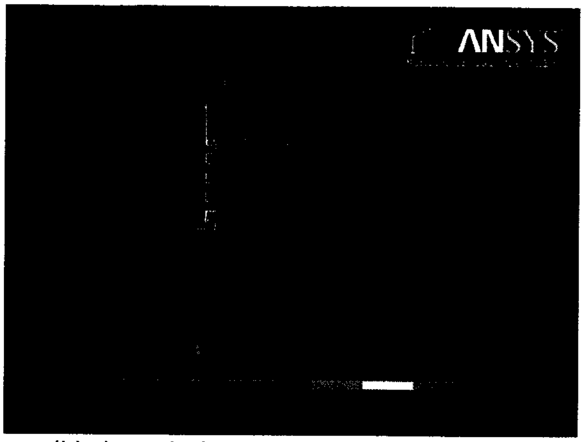

(b) Short shaft, 105 GPa Elastic modulus

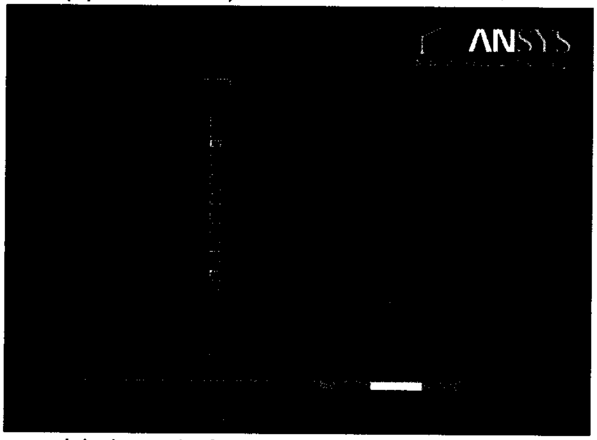

(c) Short shaft, 40 GPa Elastic modulus

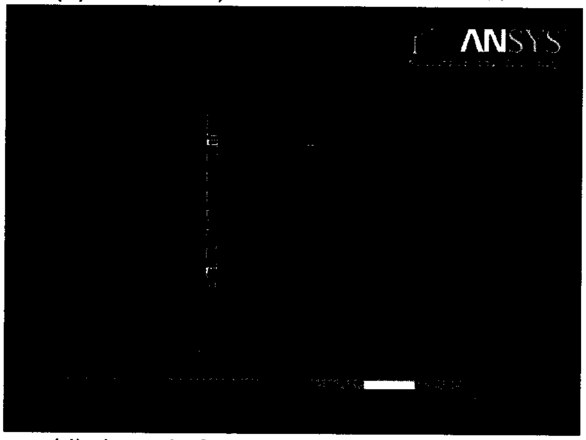

(d) Short shaft, 105 GPa Elastic modulus

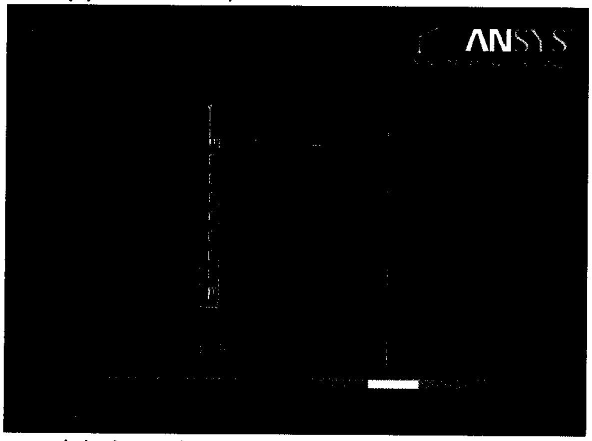

(e) Short shaft, 40 GPa Elastic modulus

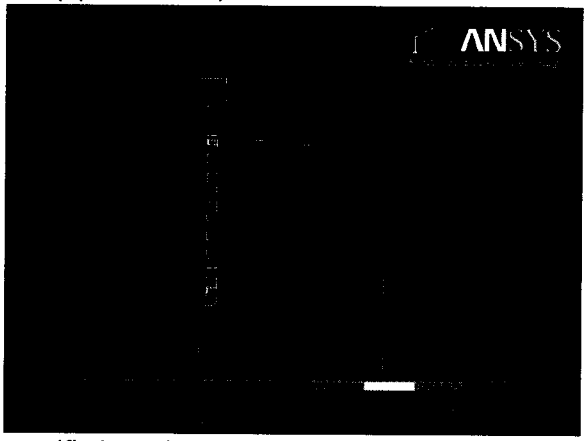

(f) Short shaft, 105 GPa Elastic modulus

Appendix E: Trapezoidal 4 mm thread diameter screw configurations

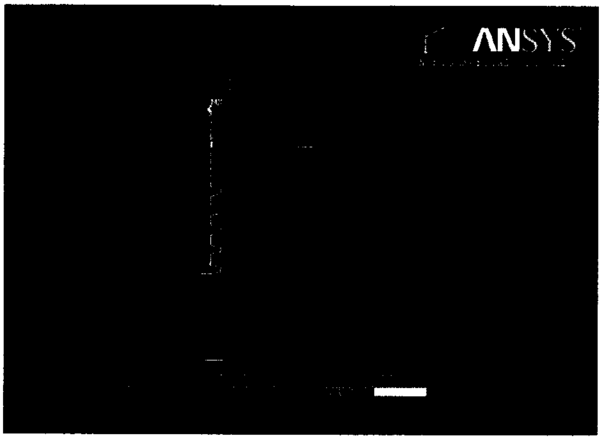

(a) Long shaft, 40 GPa Elastic modulus

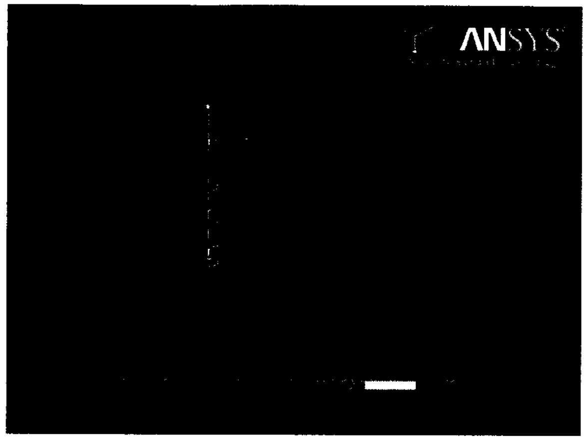

(b) Long shaft, 105 GPa Elastic modulus

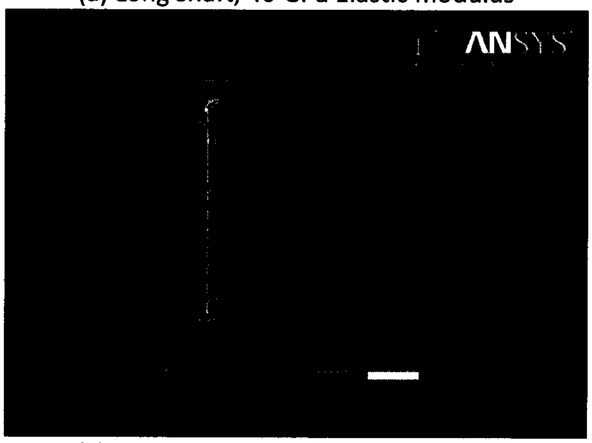

(c) Long shaft, 40 GPa Elastic modulus

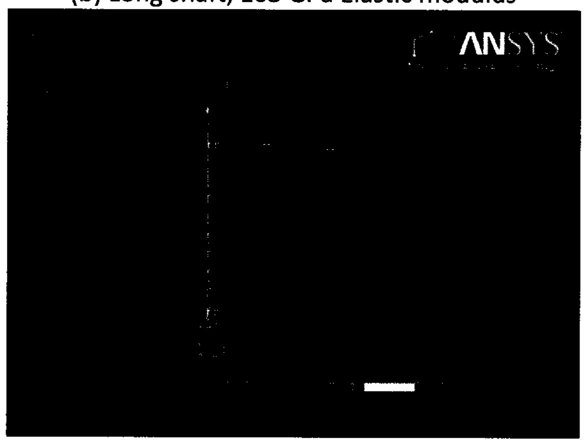

(d) Long shaft, 105 GPa Elastic modulus

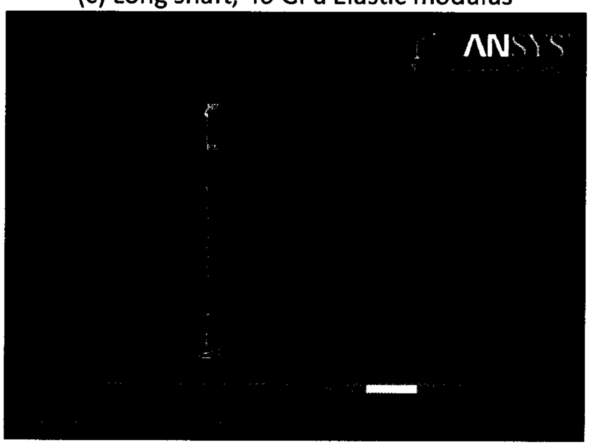

(e) Long shaft, 40 GPa Elastic modulus

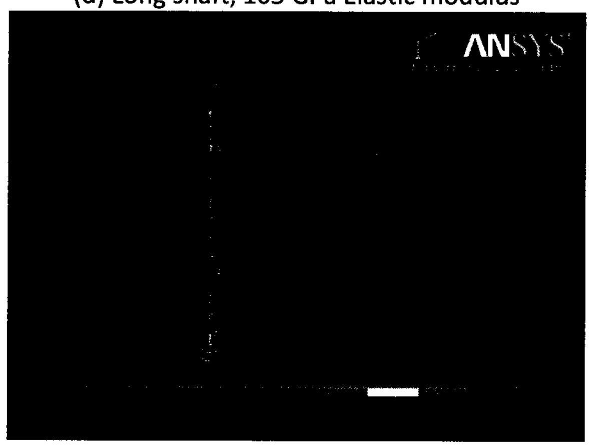

(f) Long shaft, 105 GPa Elastic modulus

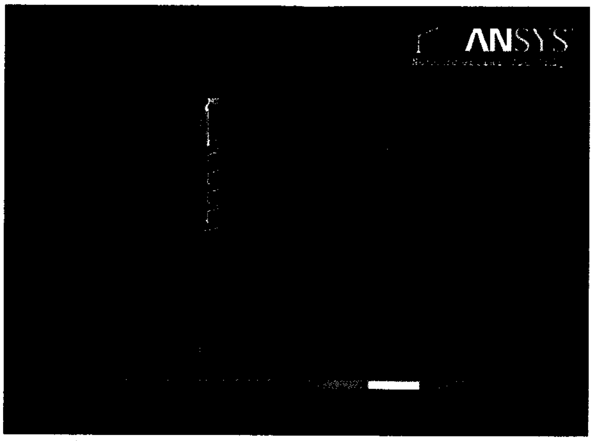

(a) Short shaft, 40 GPa Elastic modulus

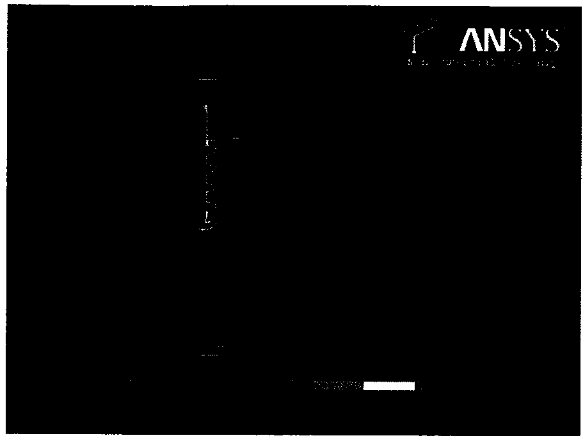

(b) Short shaft, 105 GPa Elastic modulus

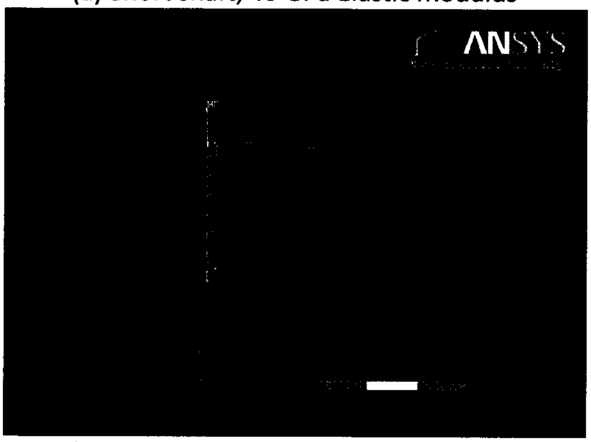

(c) Short shaft, 40 GPa Elastic modulus

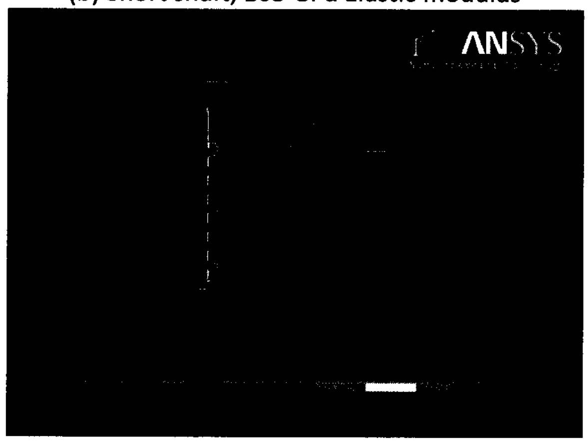

(d) Short shaft, 105 GPa Elastic modulus

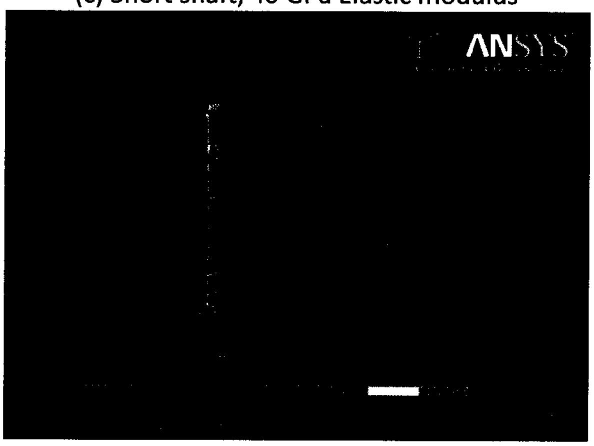

(e) Short shaft, 40 GPa Elastic modulus

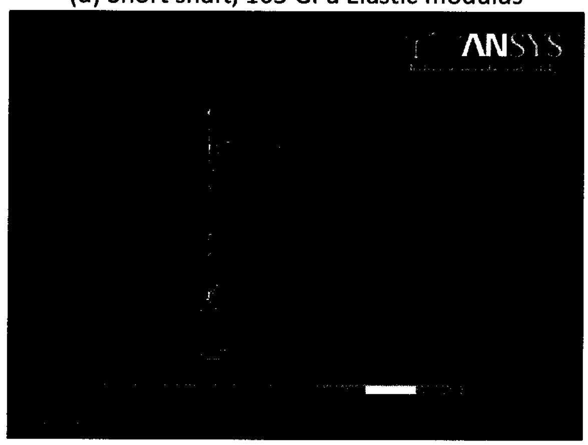

(f) Short shaft, 105 GPa Elastic modulus

Appendix F: Trapezoidal 6 mm thread diameter screw configurations

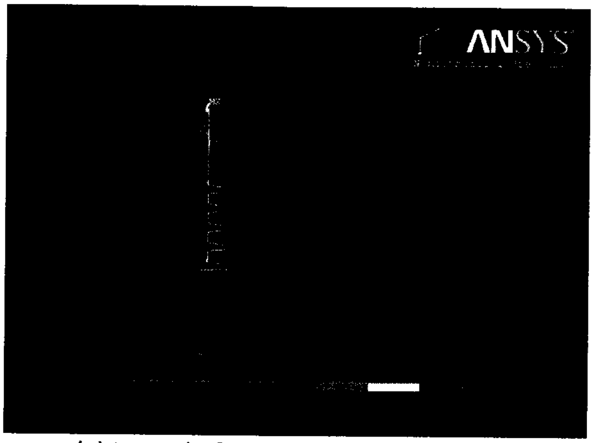

(a) Long shaft, 40 GPa Elastic modulus

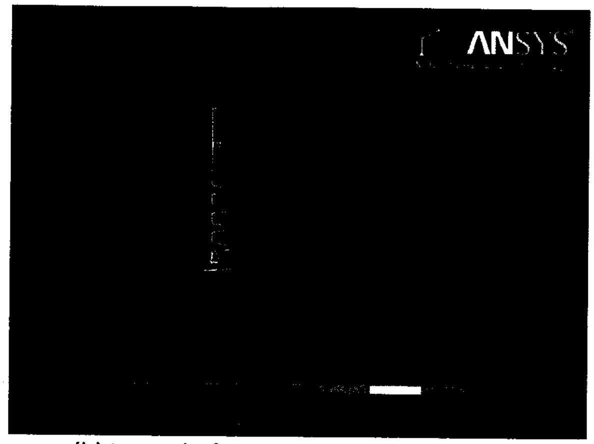

(b) Long shaft, 105 GPa Elastic modulus

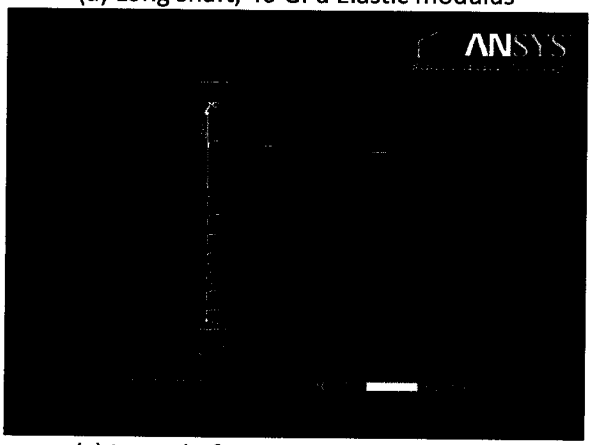

(c) Long shaft, 40 GPa Elastic modulus

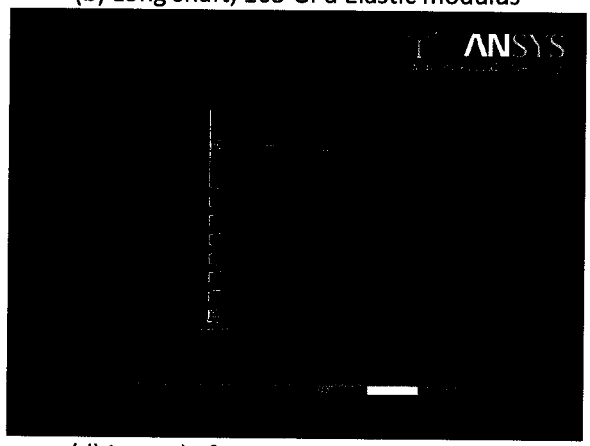

(d) Long shaft, 105 GPa Elastic modulus

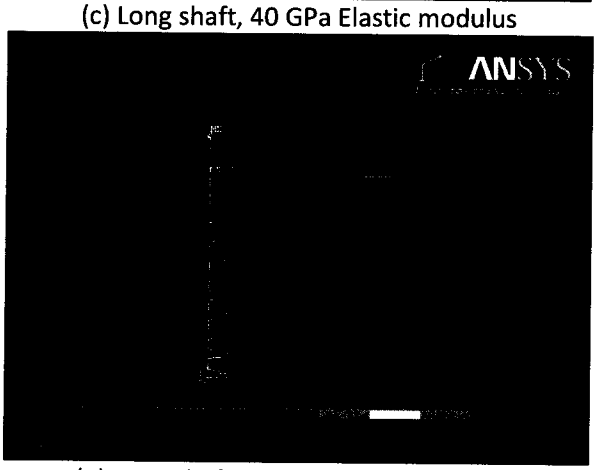

(e) Long shaft, 40 GPa Elastic modulus

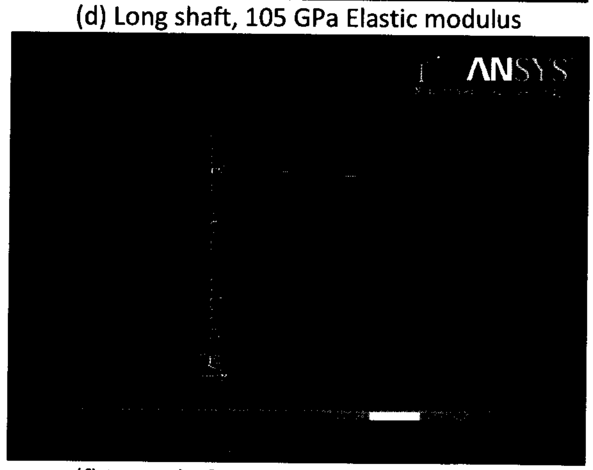

(f) Long shaft, 105 GPa Elastic modulus

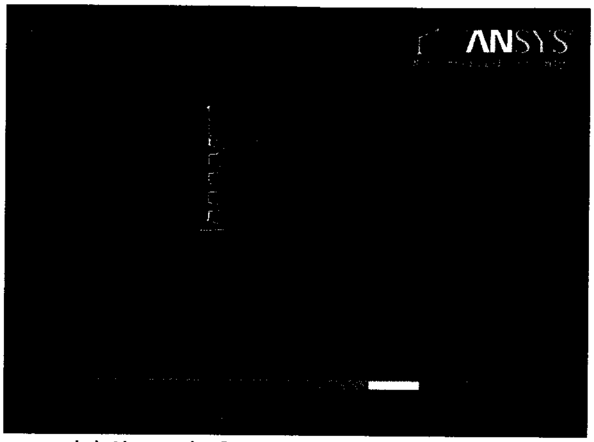

(a) Short shaft, 40 GPa Elastic modulus

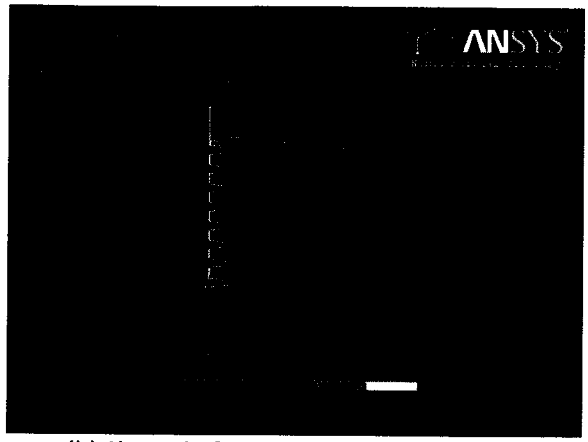

(b) Short shaft, 105 GPa Elastic modulus

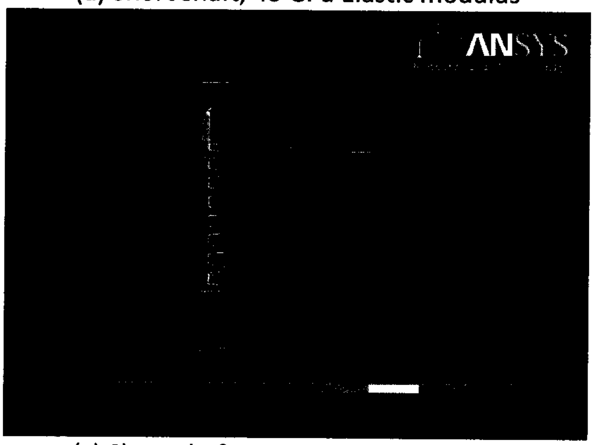

(c) Short shaft, 40 GPa Elastic modulus

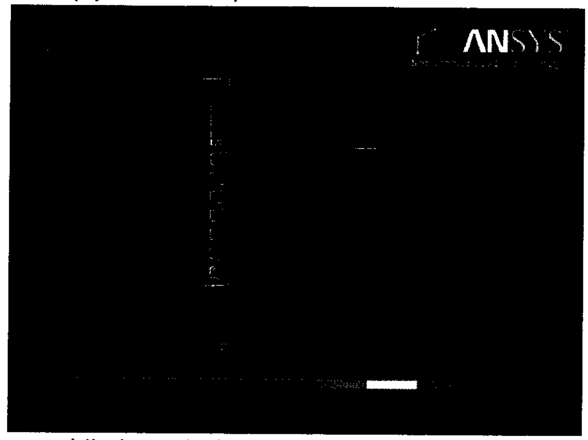

(d) Short shaft, 105 GPa Elastic modulus

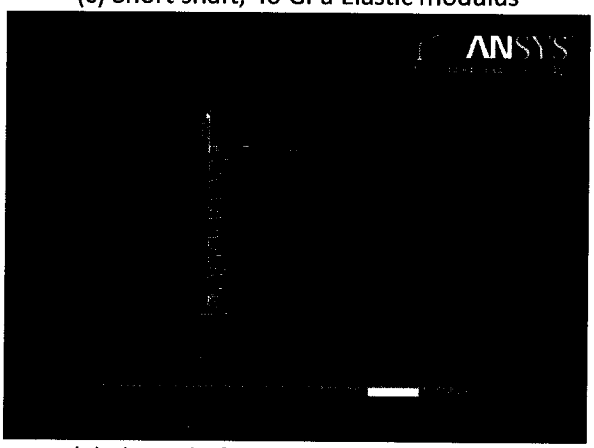

(e) Short shaft, 40 GPa Elastic modulus

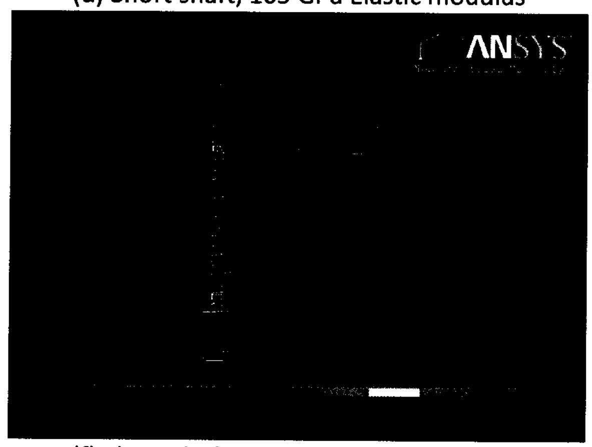

(f) Short shaft, 105 GPa Elastic modulus

Appendix G: Change in the shaft diameter

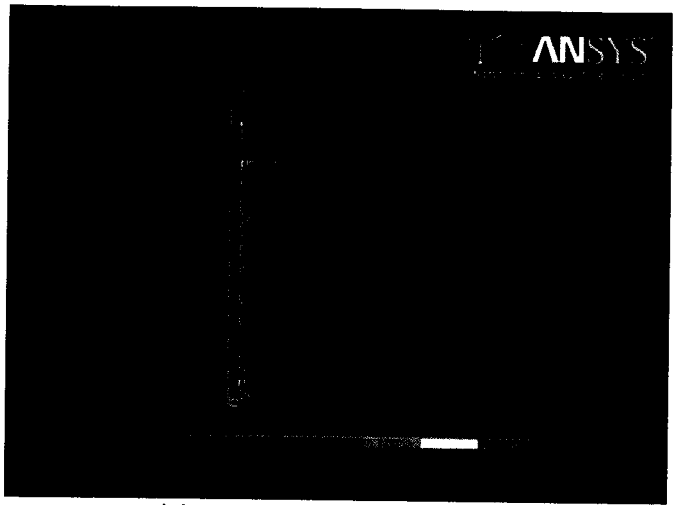

(a) 1.1 mm root diameter configuration

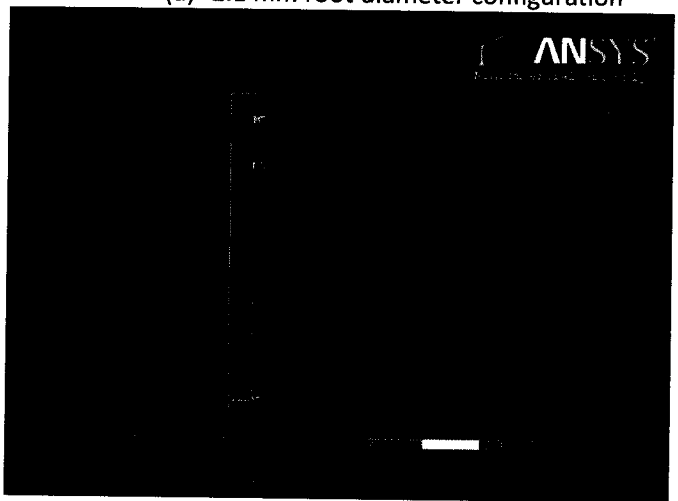

(b) 2.1 mm root diameter configuration

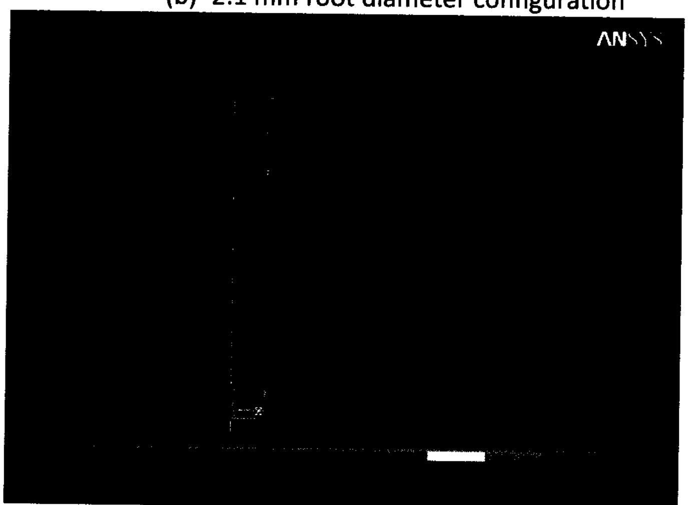

(c) 3.1 mm root diameter configuration

Appendix H: Software instructions

SolidWorks geometry instructions

SolidWorks is used to generate the 3D parametric model configurations. The radial bone shaft, fixation plate and simplified screws are all modeled and saved as parasolid parts before importing them into ANSYS workbench. The steps outlining their creation are listed below:

i. The radial bone shaft is created as a simple extrusion of a hollow cylinder with the following dimensions; 14.7 mm outer diameter and 7.4 mm inner diameter.
   - A pattern of a revolved cut is created in the plate to represent the screw holes (having the same dimensions as the simple screws).

ii. The bone plate is modeled as an extrusion of a hollow partial-cylinder. The 14.7 mm inner diameter is kept constant while the outer diameter varies as the thickness is increased from 3.0 to 4.5 mm and the angle of the cylinder is varied between 60° and 90°.
   - A revolved cut is used to model the angled holes commonly designed in fracture fixation plates to be used with cortical screws.

iii. Cortical screws are modeled as a revolved solid including the following dimensions: 2.5 mm root diameter, 3.5 mm outer diameter of two simplified threads, 4.81 mm diameter tapered head, shaft length of 5 mm, and 10.55 mm length of thread engagement (which is also the distance between the two simple threads).

iv. The 3 solid parts are then assembled using geometric relations.

ANSYS Workbench parametric model instructions

1) Import Geometry file from SolidWorks into Ansys Workbench 11.0:

   a) Select New Geometry in the top left corner of the screen.

   b) Choose the appropriate units (i.e. millimeters).

   c) From the File menu, choose Import External Geometry.

   d) Open the parasolid SolidWorks assembly file.

   e) Click on generate to view the imported file.

2) Choosing simulation options, material properties, inserting loads & boundary conditions, etc.:

   a) Click on the Project tab from the top left corner.

   b) Under DesignModeler Tasks, choose New Simulation.

   c) Static Structural analysis should be selected, for Ductile materials.

3) Inserting a local coordinate system in a desired location (to apply loads or read stresses):

   a) Under Project, Model, Geometry, click on the imported geometry.

b) Right click on Model, click insert and choose Coordinate Systems.

c) Apply a new local coordinate system to the centroid of the end of the bone.

4) Applying loads and boundary conditions:

a) Under Model, click on Static Structural.

b) At the top of the screen click on Supports, and choose Fixed Support.

c) Choose single select and apply to the faces of the bone and plate at the fracture-end of the assembly.

d) At the top of the screen click on Loads, and choose Force.

e) Under the Details of Force, choose Define by Components.

f) Under the Details of Force, Coordinate System, choose the local coordinate system that is previously created.

g) Specify the components of the load in the X, Y and Z component boxes, respectively. (For example, for the validation models apply the 324 N axial force in the Z direction)

h) Click on the origin of the local coordinate system and press apply.

5) Specifying the type of results to view in post processor:

a) From the project manager tree, right click on Solution.

b) Add equivalent stresses and strains to the default calculations.

c) Click Solve at the top of the screen.

d) Click on the Solution under menus in order to view results.

e) Click on Probe at the top of the screen in order to take readings at a specified location (along the bone-screw interface).

Repeat this process for all of the parametric configurations.

Appendix I: APDL text file

The ANSYS mechanical simulation environment is loaded for analysis of the 2D screw-bone model. From the dropdown File menu, *Read input from* is selected and the following APDL text code generates the fully solved model.

```
!ARG1:  user-defined shaft length
!ARG2:  user-defined number of threads
!ARG3:  user-defined thread profile shape
!ARG4:  user-defined thread diameter
!ARG5:  user-defined screw elastic modulus
!ARG6:  user-defined angle of trapezoidal thread profile

/Title, 2D model, variable parameters
/Prep7                        !Enter pre-processor
/Pmacro
!Define elements and material properties
ARG1=1                        !shaft length
ARG2=9                        !no. of threads
ARG3=1                        !1=triangle,2=rectangle,3=trapezoid
ARG4=6                        !thread diam.
ARG5=40e9                     !screw E
ARG6=50                       !angle

Et,1,PLANE82                  !Element type 1, 4-node quadrilateral element
Mp,ex,1,ARG5                  !Material property, Screw, Modulus of Elasticity
Mp,nuxy,1,.35                 !Material property, Screw, Poisson's ratio

Et,2,PLANE82                  !Element type 2, 4-node quadrilateral element
Mp,ex,2,20e9                  !Material property, Cortical bone, Modulus of Elasticity
Mp,nuxy,2,.35                 !Material property, Cortical bone, Poisson's ratio

Et,3,PLANE82                  !Element type 3, 4-node quadrilateral element
Mp,ex,3,1e9                   !Material property, Trabecular bone, Modulus of Elasticity
Mp,nuxy,3,.35                 !Material property, Trabecular bone, Poisson's ratio
!Define the basic geometry
Y=22-ARG1
D=1.0                         !Radius of screw shaft
K,1,0,Y-ARG2*2+1,0            !Define keypoints
K,2,0,28,0
K,3,D+2,28,0
K,4,D+2,25,0
K,5,D,25,0
K,6,D,22,0
K,7,D,Y-ARG2*2+1,0
K,8,0,-1.5,0
K,9,20,-1.5,0
K,10,20,22,0
```

```
K,11,20,25,0
K,12,D,Y,0                     !Keypoint based on shaft length input
K,13,0,22,0
L,1,2                          !Define lines by connecting keypoints
L,2,3
L,3,4
L,4,5
LESIZE,4,,,10
L,5,6
L,6,7
L,7,1
L,1,8
L,8,9
L,9,10
L,10,6
L,4,11
L,11,10
AL,1,2,3,4,5,6,7               !Define screw area (without profile thread)
!Define thread profiles
*IF,ARG3,EQ,1,THEN             !Define the triangular thread profile shape
K,14,D+(ARG4/2-1),(Y-0.5),0
K,15,D,(Y-1),0
L,12,14
L,14,15
L,15,12
AL,14,15,16
AGEN,ARG2,2,,,0,-2,0           !Generates areas - as many as thread count
AADD,ALL
A,8,9,10,13                    !Define rectangular area for trabecular region
ASBA,1,(ARG2+2),,DELETE,KEEP
RECTNG,D,20,22,25              !Define cortical bone region
*ELSEIF,ARG3,EQ,2,THEN         !Define the rectangular thread profile shape
K,14,ARG4/2,Y,0
K,15,ARG4/2,Y-1,0
K,16,D,Y-1,0
L,12,14
L,14,15
L,15,16
L,16,12
AL,14,15,16,17                 !Creates area #4 - rectangle profile
AGEN,ARG2,2,,,0,-2,0
AADD,ALL
A,8,9,10,13                    !Define rectangular area for trabecular region
ASBA,1,(ARG2+2),,DELETE,KEEP
RECTNG,D,20,22,25              !Define cortical bone region
*ELSEIF,ARG3,EQ,3,THEN         !Define the trapezoidal thread profile shape
K,14,ARG4/2,Y+((ARG4/2-1)*tan(ARG6)),0
K,15,ARG4/2,(Y-1)-((ARG4/2-1)*tan(ARG6)),0
```

```
K,16,D,Y-1,0
L,12,14
L,14,15
L,15,16
L,16,12
AL,14,15,16,17
AGEN,ARG2,2,,,0,-2,0
AADD,ALL
A,8,9,10,13                 !Define rectangular area for trabecular region
ASBA,1,(ARG2+2),,DELETE,KEEP
RECTNG,D,20,22,25           !Define cortical bone region
*ELSE                       !No profile shape
A,8,9,10,13                 !Define rectangular area for trabecular region
ASBA,2,1,,DELETE,KEEP
RECTNG,D,20,22,25           !Define cortical bone region
*ENDIF
!Meshing of separate areas
*IF,ARG3,GE,4,THEN
meshme_1=1
meshme_2=2
meshme_3=3
*ELSE
meshme_1=ARG2+2
meshme_2=1
meshme_3=2
*ENDIF
Type,1
Mat,1
MSHKEY,0                    !Use free meshing
SMRTSIZE,1
AMESH,meshme_1              !Mesh screw area
Type,2
Mat,2
MSHKEY,0                    !Use free meshing
AMESH,meshme_2              !Mesh cortical bone area
Type,3
Mat,3
MSHKEY,0
SMRTSIZE,1                  !Use free meshing
AMESH,meshme_3              !Mesh Trabecular bone area
!Mesh refinement
*IF,ARG3,LE,3,THEN
ASEL,S,,,(ARG2+2)
LSEL,S,EXT
LSEL,U,LOC,X,0
LSEL,U,LOC,Y,25
LSEL,U,LOC,Y,28
LSEL,U,LOC,X,3
```

```
LSEL,U,,,5,7,2
LSEL,STAT
LSEL,ALL
LREFINE,P,,,2
!LREFINE,ALL
*ELSE
LREFINE,6
*ENDIF
FINISH
/SOLU                          !Enter the processor
ANTYPE,0,new
SOLCONTROL,1
!Apply boundary conditions
ASEL,S,,,(ARG2+2)
LSEL,S,LOC,X,0                 !Selects a subset of lines at x=0
DL,All,ALL,SYMM
DL,All,ALL,UX,0
ASEL,S,,,1,2
LSEL,S,LOC,X,20                !Selects lines at x=20
DL,All,ALL,UX,0                !Displacement constraint in the x-direction
DL,ALL,ALL,UY,0                !Displacement constraint in the y-direction
ASEL,S,,,2
LSEL,S,LOC,Y,-1.5              !Selects line at y=-1.5
DL,All,ALL,UX,0
DL,ALL,ALL,UY,0
LSEL,S,,,2
SFL,ALL,PRES,-80
ALLSEL
SOLVE
FINISH
/POST1                         !Enter the postprocessor
PLDIS,2                        !Plot deformed shape
PLNSOL,S,EQV                   !Plot Von-Mises stress
/OUTPUT,test5,out
*GET,maxstress,PLNSOL,0,MAX
/OUTPUT
PLNSOL,EPTO,EQV                !Plot equivalent strain
/OUTPUT,test5,out,,APPEND
*GET,maxstrain,PLNSOL,0,MAX
/OUTPUT
!Create path along which to get stresses and strains
PATH,workpls,(ARG2*2+1),6,1
xstart=D+0.5*((ARG4/2)-1)      !Mid-thread x-distance
ystart=22-(ARG1/2)             !Mid-point of upper non-threaded shaft (start loc. for nodes)
PPATH,1,,xstart,ystart,0
ynext=22-(ARG1+0.5)
*DO,i,1,(ARG2*2)
PPATH,1+i,,xstart,ynext,0
```

```
ynext=ynext-1
*ENDDO
PDEF,stress,S,EQV,AVG
PDEF,strain,EPTO,EQV,AVG
/OUTPUT,test5,out,,APPEND
PRPATH,stress,strain
/OUTPUT
PLPATH,stress,strain
!*****My STOP Function
Stop=0
*IF,Stop,EQ,0,THEN
/EOF
FINISH
/EOF                              !Mark the end of file
```